University of Nevada, Reno

Aerosol-cloud-precipitation interaction based on remote sensing and cloud-resolving modeling over the Central Himalayas

A dissertation submitted in partial fulfillment of the requirements for the degree of Doctor of Philosophy in Atmospheric Science

by

Pramod Adhikari

Dr. John F. Mejia / Dissertation Advisor

August, 2022

THE GRADUATE SCHOOL

We recommend that the dissertation
prepared under our supervision by

PRAMOD ADHIKARI

entitled

Aerosol-cloud-precipitation interaction based on remote sensing and cloud-resolving modeling over the Central Himalayas

be accepted in partial fulfillment of the
requirements for the degree of

DOCTOR OF PHILOSOPHY

John F. Mejia, Ph.D.
Advisor

David Mitchell, Ph.D.
Committee Member

Eric Wilcox, Ph.D.
Committee Member

Benjamin Hatchett, Ph.D.
Committee Member

Douglas Boyle, Ph.D.
Graduate School Representative

David W. Zeh, Ph.D., Dean
Graduate School

August, 2022

Abstract

The Central Himalayan region experiences pronounced orographic precipitation related to the South Asian summer monsoon, typically occurring from June to September. Atmospheric aerosols can influence regional and global climate through aerosol-radiation (ARI) and aerosol-cloud interactions (ACI). The study of the aerosol-precipitation relationship over the Central Himalayan region during the summer monsoon season is important due to extreme pollution over the upwind Indo-Gangetic Plains, enhanced moisture supply through monsoonal flow, and steep terrain of the Himalayas modulating the orographic forcing. This dissertation aims to study the impact of atmospheric aerosols, from natural and anthropogenic sources, in modulating the monsoonal precipitation, cloud processes, and freezing isotherm over the central Himalayas. The long-term (2002 – 2017) satellite-retrieved and reanalysis datasets showed regardless of the meteorological forcing, compared to relatively cleaner days, polluted days with higher aerosol optical depth is characterized by the invigorated clouds and enhanced precipitation over the southern slopes and foothills of the Himalayas. The mean freezing isotherm increased by 136.2 meters in a polluted environment, which can be crucial and significantly impact the hydroclimate of the Himalayas. Due to the limitations of satellite-retrieved observational data, these results underlined the need for state-of-the-art Weather Research and Forecasting model coupled with Chemistry (WRF-Chem) in a cloud-resolving scale to better represent and study the impact of the aerosols from different sources through radiation and microphysics pathways over the complex terrain of the Central Himalayas. A cloud-resolving WRF-Chem simulation is performed to

assess the impact of anthropogenic and remotely transported dust aerosols on the convective processes and elevation-dependent precipitation. Long-range transported dust aerosols significantly impacted cloud microphysical properties and enhanced the precipitation by 9.3% over the southern slopes of the Nepal Himalayas. The mid-elevation of the Central Himalayas, generally between 1000 and 3000 meters, acted as the region below and above which the diurnal variation and precipitation of various intensities (light, moderate, and heavy) responded differently for ARI, ACI, and the combined effect of aerosols. Due to the ARI effect of aerosols, the light precipitation is suppressed by 17% over the Central Himalayas. The ACI effect dominated and resulted in enhanced heavy precipitation by 12% below 2000 m ASL, which can potentially increase the risk for extreme events (floods and landslides). In contrast, above 2000 m ASL, the suppression of precipitation due to aerosols can be critical for the regional supply of water resources. The overview of the study suggests that the natural and anthropogenic aerosols significantly modulate the convective processes, monsoonal precipitation, and freezing isotherm over the Central Himalayan region, which could pose significant consequences to the changing Himalayan hydroclimate.

Dedication

Dedicated to my mother, father, and entire Adhikari family

Acknowledgements

I want to express my sincere gratitude to Dr. John F. Mejia for his incredible supervision and invaluable guidance and support from the beginning of my research work. I highly appreciate Dr. John for patiently guiding and managing his precious time, ensuring my research meets the objectives and is up to the standard. Without his kind support and guidance, this work could not have come in its present form.

Besides my advisor, I would like to offer my sincere appreciation to my Ph.D. committee members: Dr. David Mitchell, Dr. Eric Wilcox, Dr. Benjamin Hatchett, and Dr. Douglas Boyle, for their insightful comments, encouragement, and time.

A special thank goes to NCAR's Computational and Information Systems Laboratory, sponsored by the National Science Foundation, for providing the computational resources. I would also like to extend my gratitude to the Department of Physics, UNR for providing Teaching Assistantship support throughout my Ph.D. In addition, I want to thank Department of Atmospheric Sciences UNR, Desert Research Institute (DRI), and DRI IPA fund for providing the summer support.

I also offer special thanks to Saroj Dhital and Subash Adhikari; they have probably been the best group of people to share this experience with for constant help and constructive comments and suggestions.

Finally, I express my profound gratitude to my parents, my sisters, and my lovely wife, Sabina, who have provided me with moral and emotional support and continuous encouragement in my life. Words are limited to describe their love and support. I am also grateful to all my friends who have supported and encouraged me along the way.

Table of Contents

List of Tables

List of Figures

Chapter 1: Introduction and Background

1.1 Introduction

The south Asian summer monsoon system, one of the largest components of the global monsoon system, is located in a region that experiences a significant occurrence of aerosol loadings. The enhanced anthropogenic activities with the fast-moving growth of urban cities, industries, and agricultural expansion contribute to a substantial amount of aerosols over the Indian subcontinent (Dey and Di Girolamo 2011; Babu et al. 2013; Kumar et al. 2018). In addition to the severe impact on human health, the increased emission of anthropogenic aerosols also influences monsoonal rainfall (Li et al. 2016). The monsoonal flow incorporates and transports the aerosol from the remote deserts and Indo Gangetic Plain (IGP), a regional hotspot, across the Himalayas to the Tibetan Plateau (Shrestha et al. 2000; Ji et al. 2015). Kang et al. (2019) suggest that the accumulated aerosols over the southern and northern slope of the Himalayas impact the hydrological processes, accelerate the melting of snowpack, and increase the risk of climatic disaster.

The increase in air pollutants over the foothills of the Himalayas and complex mountainous terrain is critical in modulating the precipitation pattern resulting in the rise of extreme events such as drought, floods, and landslides, which pose a risk to the lives and infrastructure during the monsoonal season every year. In general, aerosols have an impact on the hydrological cycle of the Central Himalayan region, which in turn affects the supply of fresh water to hundreds of millions of people residing over the Indian sub-

continent (Immerzeel et al. 2010; Mishra 2015). The better understanding of the response of elevation-dependent precipitation and temperature to the increased anthropogenic aerosols might be critical for the water resources. Improved understanding of the role of anthropogenic aerosols in perturbating the regional hydroclimate will reinforce the global need for a systematic approach to reducing the future risk on the environment of the Himalayan Cryosphere.

Aerosols can impact cloud development and precipitation through aerosol-radiation and aerosol-cloud microphysics interaction (e.g., Fan et al. 2018; Hansen et al. 1997; Rosenfeld et al. 2008; IPCC 2013). The increased aerosol concentration influences the atmospheric stability, convective processes, and circulation, modulating the regional weather and climate (Ramanathan et al. 2005; Lau and Kim 2006; Bollasina et al. 2011). To our knowledge and compared to other regions in the Indian subcontinent the central Himalayan region has received little attention in assessing the impact of the increased loading of atmospheric aerosols during the summer monsoon.

The region of interest in this study is the steep southern slope and immediate foothills of the central Himalayas (**Fig. 1.1**). The Central Himalayan region experiences pronounced orographic precipitation related to the South Asian summer monsoon, which extends from June to September (JJAS; Webster et al. 1998). The cyclonic swirl of westerly/southwesterly circulation over Southern and central India from the Arabic Ocean and southeasterly circulation from the Bay of Bengal along with the orographic forcing facilitate these regional maxima (Fu et al. 2018). The cyclonic swirl follows the path of the heavily polluted region of the Bay of Bengal coast and the IGP before it encounters the southern slope of the central Himalayas (**Fig. 1.2**). Also, the convective

uplifting of aerosols from IGP and advection to the central Himalayas makes the free troposphere more polluted during the monsoon season (Singh et al. 2020).

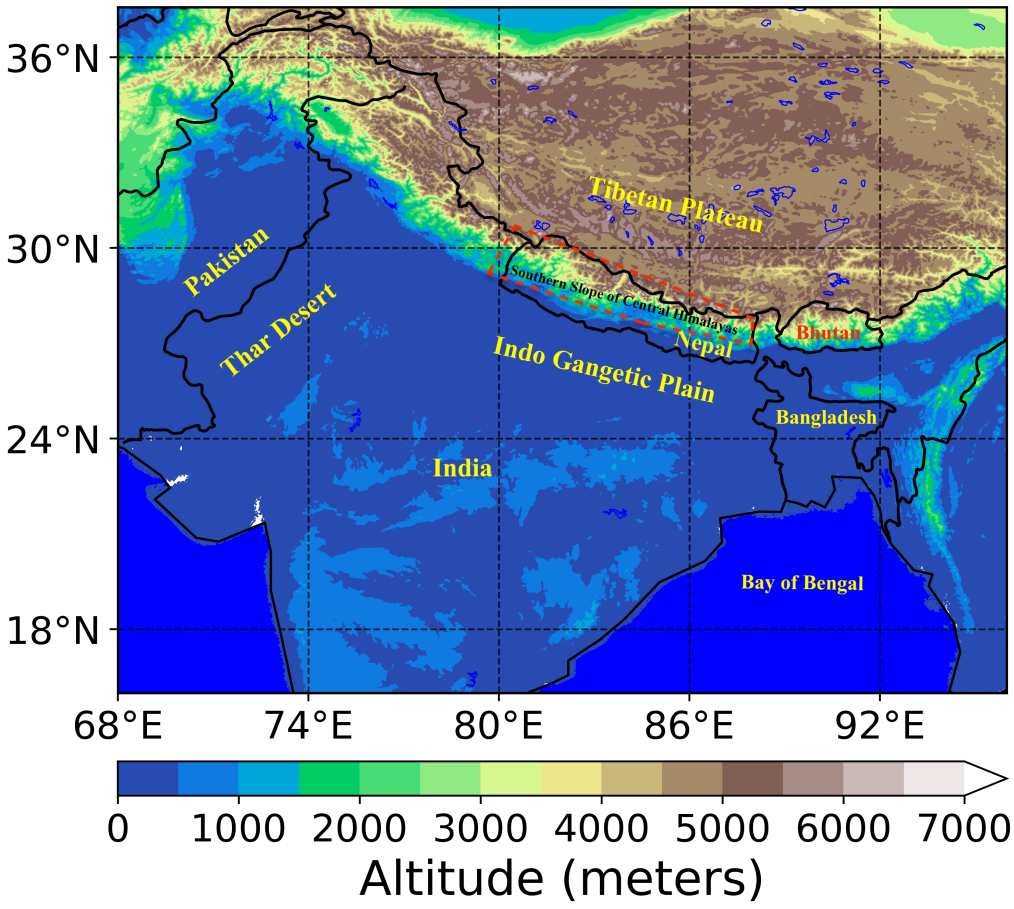

Figure 1.1: Terrain height (meters) and the red polygon represents the southern slope of central Himalayas.

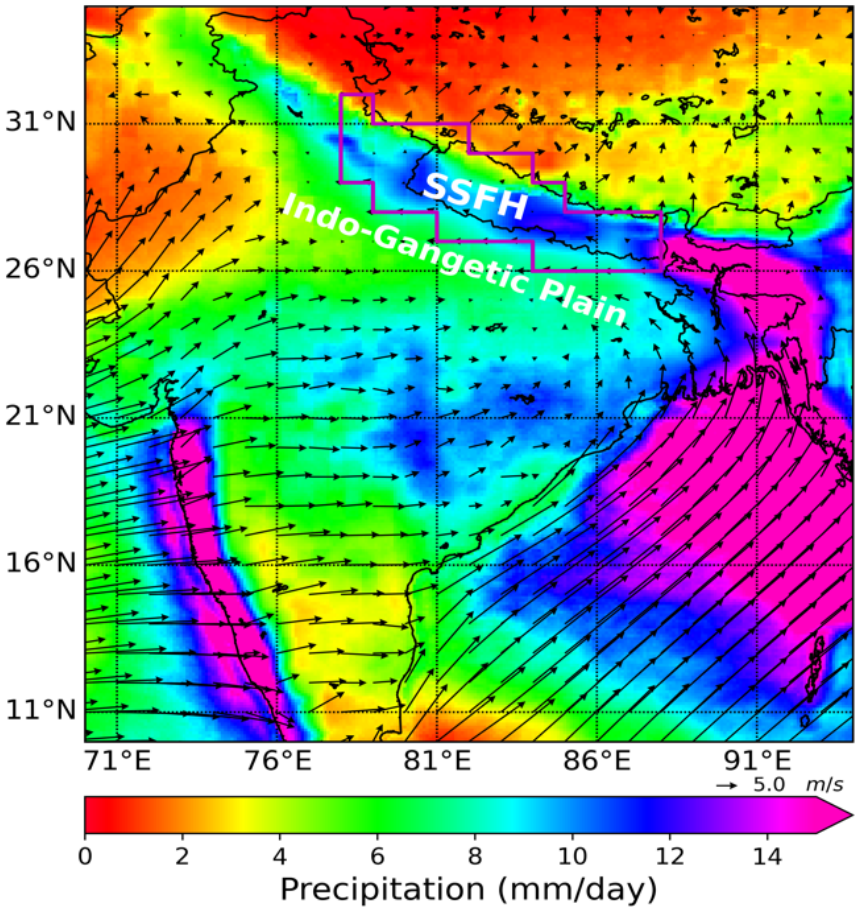

Figure 1.2: Monsoonal season (June-September; 2002-2017) daily mean of Integrated Multi-satellite retrievals for global precipitation measurement precipitation at a 10 km horizontal resolution and ERA5-reanalysis 10 m wind vectors at 0.25° spatial resolution (Adhikari and Mejia, 2021).

Due to the different associated optical properties, atmospheric aerosols can also modulate the vertical temperature distribution and freezing level height (FLH), which is critical for the hydrological conditions in the high mountainous region (Vuille et al. 2008). The positive shortwave radiative forcing over the foothills of the Himalayas during the monsoonal season due to light-absorbing (Lau et al. 2017) and mixed carbonaceous aerosols (Ji et al. 2015) can warm the upper troposphere and influences the FLH. Shrestha et al., (2017) used the numerical model over the Nepal Himalayas to

examine the sensitivity of precipitation with the increase in temperature and prescribed concentration of condensation nuclei. The fluctuation in FLH changes the state of precipitation and has potential consequences on the streamflow resulting in extreme floods over the central Himalayas and western United States (e.g., Ragettli et al. 2016; Davenport et al. 2020; Prein and Heymsfield 2020). Also, Wang et al. (2014) suggest that the variation in summer FLH is critical as it modulates snow cover and glacier mass accumulations over the high mountains of Asia, including the Himalayas.

Natural mineral dust aerosol contributes substantially to the total global atmospheric aerosol loadings (IPCC 2013). The dust aerosols also have a greater probability of emission and long-range transport (Uno et al. 2009; Dhital et al. 2020, 2021; Orza et al. 2020) and can significantly influence the convective processes, vertical temperature distribution, and the hydrological cycle due to their direct and indirect effect (Choobari et al. 2014). The intense dust storm events over the Arabian Peninsula and western Indian desert during the pre and early monsoon season from April to June can transport and severely impact the air quality of IGP and foothills of the Himalayas (Prasad and Singh 2007; Kumar et al. 2015; Sarkar et al. 2019). Also, Sijikumar et al. (2016) suggest that the mineral dust aerosols distributed over the foothills of the Himalayas and IGP during June-August mainly originate on the northwestern deserts of India. Most of the existing numerical and observational studies focused on the dynamics of dust storm origin and its impact on radiative forcing and air quality over the densely populated foothills of Northwestern India (e.g., Sarkar et al. 2019; Shukla et al. 2021; Srivastava et al. 2011).

Few studies have assessed the climatology of elevational dependent warming and precipitation over the Tibetan Plateau (TP) and the Himalayas using the climate models (e.g., Palazzi et al., 2017; Ghimire et al., 2018; Dimri et al., 2022), and highlighted the importance of need of better understanding of elevation-dependent precipitation. However, these studies did not attempt to study the effect of aerosols on elevation-dependent precipitation. A better understanding of aerosol effect on elevation-dependent warming and precipitation of this mountainous region is crucial to assess the hydrologic and climate risks for millions of people residing on the adjacent lowlands.

As the Himalayas lie downwind of the heavily polluted region, the hydroclimate of the Himalayas is sensitive to the aerosol loading through the cloud, radiation, and circulation interaction. This dissertation aims to improve our understanding of the relationship between the natural and anthropogenic aerosols and precipitation distribution over the central Himalayas. To the best of our knowledge, we believe that the impact of anthropogenic aerosols and long-range transported dust aerosols through radiation and microphysical pathways using a cloud-resolving modeling framework over the central and Nepal Himalayan region has not been assessed. Also, to our knowledge, this study is the first attempt to estimate and quantify the relationship between aerosols and freezing level isotherm during the monsoon over the Central Himalayas. Further, we examine the role of anthropogenic aerosol in modulating the elevation-dependent precipitation distribution and intensity over the complex topography of the central Himalayas. Convection-permitting or cloud-resolving numerical models are high-resolution models (< 4 km) specially configured to explicitly resolve convective clouds, which vertically transport and mix moisture, heat, and aerosol particles from the boundary layer into the

upper troposphere (Prein et al. 2015; Tao and Matsui 2015; Seinfeld et al. 2016). Furthermore, cloud-resolving models better represent the topographical features (Chow et al. 2019) and activation of aerosol as cloud droplets on the convective clouds (Chapman et al. 2009; Archer-Nicholls et al. 2016).

1.2 Background

The interaction of aerosols with different meteorological factors and their feedback process impacts the thermodynamic structure of the atmosphere, large-scale monsoonal circulation, clouds, precipitation distribution, and hydrological cycle. Indian monsoon region being collocated on the highly polluted region of Himalayan foothills due to its topographical features and the anthropogenic activities, there is a need for further understanding on the contribution of aerosols on modulating the regional and global hydroclimate. In this section, we review the aerosol and meteorology literature in the regional weather and climatological context.

1.2.1 South Asian Monsoon

The Asian monsoon system is an essential element of the global climate system, which is characterized by a distinct seasonal atmospheric response to land-ocean thermal contrast, a seasonal reversal in prevailing winds, and precipitation patterns (Webster et al. 1998; Ding 2007; Wang and Ding 2008). The south Asian summer monsoon is strongly modulated and driven by the Tibetan Plateau (TP, Figure 1.1). During summer, the immense surface heating of TP pumps up the moist air from the ocean, causing a mid-troposphere wet pool resulting in heavy precipitation over the monsoonal region (Prell

and Kutzbach 1992; Wu et al. 2012). On the other hand, during winter, the land-ocean thermal is reversed due to radiative cooling. The ocean is warmer than continental Asia, which results in a southward shift of wind and suppresses precipitation.

The south Asian summer monsoon typically occurs from June to September (JJAS) (Webster et al. 1998) and is the most significant component of the global monsoon system. The onset of the monsoon and intra-seasonal variability of the monsoonal intensity could be affected by the local land surface interaction and feedback processes between atmospheric circulation and the hydrological cycle. Also, the snow cover extent and albedo over the high land region can impact the onset and the intensity of the monsoonal circulation (Prell and Kutzbach 1992; Bamzai and Marx 2000). In addition to the natural factors, the anthropogenic emissions of greenhouse gases and absorbing aerosols interfere with solar radiation and significantly impact the monsoonal circulation, hydrological cycle, and the regional hydroclimate (Ramanathan et al. 2005; Ramanathan and Carmichael 2008; Bollasina et al. 2011).

Aerosols, the suspended particles in the atmosphere, are key component of the climate system and affect the regional and global climate. (Rosenfeld et al. 2014; Fan et al. 2016). The natural aerosols (e.g., dust, sea salt, biogenic and biomass burning emissions) and anthropogenic aerosols (e.g., sulfate, nitrate, soot, black and organic carbons, etc.) significantly impact the cloud and precipitation processes through direct, semi-direct and indirect effect, which are discussed in detail in later sections. In addition to the severe impact on human health, visibility, and air quality, the increased emission of absorbing natural and anthropogenic aerosols impacts the thermodynamic state of the

atmosphere, large-scale monsoonal circulation, and rainfall (Lau and Kim 2006; Bollasina et al. 2011).

A significant rise in seasonal aerosol optical depth from 2000 to 2015, primarily attributed to anthropogenic and dust aerosols, has been observed over the densely populated rural areas and the urban cities of India (Dey and Di Girolamo 2011; Kumar et al. 2018). The IGP (Figure 1.1) is considered the regional and global hotspot of heavier pollution, with the main contribution from anthropogenic activities. During the winter season, facilitated by the topography and meteorology of the IGP, the formation of a stable boundary layer traps aerosols, making it one of the most polluted regions of the world (Ramanathan and Ramana 2005; Kumar et al. 2018). During the pre-monsoon and summer monsoonal season, however, Babu et al. (2013) found that AOD tends to be modulated by the amount of transported remote dust aerosols and the wet deposition by the monsoonal rainfall.

1.2.2 Aerosol Radiation Interaction

The direct and semi-direct effects comprise the aerosol-radiation interaction (ARI; IPCC 2013). The direct effect of aerosol comprises the scattering and absorption of incoming solar radiation by atmospheric aerosols. Depending on the optical properties of aerosol, which is the function of size distribution, mixing state, chemical composition, and shape of the aerosols, affects the radiative forcing (Wang et al. 2013; Zhang et al. 2015; Gautam and Sorensen 2020; Gautam et al. 2020). The scattering and absorbing of solar radiation limit the amount of radiation reaching the surface, reducing the surface heating and a decreasing convective instability (Ramanathan et al. 2005). According to

Satheesh and Ramanathan (2000), mostly anthropogenic aerosols contribute to the surface forcing of -70 Wm^{-2} per unit AOD. Similarly, Moorthy et al. (2013) estimated that the solar radiation reaching the surface is reduced annually by 57 Wm^{-2} per unit of AOD over India.

Furthermore, the cooling of the surface and warming of the absorbing aerosol layer can alter the thermodynamic structure of the boundary layer through surface radiative energy, sensible heat fluxes, and the evolution of the boundary layer (Li et al. 2016). Limitation of solar radiation reaching the surface and negative surface forcing due to the increase in anthropogenic emission of absorbing aerosol results in reduced mean monsoonal (JJAS) precipitation through a reduction in surface evaporation, a slowdown of tropical-meridional and monsoonal circulation (Ramanathan et al. 2005; Bollasina et al. 2011; Ganguly et al. 2012).

During the pre-monsoon and early monsoon season (May-June), the absorbing aerosols (dust from remote deserts and black carbon from IGP) accumulate over the steep topography of the Himalayas and warms up the lower and upper troposphere (Lau and Kim 2006; Lau et al. 2006). This hypothesis, also known as the elevated heat pump (EHP) effect, suggests that the warmer layer enhances the upward motion and increases the moisture advection from the northern Indian Ocean towards northern India and Himalayan foothills. The surface cooling effect, also known as a solar dimming effect, reduces the convective instability over central India, transporting more moisture to northern India. The rising motion and the deep convection further warm the atmosphere with the release of latent heat resulting in a positive feedback process enhancing the early

tropical-meridional circulation. It results in the shift of deep convection northward and strengthens the early monsoon rainfall.

The large-scale vertical motion and strong convective updraft during the pre-monsoon and summer monsoonal season lift the absorbing aerosols to a higher altitude over the foothills of the Himalayas, resulting in elevated aerosol warming, analogous to the EHP hypothesis (Satheesh et al. 2008; Gautam et al. 2010). However, contrary to the EHP effect, Nigam and Bollasina (2010) indicate that the semi-direct effect dominates with increased aerosol loading and suppresses precipitation. The semi-direct effect refers to the warming of the atmosphere and reduction of the cloud fraction due to the absorbing aerosols, which further enhances the stability of the lower atmosphere and weakens the convective processes (Hansen et al. 1997; Cook and Highwood 2004).

In an intra-seasonal timescale, Manoj et al. (2012) shows that the radiative effect of absorbing aerosols during a period of suppressed monsoonal rainfall (inactive phase) induces a dynamical response by enhancing the inflow of large-scale moisture convergence, resulting in enhanced monsoonal rainfall (active phase). Furthermore, in a diurnal timescale, Fan et al. (2015) show that absorbing anthropogenic aerosols increases the atmospheric stability during the daytime over the polluted Sichuan basin in China. This limits the amount of moisture on the lower troposphere and allows more moisture to be transported towards the downwind mountainous region. Subsequently, the aerosol-radiation interaction enhances the conditional instability causing strong downwind convection. Further, with the support of orographic lifting, it results in heavy nighttime precipitation over the downwind mountainous region (Fan et al. 2015). Similarly, Choudhury et al., (2020) found that the extreme precipitation events over the Himalayan

foothills are associated with the aforementioned aerosol enhanced convective instability process.

1.2.3 Aerosol Cloud Interaction

The indirect effect of aerosols refers to the aerosols serving as cloud condensation nuclei (CCN) and ice nucleating particles (INP), also known as aerosol-cloud interaction (ACI; IPCC 2013) and influencing both the microphysical and radiative properties of the clouds (Rosenfeld et al. 2008; Fan et al. 2018). Aerosol particles play a pivotal role in the formation and evolution of clouds and can modulate the hydrological cycle (Li et al. 2019). The potentiality of the aerosols to serve as CCN at the typical supersaturations in the atmosphere depends on the composition, activation efficiency, and particle size distribution. For example, relatively large CCNs have a higher condensation rate and can reduce the supersaturation resulting in a reduced number of droplets (Rosenfeld et al. 2014; Li et al. 2019).

The first indirect effect, also known as the "Twomey effect", refers to the increase in CCN with a subsequent increase in aerosol concentration, which increases the number of smaller-sized cloud droplets for a constant liquid water content resulting in the enhanced reflectance and cooling effect (Twomey 1977). An extension to first indirect effect, the second indirect effect suggests that smaller droplets require a longer time to convert into the precipitating droplets, resulting in longer cloud lifetime and increased cloud cover, while suppressing the drizzle rain (Albrecht 1989; Rosenfeld 1999).

In a warm shallow cloud, higher concentration of CCN delay collision-coalescence process and slows down the conversion rates of numerous smaller-sized cloud droplets to

raindrops. The increase in aerosol concentration forms smaller cloud droplets, which are more likely to evaporate when mixing with the environment (Fan et al. 2016). However, some studies suggest that increased CCN can enhance the conversion from warmer shallow to convective clouds, amplifying the vertical development and cloud water content through microphysical and dynamical feedback (Chen et al. 2012; Saleeby et al. 2015). Furthermore, in warm cumulus clouds, the larger number of condensed droplets increases the cloud droplet surface area for vapor condensation, resulting in enhanced latent heat release, which in turn increases the vertical and horizontal extent of cloud and rainfall intensity (Koren et al. 2014).

In addition to CCN, aerosols can also serve as INP and modulate the mixed-phase and deep convective clouds (Fan et al. 2014; DeMott et al. 2015). The mixture of supercooled droplets (liquid droplets below freezing level) and ice particles forms the mixed-phase clouds. The lifetime of mixed-phase clouds depends on the balance between CCN and INP concentrations (Rosenfeld et al. 2014; Fan et al. 2016). A large number of smaller droplets, in the presence of higher anthropogenic aerosols acting as CCN, makes the riming process (accretion of supercooled water droplets on ice crystals) less efficient and reduces the snow precipitation rate (Borys et al. 2003). Fan et al. (2014) showed that the increased INP in a mixed-phase cloud enhances the riming and Wegener-Bergeron-Findeisen (WBF) process, which favors snow formation and growth and leads to enhanced precipitation. Since the saturation vapor pressure over ice is lower than over water, the WBF mechanism describes the growth of ice crystals at the expense of liquid water.

The reduced droplet effective radius in the presence of higher aerosol concentration suppresses the warm rain due to delayed collision-coalescence process, which allows smaller droplets to ascend to the higher altitude, resulting in a strengthening of an updraft and invigoration of the convection (Andreae et al. 2004; Koren et al. 2005; Rosenfeld et al. 2014). These smaller cloud droplets are carried above the freezing level, where the freezing of droplets releases additional latent heat energizing the convection and increasing the buoyancy of the clouds (Rosenfeld et al. 2008). Furthermore, the increased INP allows the depositional growth over ice crystal, releasing the latent heat and making the updraft further stronger, which results in the enhanced homogenous ice nucleation (below -38°C) and increases the anvil cloud coverage and precipitation (Fan et al. 2016). A considerable number of modeling and observational studies have shown the aerosol induced convective invigoration hypothesis, linking higher aerosol loadings with an increase in cloud cover and deepening of the convective cloud over the different parts of the globe (e.g., Niu and Li 2012; Li et al. 2011; Koren et al. 2010; Andreae et al. 2004; Sarangi et al. 2017).

In addition to different meteorological variables, the topographical structure also significantly impacts the cloud processes and precipitation distribution over the mountainous terrain (Borys et al. 2003; Fan et al. 2015; Choudhury et al. 2019; Henao et al. 2022). The orographic lifting further supports the development of clouds with an increased supply of CCN/INP particles resulting in enhanced mountainous precipitation (Ralph et al. 2015; Fan et al. 2017; Lau et al. 2017).

Dry (through gravitational setting) and wet deposition (through precipitation or in-cloud processing) are the key processes in removing atmospheric particles (Emerson et

al. 2020). In addition to the dry deposition (Yasunari et al. 2013), the monsoonal precipitation results in the increased wet deposition of the carbonaceous aerosols over the Himalayan snow surface (Ji et al. 2015). The deposition of the light-absorbing aerosols (dust and black carbon) over the Himalaya-Tibetan Plateau warms the snow surface, which reduces the surface albedo and accelerates the melting of the snowpack during pre and early monsoon season (Qian et al. 2015; Lau and Kim 2018). IPCC (2013) reports light-absorbing aerosols in snow and ice are the major contributor to the glacier retreat and global climate change.

The feedback effect of the increase in surface temperature with the melting of snowpack and warming of the troposphere due to radiation absorbance dynamically influences the monsoonal precipitation (Lau et al. 2017; Lau and Kim 2018). The climatology study by Ji et al., (2015) suggests the positive shortwave radiative forcing by the layer of carbonaceous aerosols during the monsoonal season warms the troposphere over the Himalayas. The tropospheric temperature fluctuation is critical for the change in freezing level height (FLH) over the Himalayas.

The increase in condensational latent heat release in the presence of higher CCN concentration in deep convective precipitating clouds (Tao and Li 2016) can also perturb the FLH. The increasing trend of the FLH can increase the warm cloud layer depth, which shifts snow to rainfall and potentially results in extreme precipitation (Prein and Heymsfield 2020), increasing the risk of extreme floods over the central Himalayas (Ragettli et al. 2016) and the western United States (Davenport et al. 2020). Also, the increase in liquid precipitation also shortens the snow cover season over the Himalayas and TP region (Pepin et al. 2015). Wang et al., (2014) showed that an increase in FLH by

10 m over the TP and higher latitude of Asia during summer results in a rise of equilibrium snow line altitude by 3.1 to 9.8 m, which contributes to the reduction of glacier mass balance by 7 mm to 38 mm. Furthermore, Bradley et al., (2009) attributed the rise in FLH over the tropics and the glaciated mountains of the Andes to the increase in sea surface temperature.

1.3 Data and Methodology

In this section, we provide the background and descriptions of the datasets and numerical modeling implemented.

1.3.1 Precipitation Data

This study uses Global Precipitation Measurement (GPM; active sensor) to examine the spatial patterns of precipitation. GPM is the successor of the Tropical Rainfall Measuring Mission (TRMM), launched in 2014 with scientifically advanced and well-calibrated instruments (Huffman et al. 2015a). The GPM operates in a non-sun synchronous orbit which estimates the precipitation between 60° S and 60° N latitudes covering the globe. The advanced sensitivity of dual-frequency precipitation radar (DPR) and GPM Microwave Imager (GMI) with an additional channel are capable of sensing the precipitation, including the light rain and falling snow even in severe weather (Huffman et al. 2015a).

The Integrated Multi-Satellite Retrievals for GPM (IMERG), a gridded precipitation estimation algorithm of GPM, provides the near-real-time and research (final run) products. The precipitation gauge analysis from the Global Precipitation

Climatology Center (GPCC) is used to calibrate the IMERG final product (Huffman et al. 2015b). The IMERG level-3 products (version 06) also include the TRMM-era data and provide precipitation data from June 2000 at 30 minutes temporal resolution and the finer 0.1° × 0.1° horizontal resolution.

Also, the precipitation data from the rain gauge stations over Nepal available from the Department of Hydrology and Meteorology Nepal is used to evaluate the simulated output. The DHM rain gauge stations provide daily accumulated precipitation data measured at 03 UTC (08:45 LST). In this study, we evaluated model performance using data from 90 rain gauge stations sparsely distributed around Nepal, with an altitude ranging from 60 to 2744 meters above sea level. Most of the rain gauge stations are in the valley floor and might not be able to detect the precipitation over the mountain top. Also, the manual recording of the gauge stations data and the under catch or losses due to wind speed/direction can add up the uncertainty in the precipitation data collection (Talchabhadel et al. 2017).

1.3.2 Aerosol optical depth data

Aerosol optical depth (AOD) is widely used as the proxy for aerosol loadings and CCN concentration (Andreae 2009). The cloud and aerosol properties datasets used in this study are obtained from the Moderate Resolution Imaging Spectroradiometer (MODIS) onboard of the Aqua and Terra satellites (Remer et al. 2005; Sayer et al. 2013). Both Terra and Aqua operates in a sun-synchronous orbit, crossing the equator around 10:30 and 13:30 local time, respectively. MODIS measures the light reflected from the earth in 36 spectral frequencies with a wide swath of 2330 km, almost covering the entire

globe in one day. The aerosol properties are retrieved from non-cloudy regions in the MODIS level-1 dataset to reduce the aerosol humidification effect. MODIS level-3 datasets are prepared from the level-2 products with cloud-screened aerosol retrieval and cloud retrievals (Platnick et al. 2003). The daily MODIS level 3 combined Dark Target and Deep Blue collection 6.1 AOD at 550 nm retrieval algorithm, with a horizontal resolution of 1° × 1°, are used in this study.

The hygroscopic growth of aerosol due to ambient RH influences the AOD measurement from satellites and ground networks, adding uncertainty in the aerosol-cloud-precipitation relationship (Boucher and Quaas 2013; Grandey et al. 2014). Compared to dry AOD, in a humid environment with relative humidity (RH) of 98%, AOD can elevate by 1.8 times (Haslett et al. 2019). However, the magnitude of change in AOD due to humidity depends on the aerosol properties. Also, the MODIS level-2 aerosol products attempt to reduce the humidification effect by removing the pixels if the cloud is detected within 1-km and avoiding 50% of the brightest pixels (Remer et al. 2013).

Moreover, a good correlation exists between the satellite retrieved MODIS AOD and ground-based AOD measurement from Aerosol Robotic Network (AERONET) (Remer et al. 2005; Gupta et al. 2018; Wei et al. 2019). The expected error of the AOD retrieved over land from MODIS is ± (0.05+15% of AERONET AOD) (Levy et al. 2013). The cloud and aerosol datasets from MODIS have been extensively used to study the aerosol-cloud-precipitation interaction in different parts of the globe (e.g., Koren et al. 2014; Patil et al. 2017; Ng et al. 2017).

1.3.3 Cloud-resolving simulation

The high-resolution numerical models that can explicitly resolve the convection and clouds evolution on a sub-grid scale without implementing the convective parameterization scheme are considered cloud-resolving or convection-permitting models (Kendon et al. 2021; hereafter "cloud resolving models"). The explicit microphysics options with cloud-resolving grid sizes (typically assumed as less than 3-4 km) allow interactive processes between aerosols and clouds. Activation of aerosol as a cloud droplet in a cloud-resolving scale depends on maximum supersaturation, which is a function of vertical velocity, vertical turbulent motions, and internally mixed aerosols. Also, to assess the indirect effect of aerosols or aerosol-cloud interaction in a convective system, simulations must be run in a cloud-resolving scale because cumulus parameterization approaches lack the aerosol-cloud interaction processes (Archer-Nicholls et al. 2016; Yang et al. 2011; https://ruc.noaa.gov/wrf/wrf-chem/wrf_tutorial_2018/AerosolInteractions.pdf). Prein et al. (2015) showed that the convection parameterization is linked to significant sources of uncertainty in larger-scale models and recommends cloud-resolving resolutions to add-value to simulations. Additionally, compared to coarse resolution models, cloud resolving models better represent the complex topography and coastal shapes, the contrasting land-use/land-cover, and inhomogeneous distribution of anthropogenic emission and precipitation (Wu et al. 2017).

1.3.4 Model description

In this study, the numerical simulations will be performed using WRF (Skamarock et al. 2008) coupled with Chemistry (WRF-Chem; Grell et al. 2005) model. WRF-Chem is an advanced regional model that simulates the emission, transport, and transformation of trace gases and aerosols along with the meteorological parameters. WRF-Chem consists of several chemistry components, including the emission inventories (anthropogenic, biogenic, dust, and biomass burning emissions), aerosol-chemistry mechanism, aqueous- and gas-phase mechanism, dry and wet deposition, and photolysis. The chemistry component is consistent with the meteorological component as they both use the same grid, timestep, transport scheme, and microphysical parameterization (Grell et al. 2005). The WRF-Chem can address the aerosol-chemistry and meteorological feedback, including radiation, cloud, and precipitation. It has been widely used to study the relationship between aerosol, cloud, precipitation, and regional climate (e.g., Jiang et al. 2013; Kedia et al. 2019; Wu et al. 2018).

In addition to the meteorological boundary condition data, the emission inventory and chemical boundary condition data are required to initialize the WRF-Chem. Meteorological initial conditions are provided using the WRF Pre-processing System (WPS), where it interpolates the meteorological information into the user-defined domain and model grids. The chemical boundary condition and externally prepared emission files provide the sources of chemical species into the model grids.

Several parameterization schemes are available in the WRF model to approximate the physical processes due to different limitations in the model. The WRF model includes the parameterization for microphysics of cloud and precipitation, cumulus convection, turbulence and diffusion, radiation, planetary boundary layer, and surface layer.

In this study, we implemented two one-way nested domains. The 9-km parent domain (referred as domain-1) covered the central and northern/eastern India, Bangladesh, Bhutan, and Tibetan Plateau. While the 3-km nested domain (referred as domain-2) includes the Central Himalayan region including entire Nepal (with Mount Everest), central IGP (major source of anthropogenic emissions), and the immediate Himalayan plateau region of Tibet. Refer to the chapter 3 and 4 (Figure 3.1 and Figure 4.1) for the domain design.

1.3.4.1 Radiation

The atmospheric radiation parameterization scheme accounts for atmospheric heating due to the radiative fluxes from both longwave and shortwave radiation processes (Skamarock et al. 2008). In this study, we will employ the Rapid Radiative Transfer Model for General Circulation Models (RRTMG; Iacono et al. 2008) for longwave and shortwave radiation schemes. The RRTMG radiation scheme is widely used in weather forecasting models. The longwave includes the absorption and emission from aerosols and clouds, while extinction from aerosols, clouds, and Rayleigh scattering is included in shortwave processes (Iacono et al. 2008).

1.3.4.2 Microphysics

The cloud microphysics parameterization accounts the physics of hydrometeors and explicitly resolves the water vapor, cloud, and precipitation processes. The microphysical schemes are generally divided into bulk and bin parameterization schemes. In the bulk schemes, the particle size distribution of hydrometeors is approximated using exponential/gamma distributions, whereas the bin scheme uses explicit microphysics

schemes to solve the particle size distributions (Khain et al. 2015). Also, the bin schemes solve the size distribution on a finite-difference mass grid represented by tens to hundreds of mass bins (Khain et al. 2015; Yin et al. 2017). Furthermore, the Köhler theory is used to calculate the critical radius in each bin where the supersaturation is computed at each grid and timestep (Khain et al. 2016). Therefore, the bin microphysical scheme better simulates the cloud microphysical and precipitation evolution. Though the bulk microphysics scheme has limitations and adds up the uncertainty in assessing the indirect effects of aerosols (Morrison and Grabowski 2007), it is computationally efficient (by an order of magnitude) compared to the bin scheme and is widely used in numerical models (Khain et al. 2015). Due to the limitation of the computational resources, a bulk microphysics scheme is used in this study.

We will use Morrison double moment parameterization scheme in this study. A double moment microphysics scheme includes prognostic equations for both number concentration and mixing ratios, which are essential for calculating the rate of microphysical process and evolution of cloud/precipitation (Skamarock et al. 2008). The Morrison-2 moment scheme predicts the number concentration and mass mixing ratios of vapor, cloud droplets, cloud ice, rain, snow, and graupel/hail (Morrison et al. 2009).

1.3.4.3 Cumulus Parameterization

Convective clouds are not resolved at grid-level as they occur on a scale smaller than the model grids. The cumulus parameterization scheme redistributes the moisture and temperature to resolve the vertical convective fluxes and determine the convection. For the high resolution domain (3 km nested domain), no cumulus parameterization is

used as the model explicitly resolves the convective eddies. The cumulus parameterization, however, is used for the domain size larger than 10km. The domain size between 5-10 km lies in the grey region. In this study, we used the Grell-3D Ensemble Scheme (Grell and Dévényi 2002) for the cumulus parameterization for the 9-km domain.

1.3.4.4 Planetary Boundary Layer (PBL)

The PBL schemes resolve the vertical sub-grid-scale fluxes and provide the tendencies of heat, momentum, and atmospheric constituents (e.g., moisture) due to eddy transports in the entire column of the atmosphere (Skamarock et al. 2008; Hu et al. 2010). The Land-surface and surface layers schemes provide the surface fluxes for the PBL scheme (Skamarock et al. 2008). In this study, we use the Yonsei University (YSU) PBL scheme (Hong et al. 2006). YSU is a first-order non-local scheme and has been broadly used in meteorological and chemistry simulations (e.g., Jiang et al. 2013; Wu et al. 2018).

1.3.4.5 Land-Surface

In addition to state variables and surface properties of land, the land-surface scheme uses atmospheric information, radiative forcing, and precipitation forcing from other physics schemes to compute heat and moisture fluxes over land and sea/ice points. The fluxes computed by the land-surface scheme are used as a lower boundary condition for the vertical transport to be performed in the PBL scheme (Skamarock et al. 2008). In this study, we used Community Land Model Version 4 (CLM4; Lawrence et al. 2011) and Unified NOAH (Tewari et al. 2004) land-surface scheme. The CLM4 land surface

has been successfully used in WRF-Chem in a mountainous region with higher snow surfaces (e.g., Sarangi et al. 2019; Wu et al. 2018).

1.3.4.6 Chemical and Aerosol mechanism

The CBM-Z (Carbon Bond Mechanism; Zaveri and Peters 1999) photochemical mechanism coupled with MOSAIC (Model for Simulating Aerosol Interactions and Chemistry; Zaveri et al. 2008) aerosol module is used in this study. The Fast-J photolysis scheme is used to compute the rates of photolytic reaction within the CBM-Z (Chapman et al. 2009). The CBM-Z includes the 67 chemical species and 167 reactions and treats the organic compound in a lumped structure approach depending on their internal bond types (Gery et al. 1989).

The MOSAIC aerosol module uses a sectional approach (either four or eight bins) to represent the aerosol size distribution. In this study, we implemented the MOSAIC-4 bin approach, where the aerosols are allotted to each bin depending on the dry particle diameters with bin size ranges between 0.039-0.156 μm, 0.156-0.625 μm, 0.625-2.5 μm, and 2.5-10 μm. The particles within a bin are assumed to have the same chemical composition and are internally mixed, whereas particles from different bins are mixed externally (Zaveri et al. 2008). Furthermore, Zhao et al., (2013) suggested that AOD are simulated reasonably well with a 4-bin approach (computationally cheaper) in comparison to 8-bin sectional approach. MOSAIC simulates all the major aerosol species that include sulfate, nitrate, ammonium, primary organic mass, black carbon, and liquid water (Zaveri et al. 2008).

The physical and chemical processes included in the MOSAIC aerosol module are nucleation, coagulation, condensation, water uptake by aerosols, aqueous-phase chemistry, and deposition. Both dry and wet deposition are included in the MOSAIC aerosol module. The change in the size of particles due to chemical reactions and/or physical processes such as coagulation will transfer the particles between the bins (Chapman et al. 2009). However, the transfer of the particle between the bins does not take place with hygroscopic growth or loss of water. Wet deposition of aerosol is simulated, including the cloud-borne aerosols and trace-gases dissolved and collected by rain, graupel, and snow following Chapman et al. (2009), and scavenging of aerosols below the cloud by interception and impaction method by Easter et al. (2004). Following the method by Binkowski and Shankar (1995), dry deposition is simulated, accounting for both diffusion and gravitational settlement. The current WRF-Chem model does not include the link between aerosol and ice clouds and the secondary organic aerosol formation (Chapman et al. 2009).

1.3.4.7 Boundary conditions

Any regional or limited-area model framework requires the initial and lateral boundary condition information. The initial condition provides the initial state of the environment at the start of the simulation, while the boundary condition provides the pre-defined values at the domain boundaries during the model integration. Since we are coupling the WRF with chemistry, we require initial and boundary conditions information for both meteorological and chemistry state fields. This study implemented

meteorological boundary conditions from hourly ERA5 reanalysis data at 31 km horizontal grid size and 38 vertical levels (Hersbach et al. 2020).

The initial and lateral boundary conditions for the chemical species were used from 6- hourly Community Atmosphere Model with Chemistry (CAM-Chem) simulated data, at 0.9° × 1.25° horizontal grid size and 56 vertical levels. CAM-chem is the chemistry component of the Community Earth System Model (CESM) used for simulations of global tropospheric and stratospheric composition (Emmons et al. 2020). The meteorological forcing in CAM-Chem is driven by Modern-Era Retrospective analysis for Research and Applications version 2 (MERRA2) reanalysis product. Furthermore, the anthropogenic, biogenic, and fire emissions are respectively used from the inventories specified for Coupled Model Intercomparison Project round 6 (CMIP6), Model of Emissions of Gases and Aerosols from Nature version 2.1 (MEGAN2.1), and Fire INventory from NCAR (FINN; https://doi.org/10.5065/NMP7-EP60).

1.3.4.8 Anthropogenic emission

Anthropogenic emissions are used from the Emission Database for Global Atmospheric Research - Hemispheric Transport of Air Pollutants (EDGAR-HTAP) dataset and EDGAR version 4.3.2 emissions inventory. EDGAR-HTAP version 2.2 compiles the widely-used regionally gridded inventories including US Environmental Protection Agency (EPA) and Environment Canada for North America, European Monitoring and Evaluation Programme - Netherlands Organization for Applied Scientific Research (EMEP-TNO) for Europe, Model Intercomparison Study for Asia (MICS-Asia

III) for China, India, and other Asian countries, and the EDGARv4.3 database for the rest of the world (Janssens-Maenhout et al. 2015).

EDGAR-HTAP version 2.2 emission inventory includes the black carbon (BC), organic matter (OM), particulate matter (PM2.5 and PM10), ammonia (NH3), sulfates (SO_2), oxides of nitrogen (NO_x), and carbon monoxide (CO), and non-methane volatile organic compound (NMVOC's), from each source for the year 2010. The major anthropogenic emission sources included are power generation, industry, residential, agriculture, ground and aviation transport, and shipping. The emissions inventory is provided as monthly fields at a horizontal resolution of 0.1° × 0.1° (Janssens-Maenhout et al. 2015).

1.3.4.9 Biogenic emission

The study of the air quality and the climate is critical to the emissions of reactive gases and aerosols from terrestrial ecosystems and vegetation. In this study, we use the biogenic emissions from the Model of Emissions of Gases and Aerosols from Nature (MEGAN), which quantifies the net isoprene emissions from the terrestrial biosphere (Guenther et al. 2006, 2012). The major source of isoprene emission is from the tropical broadleaf trees, which contribute around half the global emission flux, whereas widespread shrubs contribute the remaining flux to the atmosphere (Guenther et al. 2006). The MEGAN estimates the global emission of isoprene in a horizontal resolution of ~1 km^2, which is controlled and driven by the biological, physical, and chemical variables obtained from observational (satellite and ground) and modeled data. The

different driving variables use to estimate chemical species include temperature, solar radiation, leaf area index, and vegetation type (Guenther et al. 2006).

1.3.4.10 Biomass burning emission

The global emissions of particulate matter and trace gases are highly contributed by the biomass burning emissions from wildfires, agricultural or crop-residue burning, waste management burning, and controlled burns and contribute to the regional and global climate forcings. In this study, we implement Fire INventory from NCAR version 1.5 (FINNv1.5), which provides daily global estimates of open biomass burning from different sources in a 1 km grid size (Wiedinmyer et al. 2011).

1.3.4.11 Aerosol-Radiation-Cloud Interaction in WRF-Chem

The associated complex refractive indices of aerosols, which depend on the size and chemical composition, are used to compute the aerosol optical properties (Fast et al. 2006; Chapman et al. 2009). Refractive indices describe how light propagates through a medium and vary with the wavelength for some aerosol compositions. The volume averaging with Mie theory is used to compute the refractive indices of each bin (assumed to have the same composition of aerosols). It is then summed over all the bins with different size ranges to derive the composite aerosol optical properties (bulk extinction coefficient, scattering coefficient, single scattering albedo, and asymmetry factor). Providing these known values of aerosol optical properties, the RRTMG scheme (radiation transfer scheme used in this study) determines the radiative impact of aerosols (Iacono et al. 2008; Chapman et al. 2009; Archer-Nicholls et al. 2016).

The major aspect of aerosols in impacting the cloud evolution and microphysics is the concentration/composition of aerosols, aerosol size distribution, and the hygroscopicity nature of aerosols (Khain et al. 2016). Aerosols are activated as CCN when the maximum environmental supersaturation is greater than the critical supersaturation of an aerosol which is a function of aerosol size and composition. The maximum supersaturation is a function of vertical velocity, turbulent mixing, and properties of internally mixed aerosol for each bin (Abdul-Razzak and Ghan 2002). Larger and/or particles with higher hygroscopicity readily activate as condensation nuclei. The interstitial aerosols, with higher critical supersaturation than maximum environmental supersaturation, are not activated to cloud droplets (Chapman et al. 2009). The evaporation of the clouds within a grid resuspends the activated aerosols as the interstitial aerosols (Chapman et al. 2009). The assessment of aerosol-cloud interaction, only available with the cloud-resolving scale, requires the activation of aerosols which need to be coupled with a double moment microphysics scheme (includes number and mass concentrations) (Chapman et al. 2009; Yang et al. 2011; Archer-Nicholls et al. 2016).

In a convective cloud, the effect of aerosols on the microphysics of cloud is mainly determined by the number of aerosols activated as CCN, which impacts the size and number concentration of droplets (Chapman et al. 2009). The supersaturation over water for a lower number of cloud droplets is high, which allows the rapid conversion of a droplet to raindrops in a smaller vertical distance resulting in earlier onset of warm rain (Khain et al. 2016). The formation of larger drop also enhances the effectiveness of raindrop in collecting the newly formed smaller droplets and reduces the timing of

droplet that remains in the atmosphere. While for a larger number of smaller droplets in a polluted environment, the total particulate surface area is high, resulting in the reduced maximum supersaturation over water, resulting in a delayed growth of raindrops due to inefficient collision of smaller which increases the residential timing of droplets (Khain et al. 2016; Archer-Nicholls et al. 2016).

1.4 Objectives and overview of the dissertation

There is a need to extend our knowledge and advance the understanding of the impact of aerosol on clouds and precipitation over the Central Himalayan region during the monsoonal season. This dissertation aims to quantify and assess the impact of natural and anthropogenic aerosols on the cloud properties, precipitation distribution, and freezing level isotherm. The analysis is performed based on the remote sensing datasets and fully coupled regional online numerical model (WRF-Chem) and is presented and discussed in chapters 2, 3, and 4. The chapters of this dissertation aim to address the following research questions and objectives:

1. Chapter 2: How does aerosol impact the cloud properties and precipitation distribution during the polluted and clean days during the summer monsoon? What is the relationship between the aerosol loadings and freezing level height? The main objective of chapter 2 is to better understand the impact of aerosols on the precipitation and cloud properties over the immediate foothills and southern slope of the Himalayas on day-to-day and seasonal timescales. Also, we aim to investigate and quantify the degree to which the aerosol loadings modulate the variability of the observed freezing level height. In this chapter, we implement the

16 years (2002-2017) long satellite-based observational and reanalysis datasets. The peer-reviewed journal has been published in *Climate Dynamics* based on chapter 2 (Adhikari and Mejia, 2021).

2. Chapter 3: What is the role of remotely transported dust aerosols in modulating the precipitation over the Nepal Himalayas? The primary objective of chapter 3 is to evaluate and quantify the impact of long-range transported dust aerosols associated with the Thar desert dust storm event (12-15 June 2018) on the precipitation and convective processes focusing on the southern slopes of Nepal Himalayas. The cloud-resolving study in this chapter intends to provide new insights and advance our understanding of the influence of long-range transported dust aerosols in modulating the convection and precipitation processes over the mountainous region of the Central Himalayas. The peer-reviewed journal has been published in *Atmospheric Environment: X* based on chapter 3 (Adhikari and Mejia, 2022).
3. Chapter 4: How does aerosol influence the elevation-dependent precipitation over the Central Himalayas through aerosol-radiation and cloud-interaction pathways? The primary objective of chapter 4 is to assess and quantify the role of anthropogenic aerosol in modulating the elevation-dependent precipitation distribution and intensity over the complex topography of the central Himalayas. Also, we estimate and evaluate the role of increased anthropogenic aerosols in modulating the surface temperature. In this chapter, we implement WRF-Chem configured at a cloud-resolving scale, where the organization of the convection is explicitly resolved for the first monsoonal month of 2013 after the onset of the

monsoon in Nepal. The manuscript based on this chapter is in preparation to be submitted to *Atmospheric Chemistry and Physics.*

4. The summary of this dissertation with a conclusion and future recommendations are presented in chapter 5.

References

Abdul-Razzak H, Ghan SJ (2002) A parameterization of aerosol activation 3. Sectional representation. Journal of Geophysical Research: Atmospheres 107:AAC 1-1-AAC 1-6. https://doi.org/10.1029/2001JD000483

Adhikari P, Mejia JF (2021) Influence of aerosols on clouds, precipitation and freezing level height over the foothills of the Himalayas during the Indian summer monsoon. Clim Dyn 57:395–413. https://doi.org/10.1007/s00382-021-05710-2

Adhikari P, Mejia JF (2022) Impact of transported dust aerosols on precipitation over the Nepal Himalayas using convection-permitting WRF-Chem simulation. Atmospheric Environment: X 15:100179. https://doi.org/10.1016/j.aeaoa.2022.100179

Albrecht BA (1989) Aerosols, Cloud Microphysics, and Fractional Cloudiness. Science 245:1227–1230. https://doi.org/10.1126/science.245.4923.1227

Andreae MO (2009) Correlation between cloud condensation nuclei concentration and aerosol optical thickness in remote and polluted regions. Atmos Chem Phys 14. https://doi.org/10.5194/acp-9-543-2009

Andreae MO, Rosenfeld D, Artaxo P, et al (2004) Smoking rain clouds over the Amazon. Science 303:1337–1342. https://doi.org/10.1126/science.1092779

Archer-Nicholls S, Lowe D, Schultz DM, McFiggans G (2016) Aerosol–radiation–cloud interactions in a regional coupled model: the effects of convective parameterisation and resolution. Atmos Chem Phys 16:5573–5594. https://doi.org/10.5194/acp-16-5573-2016

Babu SS, Manoj MR, Moorthy KK, et al (2013) Trends in aerosol optical depth over Indian region: Potential causes and impact indicators. Journal of Geophysical Research: Atmospheres 118:11,794-11,806. https://doi.org/10.1002/2013JD020507

Bamzai AS, Marx L (2000) COLA AGCM simulation of the effect of anomalous spring snow over Eurasia on the Indian summer monsoon. Quarterly Journal of the Royal Meteorological Society 126:2575–2584. https://doi.org/10.1002/qj.49712656811

Binkowski FS, Shankar U (1995) The Regional Particulate Matter Model: 1. Model description and preliminary results. Journal of Geophysical Research: Atmospheres 100:26191–26209. https://doi.org/10.1029/95JD02093

Bollasina MA, Ming Y, Ramaswamy V (2011) Anthropogenic Aerosols and the Weakening of the South Asian Summer Monsoon. Science 334:502–505. https://doi.org/10.1126/science.1204994

Borys RD, Lowenthal DH, Cohn SA, Brown WOJ (2003) Mountaintop and radar measurements of anthropogenic aerosol effects on snow growth and snowfall rate. Geophysical Research Letters 30:. https://doi.org/10.1029/2002GL016855

Boucher O, Quaas J (2013) Water vapour affects both rain and aerosol optical depth. Nature Geoscience 6:4–5. https://doi.org/10.1038/ngeo1692

Bradley RS, Keimig FT, Diaz HF, Hardy DR (2009) Recent changes in freezing level heights in the Tropics with implications for the deglacierization of high mountain regions. Geophysical Research Letters 36:. https://doi.org/10.1029/2009GL037712

Chapman EG, Jr WIG, Easter RC, et al (2009) Coupling aerosol-cloud-radiative processes in the WRF-Chem model: Investigating the radiative impact of elevated point sources. Atmos Chem Phys 20

Chen Y-C, Christensen MW, Xue L, et al (2012) Occurrence of lower cloud albedo in ship tracks. Atmospheric Chemistry and Physics 12:8223–8235. https://doi.org/10.5194/acp-12-8223-2012

Choobari OA, Zawar-Reza P, Sturman A (2014) The global distribution of mineral dust and its impacts on the climate system: A review. Atmospheric Research 138:152–165. https://doi.org/10.1016/j.atmosres.2013.11.007

Choudhury G, Tyagi B, Singh J, et al (2019) Aerosol-orography-precipitation – A critical assessment. Atmospheric Environment 214:116831. https://doi.org/10.1016/j.atmosenv.2019.116831

Choudhury G, Tyagi B, Vissa NK, et al (2020) Aerosol-enhanced high precipitation events near the Himalayan foothills. Atmospheric Chemistry and Physics 20:15389–15399. https://doi.org/10.5194/acp-20-15389-2020

Chow FK, Schär C, Ban N, et al (2019) Crossing Multiple Gray Zones in the Transition from Mesoscale to Microscale Simulation over Complex Terrain. Atmosphere 10:274. https://doi.org/10.3390/atmos10050274

Cook J, Highwood EJ (2004) Climate response to tropospheric absorbing aerosols in an intermediate general-circulation model. Quarterly Journal of the Royal Meteorological Society 130:175–191. https://doi.org/10.1256/qj.03.64

Davenport FV, Herrera-Estrada JE, Burke M, Diffenbaugh NS (2020) Flood Size Increases Nonlinearly Across the Western United States in Response to Lower Snow-Precipitation Ratios. Water Resources Research 56:e2019WR025571. https://doi.org/10.1029/2019WR025571

DeMott PJ, Prenni AJ, McMeeking GR, et al (2015) Integrating laboratory and field data to quantify the immersion freezing ice nucleation activity of mineral dust particles. Atmospheric Chemistry and Physics 15:393–409. https://doi.org/10.5194/acp-15-393-2015

Dey S, Di Girolamo L (2011) A decade of change in aerosol properties over the Indian subcontinent. Geophysical Research Letters 38:. https://doi.org/10.1029/2011GL048153

Dhital S, Kaplan ML, Orza J a. G, Fiedler S (2020) Atmospheric Dynamics of a Saharan Dust Outbreak Over Mindelo, Cape Verde Islands, Preceded by Rossby Wave Breaking: Multiscale Observational Analyses and Simulations. Journal of Geophysical Research: Atmospheres 125:e2020JD032975. https://doi.org/10.1029/2020JD032975

Dhital S, Kaplan ML, Orza JAG, Fiedler S (2021) Poleward transport of African dust to the Iberian Peninsula organized by a barrier jet and hydraulic jumps: Observations and high-resolution simulation analyses. Atmospheric Environment 261:118574. https://doi.org/10.1016/j.atmosenv.2021.118574

Dimri AP, Palazzi E, Daloz AS (2022) Elevation dependent precipitation and temperature changes over Indian Himalayan region. Clim Dyn. https://doi.org/10.1007/s00382-021-06113-z

Ding Y (2007) The Variability of the Asian Summer Monsoon. Journal of the Meteorological Society of Japan 85B:21–54. https://doi.org/10.2151/jmsj.85B.21

Easter RC, Ghan SJ, Zhang Y, et al (2004) MIRAGE: Model description and evaluation of aerosols and trace gases. Journal of Geophysical Research: Atmospheres 109:. https://doi.org/10.1029/2004JD004571

Emerson EW, Hodshire AL, DeBolt HM, et al (2020) Revisiting particle dry deposition and its role in radiative effect estimates. Proceedings of the National Academy of Sciences 117:26076–26082. https://doi.org/10.1073/pnas.2014761117

Emmons LK, Schwantes RH, Orlando JJ, et al (2020) The Chemistry Mechanism in the Community Earth System Model Version 2 (CESM2). Journal of Advances in Modeling Earth Systems 12:e2019MS001882. https://doi.org/10.1029/2019MS001882

Fan J, Leung LR, DeMott PJ, et al (2014) Aerosol impacts on California winter clouds and precipitation during CalWater 2011: local pollution versus long-range

transported dust. Atmospheric Chemistry and Physics 14:81–101. https://doi.org/10.5194/acp-14-81-2014

Fan J, Leung LR, Rosenfeld D, DeMott PJ (2017) Effects of cloud condensation nuclei and ice nucleating particles on precipitation processes and supercooled liquid in mixed-phase orographic clouds. Atmospheric Chemistry and Physics 17:1017–1035. https://doi.org/10.5194/acp-17-1017-2017

Fan J, Rosenfeld D, Yang Y, et al (2015) Substantial contribution of anthropogenic air pollution to catastrophic floods in Southwest China. Geophysical Research Letters 42:6066–6075. https://doi.org/10.1002/2015GL064479

Fan J, Rosenfeld D, Zhang Y, et al (2018) Substantial convection and precipitation enhancements by ultrafine aerosol particles. Science 359:411–418. https://doi.org/10.1126/science.aan8461

Fan J, Wang Y, Rosenfeld D, Liu X (2016) Review of Aerosol–Cloud Interactions: Mechanisms, Significance, and Challenges. J Atmos Sci 73:4221–4252. https://doi.org/10.1175/JAS-D-16-0037.1

Fast JD, Gustafson WI, Easter RC, et al (2006) Evolution of ozone, particulates, and aerosol direct radiative forcing in the vicinity of Houston using a fully coupled meteorology-chemistry-aerosol model. Journal of Geophysical Research: Atmospheres 111:. https://doi.org/10.1029/2005JD006721

Fu Y, Pan X, Xian T, et al (2018) Precipitation characteristics over the steep slope of the Himalayas in rainy season observed by TRMM PR and VIRS. Clim Dyn 51:1971–1989. https://doi.org/10.1007/s00382-017-3992-3

Ganguly D, Rasch PJ, Wang H, Yoon J-H (2012) Climate response of the South Asian monsoon system to anthropogenic aerosols. Journal of Geophysical Research: Atmospheres 117:. https://doi.org/10.1029/2012JD017508

Gautam P, Maughan JB, Ilavsky J, Sorensen CM (2020) Light scattering study of highly absorptive, non-fractal, hematite aggregates. Journal of Quantitative Spectroscopy and Radiative Transfer 246:106919. https://doi.org/10.1016/j.jqsrt.2020.106919

Gautam P, Sorensen CM (2020) A light-scattering study of highly refractive, irregularly shaped MoS2 particles. Journal of Quantitative Spectroscopy and Radiative Transfer 242:106757. https://doi.org/10.1016/j.jqsrt.2019.106757

Gautam R, Hsu NC, Lau K-M (2010) Premonsoon aerosol characterization and radiative effects over the Indo-Gangetic Plains: Implications for regional climate warming. Journal of Geophysical Research: Atmospheres 115:. https://doi.org/10.1029/2010JD013819

Gery MW, Whitten GZ, Killus JP, Dodge MC (1989) A photochemical kinetics mechanism for urban and regional scale computer modeling. Journal of Geophysical Research: Atmospheres 94:12925–12956. https://doi.org/10.1029/JD094iD10p12925

Ghimire S, Choudhary A, Dimri AP (2018) Assessment of the performance of CORDEX-South Asia experiments for monsoonal precipitation over the Himalayan region during present climate: part I. Clim Dyn 50:2311–2334. https://doi.org/10.1007/s00382-015-2747-2

Grandey BS, Gururaj A, Stier P, Wagner TM (2014) Rainfall-aerosol relationships explained by wet scavenging and humidity. Geophysical Research Letters 41:5678–5684. https://doi.org/10.1002/2014GL060958

Grell GA, Dévényi D (2002) A generalized approach to parameterizing convection combining ensemble and data assimilation techniques. Geophysical Research Letters 29:38-1-38–4. https://doi.org/10.1029/2002GL015311

Grell GA, Peckham SE, Schmitz R, et al (2005) Fully coupled “online” chemistry within the WRF model. Atmospheric Environment 39:6957–6975. https://doi.org/10.1016/j.atmosenv.2005.04.027

Guenther A, Karl T, Harley P, et al (2006) Estimates of global terrestrial isoprene emissions using MEGAN (Model of Emissions of Gases and Aerosols from Nature). Atmospheric Chemistry and Physics 6:3181–3210. https://doi.org/10.5194/acp-6-3181-2006

Guenther AB, Jiang X, Heald CL, et al (2012) The Model of Emissions of Gases and Aerosols from Nature version 2.1 (MEGAN2.1): an extended and updated framework for modeling biogenic emissions. Geoscientific Model Development 5:1471–1492. https://doi.org/10.5194/gmd-5-1471-2012

Gupta P, Remer LA, Levy RC, Mattoo S (2018) Validation of MODIS 3 km land aerosol optical depth from NASA’s EOS Terra and Aqua missions. Atmospheric Measurement Techniques; Katlenburg-Lindau 11:3145–3159. http://dx.doi.org/10.5194/amt-11-3145-2018

Hansen J, Sato M, Ruedy R (1997) Radiative forcing and climate response. Journal of Geophysical Research: Atmospheres 102:6831–6864. https://doi.org/10.1029/96JD03436

Haslett SL, Taylor JW, Deetz K, et al (2019) The radiative impact of out-of-cloud aerosol hygroscopic growth during the summer monsoon in southern West Africa. Atmospheric Chemistry and Physics 19:1505–1520. https://doi.org/10.5194/acp-19-1505-2019

Hersbach H, Bell B, Berrisford P, et al (2020) The ERA5 global reanalysis. Quarterly Journal of the Royal Meteorological Society 146:1999–2049. https://doi.org/10.1002/qj.3803

Hong S-Y, Noh Y, Dudhia J (2006) A New Vertical Diffusion Package with an Explicit Treatment of Entrainment Processes. Mon Wea Rev 134:2318–2341. https://doi.org/10.1175/MWR3199.1

Hu X-M, Nielsen-Gammon JW, Zhang F (2010) Evaluation of Three Planetary Boundary Layer Schemes in the WRF Model. Journal of Applied Meteorology and Climatology 49:1831–1844. https://doi.org/10.1175/2010JAMC2432.1

Huffman GJ, Bolvin DT, Braithwaite D, et al (2015a) Algorithm Theoretical Basis Document (ATBD) Version 4.5: NASA Global Precipitation Measurement (GPM) Integrated Multi-satellitE Retrievals for GPM (IMERG). NASA: Greenbelt, MD, USA

Huffman GJ, Bolvin DT, Nelkin EJ (2015b) Integrated Multi-satellitE Retrievals for GPM (IMERG) Technical Documentation. NASA/GSFC Code 612, 47 pp. College Park: University of Maryland

Iacono MJ, Delamere JS, Mlawer EJ, et al (2008) Radiative forcing by long-lived greenhouse gases: Calculations with the AER radiative transfer models. Journal of Geophysical Research: Atmospheres 113:. https://doi.org/10.1029/2008JD009944

Immerzeel WW, van Beek LPH, Bierkens MFP (2010) Climate Change Will Affect the Asian Water Towers. Science 328:1382–1385. https://doi.org/10.1126/science.1183188

IPCC (2013) Climate change 2013: The Physical Science Basis: Working Group I Contribution to the Fifth Assessment Report of the Intergovernmental Panel on Climate. Cambridge University Press

Janssens-Maenhout G, Crippa M, Guizzardi D, et al (2015) HTAP_v2.2: a mosaic of regional and global emission grid maps for 2008 and 2010 to study hemispheric transport of air pollution. Atmospheric Chemistry and Physics 15:11411–11432. https://doi.org/10.5194/acp-15-11411-2015

Ji Z, Kang S, Cong Z, et al (2015) Simulation of carbonaceous aerosols over the Third Pole and adjacent regions: distribution, transportation, deposition, and climatic effects. Clim Dyn 45:2831–2846. https://doi.org/10.1007/s00382-015-2509-1

Jiang X, Barth MC, Wiedinmyer C, Massie ST (2013) Influence of anthropogenic aerosols on the Asian monsoon: A case study using the WRF-Chem model. Atmos Chem Phys Discuss 13:383–21

Kang S, Zhang Q, Qian Y, et al (2019) Linking atmospheric pollution to cryospheric change in the Third Pole region: current progress and future prospects. Natl Sci Rev 6:796–809. https://doi.org/10.1093/nsr/nwz031

Kedia S, Vellore RK, Islam S, Kaginalkar A (2019) A study of Himalayan extreme rainfall events using WRF-Chem. Meteorol Atmos Phys 131:1133–1143. https://doi.org/10.1007/s00703-018-0626-1

Kendon EJ, Prein AF, Senior CA, Stirling A (2021) Challenges and outlook for convection-permitting climate modelling. Philosophical Transactions of the Royal Society A: Mathematical, Physical and Engineering Sciences 379:20190547. https://doi.org/10.1098/rsta.2019.0547

Khain A, Lynn B, Shpund J (2016) High resolution WRF simulations of Hurricane Irene: Sensitivity to aerosols and choice of microphysical schemes. Atmospheric Research 167:129–145. https://doi.org/10.1016/j.atmosres.2015.07.014

Khain AP, Beheng KD, Heymsfield A, et al (2015) Representation of microphysical processes in cloud-resolving models: Spectral (bin) microphysics versus bulk parameterization. Reviews of Geophysics 53:247–322. https://doi.org/10.1002/2014RG000468

Koren I, Dagan G, Altaratz O (2014) From aerosol-limited to invigoration of warm convective clouds. Science 344:1143–1146. https://doi.org/10.1126/science.1252595

Koren I, Feingold G, Remer LA (2010) The invigoration of deep convective clouds over the Atlantic: aerosol effect, meteorology or retrieval artifact? https://doi.org/10.5194/acp-10-8855-2010

Koren I, Kaufman YJ, Rosenfeld D, et al (2005) Aerosol invigoration and restructuring of Atlantic convective clouds. Geophysical Research Letters 32:. https://doi.org/10.1029/2005GL023187

Kumar M, Parmar KS, Kumar DB, et al (2018) Long-term aerosol climatology over Indo-Gangetic Plain: Trend, prediction and potential source fields. Atmospheric Environment 180:37–50. https://doi.org/10.1016/j.atmosenv.2018.02.027

Kumar S, Kumar S, Kaskaoutis DG, et al (2015) Meteorological, atmospheric and climatic perturbations during major dust storms over Indo-Gangetic Basin. Aeolian Research 17:15–31. https://doi.org/10.1016/j.aeolia.2015.01.006

Lau K-M, Kim K-M (2006) Observational relationships between aerosol and Asian monsoon rainfall, and circulation. Geophysical Research Letters 33:. https://doi.org/10.1029/2006GL027546

Lau KM, Kim MK, Kim KM (2006) Asian summer monsoon anomalies induced by aerosol direct forcing: the role of the Tibetan Plateau. Clim Dyn 26:855–864. https://doi.org/10.1007/s00382-006-0114-z

Lau WKM, Kim K-M (2018) Impact of Snow Darkening by Deposition of Light-Absorbing Aerosols on Snow Cover in the Himalayas–Tibetan Plateau and Influence on the Asian Summer Monsoon: A Possible Mechanism for the Blanford Hypothesis. Atmosphere 9:438. https://doi.org/10.3390/atmos9110438

Lau WKM, Kim K-M, Shi J-J, et al (2017) Impacts of aerosol–monsoon interaction on rainfall and circulation over Northern India and the Himalaya Foothills. Clim Dyn 49:1945–1960. https://doi.org/10.1007/s00382-016-3430-y

Lawrence DM, Oleson KW, Flanner MG, et al (2011) Parameterization improvements and functional and structural advances in Version 4 of the Community Land Model. Journal of Advances in Modeling Earth Systems 3:. https://doi.org/10.1029/2011MS00045

Levy RC, Mattoo S, Munchak LA, et al (2013) The Collection 6 MODIS aerosol products over land and ocean. Atmos Meas Tech 6:2989–3034. https://doi.org/10.5194/amt-6-2989-2013

Li Z, Lau WK-M, Ramanathan V, et al (2016) Aerosol and monsoon climate interactions over Asia. Reviews of Geophysics 54:866–929. https://doi.org/10.1002/2015RG000500

Li Z, Niu F, Fan J, et al (2011) Long-term impacts of aerosols on the vertical development of clouds and precipitation. Nature Geoscience 4:888–894. https://doi.org/10.1038/ngeo1313

Li Z, Wang Y, Guo J, et al (2019) East Asian Study of Tropospheric Aerosols and their Impact on Regional Clouds, Precipitation, and Climate (EAST-AIRCPC). Journal of Geophysical Research: Atmospheres 124:13026–13054. https://doi.org/10.1029/2019JD030758

Manoj MG, Devara PCS, Joseph S, Sahai AK (2012) Aerosol indirect effect during the aberrant Indian Summer Monsoon breaks of 2009. Atmospheric Environment 60:153–163. https://doi.org/10.1016/j.atmosenv.2012.06.007

Mishra V (2015) Climatic uncertainty in Himalayan water towers. Journal of Geophysical Research: Atmospheres 120:2689–2705. https://doi.org/10.1002/2014JD022650

Moorthy KK, Babu SS, Manoj MR, Satheesh SK (2013) Buildup of aerosols over the Indian Region. Geophysical Research Letters 40:1011–1014. https://doi.org/10.1002/grl.50165

Morrison H, Grabowski WW (2007) Comparison of Bulk and Bin Warm-Rain Microphysics Models Using a Kinematic Framework. Journal of the Atmospheric Sciences 64:2839–2861. https://doi.org/10.1175/JAS3980

Morrison H, Thompson G, Tatarskii V (2009) Impact of Cloud Microphysics on the Development of Trailing Stratiform Precipitation in a Simulated Squall Line: Comparison of One- and Two-Moment Schemes. Mon Wea Rev 137:991–1007. https://doi.org/10.1175/2008MWR2556.1

Ng DHL, Li R, Raghavan SV, Liong S-Y (2017) Investigating the relationship between Aerosol Optical Depth and Precipitation over Southeast Asia with Relative Humidity as an influencing factor. Scientific Reports 7:1–13. https://doi.org/10.1038/s41598-017-10858-1

Nigam S, Bollasina M (2010) "Elevated heat pump" hypothesis for the aerosol-monsoon hydroclimate link: "Grounded" in observations? Journal of Geophysical Research: Atmospheres 115:. https://doi.org/10.1029/2009JD013800

Niu F, Li Z (2012) Systematic variations of cloud top temperature and precipitation rate with aerosols over the global tropics. Atmos Chem Phys 12:8491–8498. https://doi.org/10.5194/acp-12-8491-2012

Orza JAG, Dhital S, Fiedler S, Kaplan ML (2020) Large scale upper-level precursors for dust storm formation over North Africa and poleward transport to the Iberian Peninsula. Part I: An observational analysis. Atmospheric Environment 237:117688. https://doi.org/10.1016/j.atmosenv.2020.117688

Palazzi E, Filippi L, von Hardenberg J (2017) Insights into elevation-dependent warming in the Tibetan Plateau-Himalayas from CMIP5 model simulations. Clim Dyn 48:3991–4008. https://doi.org/10.1007/s00382-016-3316-z

Patil N, Dave P, Venkataraman C (2017) Contrasting influences of aerosols on cloud properties during deficient and abundant monsoon years. Scientific Reports 7:1–9. https://doi.org/10.1038/srep44996

Pepin N, Bradley RS, Diaz HF, et al (2015) Elevation-dependent warming in mountain regions of the world. Nature Climate Change 5:424–430. https://doi.org/10.1038/nclimate2563

Platnick S, King MD, Ackerman SA, et al (2003) The MODIS cloud products: algorithms and examples from Terra. IEEE Transactions on Geoscience and Remote Sensing 41:459–473. https://doi.org/10.1109/TGRS.2002.808301

Prasad AK, Singh RP (2007) Changes in aerosol parameters during major dust storm events (2001–2005) over the Indo-Gangetic Plains using AERONET and MODIS data. Journal of Geophysical Research: Atmospheres 112:. https://doi.org/10.1029/2006JD007778

Prein AF, Heymsfield AJ (2020) Increased melting level height impacts surface precipitation phase and intensity. Nature Climate Change 10:771–776. https://doi.org/10.1038/s41558-020-0825-x

Prein AF, Langhans W, Fosser G, et al (2015) A review on regional convection-permitting climate modeling: Demonstrations, prospects, and challenges. Reviews of Geophysics 53:323–361. https://doi.org/10.1002/2014RG000475

Prell WL, Kutzbach JE (1992) Sensitivity of the Indian monsoon to forcing parameters and implications for its evolution. Nature 360:647–652. https://doi.org/10.1038/360647a0

Qian Y, Yasunari TJ, Doherty SJ, et al (2015) Light-absorbing particles in snow and ice: Measurement and modeling of climatic and hydrological impact. Adv Atmos Sci 32:64–91. https://doi.org/10.1007/s00376-014-0010-0

Ragettli S, Immerzeel WW, Pellicciotti F (2016) Contrasting climate change impact on river flows from high-altitude catchments in the Himalayan and Andes Mountains. PNAS 113:9222–9227. https://doi.org/10.1073/pnas.1606526113

Ralph FM, Prather KA, Cayan D, et al (2015) CalWater Field Studies Designed to Quantify the Roles of Atmospheric Rivers and Aerosols in Modulating U.S. West Coast Precipitation in a Changing Climate. Bull Amer Meteor Soc 97:1209–1228. https://doi.org/10.1175/BAMS-D-14-00043.1

Ramanathan V, Carmichael G (2008) Global and regional climate changes due to black carbon. Nature Geosci 1:221–227. https://doi.org/10.1038/ngeo156

Ramanathan V, Chung C, Kim D, et al (2005) Atmospheric brown clouds: Impacts on South Asian climate and hydrological cycle. Proceedings of the National Academy of Sciences 102:5326–5333. https://doi.org/10.1073/pnas.0500656102

Ramanathan V, Ramana MV (2005) Persistent, Widespread, and Strongly Absorbing Haze Over the Himalayan Foothills and the Indo-Gangetic Plains. Pure appl geophys 162:1609–1626. https://doi.org/10.1007/s00024-005-2685-8

Remer LA, Kaufman YJ, Tanré D, et al (2005) The MODIS Aerosol Algorithm, Products, and Validation. J Atmos Sci 62:947–973. https://doi.org/10.1175/JAS3385.1

Remer LA, Mattoo S, Levy RC, Munchak LA (2013) MODIS 3 km aerosol product: algorithm and global perspective. Atmospheric Measurement Techniques 6:1829–1844. https://doi.org/10.5194/amt-6-1829-2013

Rosenfeld D (1999) TRMM observed first direct evidence of smoke from forest fires inhibiting rainfall. Geophysical Research Letters 26:3105–3108. https://doi.org/10.1029/1999GL006066

Rosenfeld D, Andreae MO, Asmi A, et al (2014) Global observations of aerosol-cloud-precipitation-climate interactions. Reviews of Geophysics 52:750–808. https://doi.org/10.1002/2013RG000441

Rosenfeld D, Lohmann U, Raga GB, et al (2008) Flood or Drought: How Do Aerosols Affect Precipitation? Science 321:1309–1313. https://doi.org/10.1126/science.1160606

Saleeby SM, Herbener SR, Heever SC van den, L'Ecuyer T (2015) Impacts of Cloud Droplet–Nucleating Aerosols on Shallow Tropical Convection. Journal of the Atmospheric Sciences 72:1369–1385. https://doi.org/10.1175/JAS-D-14-0153.1

Sarangi C, Qian Y, Rittger K, et al (2019) Impact of light-absorbing particles on snow albedo darkening and associated radiative forcing over high-mountain Asia: high-resolution WRF-Chem modeling and new satellite observations. Atmospheric Chemistry and Physics 19:7105–7128. https://doi.org/10.5194/acp-19-7105-2019

Sarangi C, Tripathi SN, Kanawade VP, et al (2017) Investigation of the aerosol–cloud–rainfall association over the Indian summer monsoon region. Atmos Chem Phys 17:5185–5204. https://doi.org/10.5194/acp-17-5185-2017

Sarkar S, Chauhan A, Kumar R, Singh RP (2019) Impact of Deadly Dust Storms (May 2018) on Air Quality, Meteorological, and Atmospheric Parameters Over the Northern Parts of India. GeoHealth 3:67–80. https://doi.org/10.1029/2018GH000170

Satheesh SK, Moorthy KK, Babu SS, et al (2008) Climate implications of large warming by elevated aerosol over India. Geophysical Research Letters 35:. https://doi.org/10.1029/2008GL034944

Satheesh SK, Ramanathan V (2000) Large differences in tropical aerosol forcing at the top of the atmosphere and Earth's surface. Nature 405:60–63. https://doi.org/10.1038/35011039

Sayer AM, Hsu NC, Bettenhausen C, Jeong M-J (2013) Validation and uncertainty estimates for MODIS Collection 6 “Deep Blue” aerosol data. Journal of Geophysical Research: Atmospheres 118:7864–7872. https://doi.org/10.1002/jgrd.50600

Seinfeld JH, Bretherton C, Carslaw KS, et al (2016) Improving our fundamental understanding of the role of aerosol−cloud interactions in the climate system. PNAS 113:5781–5790. https://doi.org/10.1073/pnas.1514043113

Shrestha AB, P. Wake C, Dibb JE, et al (2000) Seasonal variations in aerosol concentrations and compositions in the Nepal Himalaya. Atmospheric Environment 34:3349–3363. https://doi.org/10.1016/S1352-2310(99)00366-0

Shrestha RK, Connolly PJ, Gallagher MW (2017) Sensitivity of Precipitation to Aerosol and Temperature Perturbation over the Foothills of the Nepal Himalayas. Proceedings 1:144. https://doi.org/10.3390/ecas2017-04146

Shukla KK, Attada R, Khan AW, Kumar P (2021) Evaluation of extreme dust storm over the northwest Indo-Gangetic plain using WRF-Chem model. Nat Hazards. https://doi.org/10.1007/s11069-021-05017-9

Sijikumar S, Aneesh S, Rajeev K (2016) Multi-year model simulations of mineral dust distribution and transport over the Indian subcontinent during summer monsoon seasons. Meteorol Atmos Phys 128:453–464. https://doi.org/10.1007/s00703-015-0422-0

Singh P, Sarawade P, Adhikary B (2020) Transport of black carbon from planetary boundary layer to free troposphere during the summer monsoon over South Asia. Atmospheric Research 235:104761. https://doi.org/10.1016/j.atmosres.2019.104761

Skamarock WC, Klemp JB, Dudhia J, et al (2008) G.: A description of the Advanced Research WRF version 3. NCAR Tech Note NCAR/TN-475+STR

Srivastava AK, Pant P, Hegde P, et al (2011) The influence of a south Asian dust storm on aerosol radiative forcing at a high-altitude station in central Himalayas. International Journal of Remote Sensing 32:7827–7845. https://doi.org/10.1080/01431161.2010.531781

Talchabhadel R, Karki R, Parajuli B (2017) Intercomparison of precipitation measured between automatic and manual precipitation gauge in Nepal. Measurement 106:264–273. https://doi.org/10.1016/j.measurement.2016.06.047

Tao W-K, Li X (2016) The relationship between latent heating, vertical velocity, and precipitation processes: The impact of aerosols on precipitation in organized deep convective systems. Journal of Geophysical Research: Atmospheres 121:6299–6320. https://doi.org/10.1002/2015JD024267

Tao W-K, Matsui T (2015) NUMERICAL MODELS | Cloud-System Resolving Modeling and Aerosols. In: North GR, Pyle J, Zhang F (eds) Encyclopedia of Atmospheric Sciences (Second Edition). Academic Press, Oxford, pp 222–231

Tewari M, Chen F, Wang W, et al (2004) Implementation and verification of the unified NOAH land surface model in the WRF model. In: 20th conference on weather analysis and forecasting/16th conference on numerical weather prediction. pp 2165–2170

Twomey S (1977) The Influence of Pollution on the Shortwave Albedo of Clouds. J Atmos Sci 34:1149–1152. https://doi.org/10.1175/1520-0469(1977)034<1149:TIOPOT>2.0.CO;2

Uno I, Eguchi K, Yumimoto K, et al (2009) Asian dust transported one full circuit around the globe. Nature Geoscience 2:557–560. https://doi.org/10.1038/ngeo583

Vuille M, Francou B, Wagnon P, et al (2008) Climate change and tropical Andean glaciers: Past, present and future. Earth-Science Reviews 89:79–96. https://doi.org/10.1016/j.earscirev.2008.04.002

Wang B, Ding Q (2008) Global monsoon: Dominant mode of annual variation in the tropics. Dynamics of Atmospheres and Oceans 44:165–183. https://doi.org/10.1016/j.dynatmoce.2007.05.002

Wang S, Zhang M, Pepin NC, et al (2014) Recent changes in freezing level heights in High Asia and their impact on glacier changes. Journal of Geophysical Research: Atmospheres 119:1753–1765. https://doi.org/10.1002/2013JD020490

Wang Z, Zhang H, Jing X, Wei X (2013) Effect of non-spherical dust aerosol on its direct radiative forcing. Atmospheric Research 120–121:112–126. https://doi.org/10.1016/j.atmosres.2012.08.006

Webster PJ, Magaña VO, Palmer TN, et al (1998) Monsoons: Processes, predictability, and the prospects for prediction. Journal of Geophysical Research: Oceans 103:14451–14510. https://doi.org/10.1029/97JC02719@10.1002/(ISSN)2169-9291.TOGA1

Wei J, Peng Y, Guo J, Sun L (2019) Performance of MODIS Collection 6.1 Level 3 aerosol products in spatial-temporal variations over land. Atmospheric Environment 206:30–44. https://doi.org/10.1016/j.atmosenv.2019.03.001

Wiedinmyer C, Akagi SK, Yokelson RJ, et al (2011) The Fire INventory from NCAR (FINN): a high resolution global model to estimate the emissions from open burning. Geoscientific Model Development 4:625–641. https://doi.org/10.5194/gmd-4-625-2011

Wu G, Guan Y, Liu Y, et al (2012) Air–sea interaction and formation of the Asian summer monsoon onset vortex over the Bay of Bengal. Clim Dyn 38:261–279. https://doi.org/10.1007/s00382-010-0978-9

Wu L, Gu Y (ORCID:0000000234120794), Jiang JH, et al (2018) Impacts of aerosols on seasonal precipitation and snowpack in California based on convection-permitting

WRF-Chem simulations. Atmospheric Chemistry and Physics (Online) 18:. https://doi.org/10.5194/acp-18-5529-2018

Wu L, Su H, Kalashnikova OV, et al (2017) WRF-Chem simulation of aerosol seasonal variability in the San Joaquin Valley. Atmos Chem Phys 17:7291–7309. https://doi.org/10.5194/acp-17-7291-2017

Yang Q, W. I. Gustafson Jr., Fast JD, et al (2011) Assessing regional scale predictions of aerosols, marine stratocumulus, and their interactions during VOCALS-REx using WRF-Chem. Atmos Chem Phys 11:11951–11975. https://doi.org/10.5194/acp-11-11951-2011

Yasunari TJ, Tan Q, Lau K-M, et al (2013) Estimated range of black carbon dry deposition and the related snow albedo reduction over Himalayan glaciers during dry pre-monsoon periods. Atmospheric Environment 78:259–267. https://doi.org/10.1016/j.atmosenv.2012.03.031

Yin L, Ping F, Mao J (2017) A comparative study between bulk and bin microphysical schemes of a simulated squall line in East China. Atmospheric Science Letters 18:195–206. https://doi.org/10.1002/asl.742

Zaveri RA, Easter RC, Fast JD, Peters LK (2008) Model for Simulating Aerosol Interactions and Chemistry (MOSAIC). Journal of Geophysical Research: Atmospheres 113:. https://doi.org/10.1029/2007JD008782

Zaveri RA, Peters LK (1999) A new lumped structure photochemical mechanism for large-scale applications. Journal of Geophysical Research: Atmospheres 104:30387–30415. https://doi.org/10.1029/1999JD900876

Zhang H, Zhou C, Wang Z, et al (2015) The influence of different black carbon and sulfate mixing methods on their optical and radiative properties. Journal of Quantitative Spectroscopy and Radiative Transfer 161:105–116. https://doi.org/10.1016/j.jqsrt.2015.04.002

Zhao C, Chen S, Leung LR, et al (2013) Uncertainty in modeling dust mass balance and radiative forcing from size parameterization. Atmospheric Chemistry and Physics 13:10733–10753. https://doi.org/10.5194/acp-13-10733-2013

Chapter 2: Influence of aerosols on clouds, precipitation and freezing level height over the foothills of the Himalayas during the Indian summer monsoon

This chapter of dissertation is based in full on the previously published article on Climate Dynamics. I have permission from my co-authors and publishers to use this work in dissertation. 'Reproduced with permission from Springer Nature'

Adhikari, P., Mejia, J.F. Influence of aerosols on clouds, precipitation and freezing level height over the foothills of the Himalayas during the Indian summer monsoon. *Clim Dyn* **57,** 395–413 (2021). https://doi.org/10.1007/s00382-021-05710-2

2.1 Introduction

The South Asian summer monsoon occurs typically from June to September (JJAS) (Webster et al. 1998) and is the primary source of water supply required for human consumption, rainfed agriculture, and hydroelectric power generation for more than a billion people residing in this region. Rapid industrialization, urbanization, and other human activities contribute a substantial amount of anthropogenic aerosols over the Indian subcontinent with the Indo-Gangetic plain (IGP) region being the hotspot (Babu et al. 2013; Kumar et al. 2018). Over central-east and northern India, observation suggests that summer monsoonal rainfall has decreased by 10-20% since 1900 (Roxy et al. 2015). A reduction of precipitation after 1950 has been primarily attributed to anthropogenic aerosol emissions (Bollasina et al. 2011).

Numerous studies have been performed to assess the impact of aerosol loadings on the South Asian monsoon (e.g., Ramanathan et al. 2005; Lau et al. 2006; Guo et al. 2016; Patil et al. 2017; Dave et al. 2017; Singh et al. 2019). Aerosols play an essential

role in modulating the hydrological cycle through direct, indirect, and semi-direct effects (Rosenfeld et al. 2014; Fan et al. 2016). Directly, aerosol scatter and absorb the incoming solar radiation limiting the amount of radiation reaching the surface. The radiative effect of increased aerosols is associated with the reduced surface heating and decrease in convective instability, which in turn diminishes the summer monsoon (Ramanathan et al. 2005). Also, a reduction of monsoonal rainfall with higher loadings of anthropogenic aerosol impacts the hydrological cycle by increasing the drought frequency over the South Asian monsoon region (Ramanathan et al. 2005). Indirectly, aerosols act both as cloud condensation nuclei (CCN) and ice nucleating particles (INPs) and impact the microphysical and radiative properties of the clouds, leading to the changes in precipitation regime (Rosenfeld et al. 2008; Fan et al. 2018). For constant liquid water in a warm cloud, increased CCN increases the number of smaller droplets and suppresses precipitation (Twomey 1977; Rosenfeld 1999). In a convective system, the increase in cloud life-time due to suppressed warm rain allows more cloud water to be lifted and invigorates the convection forming a suitable condition for heavy precipitation (Andreae et al. 2004; Rosenfeld et al. 2008; Fan et al. 2013).

Various observational (Patil et al. 2017; Sarangi et al. 2017; Dave et al. 2017) and modeling studies (Vinoj et al. 2014; Lau et al. 2017; Singh et al. 2019) indicate that both natural and anthropogenic aerosols from local and remote sources affect monsoonal rainfall on daily to seasonal timescales. Over the monsoon region of India, aerosol loading positively correlates with cloud droplet effective radius and cloud invigoration during abundant monsoon years, while a negative relationship is observed during the deficient rainfall season, thus suppressing cloud development (Patil et al. 2017). Sarangi

et al. (2017) revealed that though aerosols delay the collision-coalescence process, they invigorate cloud development, being positively correlated with the cloud fraction (CF) and negatively correlated with cloud top pressure (CTP) and cloud top temperature (CTT), which in turn, increases monsoonal surface rainfall. Local aerosols within the South Asian region play a dominant role in suppressing precipitation and increasing the number of dry days during the monsoonal season, while remote aerosols increase the frequency of rainfall events over the northwestern part of the Indian subcontinent (Bollasina et al. 2014; Singh et al. 2019). Guo et al. (2016) suggested that higher concentrations of sulfur dioxide and black carbon aerosols due to local emissions over the IGP sector influence the rainfall over the IGP and foothills of the Himalayas, but the impact of distant aerosols are more substantial over the entire South Asian region.

The low-level convergence of warm moist air results in a substantial amount of rainfall over the foothills of the Himalayas, where most of the precipitation occurs through higher-altitude ice-phase dominated clouds (Fu et al. 2018). Along with the southwesterly monsoonal flow, aerosols are incorporated and transported from the IGP across the Himalayas to the Tibetan Plateau (Ji et al. 2015). The accumulation of dust (from remote deserts) and black carbon (from IGP) aerosols during the pre-monsoon season on the southern slope of the Himalayas absorbs shortwave radiation, leading to the northward shift of deep convection and strengthening the monsoonal rainfall, a hypothesis also known as elevated heat pump (Lau and Kim 2006; Lau et al. 2006). However, Nigam and Bollasina (2010) contradict the elevated heat pump hypothesis, suggesting instead that the increase in aerosol loading suppresses the precipitation due to the semi-direct effect of aerosols.

The accumulated aerosols over the southern slope of the Himalayas from the IGP and southern India impact the hydroclimate of the Himalayan region (Kang et al. 2019). The variability of freezing level height (FLH) impacts hydrological conditions in the high mountains region (Vuille et al. 2008) and plays an essential role in changing the state of precipitation from solid to liquid (Xiao et al. 2016). Using the Weather Research and Forecasting (WRF) model, Xiao et al. (2016) found that during the polluted environment, when the FLH is lowered over the mountain slope, orographic precipitation increases along with growth of ice crystals due to enhanced riming process. The variations in summer FLH is critical as it modulates snow cover and glacier mass accumulations over the high mountains of Asia, including the Himalayas (Wang et al. 2014). An increasing trend of 0 °C isotherm observed over the entire tropics (Diaz et al. 2003; Bradley et al. 2009), and eastern China (Zhang and Guo 2011) has been attributed to change in sea surface temperature and is linked to the decline of snow cover in the high mountain region.

Wang et al. (2014) suggests an increase in summer FLH by 10 m over high Asia results in a rise of equilibrium snow line altitude by 3.1 to 9.8 m, which contributes to the reduction of glacier mass balance by 7 mm to 38 mm. The increasing trend of melting level since 1979 over the global land region can also increase the warm cloud layer depth, which shifts snow to rainfall and potentially resulting in extreme precipitation (Prein and Heymsfield 2020). The shift from snow to rain has potential consequences on streamflow and increases the flood risk in the central Himalayas (Ragettli et al. 2016); a similar shift and impact has been found over the western United States (Davenport et al. 2020). The increase in liquid precipitation also shortens the snow cover season over the Himalayas

and Tibetan Plateau (Pepin et al. 2015). Despite the importance of FLH on Himalayan hydrology, a detailed observational study exploring the effects of aerosols on the free atmosphere 0 °C isotherm over the Himalayan region has not been investigated, to the best of our knowledge.

Numerous studies have been conducted to establish the relationship between local and remote aerosols on the South Asian monsoon over India, but the southern slope and adjacent foothills of the Himalayas have received much less attention. In this study, in addition to recent reanalysis dataset, we use the long-term (2002-2017) records of satellite-based observation to better understand the impacts of aerosols on the precipitation and cloud properties over the immediate foothills and southern slope of the Himalayas on day-to-day and seasonal timescales. The degree to which aerosol loadings modulate the variability of the observed freezing isotherm is also investigated and quantified. Section 2 describes the dataset implemented and the methods designed to characterize dirty/clean days and to calculate composite precipitation, cloud properties, and freezing level height. Section 3 examines the results and related uncertainties and offers an extended discussion on the mechanistic processes involved. Finally, Section 4 presents a summary of key findings and conclusions.

2.2 Data and Methods

2.2.1 Dataset

The area of study, indicated by a solid (magenta colored) boundary in **Fig. 2.1**, covers the territory with a topographic height ranging from ~50 m in the south to above 6,000 m in

the north. The defined region includes the steep southern slope and adjacent foothills of the Himalayas (hereafter called SSFH). The entire study region experiences the pronounced South Asian summer monsoon from June to September (**Fig. 2.4 a**). The precipitation product from the Global Precipitation Measurement [GPM; Huffman et al. 2015a; https://pmm.nasa.gov/data-access/downloads/gpm] is used in this study. The GPM, which replaced the Tropical Rainfall Measuring Mission (TRMM), was launched in 2014 and continuously provides gridded precipitation estimates between 60° S and 60° N latitudes. The Integrated Multi-Satellite Retrievals for GPM (IMERG), a precipitation estimation algorithm of GPM, level-3 products (version 06) also includes the TRMM-era data and provides a record of precipitation from June 2000 at the finer spatial resolution of 0.1° × 0.1° and temporal resolution of 30 minutes. Though the satellite estimation of orographic precipitation has uncertainties, GPM-IMERG performed better than other satellite precipitation products over India (Prakash et al. 2018) and correlated with the gridded rain gauge data over Nepal (Sunilkumar et al. 2019) during the summer monsoon season. The IMERG final product is calibrated with precipitation gauge analysis from the Global Precipitation Climatology Center [GPCC; (Huffman et al. 2015b)]. In this study, IMERG (Research/Final Run) version 06 daily Precipitation Level 3 data with a spatial resolution of 0.1° × 0.1° is used.

In this study, the level 3 data from Moderate Resolution Imaging Spectroradiometer (MODIS) onboard Aqua (MYD08_D3) and Terra (MOD08_D3) satellite are used for atmospheric aerosol optical depth (AOD), cloud macro-properties (CTP, CTT, CF), ice-phase cloud effective radius (CERI), cloud Liquid Water Path (LWP), and cloud Ice Water Path (IWP) (Remer et al. 2005; Sayer et al. 2013). The Terra

and Aqua satellites cross the equator at 1030 and 1330 local time, respectively, in sun-synchronous orbits. The combined Dark Target and Deep Blue collection 6.1 AOD retrieval algorithm, with a spatial resolution of 1° × 1°, is used in this study. The aerosol properties are retrieved from non-cloudy regions in the MODIS level-1 dataset. The MODIS level-2 aerosol retrieval is prepared, filtering out the pixels if the cloud is detected within 1-km and avoiding 50% of the brightest pixels to reduce the aerosol humidification effect (Remer et al. 2013). The cloud-screened aerosol retrieval and cloud retrievals are used from level 2 products to construct the MODIS level-3 datasets (Platnick et al. 2003). The MODIS level 3 AOD data have been extensively used to study the interaction of aerosols with clouds and precipitation in a different part of the world (e.g., Koren et al. 2012; Patil et al. 2017; Ng et al. 2017).

The MODIS AOD correlates extensively with the ground-based Aerosol Robotic Network (AERONET) observations (Remer et al. 2005; Gupta et al. 2018; Wei et al. 2019). According to Levy et al. (2013), the expected error of the MODIS AOD retrieval over land is ±(0.05+15% of AERONET AOD). The average between Aqua and Terra satellite products is computed to obtain the daily value AOD and cloud properties for 2003-2017. Only the Terra product is used for 2002, as the product from Aqua became available only after July of that year.

The meteorological variables [relative humidity (RH), upward velocity (ω), temperature, geopotential, and surface air temperature] used in this study are retrieved from ERA5, accessible through https://cds.climate.copernicus.eu. ERA5, a successor of ERA-Interim, is the fifth-generation and most recent reanalysis product of the European Center for Medium-range Weather Forecast (ECMWF). ERA5 is based on the Integrated

Forecasting System (IFS cycle 41r2) of ECMWF and uses an advanced 4D-var data assimilation schemes (Hersbach and Dee 2016). ERA5 provides an hourly global reanalysis product from 1979 at a spatial resolution of 31km with 137 vertical levels from the surface to 0.01hPa, which are improved in temporal and spatial resolution compared to ERA-Interim. Mahto and Mishra (2019) suggest that the ERA5 reanalysis product performs better than other reanalysis in assessing the hydrological variables during the monsoon season (JJAS) over India.

2.2.2 Methodology

2.2.2.1 Identification of dirty and clean days

During the JJAS of 2002 to 2017 for each day, we define the MODIS AOD index as the spatial average of AOD, which is used as a proxy for aerosol loadings and CCN concentration (Andreae 2009), over the SSFH that consists of 28 pixels of 1° × 1° grid size. In this analysis, only the pixels with AODs < 1 are included to reduce the probability of cloud contamination and aerosol humidification effect during satellite retrieval (Sarangi et al. 2017). On average 3.8% of the pixels are excluded from the analysis (AOD > 1). Furthermore, to increase confidence in the spatially averaged MODIS AOD index, we compared it with AOD from three different ground based AERONET (version 3 level 2.0) stations located in the SSFH. AERONET stations were selected based on data availability during the monsoon season. AERONET AOD averages between ± 30 minutes of MODIS overpass time were used for the effective comparison. As MODIS and AERONET AOD are retrieved at a different wavelength,

following the procedure described by Sayer et al. (2013), AERONET AOD is interpolated to 550 nm using the definition of Ångström exponent to match up with the wavelength of MODIS AOD. The Pearson correlation coefficient between the AERONET-based AOD and spatially averaged MODIS-based AOD index over SSFH is shown in Table 1. Though only a few data points are available for comparison, the spatially averaged MODIS AOD index correlates well (0.47-0.59) at a 95% significance level with a ground based AOD estimate from sparsely distributed AERONET stations within the SSFH (**Fig. 2.1**).

Table 2.1: The Pearson correlation coefficient between the MODIS AOD index and AERONET AOD during JJAS. The number of days indicates the total days in JJAS with AOD retrieval from both AERONET and MODIS which are used for comparison. The location of AERONET sites is shown in Fig 2.1b.

AERONET Station	Altitude (meters)	AERONET Data Availability	Number of Days	MODIS vs. AERONET AOD Pearson Correlation Coefficient
Pantnagar, India	241	2008-2009	99	0.58
Pokhara, Nepal	800	2010-2017	301	0.47
Kathmandu-Bode, Nepal	1297	2013-2014	52	0.59

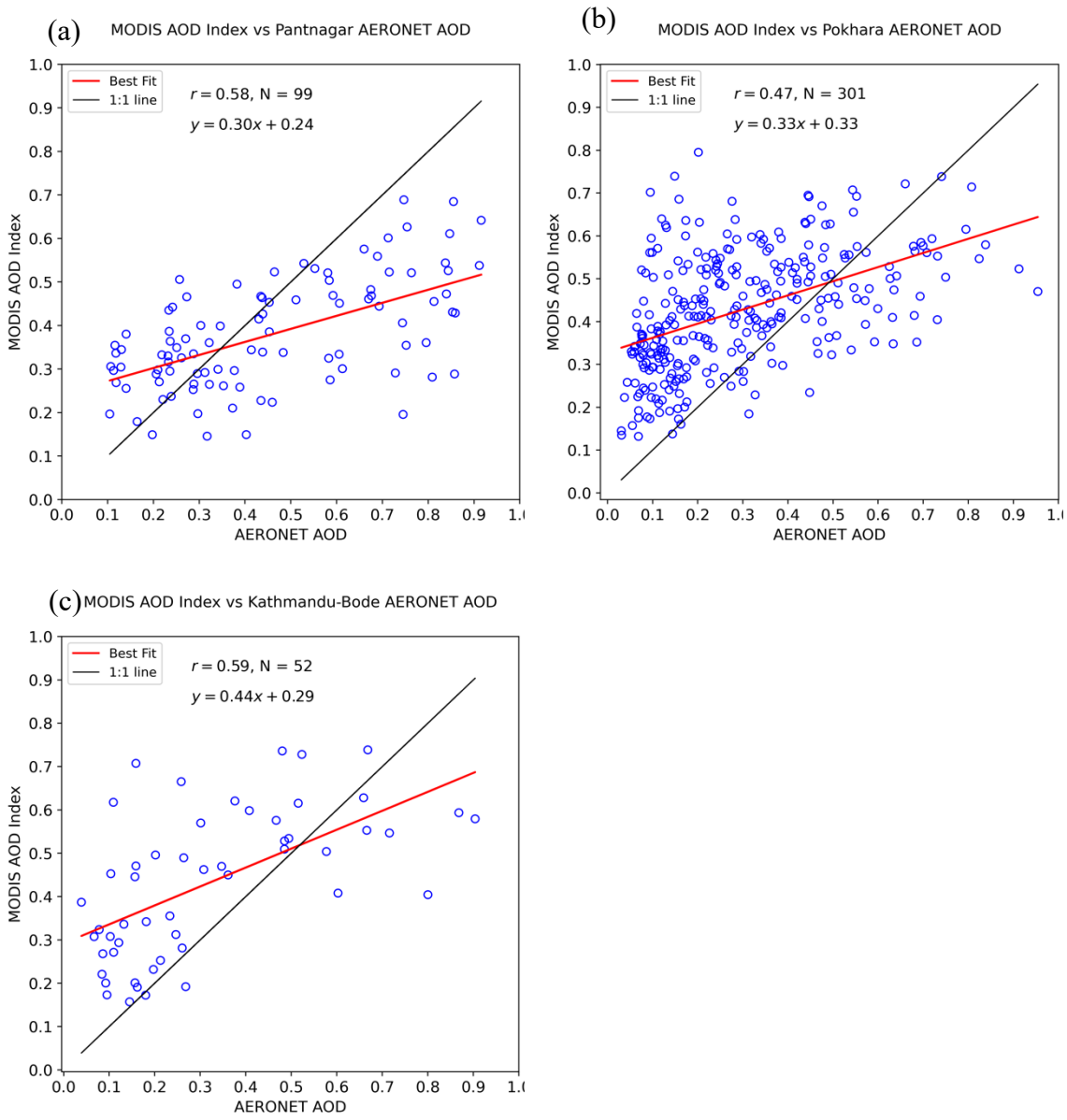

Figure 2.1: Scatter plot of statistically significant MODIS AOD index vs AERONET AOD stations at a Pantnagar, India, b Pokhara, Nepal, and c Kathmandu-Bode, Nepal.

We defined dirty (polluted) and clean (relatively pristine environment) days from the spatially averaged MODIS AOD. Dirty or clean days are those with an AOD index that falls above or below one standard deviation from the climatology (2002-2017, JJAS) mean. Out of 1952 days within the study period (JJAS of 2002 to 2017), 280 days are

classified as dirty and 275 as clean days. The mean absolute difference between the dirty and clean days AOD over SSFH is 0.39 and mean dirty days AOD is 3.5 times higher than clean days AOD. A spatial pattern of precipitation, cloud properties, and FLH were composited for the dirty and clean days to analyze the effect of aerosol loading in the atmosphere. In addition, for the available AERONET AOD retrieval days, we compared the daily (averaged for the entire day) and instantaneous (±30 minutes of Aqua/Terra overpass) AERONET AOD with the clean and dirty days AOD from individual Aqua/Terra and averages of Aqua and Terra satellite. Despite the biases, instantaneous and daily averages of AEROENT AOD from all three stations followed a similar pattern of dirty and clean days from MODIS products. Hence, the MODIS-based selection of dirty and clean days is a good indicator of daily aerosol loadings over SSFH.

2.2.2.2 Isolating the meteorological effect

The separation of the weather forcing from the aerosol-cloud-precipitation relationship is limited and has a higher uncertainty. Previous studies have implemented different methods to separate the meteorological variables and weather phenomena from aerosol-cloud interaction (e.g., Koren et al. 2010; Kourtidis et al. 2015). Here, we attempted to isolate the meteorological effect following Koren et al. (2010), with some slight modifications. To isolate the weather forcing, we used two fundamental meteorological variables, relative humidity (RH) and vertical velocity (ω), which are essential for the development of clouds and precipitation. The RH and ω at 20 pressure levels between 1000 to 300 hPa were obtained by computing the spatial average over the SSFH. We used

the mean of an hourly RH and ω data between ~0930 and ~1430 local time from ERA5 reanalysis to cover the ±1 hour of Terra and Aqua overpasses.

The correlation between the spatially averaged meteorological variables (RH and ω and cloud properties (CTP and CF) was computed at each pressure level. The maximum correlation was observed for the RH at 500 hPa and ω at 600 hPa, which were used for isolating the meteorological effect in this study. In addition, the correlation was consistent while dividing the SSFH into two subregions based on topographic height (less/greater than 2000m). Daily CTP, CF, and precipitation data at each pixel were composited by dirty and clean days and further divided into three different sub-regimes based on high, intermediate, and low values of RH and ω. The precipitation data were re-gridded to 1°× 1° pixel using bilinear interpolation to match the AOD and cloud properties data, to separate the meteorological effect. Discriminating of the data based on a similar RH also reduces the biases caused by meteorological variance and the aerosol humidification effect (Altaratz et al. 2013). Also, the correlation between the RH at 500hPa and MODIS level-3 AOD during JJAS (2002 to 2017) over SSFH is negative (**Fig. 2.2**), indicating moist condition is associated with reduced AOD over SSFH, which is consistent with Sarangi et al. (2017) over central India and Koren et al. (2010) over the tropical Atlantic Ocean.

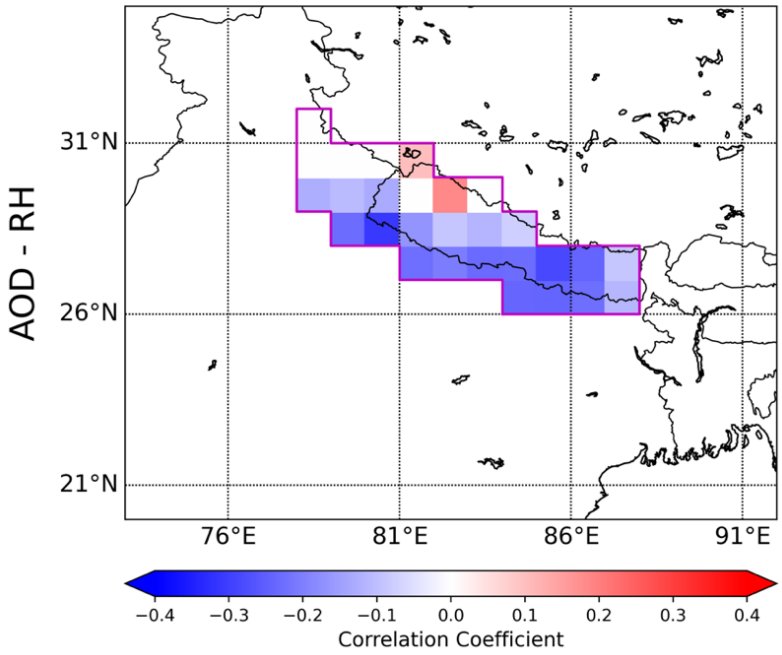

Figure 2.2: The pixel-level correlation coefficient between the RH at 500hPa and MODIS level-3 AOD during JJAS of 2002 to 2017. Only statistically significant values exceeding the 90% confidence level are shown.

Furthermore, to isolate the effect of weather forcing in the analysis, we used the bootstrapping technique for each sub-regime of dirty and clean days based on different values of RH and w. The bootstrapping technique, with replacement after each resampling, was used to generate the numerous samples empirically without assuming any specific distribution, from the original data to evaluate the sampling distribution and draw the statistical inference (Davison and Hinkley 1997). Here, for all three sub-regimes of RH and w, random sampling with replacement was performed to create 5000 individual samples. Each sample size is the same as the size of sub-regimes (see Table 3.1). The random sampling of each sub-regime was performed 5000 times. The mean values of each of the samples of size N are computed and are used to estimate the sampling distribution.

Table 2.2: The sample size of each of the sub-regimes used to isolate the meteorological effect.

	Dirty days	**Clean days**
RH < 50%	1805	1766
50% < RH < 70%	1713	1856
RH>70%	4299	4036
ω > 0	2516	2570
-0.1 < ω < 0	1926	1931
ω < -0.1	3375	3157

2.2.2.3 Freezing Level Height

The free atmosphere FLH was derived using the meteorological data from the ERA5 reanalysis datasets. Wang et al. (2014) suggest that the reanalysis product can be used to estimate the FLH, as it is in good correlation with the FLH from radiosondes over high Asia. Following the method implemented by Bradley et al. (2009), FLH was computed by interpolating the geopotential height between adjacent pressure levels for the 0^{o} C isotherm. The FLH computed and analyzed in this study includes both cloudy and non-cloudy region over the study domain.

2.2.2.4 Identification of dry and wet years

In addition to daily timescales, aerosols also influence monsoonal rainfall from intra-seasonal to inter-annual timescales (Bollasina et al. 2011; Vinoj et al. 2014; Patil et al. 2017). We further attempted to study the relationship of precipitation with cloud properties and aerosol loading on a seasonal scale during wet and dry years over the SSFH. This study did not attempt to relate precipitation anomalies to any large-scale teleconnection pattern (Mishra et al. 2012). To identify the dry and wet monsoonal (JJAS) years, in addition to GPM IMERG, precipitation products from TRMM (available through https://pmm.nasa.gov/data-access/downloads/trmm), the Climate Hazards Group Infrared Precipitation with Station [CHIRPS; Funk et al. (2015)], and the University of Delaware [UD; Willmott and Matsuura (2001)] were used. The daily precipitation data from TRMM and CHIRPS are available at 0.25° × 0.25° spatial resolution, while the UD product provides monthly total precipitation at 0.5° × 0.5° resolution.

The mean seasonal (JJAS) precipitation of all four products was obtained at each gridded cell from 2002 to 2017. The difference between each year's JJAS mean and 16-year seasonal mean precipitation was divided by the 16-year seasonal standard deviation to obtain the normalized seasonal anomaly. The spatially averaged anomaly was compared with the threshold of ± 0.1 (Patil et al. 2017) to identify the wet and dry years. If the positive (negative) anomaly of all the products existed and the IMERG seasonal anomaly was greater (smaller) than +(-) 0.1, the particular year was considered as a wet (dry) year. This technique provided robustness in the selection of dry and wet years and revealed that the results were independent of the product of choice (**Fig. 2.3**). The identified wet years were 2007, 2008, 2010, 2011, and 2013, whereas the dry years were

2002, 2005, 2006, 2009, 2014, 2015, and 2017. For both seasonal and daily scale analyses, we used the IMERG precipitation product to study the aerosol-cloud-precipitation relationship over SSFH.

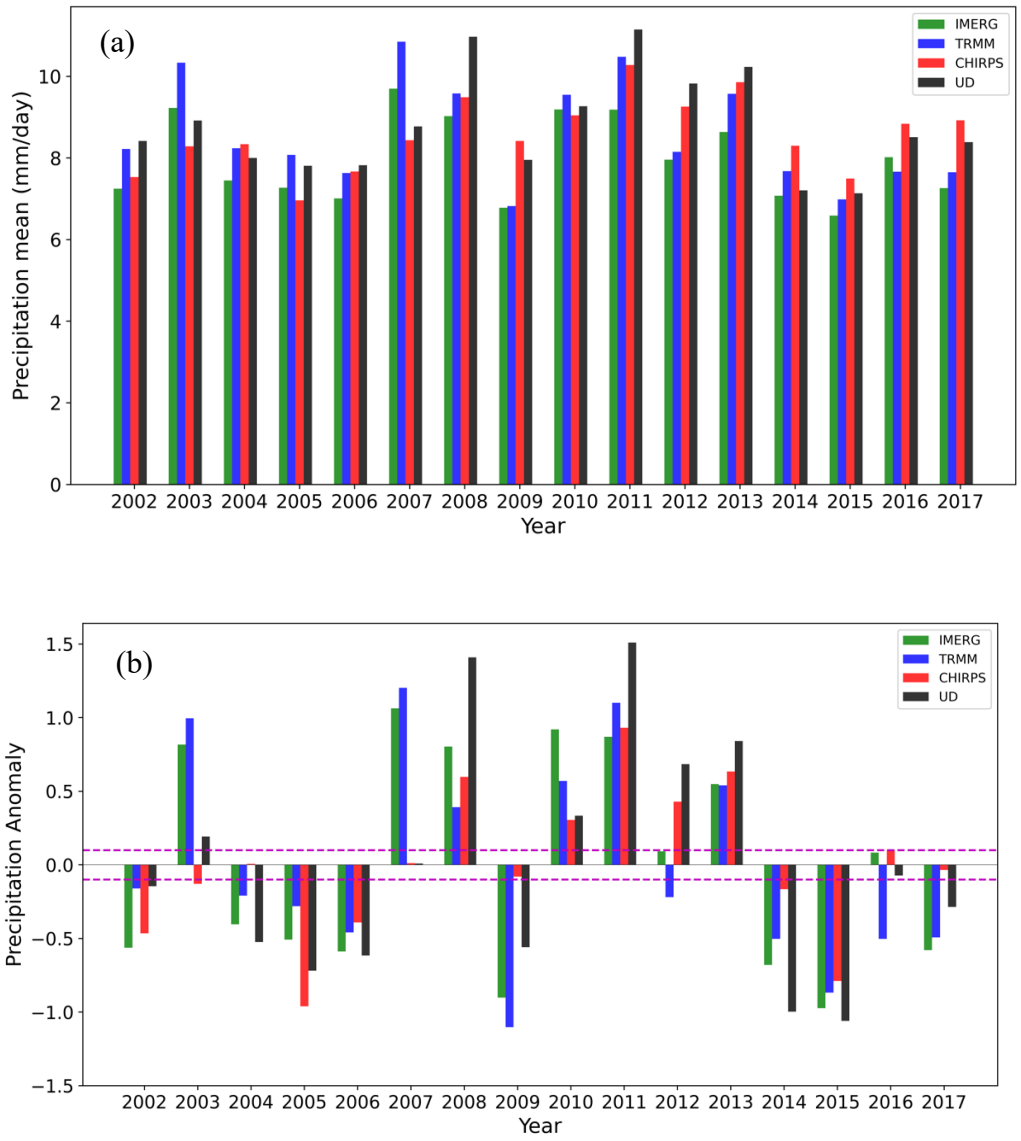

Figure 2.3: Spatially averaged a precipitation, and b precipitation anomaly computed from four different preciptitaion products (IMERG, TRMM, CHIRPS, and UD) over SSFH.

2.3 Results and Discussion

2.3.1 Day-to-day variability

Fig. 2.4a shows the climatology spatial mean of daily IMERG precipitation and AOD during the monsoon period (JJAS) from 2002 to 2017. The SSFH region received 7.98 ± 6.82 mm/day (mean ± std. dev.) of precipitation during the study period. The flow pattern conducive to these regional precipitation amounts is typically related to the cyclonic swirl of westerly/southwesterly low-level circulation over Southern India from the Arabic Ocean and southeasterly low-level circulation from the Bay of Bengal (Fu et al. 2018). The monsoonal season (2002-2017) spatial mean of daily AOD (**Fig. 2.4b**) over the SSFH region is 0.41 ± 0.16 (± std. dev.). The cyclonic swirl follows the path of the highly polluted region of the Bay of Bengal coast and the IGP before it reaches the immediate foothills and southern slope of the Himalayas; hence, our rather regional emphasis on the influence of the aerosol loadings and the downstream hydroclimate.

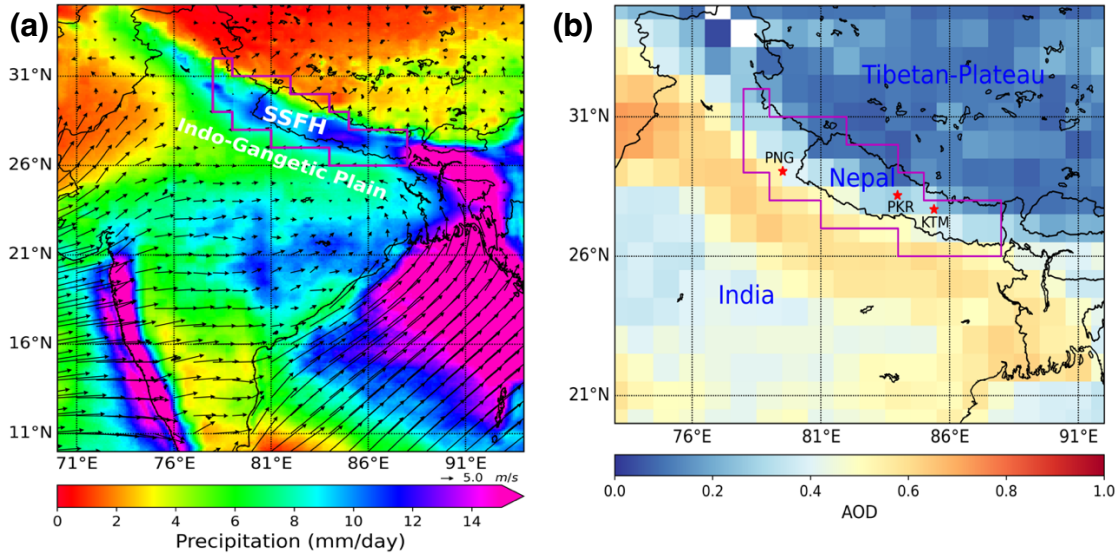

Figure 2.4: Monsoonal season (JJAS) daily mean of (a) IMERG precipitation (0.1° × 0.1°) and ERA5 10 m wind vectors (0.25° × 0.25°), and (b) MODIS-based AOD (1° × 1°). All averages are for the period 2002 to 2017. Red star labels KTM (Kathmandu-Bode), PKR (Pokhara), and PNG (Pantnagar) correspond to AERONET sites used to compare MODIS AOD index. The magenta-colored polygon encloses the southern slope and adjacent foothills of the Himalayas (SSFH).

2.3.2 Aerosol loadings, precipitation, and cloud properties

Figure 2.5 illustrates the mean composite differences of dirty minus clean days for different parameters. Not surprisingly, and by construction, the AOD over the SSFH was markedly higher during dirty days (**Fig. 2.5a**). Of note is that over the southern part of the domain, such differences were more intense, likely due to their proximity to higher aerosol loadings in the IGP. A striking feature is that mean composited precipitation differences were significantly higher during dirty days than during clean days for over 79% of the SSFH (**Fig. 2.5b**); the remaining 21% of the domain showed a decrease in precipitation during dirty days. The average increase in precipitation during dirty days over the entire domain, with a 95% confidence interval (CI), was 0.91 ± 0.05 mm day^{-1}, whereas the positive pixels in **Fig. 2.5b** experienced an increment of 1.28 mm day^{-1}. Of note is that precipitation differences were larger over the southeast part of the domain, where the aerosol loading was higher. In addition to GPM IMERG, dirty minus clean days precipitation plots were created with the TRMM and CHIRPS products (figure not shown). The positive relationship between the AOD and precipitation remained consistent for all three products, indicating the association was independent of precipitation products.

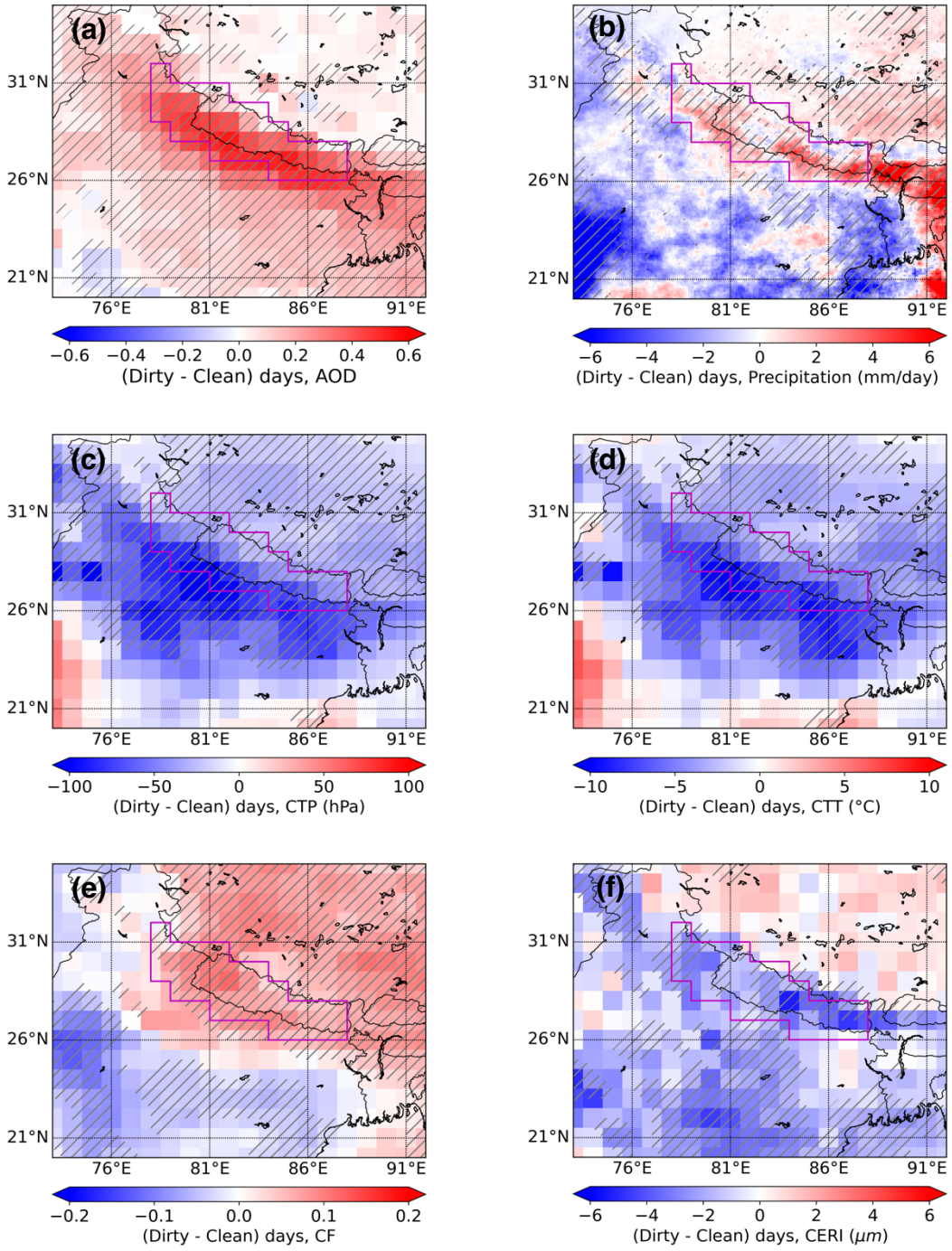

Figure 2.5: Dirty minus clean days mean differences for (a) AOD, (b) precipitation, (c) CTP in hPa, and (d) CTT in °C, (e) CF, and (f) CERI in μm. Positive values (red color) indicate the presence of higher values of the respective parameter during dirty days, and negative (blue color) represents the higher values during clean days. The hatched areas

indicate that the difference between the dirty and clean days distribution is significant at a 95% confidence level based on the Kolmogorov-Smirnov test.

The CTP and CTT were lower during dirty days, indicating a vertical intensification of the clouds during the higher aerosol loading days (**Fig. 2.5c, 2.5d**). During dirty days the mean decrease in CTP was 61.3 ± 9.52 hPa (95% CI), and CTT was 6.54 ±0.84 °C (95% CI) in comparison to clean days. Also, during the dirty days, broader clouds were observed with a mean increase in CF by 0.07 ± 0.01 (95% CI) (**Fig. 2.5e**). The ice-phased cloud effective radius was smaller by 2.22 ± 0.5 μm (95% CI) during dirty days with abundant aerosol loading of aerosols in comparison to a cleaner environment (**Fig. 2.5f**). This suggests that wider and deeper clouds with smaller ice crystals were present during the higher aerosol loading days. Also, during dirty days, though the differences are not statistically significant, the mean cloud LWP was higher (57% of the area), while the cloud IWP was lower (83% of the area) compared to the cleaner environment (**Fig. 2.6**). The association of aerosol abundance with the vertical growth of clouds and cloud fractions is comparable to the observations made in the study by Koren et al. (2012). Their result further suggests that the local rain rate intensified in the polluted environment from the tropics to mid-latitudes from June to August of 2007.

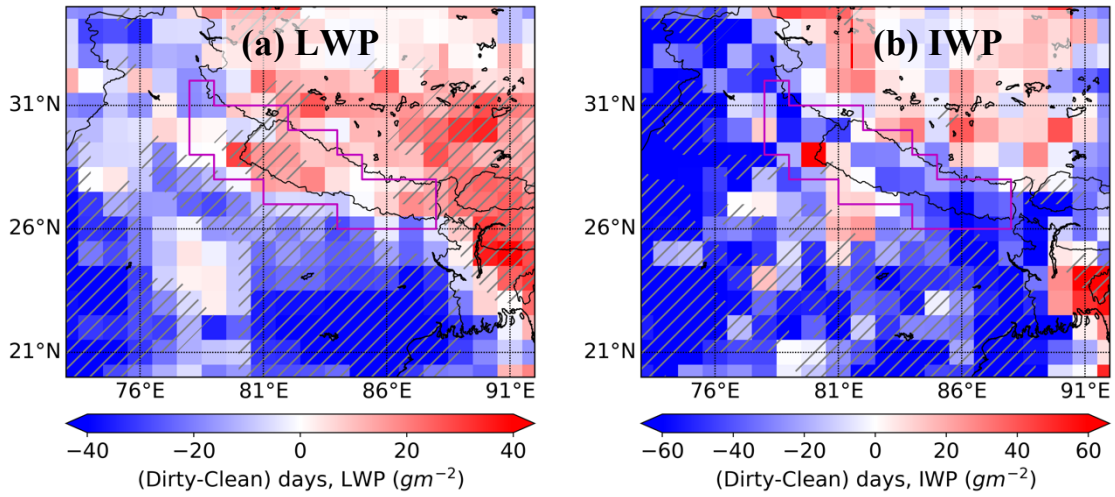

Figure 2.6: Dirty minus clean days mean differences for a Liquid Water Path (LWP) in gm-2, and b Ice Water Path (IWP) gm-2. Positive values (red color) indicate the presence of higher values of the respective parameter during dirty days, and negative (blue color) represents the higher values during clean days. The hatched areas indicate that the difference between the dirty and clean days distribution is significant at a 95% confidence level based on the Kolmogorov-Smirnov test.

A similar analysis was performed for individual pixels within SSFH and dividing the study domain into the east and west subregions. During dirty and clean days of individual pixels and east/west subregions, though the intensity was different, aerosol loading and cloud properties followed identical associations. In addition, a similar analysis carried out with the individual Terra and Aqua products illustrated the identical positive relationship between the higher aerosol loadings and cloud properties, suggesting results are independent of time and products of aerosol and cloud properties retrieval. Also, to reduce the influences of the wet-scavenging effect in determining clean and dirty days and aerosol-cloud relationship, we identified three sets of clean and dirty days excluding the AOD pixels retrieved after a rainfall events occurred at 0600, 0900, and 1200 local time. On average, 88% of the dirty and 91% of the clean days are similar with and without excluding the AOD pixels after the precipitation event. Overall, no

significant changes in the aerosol-cloud relationship result were observed for any of the three sets of clean and dirty days, suggesting that our results are robust. The high emission rate of anthropogenic aerosols rapidly builds up the absorbing aerosols in the atmosphere after the rainfall event over the Indian summer monsoon region (Devi et al. 2011), which might have resulted in no significant changes.

The observed mean CTT over the SSFH during dirty days is -19.78 ± 13.15 °C (± std. dev.) and during clean days is -13.23 ± 13.36 °C (± std. dev.), below the freezing temperature. Our result, to some extent, agrees with Fu et al. (2018), who suggest that the higher amount of precipitation over the southern slope of the Himalayas is from mixed-phase clouds. Our result is comparable with Li et al. (2011), who found that an increase in aerosol concentration significantly decreased CTT during the summer season in mixed-phase clouds, resulting in taller convective clouds and higher precipitation over the southern Great Plains of the U.S.A. Likewise, Sarangi et al. (2017) found an inverse relationship of aerosol abundance with CTT and CTP over central India, south of our study domain, indicating the invigoration of clouds during higher aerosol loadings.

Also, numerous studies have related the outlined enhancement of precipitation and the invigoration of orographic clouds to the higher loading of aerosols that act as INPs, prompting changes in the microphysics of ice-phase processes within the clouds (e.g., Ralph et al. 2015; Fan et al. 2017). An observational study by Yadav et al. (2019) suggests that during core monsoon season, the concentration of INP either decreases or remains constant and local pollution does not strongly contribute to an increase in INPs over northern India. However, the activation of available INP increases with the decrease in temperature, and the concentration varies between 2 to 3 orders of magnitude for the

observed temperature differences between dirty and clean days (Petters and Wright 2015; Yadav et al. 2019). So, the decrease in cloud temperature might also play an essential role in activating INPs during dirty days.

The increase in the natural dust INPs also can enhance the ice processes within clouds and increase precipitation over the foothills of the Himalayas (Hazra et al. 2016), and even during the early stages of the monsoon season (Lau et al. 2017). The numerical simulation over the Sierra Nevada showed a higher concentration of CCN (> 1000 cm^{-3}), which generally occurs over the foothills of Himalayas (e.g., Jayachandran et al. 2020), invigorates the mixed-phase orographic clouds and enhances the windward precipitation (Fan et al. 2017). In a polluted and humid environment, the availability of increased super-cooled water in mixed-phase orographic clouds may enhance the ice-phase growth processes and lead to increased orographic precipitation (Choudhury et al. 2019). Also, it is noteworthy that although aerosols invigorated the clouds over the region south of the SSFH, during the dirty days of our study domain, the pronounced enhancement of precipitation was observed only over the foothills and southern slope of the Himalayas.

2.3.3 Isolating the meteorological effect

There is a chance that relationship of aerosols, cloud properties, and precipitation are modulated by the strength of the weather system and the synoptic transients (meteorology) that occur during the monsoon season. RH at 500 hPa and ω at 600 hPa were used to isolate the meteorological effect from the aerosol-cloud-precipitation relationship because they correlated most closely with cloud properties at respective pressure levels. Over the SSFH, the daily spatial average RH at 500 hPa is 68.78 ±

17.91%, and ω at 600 hPa is -0.16 ± 0.08 Pa/s (mean ± std. dev.) during the monsoon season. The pixel-level precipitation, CTP, and CF data during dirty and clean days were further divided into three different weather regimes. RH is divided into three sub-regimes as: low (RH < 50%), intermediate (50% < RH < 70%), and high (RH >70%). Similarly, based on ω the data were categorized into three convective sub-regimes as: ω > 0 Pa/s (subsidence), 0 Pa/s > ω > -0.1 Pa/s (weak convective regime), and ω < -0.1 Pa/s (strong convective regime) (Koren et al. 2010). The box and whisker plot in **Fig. 2.7** show the bootstrapped distribution of each sub-regimes during dirty and clean days.

Figures **2.7 (a)** and **2.7 (b)** show that shallower clouds were formed in the presence of lower RH and downward motion (positive ω), while during higher RH and stronger upward velocity, deeper clouds with a CTP < 450 hPa were observed. Furthermore, for all three sub-regimes of RH and ω, dirty and clean days were significantly discriminated, with deeper clouds formed during the higher aerosol loading days relative to clean days. The invigoration of a mixed-phase cloud, forming taller clouds in the presence of abundant aerosol over the tropics (Niu and Li 2012) and the Amazon region (Andreae et al. 2004), agrees with our result. Notwithstanding, in all three different regimes of RH and ω, wider clouds were observed during dirty days in contrast with clean days (**Fig. 2.7 c** and **2.7 d**). Higher RH and stronger updraft environments supported the development of widespread clouds with a higher cloud fraction, while limited clouds were observed during subsidence and lower RH weather regime. This result suggests that RH and ω are important meteorological variables and significantly modulate cloud properties. **Fig. 2.7e** and **2.7f** reveal that precipitation tended to increase for the higher RH and stronger convective regime. Furthermore, higher

precipitation was observed during dirty days than during clean days regardless of the RH and w sub-regimes.

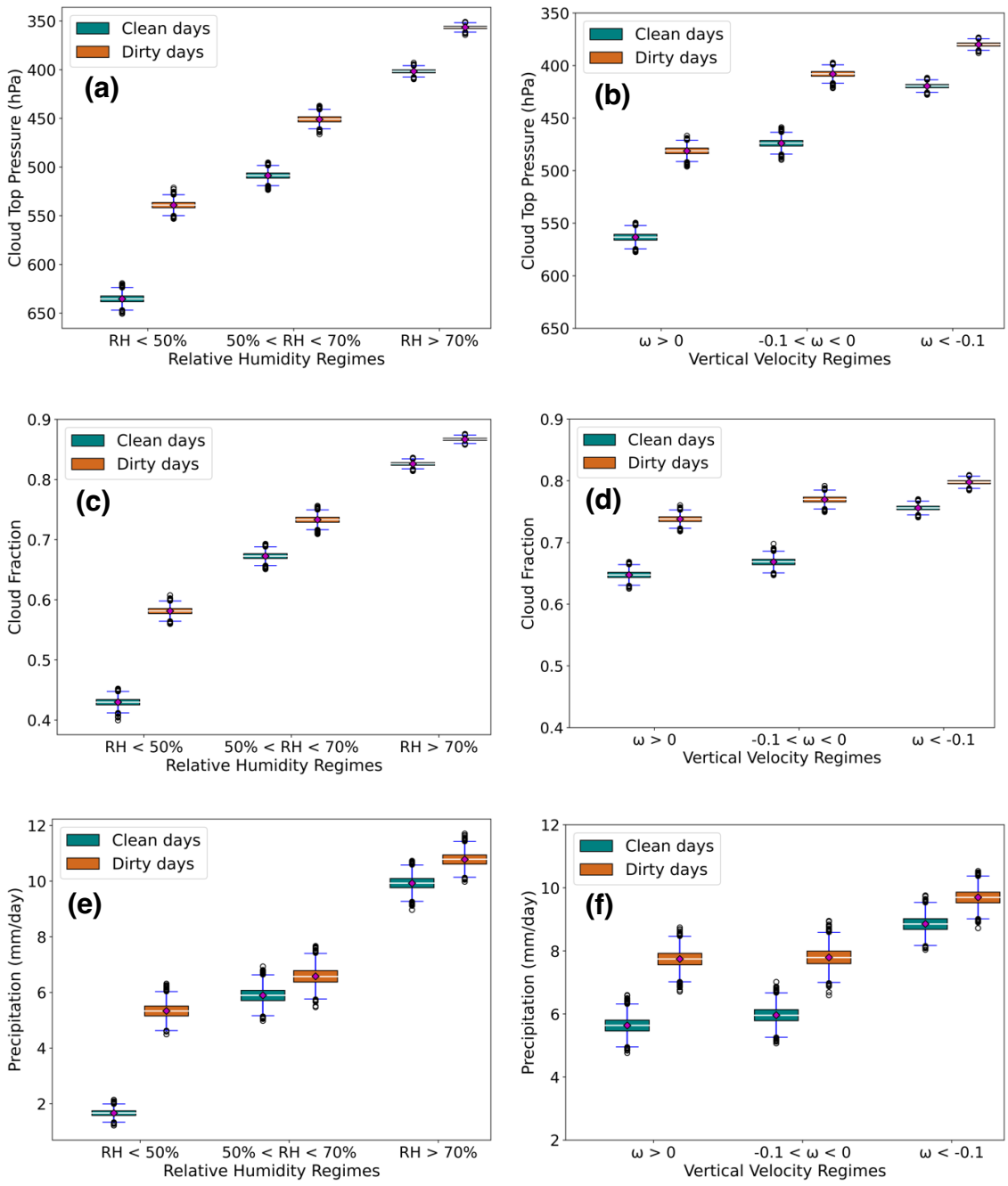

Figure 2.7: Box and whisker plot of spatially averaged CTP (a, b), CF (c, d), and precipitation (e, f) for three different RH (left column) and ω (right column) regime. For

each subgroup, the cyan color represents the clean days and the orange color indicates the dirty days. The magenta colored diamond represents the mean. Based on the Student's t-test, the mean differences between the dirty and clean bootstrapped distributions for all weather regimes are statistically significant at 95% confidence level, except for the intermediate sub-regime of precipitation-RH.

Our result was similar to previous observational-based research, indicating that the direct relationship of aerosols with cloud properties and precipitation remained almost consistent while discriminating with the RH and vertical velocity into low, intermediate, and high-value weather regimes. For example, Koren et al. (2010) showed that aerosols and meteorological variables (vertical velocity and RH) both individually influenced the invigoration of convective clouds over the Atlantic. Also, over central India, Sarangi et al. (2017) revealed that aerosol loading was proportional to precipitation and CTP during both high and low relative humidity days. An increase in aerosol concentration provides more cloud condensation nuclei (CCN), activating smaller cloud droplets and delaying the collision-coalescence process and thus, the development of the raindrop (Andreae 2009). Though the differences are not statistically significant, higher LWP and lower IWP observed during dirty days suggests, stronger warm-phase convection due to enhanced condensation might have played role in the cloud development as reported in several modeling studies (Fan et al. 2007; Sheffield et al. 2015; Chen et al. 2017). The enhanced buoyancy with the release of latent heat of condensation carries the smaller cloud droplets above the freezing level in the atmosphere (Koren et al. 2005; Fan et al. 2016). In the mixed phase, the heterogeneous freezing of a larger number of supercooled droplets releases additional latent heat of freezing in the higher and colder environments, further enhancing the updraft (Rosenfeld and Woodley 2000). In turn, these processes

might result in the formation of taller and widespread clouds with lower cloud top pressure.

The hygroscopic growth of aerosol due to environmental RH influences the AOD measurement and can add uncertainty in the aerosol-cloud-precipitation relationship (Boucher and Quaas 2013; Grandey et al. 2014). However, the magnitude of change in AOD due to humidity depends on the aerosol properties and the differences of humidity between dirty and clean days. Haslett et al. (2019) showed that in a humid environment with RH of 98%, AOD increases by 1.8 times compared to dry AOD. The difference of spatially averaged RH at 500 hPa between dirty and clean days is 1.65% (**Fig. 2.10a**). The mean dirty days AOD over SSFH is 3.5 times higher compared to clean days, which is greater than the order of magnitude presented by Haslett et al. (2019). Also, the mean differences in RH during dirty and clean days while grouping the data into different sub-regimes ranges between 0.2% and 3.53% (Table 3.3). These smaller differences in RH might not account for the change in the magnitude of AOD during dirty days, which is more than three times that of clean days (Koren et al. 2013) and further reduces the biases due to the aerosol humidification effect.

Table 2.3: Mean (±standard deviation) RH at 500 hPa of different sub-regimes used to isolate the meteorological effect.

	Dirty days (RH %)	**Clean days** (RH %)
RH < 50%	32.19 ± 12.73	28.66 ± 15.15
50% < RH < 70%	60.84 ± 5.8	61.04 ± 5.64
RH > 70%	85.65 ± 8.39	84.9 ± 8.2
$\omega > 0$	64.0 ± 24.82	67.53± 22.74
$-0.1 < \omega < 0$	70.75 ± 20.6	71.01 ± 19.86
$\omega < -0.1$	76.71 ±18.19	77.37 ± 17.0

2.3.4 Interannual variability

Our findings using day-to-day aerosol loadings variability reveal that an abundance of aerosol loading is associated with cloud invigoration and higher precipitation. In this section, our analysis focuses on examining the cumulative effect by relating the precipitation, cloud properties, and aerosol loading in the interannual time scale. **Fig. 2.8** shows composites of precipitation, AOD, and cloud properties for wet minus dry

monsoon years. By construction, the precipitation differences over the SSFH during the wet monsoonal season were higher by 2.16 ± 0.91 mm day^{-1} (mean ± std. dev.) compared to the dry period (**Fig. 2.8a**). Of note is that positive precipitation differences were more pronounced and extended over the IGP area and the western foothills. In other words, the seasonal precipitation anomaly over the SSFH was more widespread and was consistent with the drought year of 2009 (Hazra et al. 2013) and the excessive precipitation year of 2008 (Lau et al. 2017) over central and northern India. The difference between wet minus dry years mean AOD (**Fig. 2.8b**) revealed that the concentration of aerosol loading was lower during the wet years over the entire study domain.

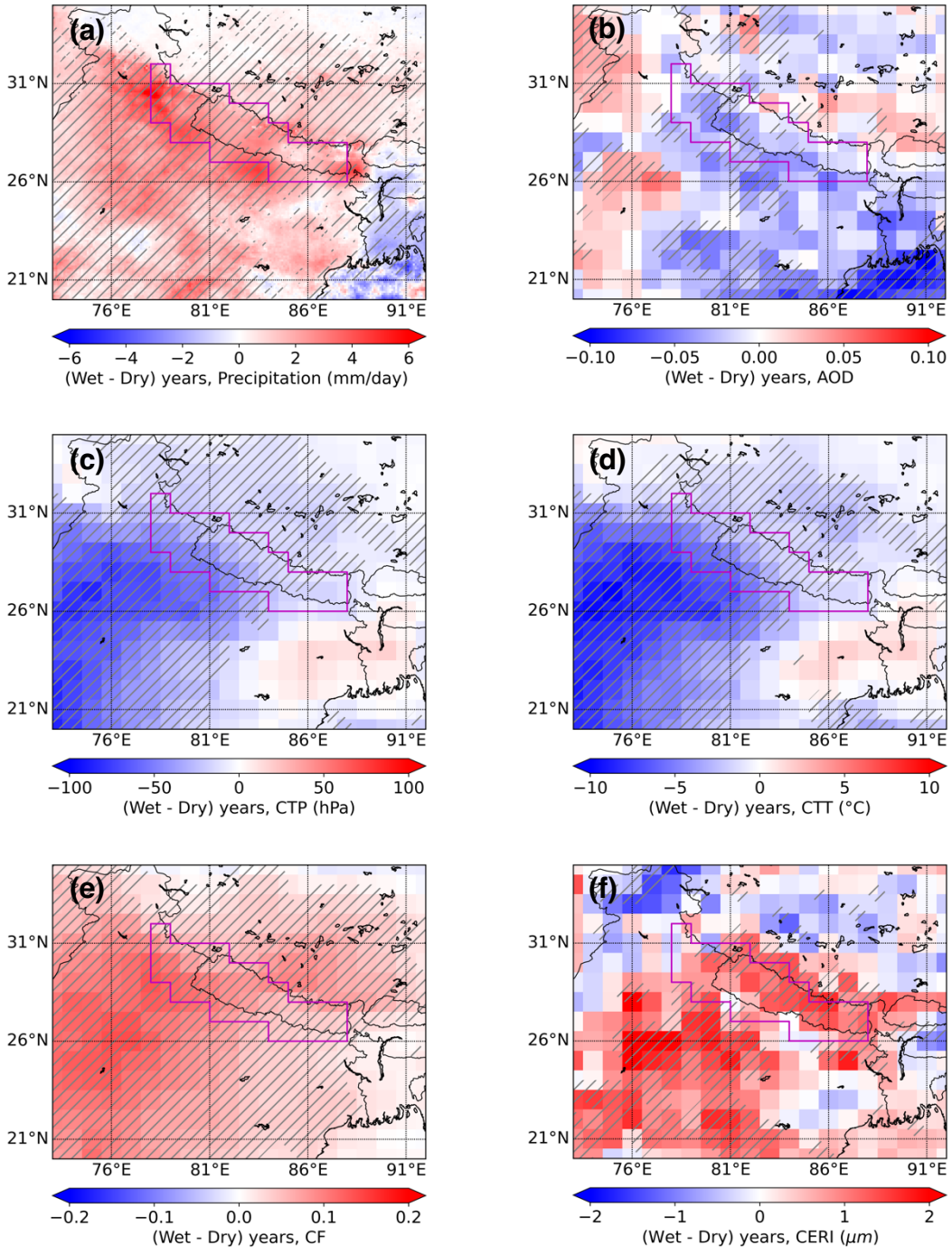

Figure 2.8: Wet minus dry years mean of (a) precipitation, (b) AOD, (c) CTP in hPa, and (d) CTT in °C, (e) CF, and (f) CERI in μm. The hatched areas indicate that the difference between the wet and dry years distribution is significant at a 90% confidence level based on the Kolmogorov-Smirnov test.

Wet years are associated with the larger vertical extent of clouds having lower CTP (**Fig. 2.8c**). During wet years, mean spatial CTP decreased by an additional 27.34 hPa compared to dry years. Also, wet years were characterized by lower CTT (**Fig. 2.8d**), with a mean reduction of 3.03 °C compared to dry years. The CF was observed to be higher during wet years (**Fig. 2.8e**), indicating the presence of broad clouds during abundant rainfall years than in dry years. Furthermore, wet years with lower aerosol loadings were characterized by larger ice crystals (**Fig. 2.8f**). The spatial mean size of CERI over the study domain was larger by 0.88 μm during the wet monsoonal season. It is worth noticing that even though this Wet minus Dry difference is statistically significant, it is relatively small compared to the retrieval uncertainties (1.8-4.2 mm, which is 7-15% of mean CERI). These estimates of retrieval uncertainties account for the atmospheric corrections, instrument calibration, model error, and surface reflectance (Hubanks et al. 2019). Hence, we prevent ourselves from drawing any conclusion on this parameter based on the differences between wet and dry monsoonal years. A similar association, with different intensity, was obtained while performing the analysis by removing the wettest and driest years with all the variables (not shown), indicating that the result was not influenced by the highest rainfall anomalies. Wet years are characterized by the presence of taller and broader clouds, but the mean seasonal aerosol loadings reduced in the atmosphere. These results are consistent with the season having diminished monsoonal rainfall characterized by presence of higher AOD and shallower clouds over the core monsoon region of India (Panicker et al. 2010; Patil et al. 2017). The

lower mean seasonal AOD observed during wet years is consistent with a cleaner environment due to the increased washout of atmospheric aerosols (Textor et al. 2006).

Since the aerosol and cloud interaction occurs at a shorter timescale, we performed the correlation analyses between the aerosol loadings and cloud properties within wet and dry years. **Figure 2.9** shows the pixel-level correlation coefficient of daily AOD with cloud properties and precipitation, significant at 90% confidence level, during wet and dry years. The negative (positive) correlation exists between the AOD and CTP (CF) during both dry and wet years (**Fig. 2.9a, 2.9b**), which is consistent with the invigoration of cloud observed during dirty days with higher aerosol loadings. Most pixels over SSFH experienced the opposite relationship between the increase in aerosol loadings and CERI (**Fig. 2.9c)** during both wet and dry years. The positive correlation of AOD with precipitation is observed over most of the pixels during wet years (**Fig. 2.9d)**. Though the similar association of aerosol loadings with cloud properties and precipitation exist, the significant correlation was widespread among SSFH during wet years compared to dry years. In addition, we also carried out the correlation analyses for each of the wet and dry years. The identical relationship of AOD with cloud properties and precipitation persist, further supporting our results.

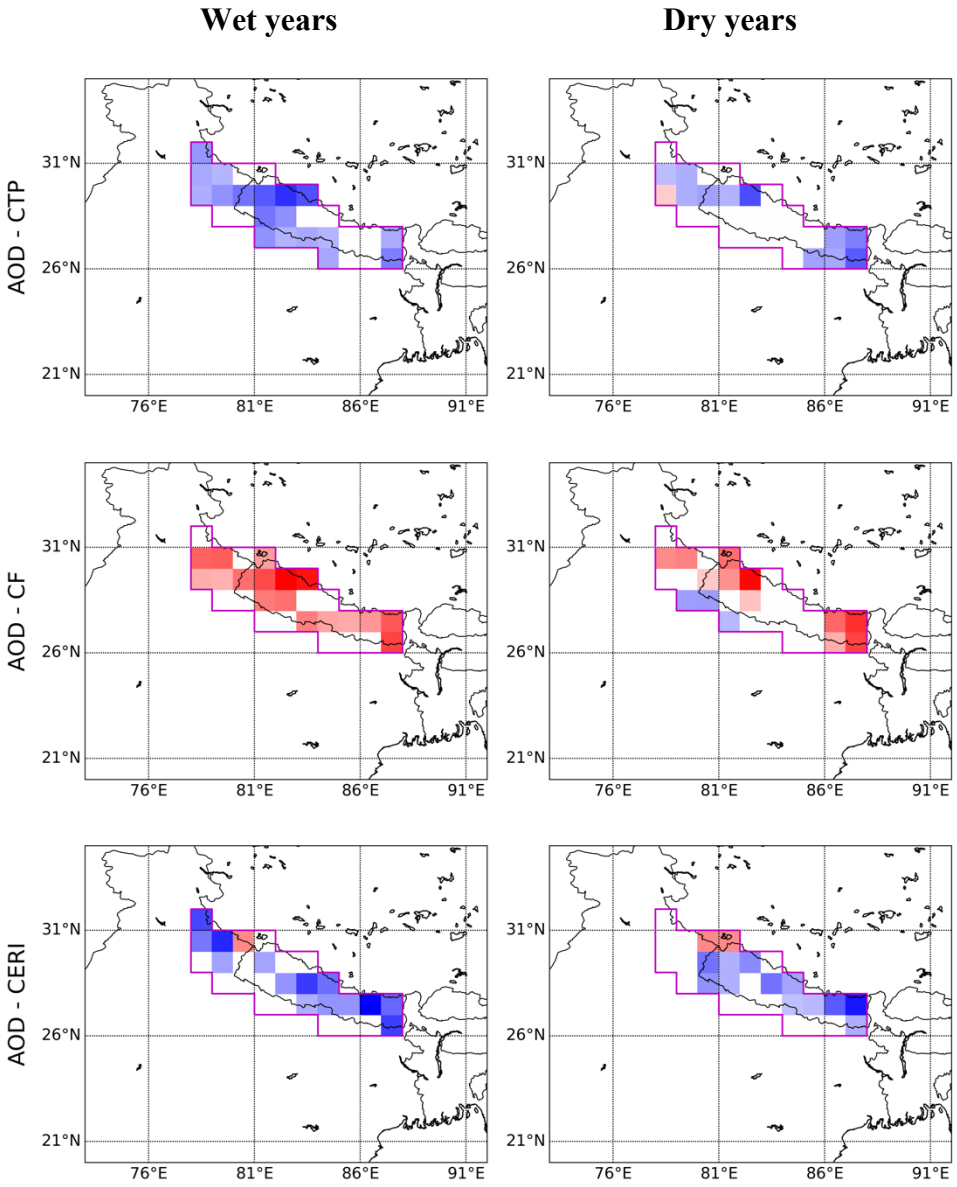
Wet years
Dry years
AOD - CTP
AOD - CF
AOD - CERI
31°N
26°N
21°N
76°E
81°E
86°E
91°E

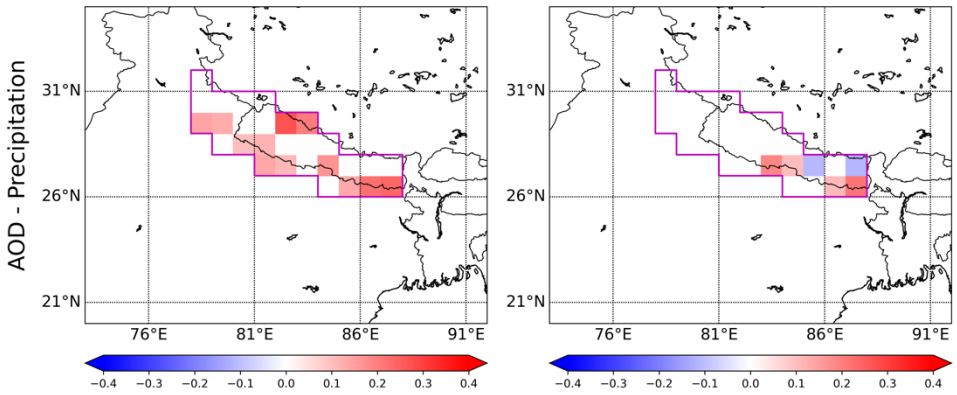

Figure 2.9: Correlation coefficients during wet (1st column) and dry (2nd column) monsoonal years between AOD and (a) CTP, (b) CF, (c) CERI, and (d) precipitation. Only statistically significant values exceeding the 90% confidence level are shown.

On a longer timescale, the changes in source and types of aerosols may influence the variability of precipitation (Ralph et al. 2015). Along with the microphysical and radiative effects, the mean seasonal influence of aerosols on precipitation is also attributed to the large-scale monsoonal circulation (Bollasina et al. 2011; Ganguly et al. 2012; Hazra et al. 2013). An increase in anthropogenic emission (although our study uses total atmospheric AOD) has been attributed to the reduction in the mean monsoonal (JJAS) precipitation (Ganguly et al. 2012) through a slowdown of tropical-meridional circulation (Bollasina et al. 2011). However, an observational study by Vinoj et al. (2014) suggests that increased dust aerosols over northern Africa and west Asia enhances moisture convergence and positively correlates with precipitation over central India on the intra-seasonal timescale. The increased aerosol concentration during dry years is largely related to the deficient moisture supply in the seasonal and intra-seasonal timescales (Manoj et al. 2012; Hazra et al. 2013). It is also consistent with the lower

mean RH observed during dry monsoonal years compared to wet monsoonal years over SSFH (**Fig. 2.10b**). The influence of RH in AOD-precipitation relationship in a daily to seasonal timescale (Ng et al. 2017) might add uncertainty to our result. However, the positive correlation of daily AOD with the cloud development and increased precipitation within dry and wet years is consistent with the dirty days. Further studies are required to quantify the relationship between the aerosols from different sources and monsoonal precipitation on a seasonal scale over the SSFH.

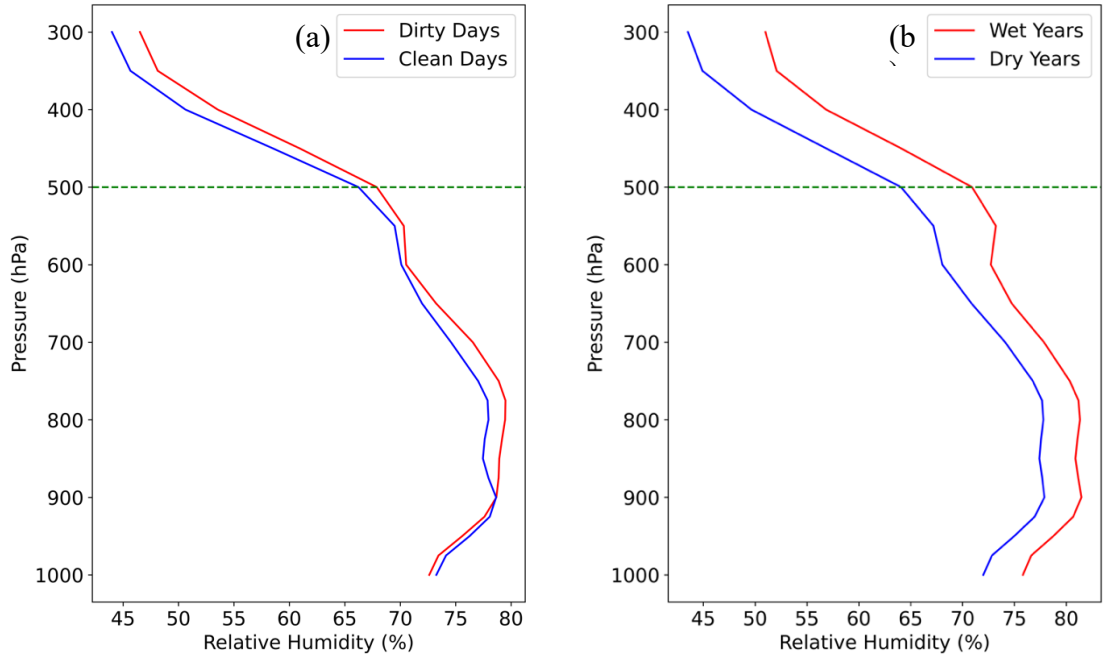

Figure 2.10: Spatially averaged mean relative humidity over SSFH during a dirty and clean days, b wet and dry years.

2.3.5 Freezing level height (FLH)

The mean daily FLH during the monsoonal season of 2002 to 2017 is shown in **Fig. 2.11a**. The FLH is higher over the Tibetan Plateau due to the extreme surface heating

during the summer season. The mean FLH during the late spring over the Himalayan foothills ranges from 4350 to 4650 m above mean sea level, which increases by ~1000 m by the beginning of June and is consistent with Wang et al. (2014). The climatology spatial mean of daily FLH during JJAS over the SSFH was 5413.63 ± 276.85 m (± std. dev.). The mean FLH was higher during dirty days than during clean days (**Fig. 2.11b**). Also, it is noteworthy that, during the dirty days of SSFH, the increase in FLH is widespread over the Himalayan region and extends to Tibetan Plateau. During higher aerosol loading days, the average increase in FLH over the domain was 136.21 ± 18.82 m and ranged between 83.92 m and 191.86 m compared to clean days. **Fig. 2.11c** presents the difference between dirty and clean years 0 ºC isotherm height. Here, dirty or clean years were defined as the years with a JJAS mean spatial AOD greater or smaller than the climatology (JJAS) AOD between 2002 to 2017. Over the study domain, the FLH increased by 12 m on average during the dirty monsoonal years compared to clean monsoonal years. Though the monsoonal averaged FLH might mask some dirty or cleaner environment signal within the season, our result suggests that the increase in FLH during the polluted environment is consistent regardless of the timescale.

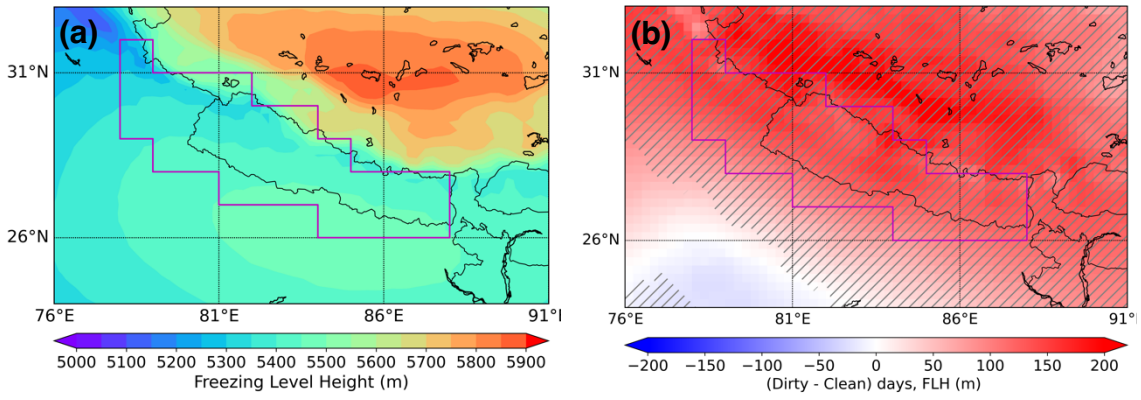

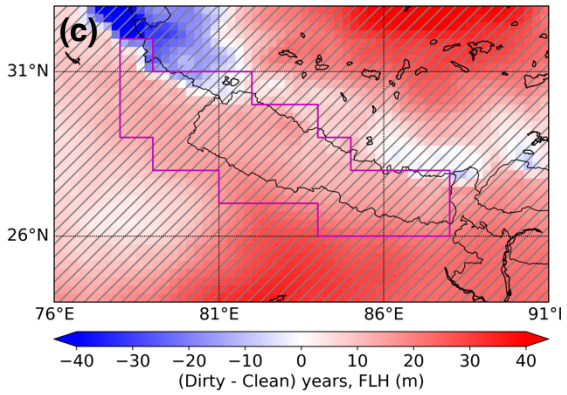

Figure 2.11 (a) Monsoonal (JJAS) (2002-2017) daily mean FLH, (b) Dirty minus clean days mean of FLH (m), and (c) Dirty minus clean monsoonal years mean FLH (m). The hatched areas in (b) and (c) indicate that the difference between the dirty and clean monsoonal season distribution is significant at a 95% confidence level based on the Kolmogorov-Smirnov test.

To isolate the potential role of weather, we divided the daily pixel-level FLH into different weather regimes of RH and ω, and implemented the bootstrapping technique to study the distribution of FLH similar to what was reported in Section 3.1.2. Also, we segregated FLH based on pixel-level CTP [low (>550 hPa), intermediate (between 400 and 550 hPa) and high (<400 hPa) convective clouds] and CF [limited (<0.6), intermediate (between 0.6 and 0.9), and widespread (>0.9) convective clouds]. Our results showed that the distribution of FLH on all three sub-regimes of RH, ω, CTP, and CF was higher during dirty days than during clean days (**Fig. 2.12 a-d**). In addition, FLH was divided into three different sub-regimes based on lower, intermediate, and upper 33 percentiles of surface (2 m) air temperature (**Fig 2.12e**). It indicated that the FLH is proportional to surface air temperature and was higher during dirty days than clean days regardless of the surface air temperature sub-regimes. This suggests that aerosol loadings impacted the FLH independent of meteorological variables and cloud macro-properties.

The direct relationship of abundance aerosol loading and FLH over the SSFH is comparable with the positive correlation between increasing trend of surface air temperature and mean summer FLH from 1970-2010 (~2.3 m/yr) over high Asia (Wang et al. 2014).

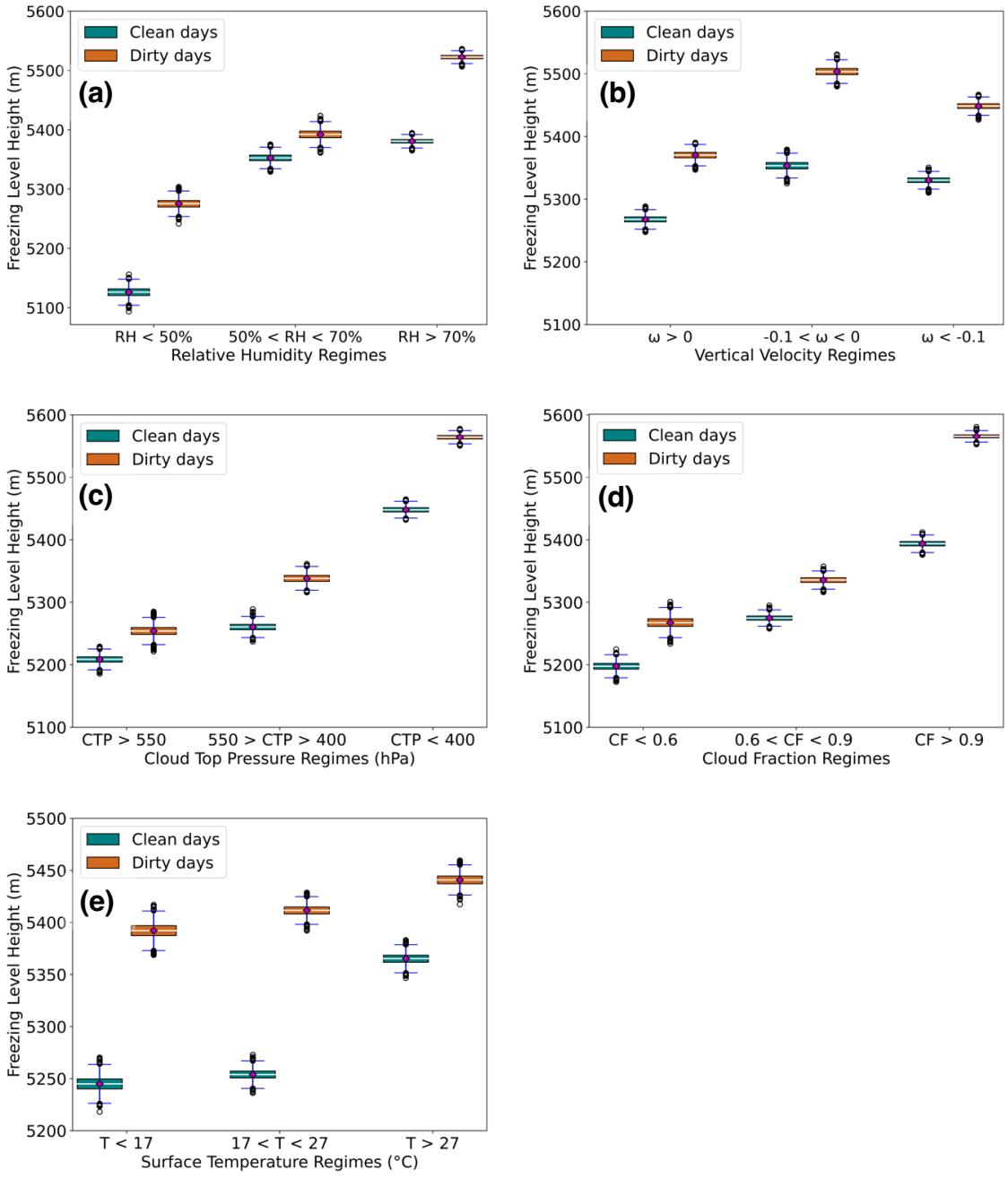

Figure 2.12: Box and whisker plot of spatially averaged FLH as a function of (a) RH, (b) ω, (c) CTP, (d) CF, and (e) surface air temperature regimes. Based on the Student's t-test, the mean difference between the dirty and clean bootstrapped distributions for all weather regimes are statistically significant at a 95% confidence level.

The interaction of aerosols with radiation and clouds may be contributing to an increase in FLH during dirty days. The warming of the upper troposphere is evident over the Himalayan foothills by the layer of light absorbing aerosols during the early monsoon (Lau et al. 2017). Also, the increase in FLH during dirty days with an abundance of aerosol loadings may be attributable to positive shortwave radiative forcing due to mixed carbonaceous aerosols over the foothills of the Himalayas during the monsoonal season (Ji et al. 2015). Furthermore, the increase in condensational latent heat release in the presence of higher CCN concentration in deep convective precipitating clouds (Tao and Li 2016) can also modulate the FLH during higher aerosol loading days.

The positive correlation of FLH and surface temperature is directly associated with the shrinkage of glacier and loss of ice mass over high latitude of Asia (Wang et al. 2014). Also, the warming of the snow surface through the deposition of the light-absorbing aerosols over the Himalaya-Tibetan Plateau reduces the surface albedo and increases the melting of the snowpack during pre- and early monsoon season (Qian et al. 2015; Lau and Kim 2018). It dynamically influences the monsoonal precipitation of the foothills through the elevated heat pump mechanism (Lau et al. 2017; Lau and Kim 2018). Alternatively, the monsoonal precipitation also increases the wet deposition of black carbon aerosols over the Himalayan snowpack (Ji et al. 2015) and has a significant impact on the melting of snow.

The enhanced precipitation observed during the dirty days might also be a potential consequence of the increase in warm cloud layer depth due to the rise in FLH, resulting in a reduction of snow to rainfall ratio (Prein and Heymsfield 2020). Furthermore, the increase in surface temperature shifts the snowline upward, resulting in more rainfall than

snowfall. It leads to an increase in streamflow during the monsoonal season, increasing the risk of landslide and flood events over the mountains and lower elevations. In addition, a positive correlation observed between the daily AOD and FLH during wet years (**Fig. 2.13**) further intensifies the runoff and flooding concern. Determining the roles of different types of local and remote aerosols on modulating the Himalayan hydroclimate through the perturbation of orographic precipitation and FLH is crucial in assessing the flood risk, landslide risk, and water resources.

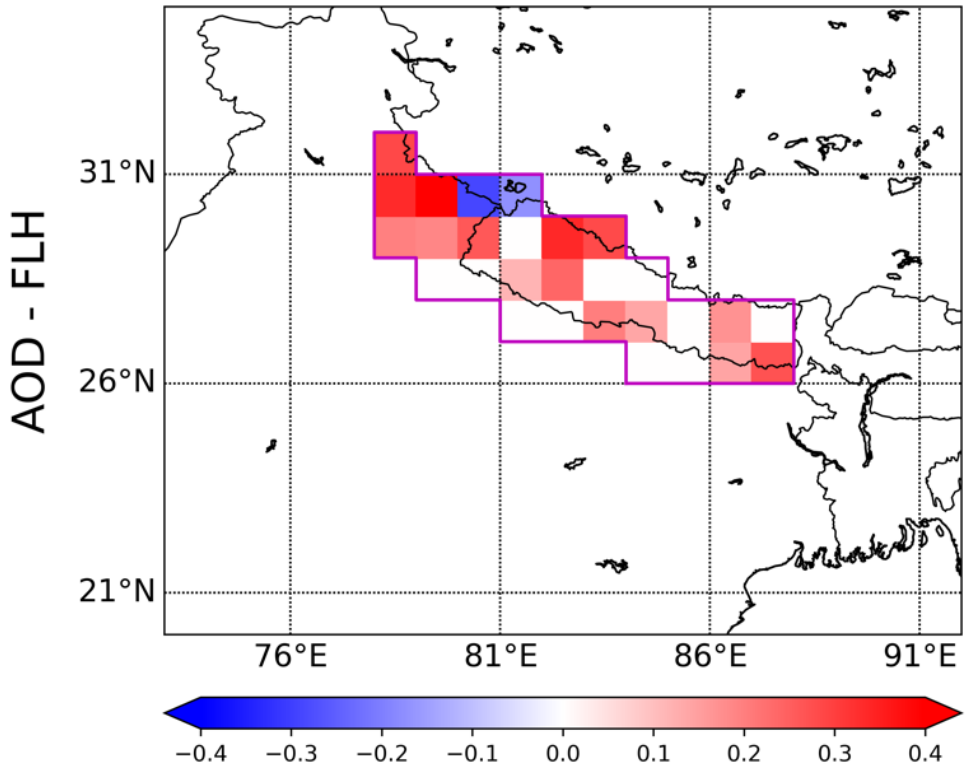

Figure 2.13: The correlation coefficients between AOD and FLH during wet years. Only statistically significant values exceeding the 90% confidence level are shown.

2.4 Conclusions

In this study, 16 years (2002-2017) of satellite and reanalysis datasets were utilized to analyze the impacts of aerosols on clouds, precipitation, and freezing level height during the summer monsoon season (JJAS) over the immediate foothills and southern slope of the Himalayas. In addition to the AOD and cloud product from MODIS, the higher-resolution GPM IMERG precipitation and recent ERA5 reanalysis datasets were used. The analysis was performed based on relatively high (dirty) and low (clean) aerosol days for day-to-day variability and dry/wet years for interannual timescale. Furthermore, significant efforts were carried out to isolate the role of weather forcing from aerosol-cloud-precipitation relationship in the daily timescale.

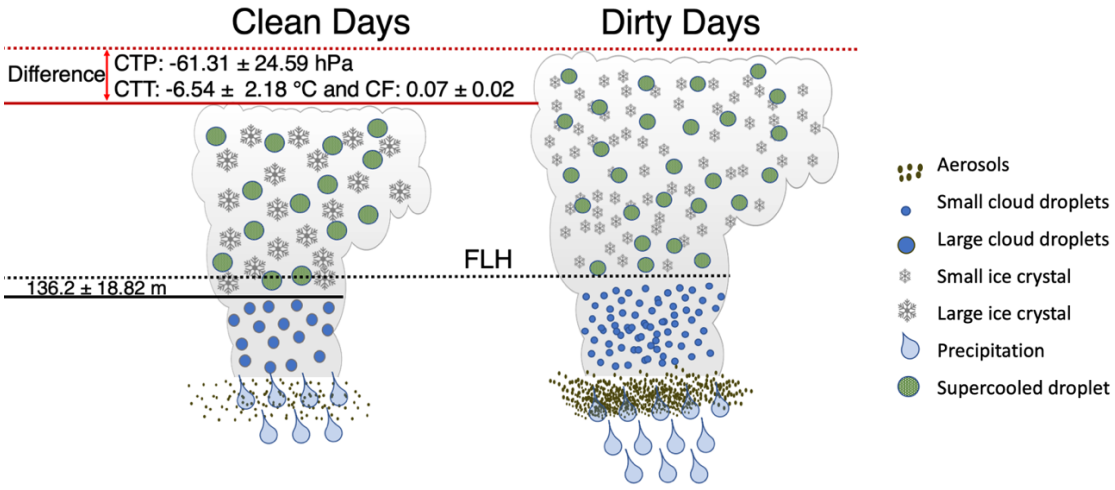

Figure 2.14 Schematic illustration of the perturbation of cloud properties and FLH during dirty and clean days. Here, the mean environmental FLH includes all the cloudy and non-

cloudy pixels over SSFH. Numerical values indicate the dirty minus clean daily differences (mean ± one standard deviation).

Our result suggests that aerosols play a crucial role to perturb monsoonal precipitation and FLH. **Fig. 2.14** shows a schematic diagram summarizing our findings based on dirty and clean days. During the dirty days, a higher fraction of the clouds with lower cloud top pressure/temperature and increased precipitation were observed in most of the study region, in comparison to clean days. We also showed that FLH is significantly higher by 136.2 ± 18.82 m during dirty days compared to clean days, a factor that can be crucial for the change in snow line and melting of Himalayan glaciers. Our findings also show that these results are consistent regardless of the meteorological regimes and cloud properties.

We further assessed the role of aerosol loading in perturbating the cloud and precipitation during relatively wet and dry monsoonal years, as aerosol can also influence the monsoonal rainfall in an interannual timescale. The anomalously wet monsoonal seasons are related to taller and broader clouds and lower mean monsoonal aerosol loadings. However, we found that despite the monsoonal precipitation anomalies, the day-to-day spatial correlation analyses reveal that AOD is directly related to cloud development and enhanced precipitation. These consistent positive relationships show that aerosol loading plays an essential part in influencing the cloud development and monsoonal rainfall over the SSFH.

In addition to terrain-induced local weather dynamics, the meteorological variables that affect the aerosol-cloud-precipitation relationship are not limited to those implemented herein and can add uncertainties to our analysis. Furthermore, the lack of

observational data that provides the concentration of CCN/INP over the Himalayas limits the understanding of the microphysical process and can impose uncertainties in our analysis.

Our findings underlined the importance of aerosols in perturbating precipitation and the FLH over the adjacent region of the Himalayas. An investigation utilizing high-resolution numerical simulation is required to better quantify and understand the relative influence of local and remote aerosols as well as to elucidate the magnitude of impact through radiative and cloud microphysical pathways.

References

Altaratz O, Bar-Or RZ, Wollner U, Koren I (2013) Relative humidity and its effect on aerosol optical depth in the vicinity of convective clouds. Environ Res Lett 8:034025. https://doi.org/10.1088/1748-9326/8/3/034025

Andreae MO (2009) Correlation between cloud condensation nuclei concentration and aerosol optical thickness in remote and polluted regions. Atmos Chem Phys 14. https://doi.org/10.5194/acp-9-543-2009

Andreae MO, Rosenfeld D, Artaxo P, et al (2004) Smoking rain clouds over the Amazon. Science 303:1337–1342. https://doi.org/10.1126/science.1092779

Babu SS, Manoj MR, Moorthy KK, et al (2013) Trends in aerosol optical depth over Indian region: Potential causes and impact indicators. Journal of Geophysical Research: Atmospheres 118:11,794-11,806. https://doi.org/10.1002/2013JD020507

Bollasina MA, Ming Y, Ramaswamy V (2011) Anthropogenic Aerosols and the Weakening of the South Asian Summer Monsoon. Science 334:502–505. https://doi.org/10.1126/science.1204994

Bollasina MA, Ming Y, Ramaswamy V, et al (2014) Contribution of local and remote anthropogenic aerosols to the twentieth century weakening of the South Asian Monsoon. Geophysical Research Letters 41:680–687. https://doi.org/10.1002/2013GL058183

Boucher O, Quaas J (2013) Water vapour affects both rain and aerosol optical depth. Nature Geoscience 6:4–5. https://doi.org/10.1038/ngeo1692

Bradley RS, Keimig FT, Diaz HF, Hardy DR (2009) Recent changes in freezing level heights in the Tropics with implications for the deglacierization of high mountain regions. Geophysical Research Letters 36:. https://doi.org/10.1029/2009GL037712

Chen Q, Koren I, Altaratz O, et al (2017) How do changes in warm-phase microphysics affect deep convective clouds? Atmos Chem Phys 17:9585–9598. https://doi.org/10.5194/acp-17-9585-2017

Choudhury G, Tyagi B, Singh J, et al (2019) Aerosol-orography-precipitation – A critical assessment. Atmospheric Environment 214:116831. https://doi.org/10.1016/j.atmosenv.2019.116831

Dave P, Bhushan M, Venkataraman C (2017) Aerosols cause intraseasonal short-term suppression of Indian monsoon rainfall. Scientific Reports 7:1–12. https://doi.org/10.1038/s41598-017-17599-1

Davenport FV, Herrera-Estrada JE, Burke M, Diffenbaugh NS (2020) Flood Size Increases Nonlinearly Across the Western United States in Response to Lower Snow-Precipitation Ratios. Water Resources Research 56:e2019WR025571. https://doi.org/10.1029/2019WR025571

Davison AC, Hinkley DV (1997) Bootstrap Methods and Their Application. Cambridge University Press

Devi JJ, Tripathi SN, Gupta T, et al (2011) Observation-based 3-D view of aerosol radiative properties over Indian Continental Tropical Convergence Zone: implications to regional climate. Tellus B: Chemical and Physical Meteorology 63:971–989. https://doi.org/10.1111/j.1600-0889.2011.00580.x

Diaz HF, Eischeid JK, Duncan C, Bradley RS (2003) Variability of Freezing Levels, Melting Season Indicators, and Snow Cover for Selected High-Elevation and Continental Regions in the Last 50 Years. Climatic Change 59:33–52. https://doi.org/10.1023/A:1024460010140

Fan J, Leung LR, Rosenfeld D, DeMott PJ (2017) Effects of cloud condensation nuclei and ice nucleating particles on precipitation processes and supercooled liquid in

mixed-phase orographic clouds. Atmospheric Chemistry and Physics 17:1017–1035. https://doi.org/10.5194/acp-17-1017-2017

Fan J, Rosenfeld D, Zhang Y, et al (2018) Substantial convection and precipitation enhancements by ultrafine aerosol particles. Science 359:411–418. https://doi.org/10.1126/science.aan8461

Fan J, Wang Y, Rosenfeld D, Liu X (2016) Review of Aerosol–Cloud Interactions: Mechanisms, Significance, and Challenges. J Atmos Sci 73:4221–4252. https://doi.org/10.1175/JAS-D-16-0037.1

Fan J, Zhang R, Li G, Tao W-K (2007) Effects of aerosols and relative humidity on cumulus clouds. Journal of Geophysical Research: Atmospheres 112:. https://doi.org/10.1029/2006JD008136

Fu Y, Pan X, Xian T, et al (2018) Precipitation characteristics over the steep slope of the Himalayas in rainy season observed by TRMM PR and VIRS. Clim Dyn 51:1971–1989. https://doi.org/10.1007/s00382-017-3992-3

Funk C, Peterson P, Landsfeld M, et al (2015) The climate hazards infrared precipitation with stations—a new environmental record for monitoring extremes. Scientific Data 2:1–21. https://doi.org/10.1038/sdata.2015.66

Ganguly D, Rasch PJ, Wang H, Yoon J-H (2012) Climate response of the South Asian monsoon system to anthropogenic aerosols. Journal of Geophysical Research: Atmospheres 117:. https://doi.org/10.1029/2012JD017508

Grandey BS, Gururaj A, Stier P, Wagner TM (2014) Rainfall-aerosol relationships explained by wet scavenging and humidity. Geophysical Research Letters 41:5678–5684. https://doi.org/10.1002/2014GL060958

Guo L, Turner AG, Highwood EJ (2016) Local and Remote Impacts of Aerosol Species on Indian Summer Monsoon Rainfall in a GCM. J Climate 29:6937–6955. https://doi.org/10.1175/JCLI-D-15-0728.1

Gupta P, Remer LA, Levy RC, Mattoo S (2018) Validation of MODIS 3 km land aerosol optical depth from NASA's EOS Terra and Aqua missions. Atmospheric Measurement Techniques; Katlenburg-Lindau 11:3145–3159. http://dx.doi.org/10.5194/amt-11-3145-2018

Haslett SL, Taylor JW, Deetz K, et al (2019) The radiative impact of out-of-cloud aerosol hygroscopic growth during the summer monsoon in southern West Africa. Atmospheric Chemistry and Physics 19:1505–1520. https://doi.org/10.5194/acp-19-1505-2019

Hazra A, Padmakumari B, Maheskumar RS, Chen J-P (2016) The effect of mineral dust and soot aerosols on ice microphysics near the foothills of the Himalayas: A numerical investigation. Atmospheric Research 171:41–55. https://doi.org/10.1016/j.atmosres.2015.12.005

Hazra A, Taraphdar S, Halder M, et al (2013) Indian summer monsoon drought 2009: role of aerosol and cloud microphysics. Atmospheric Science Letters 14:181–186. https://doi.org/10.1002/asl2.437

Heiblum RH, Koren I, Altaratz O (2012) New evidence of cloud invigoration from TRMM measurements of rain center of gravity. Geophysical Research Letters 39:. https://doi.org/10.1029/2012GL051158

Hersbach H, Dee D (2016) ERA5 reanalysis is in production. ECMWF newsletter 147:5–6

Hubanks P, Platnick S, King M, Ridgway B (2019) MODIS Atmosphere L3 Gridded Product Algorithm Theoretical Basis Document (ATBD) & Users Guide. ATBD reference number ATBD-MOD-30:129

Huffman GJ, Bolvin DT, Braithwaite D, et al (2015a) Algorithm Theoretical Basis Document (ATBD) Version 4.5: NASA Global Precipitation Measurement

(GPM) Integrated Multi-satellitE Retrievals for GPM (IMERG). NASA: Greenbelt, MD, USA

Huffman GJ, Bolvin DT, Nelkin EJ (2015b) Integrated Multi-satellitE Retrievals for GPM (IMERG) Technical Documentation. NASA/GSFC Code 612, 47 pp. College Park: University of Maryland

Jayachandran VN, Suresh Babu SN, Vaishya A, et al (2020) Altitude profiles of cloud condensation nuclei characteristics across the Indo-Gangetic Plain prior to the onset of the Indian summer monsoon. Atmos Chem Phys 20:561–576. https://doi.org/10.5194/acp-20-561-2020

Ji Z, Kang S, Cong Z, et al (2015) Simulation of carbonaceous aerosols over the Third Pole and adjacent regions: distribution, transportation, deposition, and climatic effects. Clim Dyn 45:2831–2846. https://doi.org/10.1007/s00382-015-2509-1

Kang S, Zhang Q, Qian Y, et al (2019) Linking atmospheric pollution to cryospheric change in the Third Pole region: current progress and future prospects. Natl Sci Rev 6:796–809. https://doi.org/10.1093/nsr/nwz031

Koren I, Altaratz O, Remer LA, et al (2012) Aerosol-induced intensification of rain from the tropics to the mid-latitudes. Nature Geoscience 5:118–122. https://doi.org/10.1038/ngeo1364

Koren I, Altaratz O, Remer LA, et al (2013) Reply to “Water vapour affects both rain and aerosol optical depth.” Nature Geoscience 6:5–5. https://doi.org/10.1038/ngeo1693

Koren I, Feingold G, Remer LA (2010) The invigoration of deep convective clouds over the Atlantic: aerosol effect, meteorology or retrieval artifact? https://doi.org/10.5194/acp-10-8855-2010

Koren I, Kaufman YJ, Rosenfeld D, et al (2005) Aerosol invigoration and restructuring of Atlantic convective clouds. Geophysical Research Letters 32:. https://doi.org/10.1029/2005GL023187

Kourtidis K, Stathopoulos S, Georgoulias AK, et al (2015) A study of the impact of synoptic weather conditions and water vapor on aerosol-cloud relationships over major urban clusters of China. Atmos Chem Phys Discuss 15:14007–14026. https://doi.org/10.5194/acpd-15-14007-2015

Kumar M, Parmar KS, Kumar DB, et al (2018) Long-term aerosol climatology over Indo-Gangetic Plain: Trend, prediction and potential source fields. Atmospheric Environment 180:37–50. https://doi.org/10.1016/j.atmosenv.2018.02.027

Lau K-M, Kim K-M (2006) Observational relationships between aerosol and Asian monsoon rainfall, and circulation. Geophysical Research Letters 33:. https://doi.org/10.1029/2006GL027546

Lau KM, Kim MK, Kim KM (2006) Asian summer monsoon anomalies induced by aerosol direct forcing: the role of the Tibetan Plateau. Clim Dyn 26:855–864. https://doi.org/10.1007/s00382-006-0114-z

Lau WKM, Kim K-M (2018) Impact of Snow Darkening by Deposition of Light-Absorbing Aerosols on Snow Cover in the Himalayas–Tibetan Plateau and Influence on the Asian Summer Monsoon: A Possible Mechanism for the Blanford Hypothesis. Atmosphere 9:438. https://doi.org/10.3390/atmos9110438

Lau WKM, Kim K-M, Shi J-J, et al (2017) Impacts of aerosol–monsoon interaction on rainfall and circulation over Northern India and the Himalaya Foothills. Clim Dyn 49:1945–1960. https://doi.org/10.1007/s00382-016-3430-y

Levy RC, Mattoo S, Munchak LA, et al (2013) The Collection 6 MODIS aerosol products over land and ocean. Atmos Meas Tech 6:2989–3034. https://doi.org/10.5194/amt-6-2989-2013

Li Z, Niu F, Fan J, et al (2011) Long-term impacts of aerosols on the vertical development of clouds and precipitation. Nature Geoscience 4:888–894. https://doi.org/10.1038/ngeo1313

Mahto SS, Mishra V (2019) Does ERA-5 Outperform Other Reanalysis Products for Hydrologic Applications in India? Journal of Geophysical Research: Atmospheres 124:9423–9441. https://doi.org/10.1029/2019JD031155

Manoj MG, Devara PCS, Joseph S, Sahai AK (2012) Aerosol indirect effect during the aberrant Indian Summer Monsoon breaks of 2009. Atmospheric Environment 60:153–163. https://doi.org/10.1016/j.atmosenv.2012.06.007

Mishra V, Smoliak BV, Lettenmaier DP, Wallace JM (2012) A prominent pattern of year-to-year variability in Indian Summer Monsoon Rainfall. PNAS 109:7213–7217. https://doi.org/10.1073/pnas.1119150109

Ng DHL, Li R, Raghavan SV, Liong S-Y (2017) Investigating the relationship between Aerosol Optical Depth and Precipitation over Southeast Asia with Relative Humidity as an influencing factor. Scientific Reports 7:1–13. https://doi.org/10.1038/s41598-017-10858-1

Nigam S, Bollasina M (2010) "Elevated heat pump" hypothesis for the aerosol-monsoon hydroclimate link: "Grounded" in observations? Journal of Geophysical Research: Atmospheres 115:. https://doi.org/10.1029/2009JD013800

Niu F, Li Z (2012) Systematic variations of cloud top temperature and precipitation rate with aerosols over the global tropics. Atmos Chem Phys 12:8491–8498. https://doi.org/10.5194/acp-12-8491-2012

Panicker AS, Pandithurai G, Dipu S (2010) Aerosol indirect effect during successive contrasting monsoon seasons over Indian subcontinent using MODIS data. Atmospheric Environment 44:1937–1943. https://doi.org/10.1016/j.atmosenv.2010.02.015

Patil N, Dave P, Venkataraman C (2017) Contrasting influences of aerosols on cloud properties during deficient and abundant monsoon years. Scientific Reports 7:1–9. https://doi.org/10.1038/srep44996

Pepin N, Bradley RS, Diaz HF, et al (2015) Elevation-dependent warming in mountain regions of the world. Nature Climate Change 5:424–430. https://doi.org/10.1038/nclimate2563

Petters MD, Wright TP (2015) Revisiting ice nucleation from precipitation samples. Geophysical Research Letters 42:8758–8766. https://doi.org/10.1002/2015GL065733

Platnick S, King MD, Ackerman SA, et al (2003) The MODIS cloud products: algorithms and examples from Terra. IEEE Transactions on Geoscience and Remote Sensing 41:459–473. https://doi.org/10.1109/TGRS.2002.808301

Prakash S, Mitra AK, AghaKouchak A, et al (2018) A preliminary assessment of GPM-based multi-satellite precipitation estimates over a monsoon dominated region. Journal of Hydrology 556:865–876. https://doi.org/10.1016/j.jhydrol.2016.01.029

Prein AF, Heymsfield AJ (2020) Increased melting level height impacts surface precipitation phase and intensity. Nature Climate Change 10:771–776. https://doi.org/10.1038/s41558-020-0825-x

Qian Y, Yasunari TJ, Doherty SJ, et al (2015) Light-absorbing particles in snow and ice: Measurement and modeling of climatic and hydrological impact. Adv Atmos Sci 32:64–91. https://doi.org/10.1007/s00376-014-0010-0

Ragettli S, Immerzeel WW, Pellicciotti F (2016) Contrasting climate change impact on river flows from high-altitude catchments in the Himalayan and Andes Mountains. PNAS 113:9222–9227. https://doi.org/10.1073/pnas.1606526113

Ralph FM, Prather KA, Cayan D, et al (2015) CalWater Field Studies Designed to Quantify the Roles of Atmospheric Rivers and Aerosols in Modulating U.S. West

Coast Precipitation in a Changing Climate. Bull Amer Meteor Soc 97:1209–1228. https://doi.org/10.1175/BAMS-D-14-00043.1

Ramanathan V, Chung C, Kim D, et al (2005) Atmospheric brown clouds: Impacts on South Asian climate and hydrological cycle. Proceedings of the National Academy of Sciences 102:5326–5333. https://doi.org/10.1073/pnas.0500656102

Remer LA, Kaufman YJ, Tanré D, et al (2005) The MODIS Aerosol Algorithm, Products, and Validation. J Atmos Sci 62:947–973. https://doi.org/10.1175/JAS3385.1

Remer LA, Mattoo S, Levy RC, Munchak LA (2013) MODIS 3 km aerosol product: algorithm and global perspective. Atmospheric Measurement Techniques 6:1829–1844. https://doi.org/10.5194/amt-6-1829-2013

Rosenfeld D (1999) TRMM observed first direct evidence of smoke from forest fires inhibiting rainfall. Geophysical Research Letters 26:3105–3108. https://doi.org/10.1029/1999GL006066

Rosenfeld D, Andreae MO, Asmi A, et al (2014) Global observations of aerosol-cloud-precipitation-climate interactions. Reviews of Geophysics 52:750–808. https://doi.org/10.1002/2013RG000441

Rosenfeld D, Lohmann U, Raga GB, et al (2008) Flood or Drought: How Do Aerosols Affect Precipitation? Science 321:1309–1313. https://doi.org/10.1126/science.1160606

Rosenfeld D, Woodley WL (2000) Deep convective clouds with sustained supercooled liquid water down to -37.5 °C. Nature 405:440–442. https://doi.org/10.1038/35013030

Roxy MK, Ritika K, Terray P, et al (2015) Drying of Indian subcontinent by rapid Indian Ocean warming and a weakening land-sea thermal gradient. Nat Commun 6:7423. https://doi.org/10.1038/ncomms8423

Sarangi C, Tripathi SN, Kanawade VP, et al (2017) Investigation of the aerosol–cloud–rainfall association over the Indian summer monsoon region. Atmos Chem Phys 17:5185–5204. https://doi.org/10.5194/acp-17-5185-2017

Sayer AM, Hsu NC, Bettenhausen C, Jeong M-J (2013) Validation and uncertainty estimates for MODIS Collection 6 “Deep Blue” aerosol data. Journal of Geophysical Research: Atmospheres 118:7864–7872. https://doi.org/10.1002/jgrd.50600

Sheffield AM, Saleeby SM, Heever SC van den (2015) Aerosol-induced mechanisms for cumulus congestus growth. Journal of Geophysical Research: Atmospheres 120:8941–8952. https://doi.org/10.1002/2015JD023743

Singh D, Bollasina M, Ting M, Diffenbaugh NS (2019) Disentangling the influence of local and remote anthropogenic aerosols on South Asian monsoon daily rainfall characteristics. Clim Dyn 52:6301–6320. https://doi.org/10.1007/s00382-018-4512-9

Sunilkumar K, Yatagai A, Masuda M (2019) Preliminary Evaluation of GPM-IMERG Rainfall Estimates Over Three Distinct Climate Zones With APHRODITE. Earth and Space Science 6:1321–1335. https://doi.org/10.1029/2018EA000503

Tao W-K, Li X (2016) The relationship between latent heating, vertical velocity, and precipitation processes: The impact of aerosols on precipitation in organized deep convective systems. Journal of Geophysical Research: Atmospheres 121:6299–6320. https://doi.org/10.1002/2015JD024267

Textor C, Schulz M, Guibert S, et al (2006) Analysis and quantification of the diversities of aerosol life cycles within AeroCom. Atmos Chem Phys 37

Twomey S (1977) The Influence of Pollution on the Shortwave Albedo of Clouds. J Atmos Sci 34:1149–1152. https://doi.org/10.1175/1520-0469(1977)034<1149:TIOPOT>2.0.CO;2

Vinoj V, Rasch PJ, Wang H, et al (2014) Short-term modulation of Indian summer monsoon rainfall by West Asian dust. Nature Geoscience 7:308–313. https://doi.org/10.1038/ngeo2107

Vuille M, Francou B, Wagnon P, et al (2008) Climate change and tropical Andean glaciers: Past, present and future. Earth-Science Reviews 89:79–96. https://doi.org/10.1016/j.earscirev.2008.04.002

Wang S, Zhang M, Pepin NC, et al (2014) Recent changes in freezing level heights in High Asia and their impact on glacier changes. Journal of Geophysical Research: Atmospheres 119:1753–1765. https://doi.org/10.1002/2013JD020490

Webster PJ, Magaña VO, Palmer TN, et al (1998) Monsoons: Processes, predictability, and the prospects for prediction. Journal of Geophysical Research: Oceans 103:14451–14510. https://doi.org/10.1029/97JC02719

Wei J, Peng Y, Guo J, Sun L (2019) Performance of MODIS Collection 6.1 Level 3 aerosol products in spatial-temporal variations over land. Atmospheric Environment 206:30–44. https://doi.org/10.1016/j.atmosenv.2019.03.001

Willmott CJ, Matsuura K (2001) Terrestrial air temperature and precipitation: Monthly and annual time series (1950–1999) Version 1.02. Center for Climatic Research, University of Delaware, Newark

Xiao H, Yin Y, Chen Q, Zhao P (2016) Impact of aerosol and freezing level on orographic clouds: A sensitivity study. Atmospheric Research 176–177:19–28. https://doi.org/10.1016/j.atmosres.2016.02.014

Yadav S, Venezia RE, Paerl RW, Petters MD (2019) Characterization of Ice-Nucleating Particles Over Northern India. Journal of Geophysical Research: Atmospheres 124:10467–10482. https://doi.org/10.1029/2019JD030702

Zhang Y, Guo Y (2011) Variability of atmospheric freezing-level height and its impact on the cryosphere in China. Annals of Glaciology 52:81–88. https://doi.org/10.3189/172756411797252095

Chapter 3: Impact of transported dust aerosols on precipitation over the Nepal Himalayas using convection-permitting WRF-Chem simulation

This chapter of dissertation is based in full on the previously published article on *Atmospheric Environment: X*. I have permission from my co-authors and publishers to use this work in the dissertation.

Adhikari, P., Mejia, J.F., 2022. Impact of transported dust aerosols on precipitation over the Nepal Himalayas using convection-permitting WRF-Chem simulation. Atmospheric Environment: X 100179. https://doi.org/10.1016/j.aeaoa.2022.100179

3.1 Introduction

Natural and anthropogenic aerosols impact the regional weather and climate directly through aerosol-radiation and indirectly via aerosol-cloud interaction (IPCC, 2013). Numerous studies conducted around the globe have suggested that aerosol influences cloud properties and modulate regional precipitation in frequency and intensity (e.g., Dave et al., 2017; Koren et al., 2012; Li et al., 2011; Rosenfeld et al., 2008; Wu et al., 2018). During the Indian summer monsoon (June to September), the aerosol invigorates the cloud development and enhances the surface precipitation over the slopes/foothills of the central Himalayas (Adhikari and Mejia, 2021) and central northern India (Sarangi et al., 2017; Wang et al., 2009). Adhikari and Mejia (2021) also illustrated that the abundant aerosol loading increases the freezing level height over the Himalayan foothills and can be critical for the hydrometeors phase change and precipitation intensity, as suggested by Prein and Heymsfield (2020).

Mineral dust aerosol is a major contributor to the total global atmospheric aerosols due to the high emission rate (IPCC, 2013) and can be carried away over long distances (Dhital et al., 2021; Orza et al., 2020; Uno et al., 2009). Mineral dust significantly influences the vertical temperature distribution, convective processes, and the hydrological cycle due to its radiative and cloud-microphysical interaction (Choobari et al., 2014). The radiative effect of dust aerosols over the remote desert strengthens the moisture convergence and enhances the monsoonal precipitation over central and northern India on a sub-seasonal timescale (Jin et al., 2021, 2015; Lau et al., 2017; Vinoj et al., 2014). According to the Elevated Heat Pump (EHP) mechanism, a hypothesis proposed by Lau et al. (2006), absorbing aerosols such as dust aerosols from the remote deserts (Arabian Peninsula, North Africa, and north-western India) accumulate over the complex topography of the Himalayas and warm the atmospheric layer due to radiative heating. The dynamical feedback process due to the warming of the upper-tropospheric layer increases the north-south temperature gradient. It plays a significant role in strengthening the monsoonal circulation, resulting in a northward shift of early monsoonal precipitation to the foothills of the Himalayas (Lau et al., 2006, 2017; Lau and Kim, 2006).

In a shorter timescale, the modeling study by Fan et al. (2015) suggests that the radiative effect of absorbing aerosols (dust and carbonaceous) over the Sichuan Basin increases the upwind stability during the daytime. It allows more moisture to be transported downwind towards the mountain, which with the orographic lifting results in heavy precipitation during the nighttime over the mountainous region. Similarly, Choudhury et al. (2020) illustrated that the extreme precipitation events over the

Himalayan foothills are associated with the aerosol enhanced convective instability. Furthermore, mineral dust aerosols serve as both Cloud Condensation Nuclei (CCN) and ice-nucleating particles (INPs) and impact cloud microphysics due to their effective and stronger nucleating capacity (DeMott et al., 2015; Hoose and Möhler, 2012; Kanji et al., 2017). Several studies have shown that dust particles effectively initiate mixed-phase clouds with ice production and enhance surface precipitation (Fan et al., 2014; Zhang et al., 2020). Hazra et al. (2016) suggested that dust INPs are more effective than soot INPs in generating cloud ice particles, resulting in higher precipitation over the foothills of the Himalayas during the pre-monsoon season. The satellite-based observational and reanalysis study by Yuan et al. (2021) suggested that a dust storm might result in heavy rain due to dust-ice nuclei invigorating the deep clouds.

The foothills of the Himalayas and Indo-Gangetic Plain (IGP) encounters severe dust storm events during the pre and early monsoon season from April to June, mainly from the Arabian Peninsula and Thar desert over western India (S. Kumar et al., 2015; Prasad and Singh, 2007; Sarkar et al., 2019). Also, the multi-year simulation during the summer (June to August) by Sijikumar et al. (2016) suggests that the mineral dust aerosols distributed over the foothills of the Himalayas and IGP originate on the northwestern deserts of India. Over the foothills of Northwestern India, most of the previous studies using numerical simulation and observational data focused on the dynamics of dust storm origin and its impact on radiative forcing and air quality (e.g., Sarkar et al., 2019; Shukla et al., 2021; Srivastava et al., 2011). The strong wind gust and buoyancy during a severe thunderstorm event caused the dust outbreak over the Thar desert from 12th to 15th June 2018 and transported a significant amount of dust aerosols to

the central Himalayan region with north/northwesterly winds and is coincident with the precipitation event over Nepal (Pokharel et al., 2020). The onset of the summer monsoon season over Nepal occurred on the 8 June 2018, according to the Department of Hydrology and Meteorology (DHM), Nepal (http://www.dhm.gov.np/climate/).

In this study, we employ the high resolution (cloud-resolving) Weather Research and Forecasting (WRF) model coupled with Chemistry (WRF-Chem). The primary objective is to evaluate and quantify the impact of long-range transported dust aerosols associated with the Thar desert dust storm event (12-15 June 2018) on the precipitation and convective processes focusing on the southern slopes of Nepal Himalayas. The convection-permitting finer resolution (less than 4 km) with explicit microphysics option allows interactive processes between aerosols and cloud. Compared to parameterized convection, the cloud-resolving scale better simulates the evolution of cloud structures, optical properties, latent heat release, and vertical transport and mixing of moisture, heat, and aerosols (Prein et al., 2015; Tao and Matsui, 2015). This cloud-resolving study intends to provide new insights and advance our understanding of the influence of long-range transported dust aerosols in modulating the convection and precipitation processes over the mountainous region of the Central Himalayas. The rest of the article is organized as follows: Section 3.2 provides the description of the model setup and experimental design. In section 3.3, model results are presented and discussed. The conclusion of this study is summarized in section 3.4.

3.2 Methods and Data

3.2.1 Model setup and experiment design

The WRF-Chem model is capable of simulating the aerosol interaction with meteorology, radiation, and atmospheric feedback processes (Chapman et al., 2009; Fast et al., 2006). The WRF-Chem has been successfully used around the globe to study the locally emitted and remotely transported aerosol interaction with cloud and precipitation (e.g., Fan et al., 2015; Naeger, 2018; Sarangi et al., 2015; Wu et al., 2018; Zhang et al., 2021). In this study, we use the WRF-Chem model [version 4.1.5; Grell et al. (2005)] with two domains having horizontal grid resolution of 9 km (194 × 219 grid points) and a nested 3 km (273 × 333 grid points) domain. The topographical elevation with the model domain configuration is shown in **Fig. 3.1a**. The larger 9 km domain includes central India and Tibetan Plateau, while the inner 3 km domain includes IGP and all Nepal with lowlands and mountains to better characterize the orographic forcing. In the vertical, we used 71 layers from surface to 50 hPa. We integrated the model from 00 UTC 11th to 00 UTC 17th June 2018, corresponding all the lifetime, from onset to demise, of the dust storm (Pokharel et al., 2020) and the first 72 hours of simulation used as spin-up period.

The model configuration with the physical parameterizations implemented in this study is listed in **Table 3.1**. The model was initialized using the meteorological fields for initial and boundary conditions from ERA5, a recent reanalysis product by European Centre for Medium range Weather Forecasting (ECMWF), with hourly temporal and 31-km horizontal resolution. Other studies have used the hourly ERA5 reanalysis product adequately as boundary conditions (e.g., Barman and Gokhale, 2022; Sicard et al., 2021). A convective parameterization scheme was used for the outer 9km domain, while no cumulus parameterization was used for the inner 3km domain as the model explicitly resolves the convective eddies for these grid sizes. Also, CLM4 land-surface scheme has

been previously implemented in WRF-Chem in mountainous terrain (e.g., Sarangi et al. 2019; Wu et al. 2018).

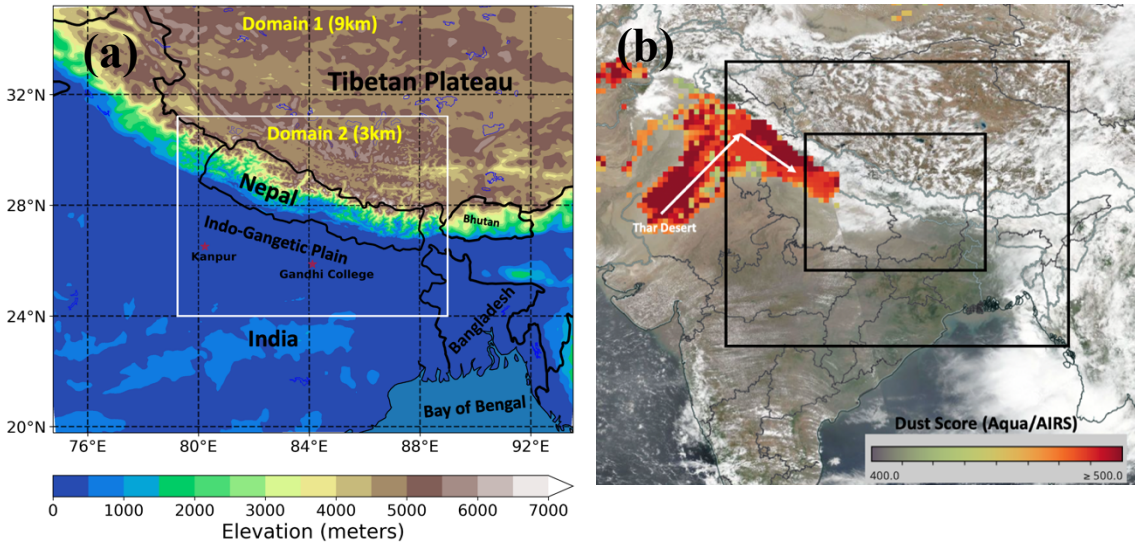

Figure 3.1: (a) The WRF-Chem domain configuration with terrain height. Red star labels Kanpur and Gandhi College corresponds to the AERONET sites. (b) MODIS/Terra reflectance image (June 15th, 2018) with an added layer of dust score from Atmospheric Infrared Sounder (AIRS) aboard MODIS/Aqua (https://worldview.earthdata.nasa.gov/). A dust score above 380 is considered as the presence of dust. Black boxes indicate the model domains.

Table 3.1: Model configuration.

Physics/Chemistry option	Scheme
Microphysics	Morrsion-2 moment (Morrison et al.,
Radiation	RRTMG (Iacono et al., 2008)
Land surface	CLM4 (Lawrence et al., 2011)
Planetary Boundary Layer (PBL)	YSU (Hong et al., 2006)
Cumulus	Grell-3D for 9 km (Grell and Dévényi, 2002); Cloud resolving (3km)
Meteorological boundary condition	ERA5 (31km, hourly)
Chemical boundary condition	CAM-Chem (0.9° × 1.25°, 6 hourly)
Aerosol mechanism	MOSAIC-4bin (Zaveri et al., 2008)
Chemical mechanism	CBMZ (Zaveri and Peters, 1999)
Anthropogenic Emission	EDGAR-HTAP v2.2 and EDGAR v4.3.2 (0.1°× 0.1° and monthly; (Janssens-Maenhout et al., 2015)
Biogenic Emission	MEGAN (Guenther et al., 2006)
Biomass burning emission	FINNv1.5 (Wiedinmyer et al., 2011)
RRTMG (Rapid Radiative Transfer Model for General Circulation Models); YSU (Yonsei University); CLM4 (Community Land Model Version 4); CBM-Z (Carbon Bond Mechanism); MOSAIC (Model for Simulating Aerosol Interactions and Chemistry); MEGAN (Model of Emissions of Gases and Aerosols from Nature; FINN (Fire Inventory from NCAR); GOCART (Goddard Chemistry Aerosol Radiative and Transport model); EDGAR-HTAP (Emission Database for Global Atmospheric Research-Hemispheric Transport of Air Pollutants)	

The anthropogenic emissions are used from the EDGAR-HTAP emission inventory, including black carbon, organic matter, particulate matter (PM2.5 and PM10), ammonia, sulfates, oxides of nitrogen, and carbon monoxide. The non-methane volatile organic compounds (NMVOC's) are used from the EDGARv4.3.2 emission inventory. In this study, the Carbon Bond Mechanism (CBM-Z; Zaveri and Peters, 1999), a photochemical

mechanism coupled with the Model for Simulating Aerosol Interactions and Chemistry (MOSAIC; Zaveri et al., 2008) aerosol module was used. We used the MOSAIC four sectional bin approach to represent the aerosol size distribution, where the aerosols are allotted to each bin (0.039-0.156 μm, 0.156-0.625 μm, 0.625-2.5 μm, and 2.5-10 μm) depending on the dry particle diameter. The particles within a bin are assumed to have the same chemical composition and are internally mixed, whereas particles from different bins are mixed externally (Zaveri et al., 2008). Furthermore, Zhao et al. (2013) suggested that dust mass loading and AOD are simulated reasonably well with a 4-bin approach in comparison to 8-bin sectional approach.

This current study simulates the long-range transported dust aerosols after the Thar dust storm event that started on June 12th, 2018. After the origin of the dust storm, the north/northwesterly wind transported a large amount of dust aerosols towards the IGP and southern slopes of the central Himalayas. The MODIS/Terra reflectance image of June 15th (**Fig. 3.1b**) with an added layer of the dust score from Atmospheric Infrared Sounder aboard MODIS/Aqua (https://worldview.earthdata.nasa.gov/) shows the transport path of the dust aerosols towards the central Himalayan region. In this study, we do not simulate the genesis of the dust storm. The source of dust aerosols in our domain is the dust plume originating from the Thar-Desert dust storm event-related concentrations that come through those as prescribed by the chemistry boundary conditions.

The initial and lateral boundary conditions for the chemical species were used from Community Atmosphere Model with Chemistry (CAM-Chem), having 0.9° × 1.25°

horizontal with 56 vertical levels and 6- hourly temporal resolution (Buchholz et al., 2019). CAM-Chem is a chemistry component of the Community Earth System Model (CESM) and is used for simulations of global tropospheric and stratospheric composition (Emmons et al., 2020). The meteorology in the CAM-Chem is driven by the Modern-Era Retrospective analysis for Research and Applications version 2 (MERRA-2) reanalysis product. Also, CAM-Chem includes the anthropogenic, biogenic, and fire emissions respectively from the inventories specified for Coupled Model Intercomparison Project round 6 (CMIP6), MEGAN version 2.1, and Fire Inventory from NCAR (Buchholz et al., 2019). The emission of dust aerosols in the CAM-Chem is computed online as the function of wind speed (Emmons et al., 2020). CAM-Chem has been adequately used as boundary condition for chemistry in WRF-Chem over India, including the Indo-Gangetic plain (e.g., Jat et al., 2021; Mogno et al., 2021).

We performed two different model simulations to assess the impact of transported dust aerosols on the precipitation processes. The first simulation is the control (CTL) run, where the dust aerosols are specified from the boundary condition file. The second simulation is the no dust run (ND), performed with a similar model configuration but excluding the dust aerosols transported into the model domain by setting the dust concentration from the boundary condition file to zero. No dust emission was simulated within the domain for both runs. A similar approach has been implemented to zero out the transported aerosols to study the impact of long range transported aerosols over the Sierra Nevada using WRF-Chem (Naeger, 2018; Wu et al., 2018). In both CTL and ND simulations, we also included other locally emitted and transported aerosols, including

the aerosols from anthropogenic, biogenic, and biomass burning sources, to better represent the composition of atmospheric aerosols. The aerosol radiative feedback, wet and dry deposition, aqueous-phase chemistry, and processes of nucleation, condensation, and coagulation are included in both the simulations.

3.2.2 Datasets

The simulated precipitation results were evaluated using the precipitation product from Integrated Multi-satellite Retrievals for Global Precipitation Measurement (GPM-IMERG). GPM-IMERG level-3 (version 06) data provides satellite precipitation retrievals at half-hourly temporal resolution and in a 0.1° × 0.1° spatial resolution (Huffman et al., 2019). The modeled Aerosol Optical Depth (AOD) is evaluated with the ground-based Aerosol Robotic Network (AERONET) AOD data from Kanpur and Gandhi College stations (shown in **Fig. 3.1a**).

The vertical extension of the dust plume was validated with the Cloud-Aerosol Lidar and Infrared Pathfinder Satellite Observation (CALIPSO) vertical feature mask (Vaughan et al., 2009). Furthermore, three hourly MERRA-2 reanalysis product (GMAO, 2015), at a horizontal resolution of 0.5° × 0.625° and 72 vertical levels, were used to compare the dust aerosols from boundary conditions and simulated output. The dust emission in MERRA2 is driven by wind, and Goddard Chemistry Aerosol Radiation and Transport coupled with the Goddard Earth Observing System model simulates the life cycle of the dust (Gelaro et al., 2017).

3.3 Results and Discussion

The mean of 72-hour (06-14:00 to 06-17:00 UTC) accumulated precipitation over the Nepal Himalayas from both the simulation run with (CTL) and without (ND) dust aerosols and differences (CTL-ND) are shown in **Fig. 3.2 (a, b, c)**. In this study, we focus on the southern slopes of the Nepal Himalayas, represented by the black box in **Fig. 3.2**, which is also the region with heavier precipitation in the domain. The area-averaged (enclosed by the black box in **Fig. 3.2**) hourly precipitation of the southern slopes from the simulation and half-hourly precipitation from GPM-IMERG is shown in **Fig. 3.3a**. Noticeably, both the simulations (CTL and ND) overestimated the precipitation compared to the satellite-based IMERG observation spatially over the higher terrains (**Fig. 3.2d, 3.2e**) and during the full simulation period (**Fig. 3.3a**). The discrepancy between the observation and model precipitation can also be associated with the uncertainties from the physical parametrizations, as the model is highly sensitive to the model configuration (e.g., Baró et al., 2015; Zhang et al., 2021). The overestimation of the simulated rainfall by WRF-Chem has also been indicated over the foothills and higher terrain of the Himalayas (Barman and Gokhale, 2022; R. Kumar et al., 2015; Sarangi et al., 2015) and mountainous region of Sierra Nevada (Wu et al., 2018). Also, it must be noted that the IMERG satellite product is at a coarser resolution than the model and uncertainties of IMERG can underrepresent the concentrated precipitating events over the complex terrain, increasing the discrepancies. For example, Sharma et al. (2020b, 2020a) suggested that the IMERG products tend to underestimate the orographic precipitation over the Nepal Himalayas compared to the in situ observational network of

rain gauge stations. However, the **Fig. 3.3a** shows the area averaged simulated hourly precipitation from both runs generally follows the GPM-IMERG diurnal bimodal distribution pattern. The bimodal diurnal cycle of precipitation during the monsoon over the Nepal Himalayas has also been observed by Fujinami et al. (2021) and suggested that the daytime peak is due to the upslope flows with surface heating. In contrast, the nighttime precipitation maxima are associated with the convergence of downslope winds with the low-level monsoonal flow towards the mountains.

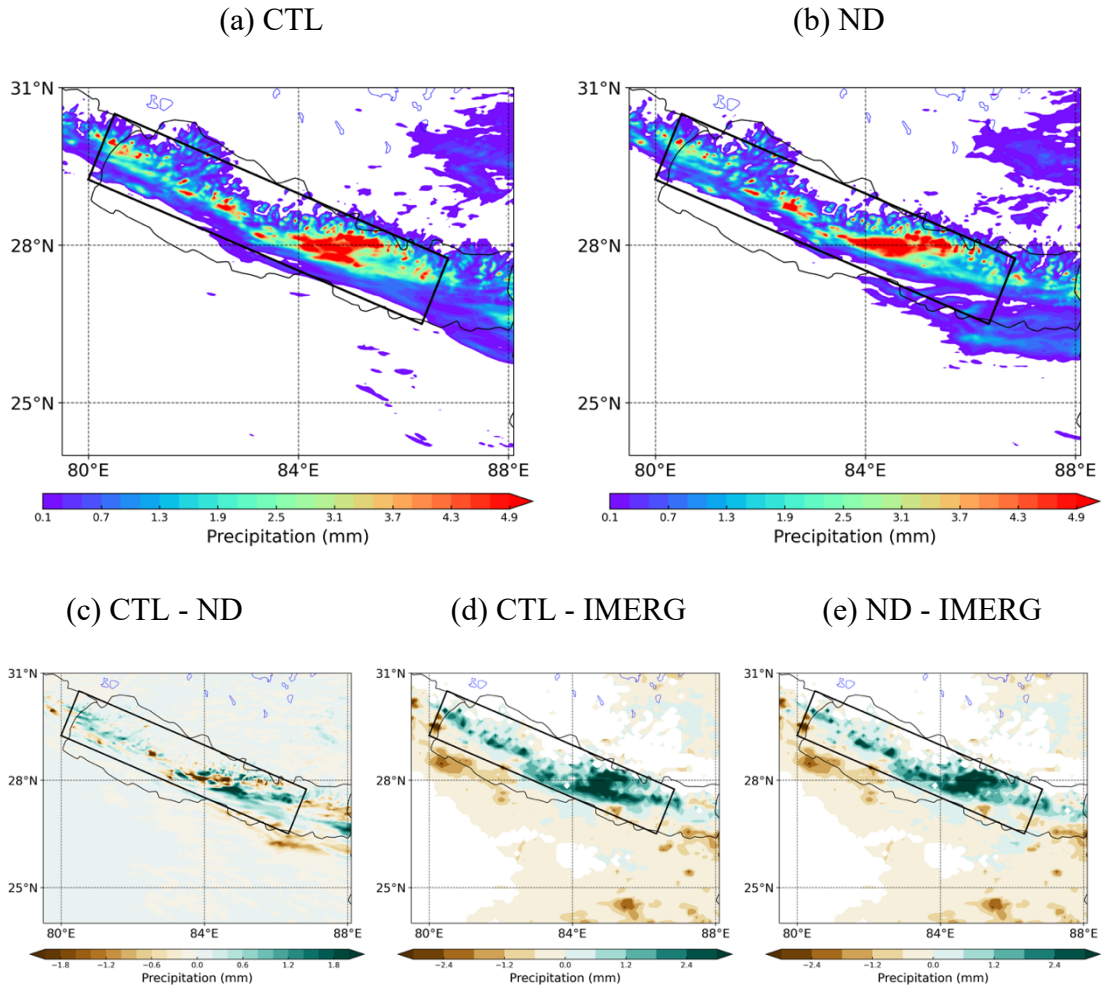

Figure 3.2: The 72-hour (06-14:00 to 06-17:00 UTC) mean precipitation for (a) CTL and (b) ND run, and the precipitation differences between (c) CTL - ND, (d) CTL – IMERG, and (e) ND - IMERG. The domain 2 model precipitation output is re-gridded to 10 km resolution to compare with the IMERG spatial resolution using the bilinear interpolation method. The area enclosed by the black box represents the southern slopes of the central Himalayas and our area of interest.

Though only a few data points are available for comparison (**Fig. C3S1**), in the presence of dust, simulated AOD correlates well (R-squared 0.69 at 99% significance level) with a ground-based AERONET AOD observed at Gandhi College and Kanpur stations. **Figure 3.4** compares the spatial distribution of column integrated dust

concentration between the MERRA-2 reanalysis product and WRF-Chem. The WRF-Chem overestimated the columnar dust concentration mainly over the south of Nepal compared to the MERRA2 reanalysis product. As expected, the columnar dust concentration in both products is largely accumulated over the Northwestern part of the domain, which is in the transport path and closest to the location of storm outbreaks. Also, the WRF-Chem with the finer resolution emphasized the topographical feature and depicted the elevational gradient of dust distribution due to the limited transport caused by a higher barrier of the Himalayas, which is absent in the MERRA-2 due to the coarser resolution. Compared to the MERRA-2, the WRF-Chem overestimated the average column integrated dust load over the inner domain by 4.5% (not shown). The bias in the dust concentration can be associated with the overestimation of the dust emissions in the CAM-Chem (Emmons et al., 2020) or the underestimation in the MERRA-2 compared to satellite observation due to the partial representation of the dust sources (Gkikas et al., 2021). However, the WRF-Chem captured the spatial distribution of dust plumes compared to the spatial distribution of the coarser-resolution MERRA-2 reanalysis product. The large plume of dust entered our area of interest with the northwesterly wind (**Fig. 3.4**) and contributed to a substantial rise of AOD after around 14:00 LST on June 15th (**Fig. 3.3b**). Before the arrival of the dust plume, the AOD over the southern slopes generally remained similar between the CTL and ND run and is contributed mainly by the anthropogenic aerosols. After the arrival of the dust plume at around 1400 LST, the AOD increases for the CTL run abruptly compared to the ND run. The dust aerosols are present over the southern slopes below 550 hPa with a maximum concentration at around 750 hPa and are heavily present after 1400 LST, June 15th (**Fig. 3.3c)**. Hereafter, we

focus our analysis on the southern slopes and the period after the arrival of the dust plume. Of note is that precipitating pixels during this 40-hour dusty period (precipitation > 0 mm) and over the southern slopes increased by 9.31% for the CTL simulations (80.7 mm) relative to the ND (73.8 mm).

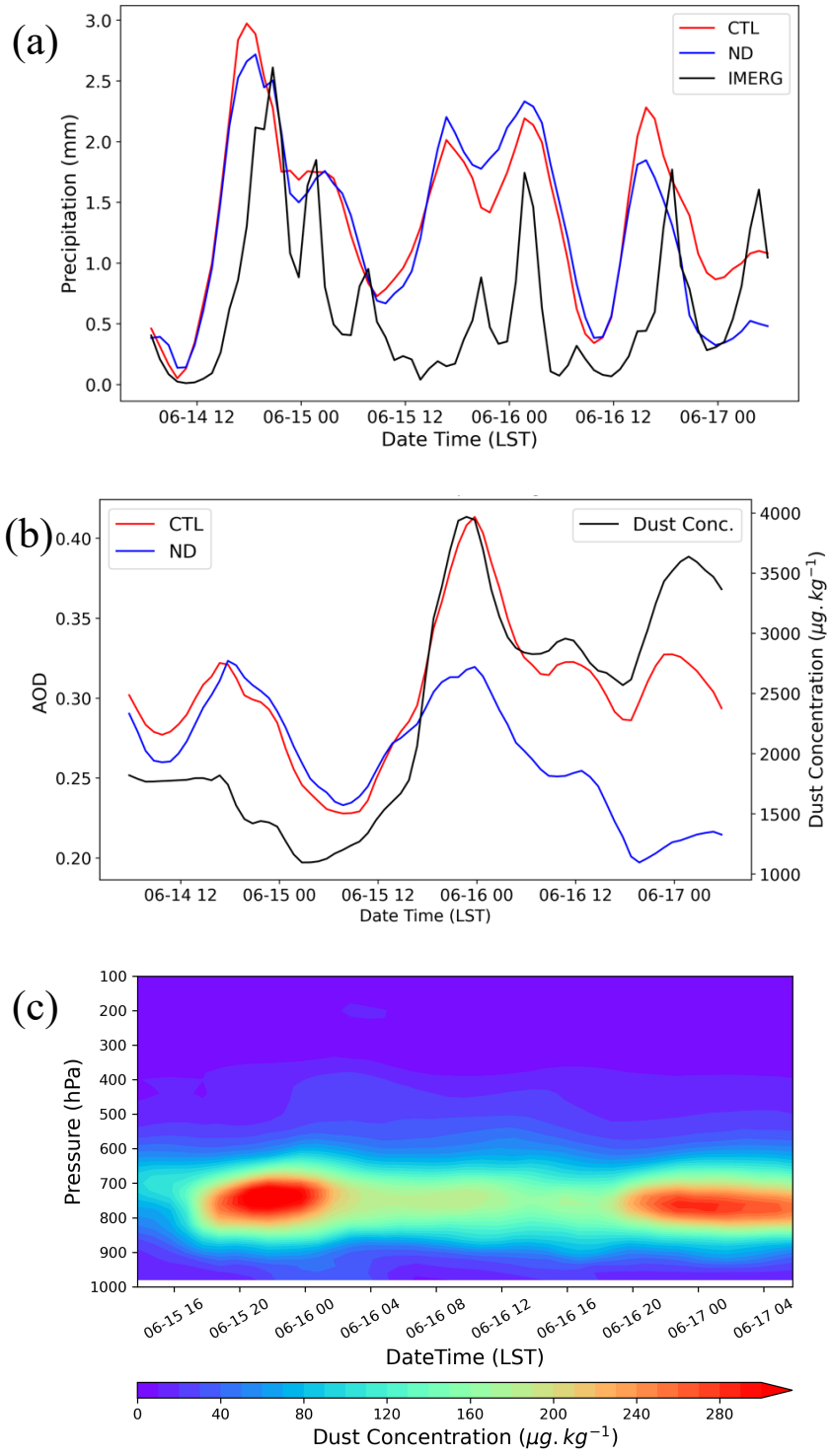

Figure 3.3: Timeseries of area averaged (enclosed by the black box in Fig. 3.2) of (a) hourly simulated and IMERG precipitation, (b) column integrated AOD and Dust

Concentration, for different runs over the southern slopes, (c) time series of vertically distributed area-averaged dust concentration over the southern slopes.

MERRA-2 WRF-Chem

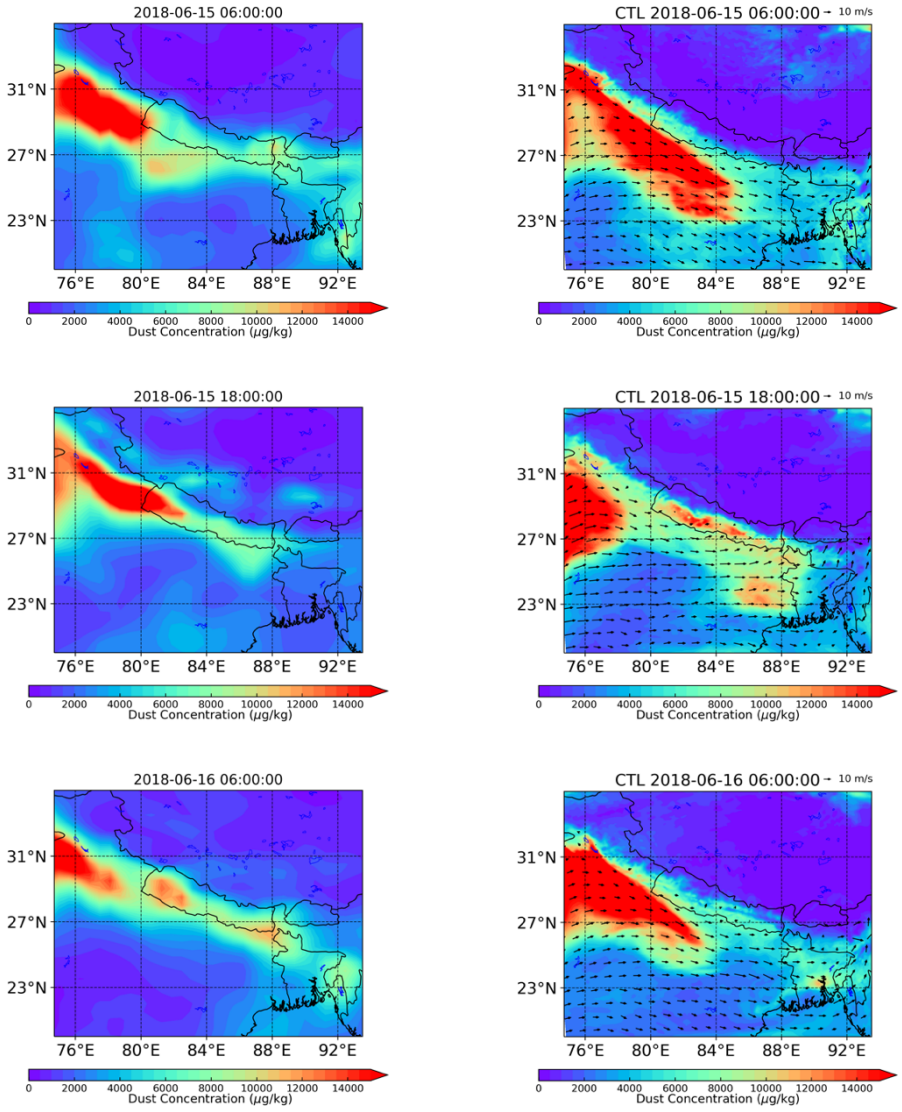

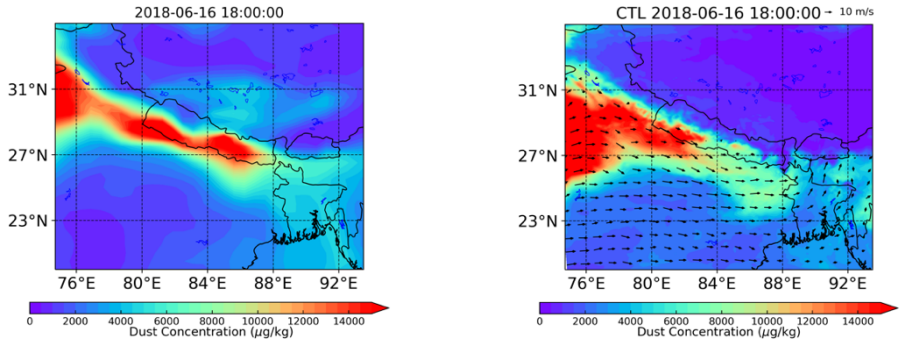

Figure 3.4: Spatial distribution of column integrated dust concentration from MERRA-2 reanalysis product (first column), CTL simulation for outer 9 km domain with 850 hPa wind vectors (second column).

Fig. 3.5a presents the vertical distribution of aerosol classification captured by the CALIPSO at 2030 UTC on June 15th. The mixture of mineral dust and polluted dust (mixed with the component of the urban pollution) has been stretched out to about 6 km over 25.13°N and 80.46°E. **Fig. 3.5b** shows that the dust plume is confined below ~ 5.5 km in the CTL simulation, approximately at the location as captured by the CALIPSO vertical feature mask. Comparing the vertical distribution of dust aerosols between the CALIPSO and simulated results indicates that the model reasonably simulated the vertical extension of dust aerosols.

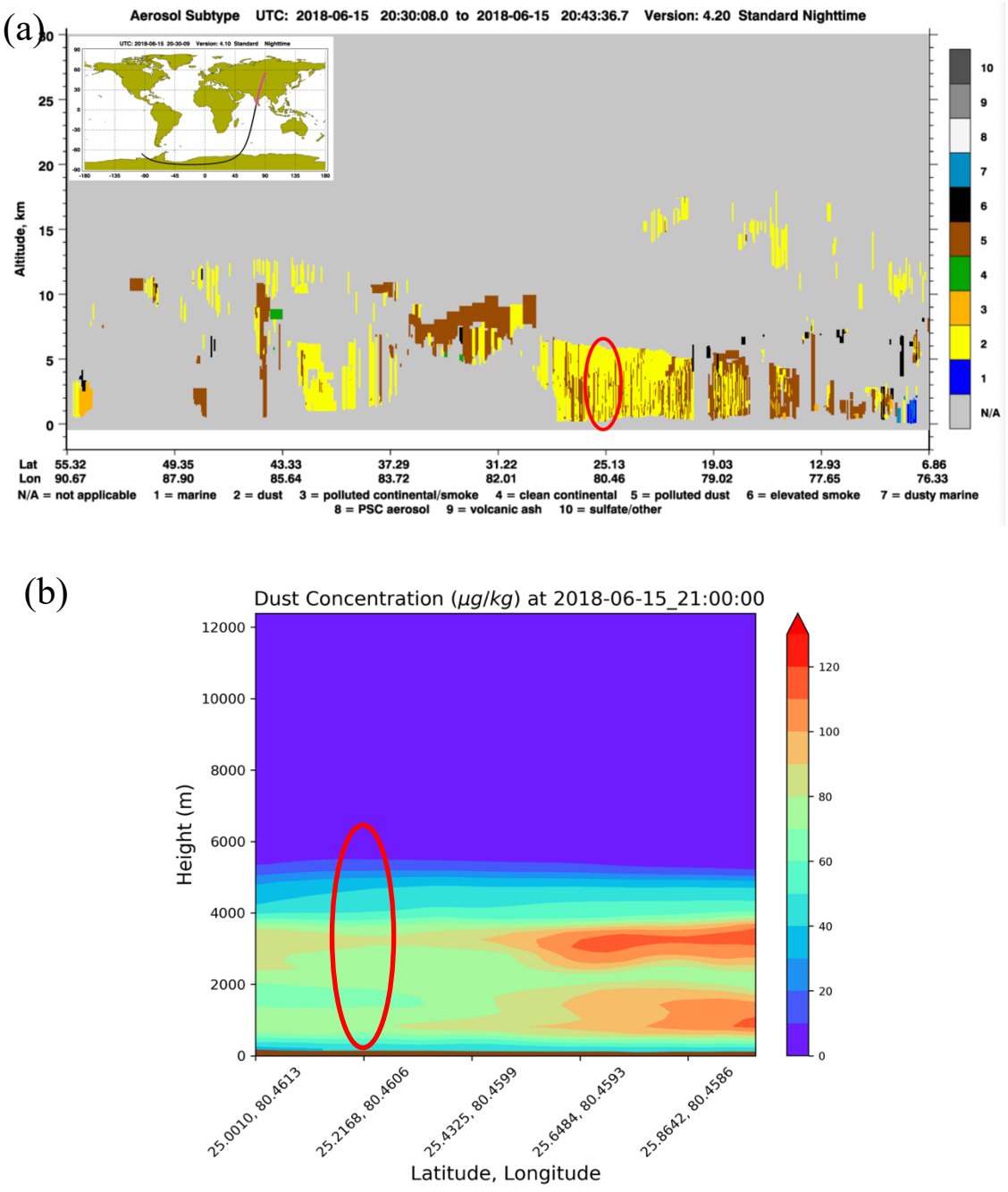

Figure 3.5: (a) Vertical distribution of aerosol subtype from CALIPSO overpass (inset image) over model domain 2. (b) Vertical distribution of dust concentration approximately at the same location as spotted in CALIPSO overpass. The red oval indicates the time-location for comparison between model output and CALIPSO image.

3.3.1 Direct aerosol forcing

The time variation of surface fluxes, temperature, and PBL height for the clear sky pixels (total cloud hydrometeors < 10^{-6} kg/kg; e.g., Fan et al., 2014; Huang et al., 2019), over the lower elevation (terrain height < 500 meters) where the dust concentration is higher are shown in **Fig. 3.6 (a-e)**. The scattering and absorption of solar radiation by dust aerosols limit the amount of shortwave radiation reaching the surface during the day (**Fig. 3.6a**). The net negative radiative forcing at the surface during the day is due to the attenuated incoming shortwave solar radiation (-26 W m^{-2}), which is negligibly compensated by surface downward longwave radiation (+2 W m^{-2}; not shown). The reduced solar radiation resulted in a lower surface temperature (maximum up to -3 °C) during the daytime compared to the ND run (**Fig. 3.6b**). The cooling of the surface during the daytime resulted in diminished mean sensible and latent heat fluxes (**Fig. 3.6c and 3.6d**). The negative surface radiative forcing and the cooling of the surface due to the dust-radiation interaction are also evident in different parts of the world (e.g., Huang et al., 2019; Kedia et al., 2018; Mamun et al., 2021). Consistent with our findings, the reduction of the surface fluxes due to the dust-radiative forcing has also been simulated in a season-long WRF-Chem model run over west Africa (Saidou Chaibou et al., 2020). Furthermore, the CTL simulated the significant reduction of daytime PBL height (11:00 - 15:00 LST) by 123 meters (12%) compared to the ND run (**Fig. 3.6e**). The dust-radiation interaction resulted in the shallow cooling in the boundary layer and warming of the mid-troposphere due to the solar radiation absorption (**Fig. C3S2**), which stabilized and lowered the boundary layer height and reduced heat flux transport.

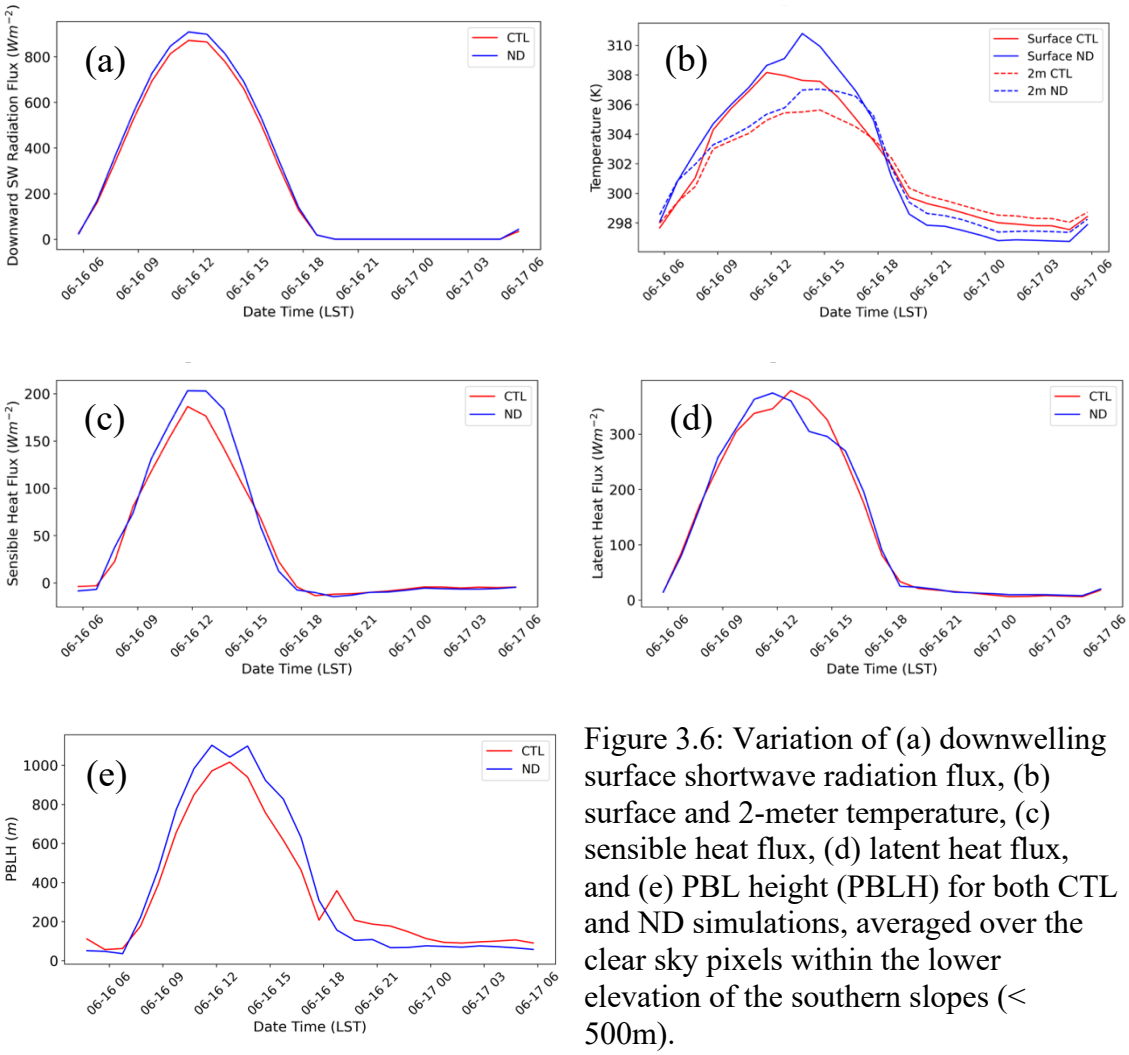

Figure 3.6: Variation of (a) downwelling surface shortwave radiation flux, (b) surface and 2-meter temperature, (c) sensible heat flux, (d) latent heat flux, and (e) PBL height (PBLH) for both CTL and ND simulations, averaged over the clear sky pixels within the lower elevation of the southern slopes (< 500m).

3.3.2 Indirect aerosol forcing

Fig. 3.7 shows the time and spatially averaged CTL and ND run AOD and precipitation over the different altitudinal ranges. For the topographical altitude less than 500 meters, the increase in AOD is higher by 37% for the CTL with a contribution from the remotely transported dust aerosols (**Fig. 3.7a**). While over the mountainous slopes (between 500 and 3000 meters), the AOD change between CTL and ND is 23.3%. On the

other hand, the mean CTL precipitation is enhanced by 9.6% over the higher terrains, while lower elevation (< 500 meters) only observed the 3% increase compared to the ND run (**Fig. 3.7b**). The comparison of the CTL and ND run over the different altitudinal ranges indicates that the impact of the remote dust aerosols is higher on the mountain precipitation compared to a lower elevation. Similar enhancement of the precipitation due to the long-range transported dust aerosols have been reported over the windward slopes of the mountain ranges of Taiwan (Zhang et al., 2020) and Sierra Nevada (Naeger, 2018). (Naeger, 2018) suggested that the efficient activation of dust aerosols as condensation nuclei resulted in a higher amount of cloud water over the windward slopes, resulting in the enhanced snow accretion process and precipitation over the higher terrain. The impact of dust aerosols on the convective processes and clouds over the southern slopes of the Himalayas is apparent.

The difference between the CTL and ND time-series of the area-averaged vertical profiles of water vapor mixing ratio and convective updraft mass flux (density × vertical velocity) for the precipitating pixels is shown in **Fig. 3.8**. After the morning of June 16th, the convection for the CTL run intensified with the higher low-level water vapor and stronger updraft mass flux. The dust aerosols activated as the cloud droplets (**Fig C3S3**) and higher vertical velocity further intensified convective processes. The increase of aerosol concentration in the moist environment has a more significant effect on the cloud properties by enhancing the release of latent heat of condensation, increasing collision-coalescence efficiency, the early invigoration of mixed-phase cloud, and increasing the amount of supercooled liquid water (Fan et al., 2007; Gayatri et al., 2022).

The time-varying water vapor mixing ratio over the foothills exhibited by the model (**Fig. 3.8**) might be due to the mesoscale feedback processes of aerosol radiative effect, moisture flux convergence, and aerosol-indirect effect. The variability in low-level (850 hPa) winds, probably associated with the dust-radiative impact, modulated the moisture flux at different periods (**Fig. C3S4**) over the foothills of the Himalayas. The solar dimming effect due to dust-radiation interaction and suppressed convection over the lowland strengthens the low-level moisture convergence over the downwind mountainous region (Choudhury et al., 2020; Fan et al., 2015). The reduced low-level moisture on the afternoon/night of the 15th resulted in the suppression of precipitation (**Fig. 3.8)**. Due to the depleted moisture supply and higher aerosols concentration, the water vapor competition increases among the activated cloud droplets and reduces droplet growth due to inefficient coalescence (Fan et al., 2007). Of note is that the aerosol loading from other sources, including dust, is higher during this period (**Fig. 3.3b**), increasing the competition for moisture. Moreover, due to the warming of the dusty layer and reduced relative humidity, the smaller droplets are more likely to evaporate. This distinct impact of dust aerosol on the variable moisture supply is consistent with the other satellite-based observational study in Mongolia (Zhao et al., 2022) and southern India (Kuriakose et al., 2022). The moisture distribution in the presence of dust aerosols explains the precipitation responses; however, the relative importance of the processes responsible for the variation in water vapor mixing ratio over the foothills requires further exploration.

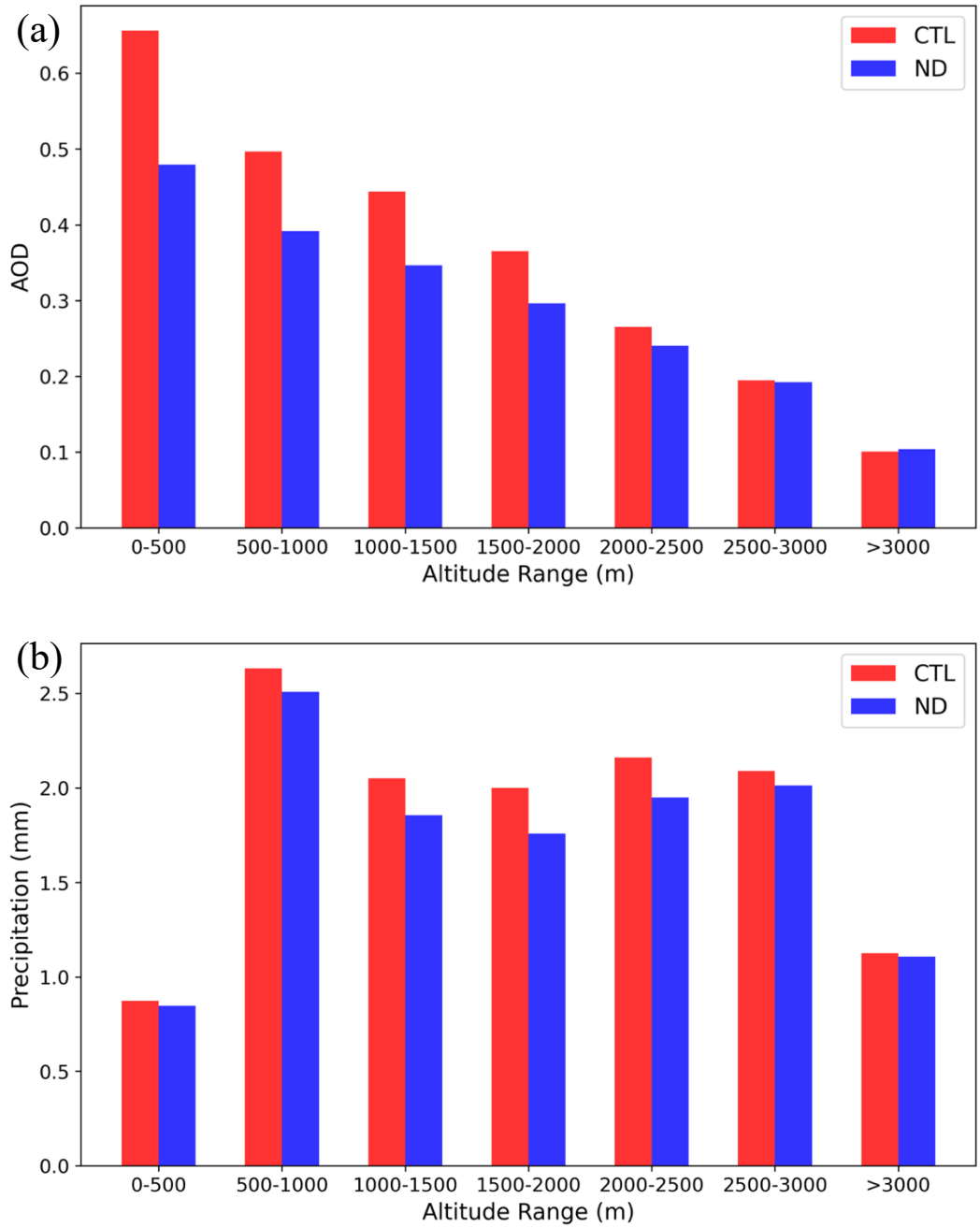

Figure 3.7: Area and time averaged (a) AOD and (b) precipitation of precipitating pixels for the altitudinal range over the southern slopes (area enclosed by the black box in Fig.3.2).

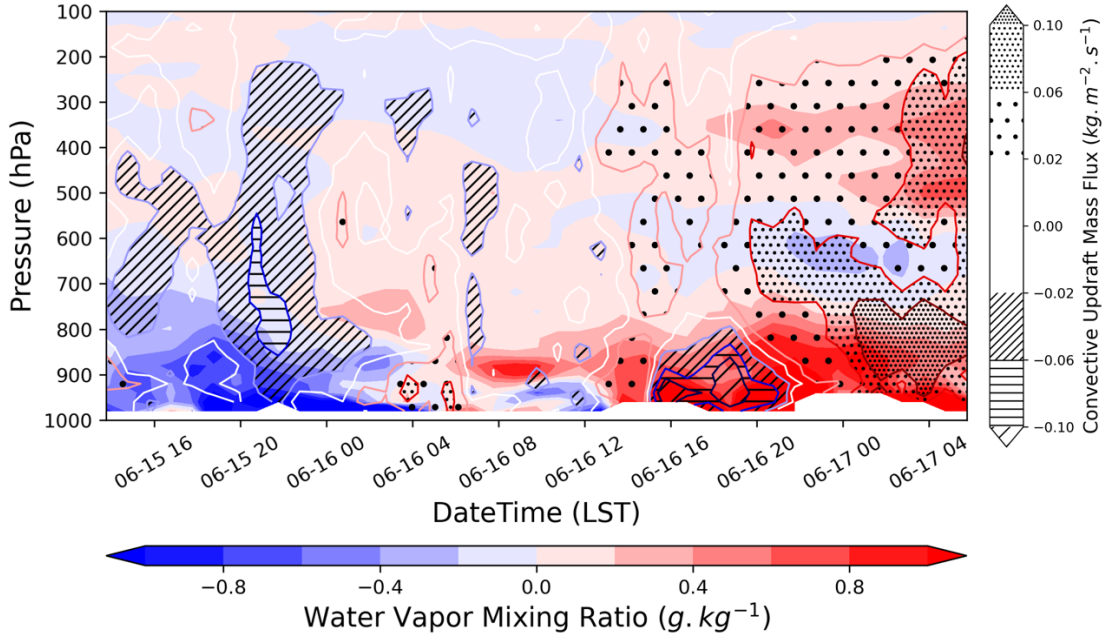

Figure 3.8: Time series of vertical profiles of the differences (CTL - ND) of water vapor mixing ratio (shaded) and convective updraft mass flux for ω > 0 ms-1 (contour with hatched) averaged among precipitation grids over the southern slopes (area enclosed by the black box in Fig. 3.2).

Fig. 3.9 shows the vertical profiles of the time and area-averaged (area enclosed by the black box in Fig. 3.2) vertical velocity, latent heat rate, condensation rate, and cloud fraction for the precipitating pixels over the southern slopes. The variation in the condensation and latent heat rate in the presence of dust aerosols modifies the buoyancy and cloud structure enhancing the intensity of convection. The condensation rate is observed to be maximum between 750hPa and 600hPa, consistent with the presence of the dust aerosols (**Fig. 3.9c**). The increased vertical velocity and stronger convection intensity for the CTL run are associated with the enhanced latent heat release with the increasing condensation rate (enhanced by 10%). The mean latent heat release for the CTL run is higher by 15% (**Fig. 3.9b**), which resulted in the enhanced updraft vertical

velocity by 13% compared to the run without dust aerosols (**Fig. 3.9a**). The higher release of freezing latent heat in the CTL run with dust aerosols above the freezing level resulted in enhanced vertical velocity, further invigorating the convection. Furthermore, when taking the dust aerosols into account, the mean cloud fraction increased by 4.1% (**Fig. 3.9d**) compared to the ND run. The increase in cloud coverage due to dust aerosols is consistent with the findings of other studies (Small et al., 2011; Zhang et al., 2021), and is driven by microphysical properties and thermodynamic invigoration (Fan et al., 2013). The rate of change in cloud cover can also be altered by the dynamic and meteorological conditions as well as the size distribution of aerosols (Small et al., 2011). The intensification of the convection with stronger vertical motion in the presence of the dust aerosols is consistent with the findings of previous cloud-resolving WRF modeling studies (e.g., Huang et al., 2019; Zhang et al., 2021).

The mean freezing level altitude for the CTL run is higher by 58.5 meters compared to the ND run, which might relate to the combined result of the radiative and microphysical impact of the dust aerosols. Though this result is based on one short-term case study, rise of 10 meter summer FLH can be crucial for snowpack melting and increased snowline altitude over the Himalayas in the long term (Wang et al., 2014). After isolating the weather, Adhikari and Mejia (2021) found that the freezing level height increased by 136 meters over the Central Himalayan region during an enhanced polluted environment (accounting for the total atmospheric aerosols) compared to a relatively pristine environment, comparable to our findings. Since our simulations isolated the role of dust aerosols alone from other aerosols, it is possible that the

tropospheric warming by the total atmospheric aerosols is more extensive, as indicated by (Adhikari and Mejia, 2021), than our simulated warming signal.

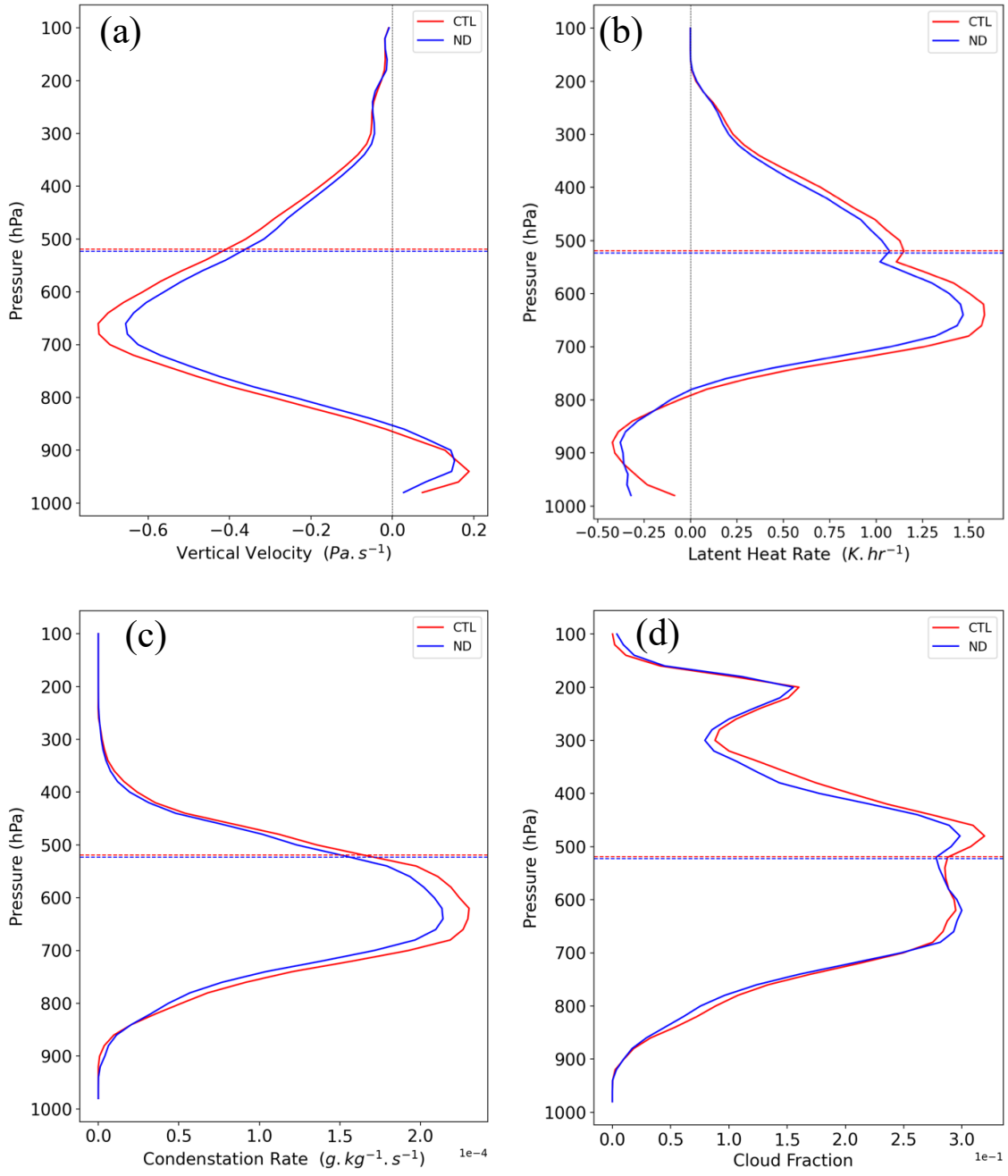

Figure 3.9: Vertical profiles of (a) vertical velocity, (b) Latent heating rate, (c) condensation rate, and (d) cloud fraction over the precipitating pixels of southern slopes (area enclosed by the black box in Fig. 3.1). The horizontal dotted lines represent the mean freezing level altitude (red for CTL and blue for ND).

Furthermore, we compare the vertical distribution of simulated cloud hydrometeors over the southern slopes of the Himalayas between the CTL and ND simulations. The averaged vertical profiles of different hydrometeors (cloud, droplet, rain, ice, snow, and graupel) for precipitating pixels over the southern slopes are shown in **Fig. 3.10**. The area-averaged droplet number concentration increased by 18%, and the difference is maximum at around the same altitude with maximum dust aerosols (**Fig. 3.10a**). The fewer but larger droplets in the ND run can effectively enhance the rain production over the foothills. However, an increased number of smaller droplets allows more cloud water to transport downwind over the elevated mountainous terrain resulting in enhanced cloud ice formation and orographic precipitation. Also, the mean ice water path for the dust run increased respectively by 13% (not shown) compared to the ND run, resulting in the thicker and colder clouds (mean cloud top temperature reduced by 5%). The increased condensation rate and the convection in the CTL run resulted in the higher number concentration (**Fig. 3.10b**) and enhanced mass mixing ratio (**Fig. 3.10c**) of different cloud hydrometeors including rain, ice, snow, and graupel. Furthermore, the supercooled liquid water concentration in a CTL run increased by 19% (not shown) compared to the ND run. The sustained and enhanced supercooled liquid water in the presence of the dust aerosol enhances the production of snow and graupel mass in mixed-phase orographic cloud processes (Choudhury et al., 2019; Fan et al., 2017). The growth of ice and snow particles further intensifies the convection with latent heat release and enhances the precipitation. The amplified precipitation over the elevated terrain due to the presence of long-range transported dust aerosols as a result of deeper and colder

clouds has also been reported in previous studies (e.g., Creamean et al., 2013; Fan et al., 2014).

The parameterization schemes associated with aerosols activation as INPs are lacking in the current WRF-Chem model. Therefore, the simulations in this study might have underestimated a complete assessment of the impact of dust aerosols on cold cloud processes and accumulated precipitation. Dust aerosols are considered efficient INPs (Kanji et al., 2017) and can contribute to an increased number of ice concentrations in the presence of sufficient moisture resulting in enhanced precipitation (Ault et al., 2011; Creamean et al., 2013). Also, though our simulation better represented the topography using the 3km resolution, it might be relatively coarser for the steep terrain of the Himalayas and poorly resolve the mountain-valley circulation and orographic forcing.

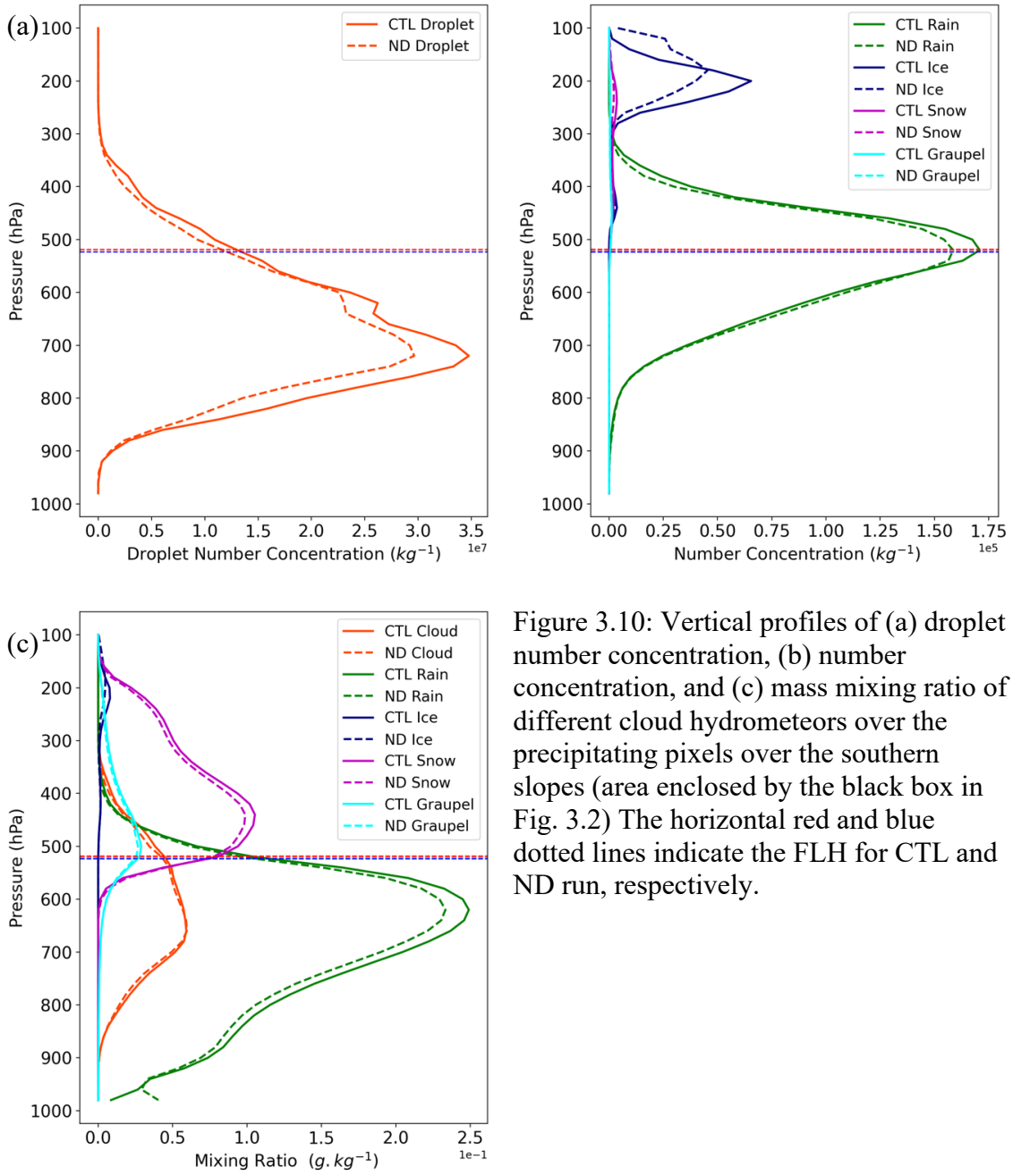

Figure 3.10: Vertical profiles of (a) droplet number concentration, (b) number concentration, and (c) mass mixing ratio of different cloud hydrometeors over the precipitating pixels over the southern slopes (area enclosed by the black box in Fig. 3.2) The horizontal red and blue dotted lines indicate the FLH for CTL and ND run, respectively.

3.4 Summary and Conclusions

This study highlights the impact of long-range transported dust aerosols on the precipitation and convective processes over the southern slopes of Nepal Himalayas. Though we do not know the overall seasonal effects of a severe Thar desert dust storm on the monsoon, Thar desert contributes a significant amount of mineral dust aerosols to the IGP and foothills of the Himalayas during the summer-monsoonal (June-August) season (Sijikumar et al., 2016). The dust storm event that occurred (12-15 June 2018) over the Thar desert transported a substantial amount of dust aerosols towards the central Himalayan region. In this case study, two different sensitivity runs are simulated, with and without transported dust aerosols, implementing the cloud-resolving scale (3km horizontal resolution) WRF-Chem model. We isolated the transported dust aerosols by zeroing out dust aerosols from lateral boundary conditions. The composition of atmospheric aerosols is effectively represented in this study by including the species of aerosols from anthropogenic, biogenic, and biomass burning sources that are locally emitted and remotely transported in both simulations.

The inclusion of the transported dust aerosols into the model domain enhanced the precipitation by 9.3% over the southern slopes of the Nepal Himalayas. In the presence of dust aerosols, precipitation is enhanced by 9.6% over the higher terrains (500 to 3000 meters), while the total accumulated precipitation increased by 3% over the lower elevation (< 500 meters). The total accumulated precipitation has been highly impacted over the higher terrains of the Nepal Himalayas than the lower elevation due to the transported dust aerosols. Furthermore, a significant increase in droplet concentration at

around 700 hPa in the CTL run indicates more dust aerosols activated as CCN, resulting in enhanced upward velocity with the release of latent heat of condensation. In the presence of higher low-level moisture, the enhanced cloud water mixing ratio with a higher updraft facilitated snow and raindrop growth, resulting in higher precipitation.

The result of our study indicates that the remote dust aerosols play a significant role in modulating the convective processes, microphysical properties of the cloud, and precipitation over the Nepal Himalayas. Though we only investigated one case study, these results complement the satellite-based observational findings of Adhikari and Mejia (2021), which suggests that total atmospheric aerosols enhance the precipitation and freezing isotherm during the polluted days over the central Himalayas compared to a relatively cleaner environment. Our results underline the need for a better representation of terrain-induced convective processes to understand further and quantify the complete impact of aerosol on cloud microphysics and precipitation over complex topography such as the Himalayas, which are challenging to resolve in coarser resolution numerical models. Furthermore, simulating additional case studies with the inclusion of aerosol effects on ice clouds under different environmental and meteorological conditions will provide better insight and quantification of the impact of dust aerosols in convective processes over the Himalayas.

References

Adhikari, P., Mejia, J.F., 2021. Influence of aerosols on clouds, precipitation and freezing level height over the foothills of the Himalayas during the Indian summer monsoon. Clim Dyn 57, 395–413. https://doi.org/10.1007/s00382-021-05710-2

Ault, A.P., Williams, C.R., White, A.B., Neiman, P.J., Creamean, J.M., Gaston, C.J., Ralph, F.M., Prather, K.A., 2011. Detection of Asian dust in California orographic precipitation. Journal of Geophysical Research: Atmospheres 116. https://doi.org/10.1029/2010JD015351

Barman, N., Gokhale, S., 2022. Aerosol influence on the pre-monsoon rainfall mechanisms over North-East India: A WRF-Chem study. Atmospheric Research 268, 106002. https://doi.org/10.1016/j.atmosres.2021.106002

Baró, R., Jiménez-Guerrero, P., Balzarini, A., Curci, G., Forkel, R., Grell, G., Hirtl, M., Honzak, L., Langer, M., Pérez, J.L., Pirovano, G., San José, R., Tuccella, P., Werhahn, J., Žabkar, R., 2015. Sensitivity analysis of the microphysics scheme in WRF-Chem contributions to AQMEII phase 2. Atmospheric Environment 115, 620–629. https://doi.org/10.1016/j.atmosenv.2015.01.047

Buchholz, R.R., Emmons, L.K., Tilmes, S., The CESM2 Development Team, 2019. CESM2. 1/CAM-chem instantaneous output for boundary conditions. UCAR/NCAR-Atmospheric Chemistry Observations and Modeling Laboratory. https://doi.org/10.5065/NMP7-EP60

Chapman, E.G., Jr, W.I.G., Easter, R.C., Barnard, J.C., Ghan, S.J., Pekour, M.S., Fast, J.D., 2009. Coupling aerosol-cloud-radiative processes in the WRF-Chem model: Investigating the radiative impact of elevated point sources. Atmos. Chem. Phys. 20.

Choobari, O.A., Zawar-Reza, P., Sturman, A., 2014. The global distribution of mineral dust and its impacts on the climate system: A review. Atmospheric Research 138, 152–165. https://doi.org/10.1016/j.atmosres.2013.11.007

Choudhury, G., Tyagi, B., Singh, J., Sarangi, C., Tripathi, S.N., 2019. Aerosol-orography-precipitation – A critical assessment. Atmospheric Environment 214, 116831. https://doi.org/10.1016/j.atmosenv.2019.116831

Choudhury, G., Tyagi, B., Vissa, N.K., Singh, J., Sarangi, C., Tripathi, S.N., Tesche, M., 2020. Aerosol-enhanced high precipitation events near the Himalayan foothills. Atmospheric Chemistry and Physics 20, 15389–15399. https://doi.org/10.5194/acp-20-15389-2020

Creamean, J.M., Suski, K.J., Rosenfeld, D., Cazorla, A., DeMott, P.J., Sullivan, R.C., White, A.B., Ralph, F.M., Minnis, P., Comstock, J.M., Tomlinson, J.M., Prather, K.A., 2013. Dust and Biological Aerosols from the Sahara and Asia Influence Precipitation in the Western U.S. Science 339, 1572–1578. https://doi.org/10.1126/science.1227279

Dave, P., Bhushan, M., Venkataraman, C., 2017. Aerosols cause intraseasonal short-term suppression of Indian monsoon rainfall. Scientific Reports 7, 1–12. https://doi.org/10.1038/s41598-017-17599-1

DeMott, P.J., Prenni, A.J., McMeeking, G.R., Sullivan, R.C., Petters, M.D., Tobo, Y., Niemand, M., Möhler, O., Snider, J.R., Wang, Z., Kreidenweis, S.M., 2015. Integrating laboratory and field data to quantify the immersion freezing ice nucleation activity of mineral dust particles. Atmospheric Chemistry and Physics 15, 393–409. https://doi.org/10.5194/acp-15-393-2015

Dhital, S., Kaplan, M.L., Orza, J.A.G., Fiedler, S., 2021. Poleward transport of African dust to the Iberian Peninsula organized by a barrier jet and hydraulic jumps: Observations and high-resolution simulation analyses. Atmospheric Environment 261, 118574. https://doi.org/10.1016/j.atmosenv.2021.118574

Emmons, L.K., Schwantes, R.H., Orlando, J.J., Tyndall, G., Kinnison, D., Lamarque, J.-F., Marsh, D., Mills, M.J., Tilmes, S., Bardeen, C., Buchholz, R.R., Conley, A., Gettelman, A., Garcia, R., Simpson, I., Blake, D.R., Meinardi, S., Pétron, G., 2020. The Chemistry Mechanism in the Community Earth System Model Version 2 (CESM2). Journal of Advances in Modeling Earth Systems 12, e2019MS001882. https://doi.org/10.1029/2019MS001882

Fan, J., Leung, L.R., DeMott, P.J., Comstock, J.M., Singh, B., Rosenfeld, D., Tomlinson, J.M., White, A., Prather, K.A., Minnis, P., Ayers, J.K., Min, Q., 2014. Aerosol impacts on California winter clouds and precipitation during CalWater 2011: local pollution versus long-range transported dust. Atmospheric Chemistry and Physics 14, 81–101. https://doi.org/10.5194/acp-14-81-2014

Fan, J., Leung, L.R., Rosenfeld, D., Chen, Q., Li, Z., Zhang, J., Yan, H., 2013. Microphysical effects determine macrophysical response for aerosol impacts on deep convective clouds. PNAS 110, E4581–E4590. https://doi.org/10.1073/pnas.1316830110

Fan, J., Leung, L.R., Rosenfeld, D., DeMott, P.J., 2017. Effects of cloud condensation nuclei and ice nucleating particles on precipitation processes and supercooled liquid in mixed-phase orographic clouds. Atmospheric Chemistry and Physics 17, 1017–1035. https://doi.org/10.5194/acp-17-1017-2017

Fan, J., Rosenfeld, D., Yang, Y., Zhao, C., Leung, L.R., Li, Z., 2015. Substantial contribution of anthropogenic air pollution to catastrophic floods in Southwest China. Geophysical Research Letters 42, 6066–6075. https://doi.org/10.1002/2015GL064479

Fan, J., Zhang, R., Li, G., Tao, W.-K., 2007. Effects of aerosols and relative humidity on cumulus clouds. Journal of Geophysical Research: Atmospheres 112. https://doi.org/10.1029/2006JD008136

Fast, J.D., Gustafson, W.I., Easter, R.C., Zaveri, R.A., Barnard, J.C., Chapman, E.G., Grell, G.A., Peckham, S.E., 2006. Evolution of ozone, particulates, and aerosol direct radiative forcing in the vicinity of Houston using a fully coupled meteorology-chemistry-aerosol model. Journal of Geophysical Research: Atmospheres 111. https://doi.org/10.1029/2005JD006721

Fujinami, H., Fujita, K., Takahashi, N., Sato, T., Kanamori, H., Sunako, S., Kayastha, R.B., 2021. Twice-Daily Monsoon Precipitation Maxima in the Himalayas Driven by Land Surface Effects. Journal of Geophysical Research: Atmospheres 126, e2020JD034255. https://doi.org/10.1029/2020JD034255

Gayatri, K., Patade, S., Fan, J., Prabhakaran, T., 2022. Pathways of precipitation formation in different thermodynamic and aerosol environments over the Indian Peninsula. Atmospheric Research 266, 105934. https://doi.org/10.1016/j.atmosres.2021.105934

Gelaro, R., McCarty, W., Suárez, M.J., Todling, R., Molod, A., Takacs, L., Randles, C.A., Darmenov, A., Bosilovich, M.G., Reichle, R., Wargan, K., Coy, L., Cullather, R., Draper, C., Akella, S., Buchard, V., Conaty, A., Silva, A.M. da, Gu, W., Kim, G.-K., Koster, R., Lucchesi, R., Merkova, D., Nielsen, J.E., Partyka, G., Pawson, S., Putman, W., Rienecker, M., Schubert, S.D., Sienkiewicz, M., Zhao, B., 2017. The Modern-Era Retrospective Analysis for Research and Applications, Version 2 (MERRA-2). Journal of Climate 30, 5419–5454. https://doi.org/10.1175/JCLI-D-16-0758.1

Gkikas, A., Proestakis, E., Amiridis, V., Kazadzis, S., Di Tomaso, E., Tsekeri, A., Marinou, E., Hatzianastassiou, N., Pérez García-Pando, C., 2021. ModIs Dust AeroSol (MIDAS): a global fine-resolution dust optical depth data set. Atmospheric Measurement Techniques 14, 309–334. https://doi.org/10.5194/amt-14-309-2021

GMAO, 2015. Global Modeling and Assimilation Office (GMAO), MERRA-2 inst3_3d_aer_Nv: 3d,3-Hourly,Instantaneous,Model-Level,Assimilation,Aerosol Mixing Ratio V5.12.4. Greenbelt, MD, USA, Goddard Earth Sciences Data and Information Services Center (GES DISC). https://doi.org/10.5067/LTVB4GPCOTK2

Grell, G.A., Dévényi, D., 2002. A generalized approach to parameterizing convection combining ensemble and data assimilation techniques. Geophysical Research Letters 29, 38-1-38–4. https://doi.org/10.1029/2002GL015311

Grell, G.A., Peckham, S.E., Schmitz, R., McKeen, S.A., Frost, G., Skamarock, W.C., Eder, B., 2005. Fully coupled "online" chemistry within the WRF model. Atmospheric Environment 39, 6957–6975. https://doi.org/10.1016/j.atmosenv.2005.04.027

Guenther, A., Karl, T., Harley, P., Wiedinmyer, C., Palmer, P.I., Geron, C., 2006. Estimates of global terrestrial isoprene emissions using MEGAN (Model of Emissions of Gases and Aerosols from Nature). Atmospheric Chemistry and Physics 6, 3181–3210. https://doi.org/10.5194/acp-6-3181-2006

Hazra, A., Padmakumari, B., Maheskumar, R.S., Chen, J.-P., 2016. The effect of mineral dust and soot aerosols on ice microphysics near the foothills of the Himalayas: A numerical investigation. Atmospheric Research 171, 41–55. https://doi.org/10.1016/j.atmosres.2015.12.005

Hong, S.-Y., Noh, Y., Dudhia, J., 2006. A New Vertical Diffusion Package with an Explicit Treatment of Entrainment Processes. Mon. Wea. Rev. 134, 2318–2341. https://doi.org/10.1175/MWR3199.1

Hoose, C., Möhler, O., 2012. Heterogeneous ice nucleation on atmospheric aerosols: a review of results from laboratory experiments. Atmospheric Chemistry and Physics 12, 9817–9854. https://doi.org/10.5194/acp-12-9817-2012

Huang, C.-C., Chen, S.-H., Lin, Y.-C., Earl, K., Matsui, T., Lee, H.-H., Tsai, I.-C., Chen, J.-P., Cheng, C.-T., 2019. Impacts of Dust–Radiation versus Dust–Cloud Interactions on the Development of a Modeled Mesoscale Convective System over North Africa. Monthly Weather Review 147, 3301–3326. https://doi.org/10.1175/MWR-D-18-0459.1

Huffman, G.J., Stocker, E.F., Bolvin, D.T., Nelkin, E.J., Tan, J., 2019. GPM IMERG Early Precipitation L3 Half Hourly 0.1 degree x 0.1 degree V06. Goddard Earth Sciences Data and Information Services Center (GES DISC), Greenbelt, MD. https://doi.org/10.5067/GPM/IMERG/3B-HH-E/06

Iacono, M.J., Delamere, J.S., Mlawer, E.J., Shephard, M.W., Clough, S.A., Collins, W.D., 2008. Radiative forcing by long-lived greenhouse gases: Calculations with the AER radiative transfer models. Journal of Geophysical Research: Atmospheres 113. https://doi.org/10.1029/2008JD009944

IPCC, 2013. Climate change 2013: The Physical Science Basis: Working Group I Contribution to the Fifth Assessment Report of the Intergovernmental Panel on Climate. Cambridge University Press.

Janssens-Maenhout, G., Crippa, M., Guizzardi, D., Dentener, F., Muntean, M., Pouliot, G., Keating, T., Zhang, Q., Kurokawa, J., Wankmüller, R., Denier van der Gon, H., Kuenen, J.J.P., Klimont, Z., Frost, G., Darras, S., Koffi, B., Li, M., 2015. HTAP_v2.2: a mosaic of regional and global emission grid maps for 2008 and 2010 to study hemispheric transport of air pollution. Atmospheric Chemistry and Physics 15, 11411–11432. https://doi.org/10.5194/acp-15-11411-2015

Jat, R., Gurjar, B.R., Lowe, D., 2021. Regional pollution loading in winter months over India using high resolution WRF-Chem simulation. Atmospheric Research 249, 105326. https://doi.org/10.1016/j.atmosres.2020.105326

Jin, Q., Wei, J., Lau, W.K.M., Pu, B., Wang, C., 2021. Interactions of Asian mineral dust with Indian summer monsoon: Recent advances and challenges. Earth-Science Reviews 215, 103562. https://doi.org/10.1016/j.earscirev.2021.103562

Jin, Q., Wei, J., Yang, Z.-L., Pu, B., Huang, J., 2015. Consistent response of Indian summer monsoon to Middle East dust in observations and simulations. Atmospheric Chemistry and Physics 15, 9897–9915. https://doi.org/10.5194/acp-15-9897-2015

Kanji, Z.A., Ladino, L.A., Wex, H., Boose, Y., Burkert-Kohn, M., Cziczo, D.J., Krämer, M., 2017. Overview of Ice Nucleating Particles. Meteorological Monographs 58, 1.1-1.33. https://doi.org/10.1175/AMSMONOGRAPHS-D-16-0006.1

Kedia, S., Kumar, R., Islam, S., Sathe, Y., Kaginalkar, A., 2018. Radiative impact of a heavy dust storm over India and surrounding oceanic regions. Atmospheric Environment 185, 109–120. https://doi.org/10.1016/j.atmosenv.2018.05.005

Koren, I., Altaratz, O., Remer, L.A., Feingold, G., Martins, J.V., Heiblum, R.H., 2012. Aerosol-induced intensification of rain from the tropics to the mid-latitudes. Nature Geoscience 5, 118–122. https://doi.org/10.1038/ngeo1364

Kumar, R., Barth, M.C., Pfister, G.G., Nair, V.S., Ghude, S.D., Ojha, N., 2015. What controls the seasonal cycle of black carbon aerosols in India? Journal of Geophysical Research: Atmospheres 120, 7788–7812. https://doi.org/10.1002/2015JD023298

Kumar, S., Kumar, Sanjay, Kaskaoutis, D.G., Singh, R.P., Singh, R.K., Mishra, A.K., Srivastava, M.K., Singh, A.K., 2015. Meteorological, atmospheric and climatic perturbations during major dust storms over Indo-Gangetic Basin. Aeolian Research 17, 15–31. https://doi.org/10.1016/j.aeolia.2015.01.006

Kuriakose, J.M., Aloysius, M., Jayaprakash, R., Fathima, C.P., Prijith, S.S., Mohan, M., 2022. Investigation on the role of aerosols on precipitation enhancement over

Kerala during August 2018. Atmospheric Environment 119101. https://doi.org/10.1016/j.atmosenv.2022.119101

Lau, K.-M., Kim, K.-M., 2006. Observational relationships between aerosol and Asian monsoon rainfall, and circulation. Geophysical Research Letters 33. https://doi.org/10.1029/2006GL027546

Lau, K.M., Kim, M.K., Kim, K.M., 2006. Asian summer monsoon anomalies induced by aerosol direct forcing: the role of the Tibetan Plateau. Clim Dyn 26, 855–864. https://doi.org/10.1007/s00382-006-0114-z

Lau, W.K.M., Kim, K.-M., Shi, J.-J., Matsui, T., Chin, M., Tan, Q., Peters-Lidard, C., Tao, W.K., 2017. Impacts of aerosol–monsoon interaction on rainfall and circulation over Northern India and the Himalaya Foothills. Clim Dyn 49, 1945–1960. https://doi.org/10.1007/s00382-016-3430-y

Lawrence, D.M., Oleson, K.W., Flanner, M.G., Thornton, P.E., Swenson, S.C., Lawrence, P.J., Zeng, X., Yang, Z.-L., Levis, S., Sakaguchi, K., Bonan, G.B., Slater, A.G., 2011. Parameterization improvements and functional and structural advances in Version 4 of the Community Land Model. Journal of Advances in Modeling Earth Systems 3. https://doi.org/10.1029/2011MS00045

Li, Z., Niu, F., Fan, J., Liu, Y., Rosenfeld, D., Ding, Y., 2011. Long-term impacts of aerosols on the vertical development of clouds and precipitation. Nature Geoscience 4, 888–894. https://doi.org/10.1038/ngeo1313

Mamun, A., Chen, Y., Liang, J., 2021. Radiative and cloud microphysical effects of the Saharan dust simulated by the WRF-Chem model. Journal of Atmospheric and Solar-Terrestrial Physics 219, 105646. https://doi.org/10.1016/j.jastp.2021.105646

Mogno, C., Palmer, P.I., Knote, C., Yao, F., Wallington, T.J., 2021. Seasonal distribution and drivers of surface fine particulate matter and organic aerosol over the Indo-

Gangetic Plain. Atmospheric Chemistry and Physics 21, 10881–10909. https://doi.org/10.5194/acp-21-10881-2021

Morrison, H., Thompson, G., Tatarskii, V., 2009. Impact of Cloud Microphysics on the Development of Trailing Stratiform Precipitation in a Simulated Squall Line: Comparison of One- and Two-Moment Schemes. Mon. Wea. Rev. 137, 991–1007. https://doi.org/10.1175/2008MWR2556.1

Naeger, A.R., 2018. Impact of dust aerosols on precipitation associated with atmospheric rivers using WRF-Chem simulations. Results in Physics 10, 217–221. https://doi.org/10.1016/j.rinp.2018.05.027

Orza, J.A.G., Dhital, S., Fiedler, S., Kaplan, M.L., 2020. Large scale upper-level precursors for dust storm formation over North Africa and poleward transport to the Iberian Peninsula. Part I: An observational analysis. Atmospheric Environment 237, 117688. https://doi.org/10.1016/j.atmosenv.2020.117688

Pokharel, A.K., Xu, T., Liu, X., Dawadi, B., 2020. Dynamics of Muddy Rain of 15 June 2018 in Nepal. Atmosphere 11, 529. https://doi.org/10.3390/atmos11050529

Prasad, A.K., Singh, R.P., 2007. Changes in aerosol parameters during major dust storm events (2001–2005) over the Indo-Gangetic Plains using AERONET and MODIS data. Journal of Geophysical Research: Atmospheres 112. https://doi.org/10.1029/2006JD007778

Prein, A.F., Heymsfield, A.J., 2020. Increased melting level height impacts surface precipitation phase and intensity. Nature Climate Change 10, 771–776. https://doi.org/10.1038/s41558-020-0825-x

Prein, A.F., Langhans, W., Fosser, G., Ferrone, A., Ban, N., Goergen, K., Keller, M., Tölle, M., Gutjahr, O., Feser, F., Brisson, E., Kollet, S., Schmidli, J., Lipzig, N.P.M. van, Leung, R., 2015. A review on regional convection-permitting climate

modeling: Demonstrations, prospects, and challenges. Reviews of Geophysics 53, 323–361. https://doi.org/10.1002/2014RG000475

Rosenfeld, D., Lohmann, U., Raga, G.B., O'Dowd, C.D., Kulmala, M., Fuzzi, S., Reissell, A., Andreae, M.O., 2008. Flood or Drought: How Do Aerosols Affect Precipitation? Science 321, 1309–1313. https://doi.org/10.1126/science.1160606

Saidou Chaibou, A.A., Ma, X., Sha, T., 2020. Dust radiative forcing and its impact on surface energy budget over West Africa. Sci Rep 10, 12236. https://doi.org/10.1038/s41598-020-69223-4

Sarangi, C., Qian, Y., Rittger, K., Bormann, K.J., Liu, Y., Wang, H., Wan, H., Lin, G., Painter, T.H., 2019. Impact of light-absorbing particles on snow albedo darkening and associated radiative forcing over high-mountain Asia: high-resolution WRF-Chem modeling and new satellite observations. Atmospheric Chemistry and Physics 19, 7105–7128. https://doi.org/10.5194/acp-19-7105-2019

Sarangi, C., Tripathi, S.N., Kanawade, V.P., Koren, I., Pai, D.S., 2017. Investigation of the aerosol–cloud–rainfall association over the Indian summer monsoon region. Atmos. Chem. Phys. 17, 5185–5204. https://doi.org/10.5194/acp-17-5185-2017

Sarangi, C., Tripathi, S.N., Tripathi, S., Barth, M.C., 2015. Aerosol-cloud associations over Gangetic Basin during a typical monsoon depression event using WRF-Chem simulation. Journal of Geophysical Research: Atmospheres 120, 10,974-10,995. https://doi.org/10.1002/2015JD023634

Sarkar, S., Chauhan, A., Kumar, R., Singh, R.P., 2019. Impact of Deadly Dust Storms (May 2018) on Air Quality, Meteorological, and Atmospheric Parameters Over the Northern Parts of India. GeoHealth 3, 67–80. https://doi.org/10.1029/2018GH000170

Sharma, S., Chen, Y., Zhou, X., Yang, K., Li, X., Niu, X., Hu, X., Khadka, N., 2020a. Evaluation of GPM-Era Satellite Precipitation Products on the Southern Slopes of

the Central Himalayas Against Rain Gauge Data. Remote Sensing 12, 1836. https://doi.org/10.3390/rs12111836

Sharma, S., Khadka, N., Hamal, K., Shrestha, D., Talchabhadel, R., Chen, Y., 2020b. How Accurately Can Satellite Products (TMPA and IMERG) Detect Precipitation Patterns, Extremities, and Drought Across the Nepalese Himalaya? Earth and Space Science 7, e2020EA001315. https://doi.org/10.1029/2020EA001315

Shukla, K.K., Attada, R., Khan, A.W., Kumar, P., 2021. Evaluation of extreme dust storm over the northwest Indo-Gangetic plain using WRF-Chem model. Nat Hazards. https://doi.org/10.1007/s11069-021-05017-9

Sicard, P., Crippa, P., De Marco, A., Castruccio, S., Giani, P., Cuesta, J., Paoletti, E., Feng, Z., Anav, A., 2021. High spatial resolution WRF-Chem model over Asia: Physics and chemistry evaluation. Atmospheric Environment 244, 118004. https://doi.org/10.1016/j.atmosenv.2020.118004

Sijikumar, S., Aneesh, S., Rajeev, K., 2016. Multi-year model simulations of mineral dust distribution and transport over the Indian subcontinent during summer monsoon seasons. Meteorol Atmos Phys 128, 453–464. https://doi.org/10.1007/s00703-015-0422-0

Small, J.D., Jiang, J.H., Su, H., Zhai, C., 2011. Relationship between aerosol and cloud fraction over Australia. Geophysical Research Letters 38. https://doi.org/10.1029/2011GL049404

Srivastava, A.K., Pant, P., Hegde, P., Singh, S., Dumka, U.C., Naja, M., Singh, N., Bhavanikumar, Y., 2011. The influence of a south Asian dust storm on aerosol radiative forcing at a high-altitude station in central Himalayas. International Journal of Remote Sensing 32, 7827–7845. https://doi.org/10.1080/01431161.2010.531781

Tao, W.-K., Matsui, T., 2015. NUMERICAL MODELS | Cloud-System Resolving Modeling and Aerosols, in: North, G.R., Pyle, J., Zhang, F. (Eds.), Encyclopedia of Atmospheric Sciences (Second Edition). Academic Press, Oxford, pp. 222–231. https://doi.org/10.1016/B978-0-12-382225-3.00511-9

Uno, I., Eguchi, K., Yumimoto, K., Takemura, T., Shimizu, A., Uematsu, M., Liu, Z., Wang, Z., Hara, Y., Sugimoto, N., 2009. Asian dust transported one full circuit around the globe. Nature Geoscience 2, 557–560. https://doi.org/10.1038/ngeo583

Vaughan, M.A., Powell, K.A., Winker, D.M., Hostetler, C.A., Kuehn, R.E., Hunt, W.H., Getzewich, B.J., Young, S.A., Liu, Z., McGill, M.J., 2009. Fully Automated Detection of Cloud and Aerosol Layers in the CALIPSO Lidar Measurements. Journal of Atmospheric and Oceanic Technology 26, 2034–2050. https://doi.org/10.1175/2009JTECHA1228.1

Vinoj, V., Rasch, P.J., Wang, H., Yoon, J.-H., Ma, P.-L., Landu, K., Singh, B., 2014. Short-term modulation of Indian summer monsoon rainfall by West Asian dust. Nature Geoscience 7, 308–313. https://doi.org/10.1038/ngeo2107

Wang, C., Kim, D., Ekman, A.M.L., Barth, M.C., Rasch, P.J., 2009. Impact of anthropogenic aerosols on Indian summer monsoon. Geophysical Research Letters 36. https://doi.org/10.1029/2009GL040114

Wang, S., Zhang, M., Pepin, N.C., Li, Z., Sun, M., Huang, X., Wang, Q., 2014. Recent changes in freezing level heights in High Asia and their impact on glacier changes. Journal of Geophysical Research: Atmospheres 119, 1753–1765. https://doi.org/10.1002/2013JD020490

Wiedinmyer, C., Akagi, S.K., Yokelson, R.J., Emmons, L.K., Al-Saadi, J.A., Orlando, J.J., Soja, A.J., 2011. The Fire INventory from NCAR (FINN): a high resolution global model to estimate the emissions from open burning. Geoscientific Model Development 4, 625–641. https://doi.org/10.5194/gmd-4-625-2011

Wu, L., Gu, Y. (ORCID:0000000234120794), Jiang, J.H., Su, H., Yu, N., Zhao, C., Qian, Y., Zhao, B. (ORCID:0000000184389188), Liou, K.-N., Choi, Y.-S., 2018. Impacts of aerosols on seasonal precipitation and snowpack in California based on convection-permitting WRF-Chem simulations. Atmospheric Chemistry and Physics (Online) 18. https://doi.org/10.5194/acp-18-5529-2018

Yuan, T., Huang, J., Cao, J., Zhang, G., Ma, X., 2021. Indian dust-rain storm: Possible influences of dust ice nuclei on deep convective clouds. Science of The Total Environment 779, 146439. https://doi.org/10.1016/j.scitotenv.2021.146439

Zaveri, R.A., Easter, R.C., Fast, J.D., Peters, L.K., 2008. Model for Simulating Aerosol Interactions and Chemistry (MOSAIC). Journal of Geophysical Research: Atmospheres 113. https://doi.org/10.1029/2007JD008782

Zaveri, R.A., Peters, L.K., 1999. A new lumped structure photochemical mechanism for large-scale applications. Journal of Geophysical Research: Atmospheres 104, 30387–30415. https://doi.org/10.1029/1999JD900876

Zhang, Y., Yu, F., Luo, G., Chen, J.-P., Chou, C.C.-K., 2020. Impact of Mineral Dust on Summertime Precipitation Over the Taiwan Region. Journal of Geophysical Research: Atmospheres 125, e2020JD033120. https://doi.org/10.1029/2020JD033120

Zhang, Y., Yu, F., Luo, G., Fan, J., Liu, S., 2021. Impacts of long-range-transported mineral dust on summertime convective cloud and precipitation: a case study over the Taiwan region. Atmos. Chem. Phys. 21, 17433–17451. https://doi.org/10.5194/acp-21-17433-2021

Zhao, C., Chen, S., Leung, L.R., Qian, Y., Kok, J.F., Zaveri, R.A., Huang, J., 2013. Uncertainty in modeling dust mass balance and radiative forcing from size parameterization. Atmospheric Chemistry and Physics 13, 10733–10753. https://doi.org/10.5194/acp-13-10733-2013

Zhao, X., Zhao, C., Yang, Y., Sun, Y., Xia, Y., Yang, X., Fan, T., 2022. Distinct changes of cloud microphysical properties and height development by dust aerosols from a case study over Inner-Mongolia region. Atmospheric Research 273, 106175. https://doi.org/10.1016/j.atmosres.2022.106175

Supplementary Figures for Chapter 3

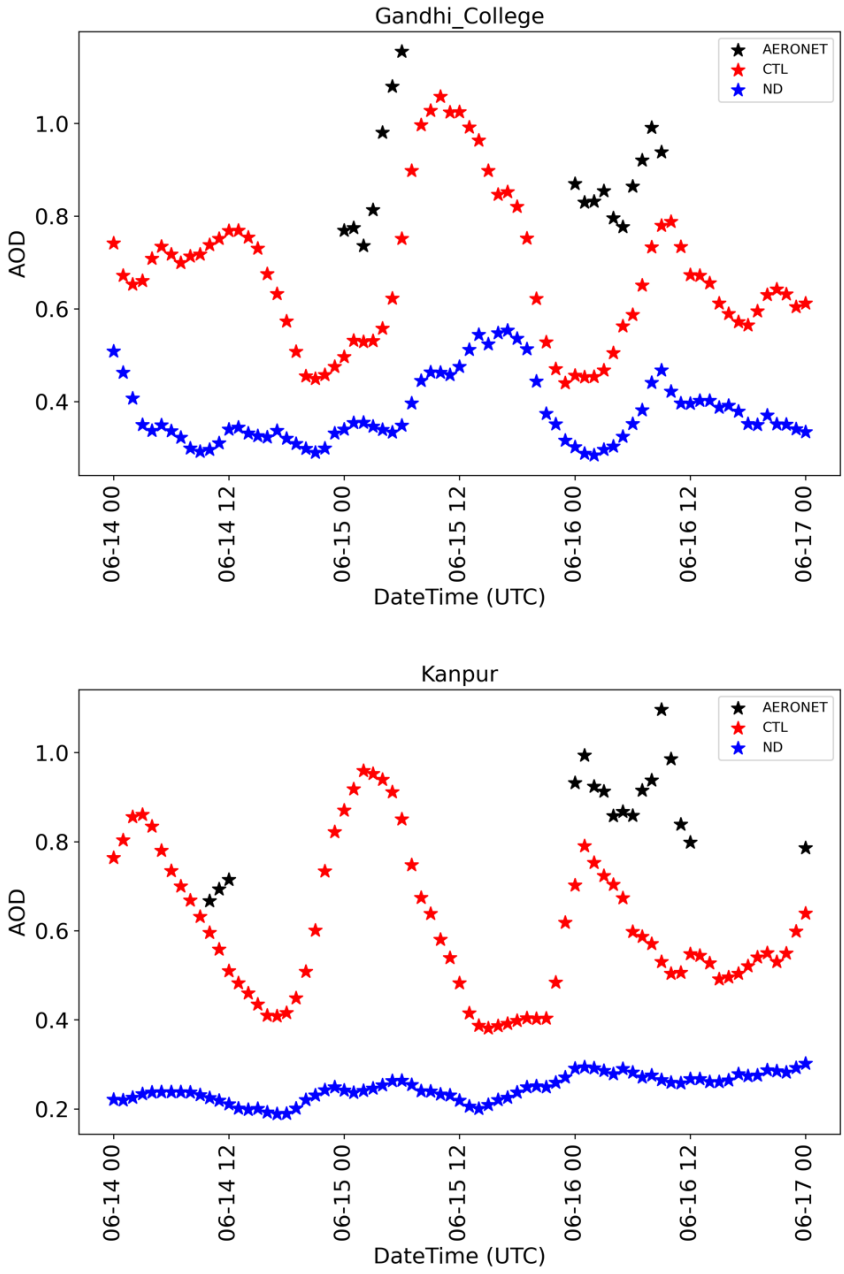

Supplementary Figure (C3S1): Scatter plot of statistically significant modeled AOD (CTL and ND; 3km domain) and available AERONET AOD at Kanpur station, India, and Gandhi College station, India.

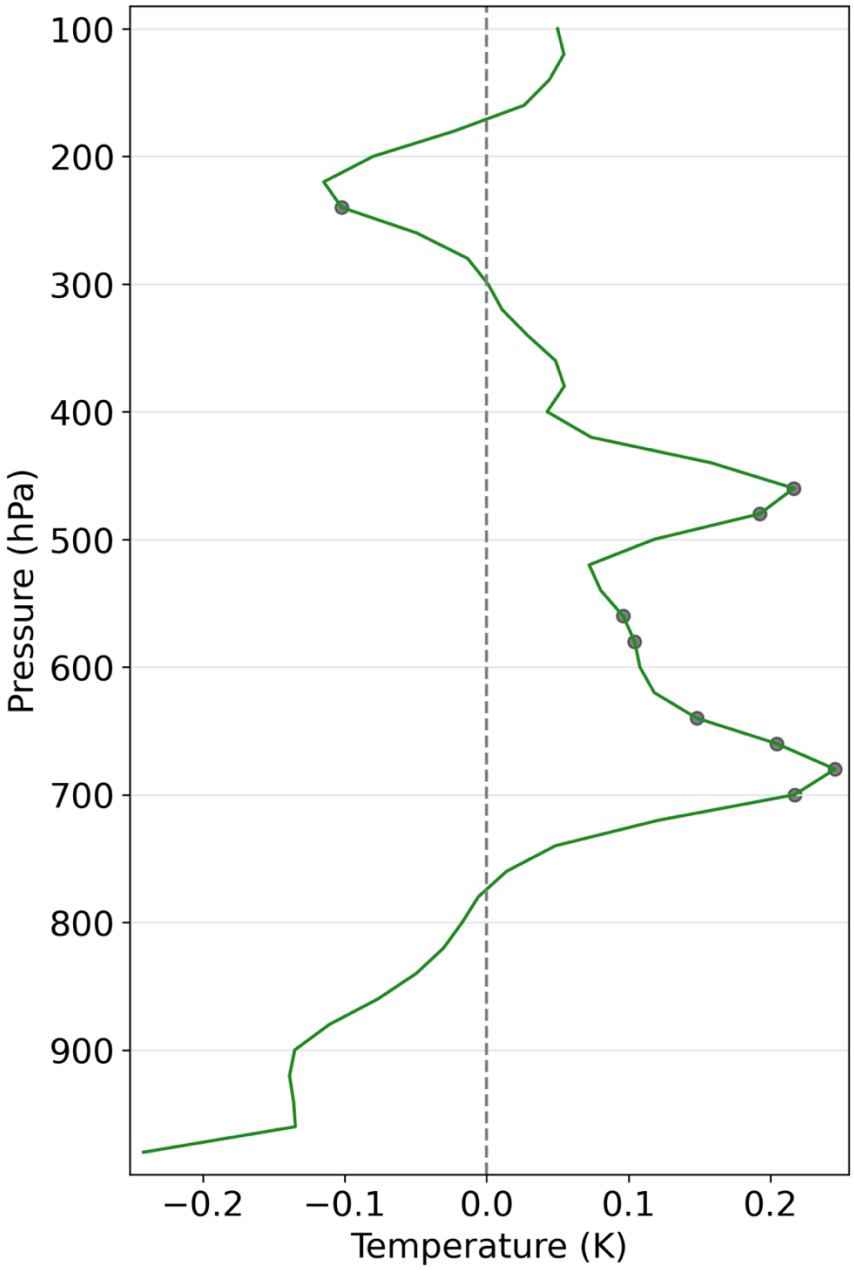

Supplementary Figure (C3S2): The mean temperature difference between CTL and ND run. The dot represents that the difference between the simulations is not significant at 90% confidence interval.

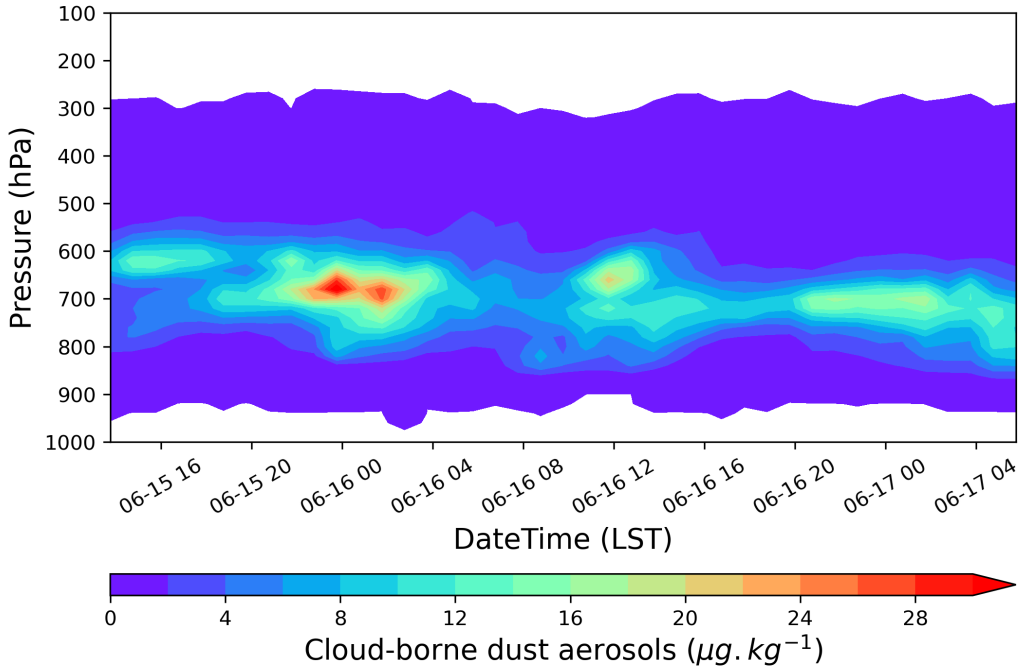

Supplementary Figure (C3S3): Timeseries of mixing ratio of activated dust aerosols to cloud droplets over the southern slopes (area enclosed by the black box in Fig. 3.1).

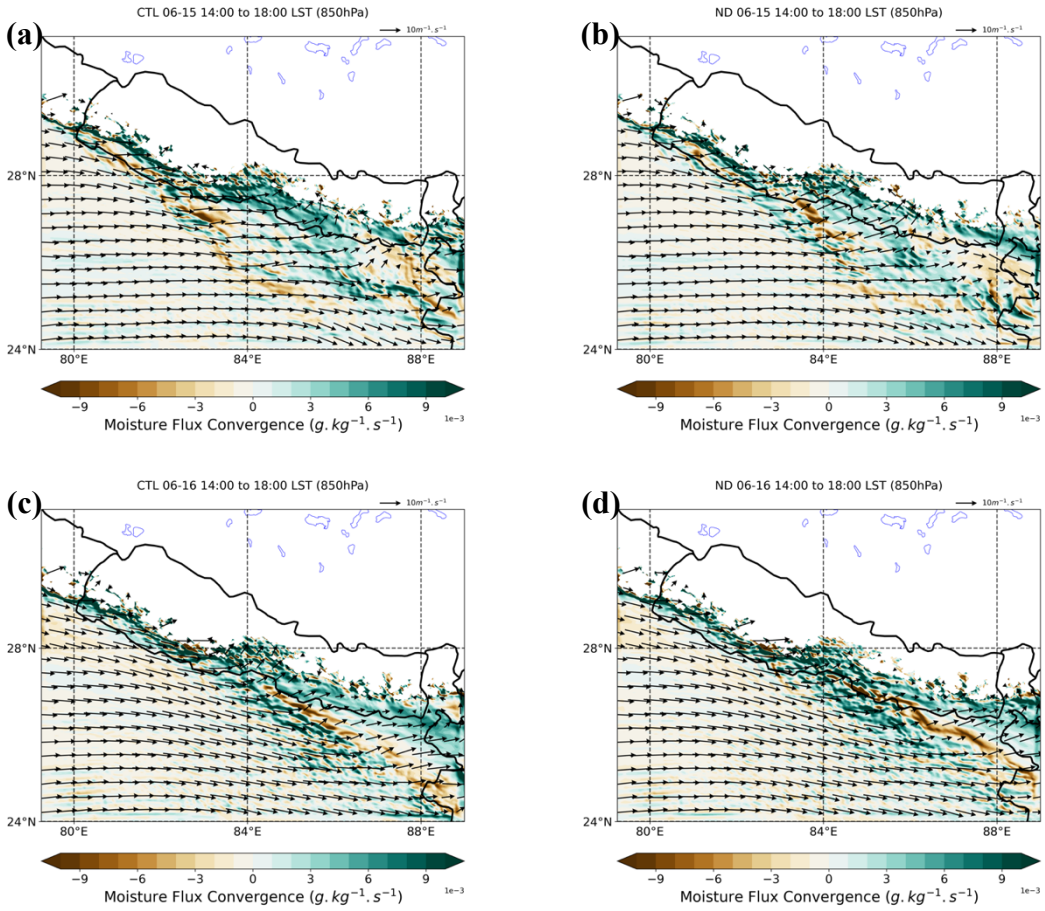

Supplementary Figure (C3S4): Moisture Flux convergence (shaded) and wind vectors at 850 hPa for CTL (a, c) and ND (b, d) run for 1400 to 1800 LST on June 15th (a, b) and 16th (c, d).

Chapter 4: Aerosols-precipitation elevation dependence over the Central Himalayas using cloud-resolving WRF-Chem numerical modeling

4.1 Introduction

The south Asian summer monsoon system, one of the major monsoonal systems on Earth, is located in the region with the persistent occurrence of substantial loadings of atmospheric aerosols (Li et al., 2016). The densely populated and rapidly growing urban centers of the Indo-Gangetic Plain (IGP), located over the northern India at the foothills of the Himalayas, experiences frequent events of severe air pollution with significant contribution from local anthropogenic activities and remotely transported mineral dust aerosols (Dey and Di Girolamo, 2011; Kumar et al., 2018; Sijikumar et al., 2016). Atmospheric aerosols, from both natural and anthropogenic sources, can impact the weather and climate on a local to global scale through interactions with radiation and cloud, as well as through albedo and hydrologic pathways due to deposition over the snow (e.g., Sarangi et al., 2019; Wu et al., 2018; Andreae and Rosenfeld, 2008; Haywood and Boucher, 2000; Mahowald et al., 2011; Ramanathan and Carmichael, 2008). However, due to inhomogeneous distribution and complex radiation and cloud interaction, aerosol also contributes to the larger uncertainties in assessing the Earth's changing climate (IPCC, 2013).

The direct radiative effects due to the scattering and absorption of radiation depending on the optical properties of aerosols and semi-direct effect comprise the Aerosol-Radiation Interaction (ARI; IPCC, 2013). The semi-direct effect refers to the heating of the cloud due to the absorbing aerosols, which reduces the relative humidity

and increases the cloud burn-off process resulting in lower planetary albedo (Hansen et al., 1997; Huang et al., 2006a; Ackerman et al., 2000). The ARI can alter the surface energy budget, atmospheric thermodynamic structure, convective stability, and tropical-meridional circulation, which modulates the frequency and intensity of the monsoonal rainfall (e.g., Li et al., 2016; Ramanathan et al., 2005; Lau et al., 2006). In a daily timescale, compared to the relatively pristine environment, the polluted urban plains increase the low-level stability due to the direct radiative effect during the daytime, resulting in enhanced moisture transport and abnormally increasing precipitation over the downwind mountains at night (Choudhury et al., 2020; Fan et al., 2015).

IPCC (2013) refers to the Aerosol-Cloud Interaction (ACI) to the modification of cloud microphysical properties or cloud evolution through the ability of aerosol to act as cloud condensation nuclei (CCN) or Ice-Nucleating particles (INPs). The higher concentration of CCN in a polluted cloud increases the number of smaller cloud droplets for a constant liquid water path and enhances the reflection, also known as the first indirect effect (Twomey, 1977). Smaller cloud droplets result in increased cloud lifetime and height and suppress the drizzle precipitation, also known as second indirect or cloud lifetime effect (Pincus and Baker, 1994; Albrecht, 1989; Rosenfeld, 1999). The continuing and intensified updrafts with the release of latent heat of condensation and freezing and additional thermal buoyancy invigorates the convection strength and cloud development (Rosenfeld et al., 2008; Andreae et al., 2004; Koren et al., 2005). Additionally, Fan et al. (2017) proposed that the increase in latent heat release with CCN concentration strengthens the moisture transport to the windward slope and can

invigorate the mixed phase orographic clouds resulting in higher precipitation over the Sierra Nevada, California.

The deep convective activity and southwesterly monsoonal flow incorporates the remote dust and anthropogenic aerosols from the IGP and transports them to the southern slopes of the Himalayas and even to the Tibetan Plateau (Kang et al., 2019; Ji et al., 2015; Vernier et al., 2011). The transport and local emission of the anthropogenic aerosols can impact the precipitation, vertical temperature distribution and regional hydroclimate of the Himalayan and the adjacent region. The increasing trend of the freezing level height (FLH) has been reported around the globe (e.g., Wang et al., 2014; Bradley et al., 2009; Zhang and Guo, 2011; Prein and Heymsfield, 2020; Lynn et al., 2020). The elevation-dependent warming or the amplified warming of the mountainous terrain around the globe can be associated with the change in snow cover and albedo, radiative and surface fluxes, changes in water vapor and latent heat release, deposition of aerosols on snowpack, and aerosol concentrations (Pepin et al., 2015; Rangwala et al., 2010). Depending on the location and topographical altitude, different factors can dominate elevation-dependent warming; e.g., snow albedo feedback, change in specific humidity, and radiative impact of concentrated aerosol loading can play a significant role in modulating the temperature over the slopes of the Himalayas and mid-latitude Asia (Pepin et al., 2015; Rangwala and Miller, 2012; Palazzi et al., 2017). Adhikari and Mejia (2021) indicated that the FLH increased over the Central Himalayas during the polluted days with heavier aerosol loadings compared to cleaner environment, which can impact the snowline altitude (Wang et al., 2014; Prein and Heymsfield, 2020).

The localized extreme weather events over the complex mountainous terrain pose a higher hazard due to the flash floods and landslides. The variability in the orographic precipitation has been linked to atmospheric aerosols around the globe (Napoli et al., 2019; Wu et al., 2018; Choudhury et al., 2020; Adhikari and Mejia, 2021, 2022). Cho et al. (2016) suggested that anthropogenic climate forcing modifies the circulation structure and triggers the intense rainfall over northern south Asia and increase the risk of flood severity. The atmospheric heating due to the accumulated remote dust and carbonaceous aerosols from IGP leads to the northward shift of deep convection and heavier monsoonal rainfall over the foothills of the Himalayas during the early monsoon period (Lau et al., 2006, 2017). Furthermore, the long term (2002 to 2016) satellite-based observational study by Adhikari and Mejia (2021) also shown that the aerosol invigorated the cloud development and enhances the precipitation over the southern slopes of the central Himalayas.

Few studies have assessed the climatology of elevational dependent warming and precipitation over the Tibetan Plateau (TP) and the Himalayas using the climate models (e.g., Palazzi et al., 2017; Ghimire et al., 2018; Dimri et al., 2022), but without including aerosols effects. The response of elevational dependent precipitation to anthropogenic aerosols within the Central Himalayan region using cloud-resolving simulations is lacking, to the best of our knowledge. A better understanding of elevation-dependent warming and precipitation of this mountainous region is crucial to assess the hydrologic and climate risks for millions of people residing on the adjacent lowlands. The present study attempts to examine the role of anthropogenic aerosol in modulating the elevation-dependent precipitation distribution and intensity over the complex topography of the

central Himalayas. Also, we estimate and evaluate the role of increased anthropogenic aerosols in modulating the surface temperature distribution. In this study, we implement the Weather Research and Forecasting (WRF) model coupled with chemistry (WRF-Chem) configured at a cloud-resolving scale, where the organization of the convection is explicitly resolved, for the first monsoonal month of 2013 after the onset of the monsoon in Nepal. In section 4.2, we describe the details of the model used. In section 4.3, we present and discuss the model evaluation, simulation results, and limitations of the study. Conclusion of this study are summarized in section 4.4.

4.2. Methodology

4.2.1 Model description

In this study we implement the Weather Research and Forecasting (WRF) model coupled with Chemistry (WRF-Chem) version 4.1.5 for numerical simulations (Grell et al., 2005). WRF-Chem is an advanced online coupled regional model which can simulate the emission, transport and transformation of trace gases and aerosols with atmospheric feedback processes from radiation and meteorology (Chapman et al., 2009; Fast et al., 2006). WRF-Chem consists of several chemistry components, e.g., emission inventories, aerosol-chemistry mechanism, aqueous- and gas-phase mechanism, dry and wet deposition, and photolysis, and has been widely used to study aerosol-cloud-radiation-climate interaction around the globe (e.g., Wu et al., 2018; Fan et al., 2015; Sarangi et al., 2015; Archer-Nicholls et al., 2016; Liu et al., 2020).

The Carbon Bond Mechanism (CBM-Z; Zaveri and Peters 1999), a gas-phase chemistry mechanism coupled with MOSAIC (Model for Simulating Aerosol Interactions

and Chemistry; Zaveri et al. 2008) aerosol module was utilized. The CBM-Z includes 67 chemical species and 164 reactions and treats the organic compound in a lumped structure approach depending on their internal bond types (Gery et al., 1989; Zaveri et al., 2008). MOSAIC aerosol module simulates all the major aerosol species (including sulfate, nitrate, ammonium, primary organic mass, black carbon, and liquid water) that are deemed to be significant at urban, regional and global scales (Zaveri et al., 2008). Of note is that the MOSAIC version implemented in this study does not treat the secondary organic aerosols, which is expected to modulate the physical and chemical properties of atmospheric aerosols (Kaul et al., 2011; Hallquist et al., 2009) and can add up the uncertainties in the result. The aerosol size distribution within the MOSAIC aerosol module is represented by 4 or 8 sectional bin approach. To reduce the computational burden, the aerosol size distribution in the MOSAIC was represented using 4-bins, ranging between 39 nm to 10 μm based on dry particle diameters. The four bin approach reasonably produce similar results in comparison to the eight sized bins approach (Eidhammer et al., 2014; Zhao et al., 2013). All particles within a bin are considered to be internally mixed which have similar chemical composition, while particles from different sized bins are mixed externally (Zaveri et al., 2008).

Composite aerosol optical properties, such as the extinction and scattering coefficient, single scattering albedo and asymmetry factor, are estimated as a function of the size and chemical composition of aerosols using the volume averaging method with Mie theory (Fast et al., 2006; Chapman et al., 2009). The total integrated aerosol optical properties across all sized bins are then used in the radiation transfer scheme to compute the net radiative effect of aerosols (Chapman et al., 2009; Iacono et al., 2008). The major aspect

of aerosols in impacting the cloud evolution and microphysics are the concentration and composition, size distribution, and the hygroscopicity nature of aerosols (Khain et al., 2016). In a convective cloud, the effect of aerosols on the microphysics of the cloud is mainly determined by the number of aerosols activated as CCN, which impacts the size and cloud droplet number concentration (Chapman et al., 2009). Aerosols are activated as CCN when the maximum environmental supersaturation is greater than the critical supersaturation of an aerosol, which is a function of aerosol size and composition. The maximum supersaturation of rising air parcel within each size bin is computed as a function of vertical velocity and composition of internally mixed aerosols (Abdul-Razzak and Ghan, 2002). The interstitial aerosols with higher critical supersaturation than maximum ambient supersaturation are not activated as CCN (Chapman et al., 2009). Also, the WRF-Chem can resuspend cloud-borne aerosols to interstitial state when the cloud particles evaporate within a grid cell (Chapman et al., 2009). The main advantage of using cloud-resolving scales in this aerosol-cloud interacting study is that the activation of aerosols is explicitly resolved by the double-moment microphysics scheme (Archer-Nicholls et al., 2016; Chapman et al., 2009; Yang et al., 2011).

This study uses the anthropogenic emission inventories from the Emission Database for Global Atmospheric Research - Hemispheric Transport of Air Pollutants (EDGAR-HTAP) and EDGARv4.3.2 (Janssens-Maenhout et al., 2015). EDGAR-HTAP is a global monthly emission inventory for the year 2010 at a spatial resolution of 0.1° × 0.1°. EDGAR-HTAP emission inventory includes the black carbon, organic matter, particulate matter, ammonia, sulfates, oxides of nitrogen, and carbon monoxide, from the major anthropogenic sources from power generation, industry, residential, agriculture,

ground, and aviation transport, and shipping. The non-methane volatile organic compounds in this study are provided from EDGARv4.3.2. This study utilizes the biogenic emissions from the Model of Emissions of Gases and Aerosols from Nature (MEGAN), which quantifies the net emissions from the terrestrial biosphere at a horizontal resolution of one square km (Guenther et al., 2006, 2012). Fire INventory from NCAR version 1.5 (FINNv1.5), which provides the global estimates of open episodic fires from different sources in a 1 km spatial and daily temporal resolution (Wiedinmyer et al., 2011), is used as biomass burning emissions. Though fire events are less relevant during the monsoon season (2002-2013) in our area of interest (Matin et al., 2017), we used biomass burning information to include all the primary sources of aerosols.

The Community Atmosphere Model with Chemistry (CAM-Chem), with 0.9° × 1.25° spatial resolution with 56 vertical levels and six hourly temporal resolution, is used as initial and boundary conditions for the chemical species (Buchholz et al., 2019). The meteorological forcing in CAM-Chem is driven by Modern-Era Retrospective analysis for Research and Applications version 2 (MERRA-2) reanalysis product (Emmons et al. 2020). Furthermore, the Coupled Model Intercomparison Project round 6 (CMIP6) provides the anthropogenic aerosols within CAM-Chem. The meteorological initial and boundary condition from ERA5 (Hersbach et al., 2020), a most recent reanalysis product from European Centre for Medium range Weather Forecasting (ECMWF), with 31 km spatial and hourly temporal resolution, was used to initialize the model.

4.2.2 Experimental setup

According to the Department Of Hydrology and Meteorology (DHM) of Nepal, the onset of the monsoon occurred on June 14th, 2013, about a day after a normal onset date over eastern Nepal (DHM Nepal, 2022), and generally overs the entire country within a week. Model simulations were performed for 31 days, from June 14th 00 UTC to July 15th 00 UTC, 2013. The mean precipitation over the Central Himalayan region (hereafter CenHim; area indicated by the white-colored polygon in Fig. 4.1b) during the first month of the monsoon (31 days after the monsoonal onset) from 2000-2021 is 11.84 mm/day with a standard deviation (SD) of 2.97 mm/day (see Fig. C4S1). For the same period, the CenHim region received 14.62 mm/day of precipitation which is within +1 SD of the climatology mean.

Two one-way nested domains with a horizontal resolution of 9 km and 3 km were set up (see **Fig. 4.1**). The model was divided into 61 vertical layers with the 50 hPa model top. The 9km parent domain with 179 × 221 grids covered the central and northern/eastern India, Bangladesh, Bhutan, and TP. The 3km nested domain with 273 × 321 grid points was designed to include the CenHim, Nepal (with Mount Everest), the areas of most anthropogenic emission sources over the central IGP, and the immediate Himalayan plateau region of Tibet. The model configuration with the physical parameterizations used in this study is listed in **Table 4.1**. The double moment Morrison microphysics scheme simulates the number and mass mixing ratio of hydrometeors, including cloud droplets, rain, ice, snow, and graupel (Morrison et al., 2009). Previous studies have reasonably implemented the Morrison microphysics, RRTMG for radiation, and YSU for the boundary layer to simulate and study the aerosol-cloud-precipitation

interaction on a cloud-resolving scale (e.g., Kant et al., 2021; Wu et al., 2018). The convective parametrization was turned off for the 3 km domain. This consideration assumes that the model explicitly resolves convective eddies, hence the term cloud-resolving scale.

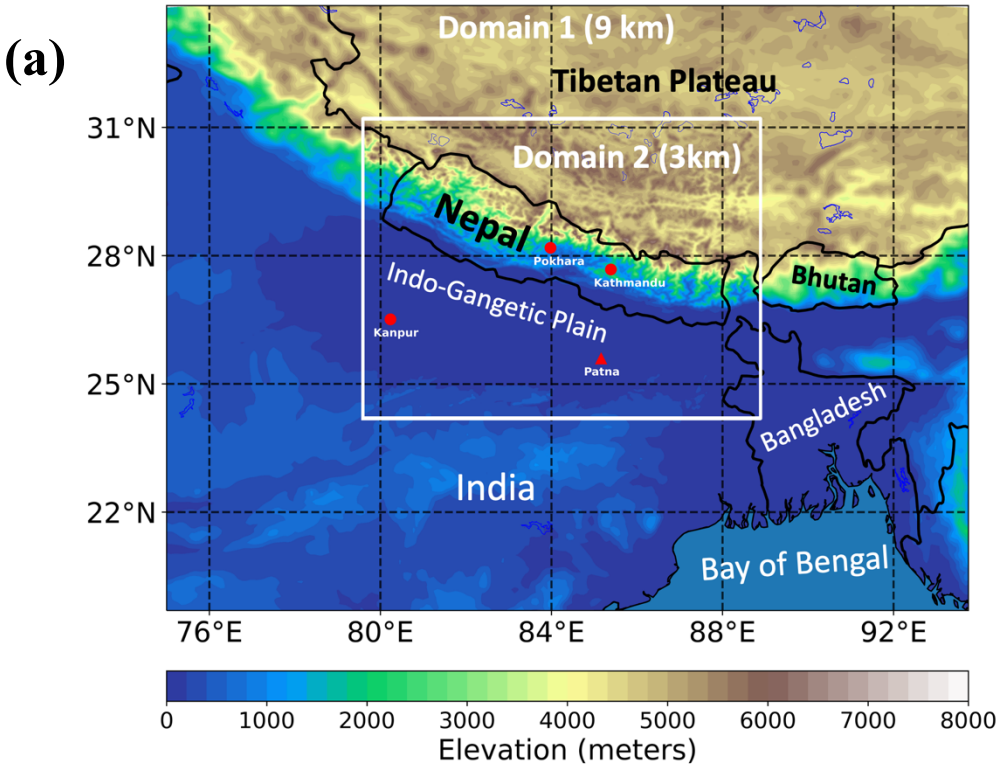

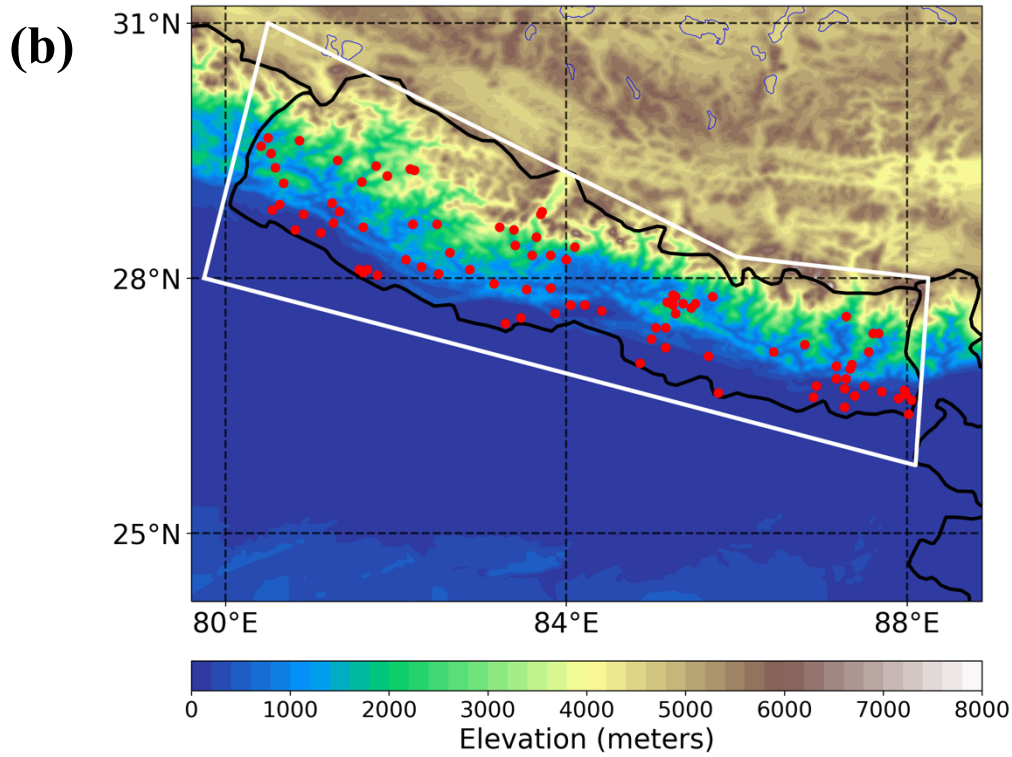

Figure 4.1: (a) The topography of the domains used in the simulation. The red marker represents the station locations for AERONET (circle) and upper air sounding (triangle). (b) The red marker represents the locations of DHM Nepal rain gauge stations. The white-colored polygon represents the Central Himalayan region (CenHim) region in the text.

Table 4.1: Model configuration.

Physics option	**Scheme**
Microphysics	Morrsion-2 moment (Morrison et al., 2009)
Radiation	Rapid Radiative Transfer Model for General Circulation Models (RRTMG; Iacono et al., 2008)
Land surface	Unified Noah (Tewari et al., 2004)
Planetary Boundary layer	Yonsei University (YSU; Hong et al., 2006)
Cumulus	Grell-3D for 9 km (Grell and Dévényi, 2002) and Turned off for 3km
Chemical and Aerosol	CBM-Z and MOSAIC-4bin
Boundary Condition	ERA5 (meteorology) and CAM-Chem (Chemistry)

Three simulations were performed to assess the sensitivity of the model to aerosol effects. A baseline or control simulation (hereafter "CTL") includes all the emissions (anthropogenic, biogenic, fire, and aerosols from chemistry boundary conditions). CTL includes the aerosol-radiation interaction, indirect effect of aerosols, wet scavenging, and dry deposition of aerosols. To isolate the impact of aerosol direct effect, the second simulations resemble the CTL simulation, but it is performed by turning off aerosol-radiation feedback (hereafter "NoARI"). The comparison between the CTL and NoARI enables the assessment of effect of aerosol-radiation interaction (ARI effect). The third experiment resembles the CTL, but it is performed by reducing anthropogenic aerosols from the boundary condition and emission inventory by a factor of 10% (hereafter "CLEAN"). Reducing polluted aerosol concentration to a more pristine environment is a common practice in studying the impact of aerosols on clouds and precipitation (e.g., Manoj et al., 2021; Fan et al., 2013, 2007). We attempt to broadly examine the microphysical effect of anthropogenic aerosols by comparing NoARI to CLEAN simulations (ACI effect). For completeness and as an effort to assess the uncertainty of anthropogenic aerosol loading in the region, a fourth simulation was performed using CTL but doubling anthropogenic aerosol concentration (D_AERO). Early results in this study suggested that the CTL simulation predicted a relatively low AOD compared to remote sensing retrievals. We use results and discuss the effect of the D_AERO simulations when necessary. Also, unless mentioned, we examine and present the results using the analysis from the inner domain.

To examine the aerosol-precipitation elevational dependence, we divided the CenHim into 30 different bins at an increasing interval of 200 m up to 6000 m and one

bin for elevation above 6000 m above sea level (ASL). **Figure 4.2** shows the elevation distribution of the number of grid points in the CenHim and the corresponding mean CTL precipitation. The relatively small number of grid points at higher elevations suggests a drop in the statistical robustness of the analyses. When possible, we perform statistical significance tests using the student's t-test at the 90% confidence level to control for the statistical signal and noise. The maximum number of grid points (7113) is present below 200 meters, while only 176 grid points are present above 6000 meters over the CenHim. The diurnal variation and the elevational dependency of each variable are obtained by computing the average among all the grid points within each bin of the elevational range.

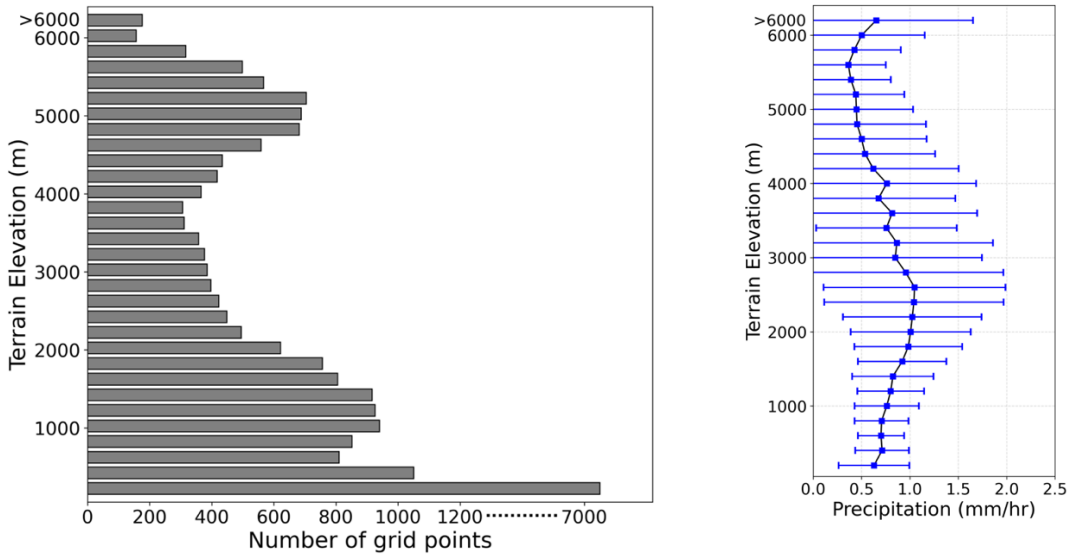

Figure 4.2: (a) The total number of grids per elevation range for 200 m bins up to 6000 m and one bin above 6000 m. (b) Variation of CTL mean (± 1 standard deviation) precipitation over the CenHim as a function of altitude.

4.2.3 Model Evaluation

CTL precipitation fields were evaluated using the sparsely distributed network of 90 rain gauge stations measuring daily accumulations (measured at 03 UTC) and provided by the Department of Hydrology and Meteorology, Nepal (see **Fig. 4.1b**). The altitudinal

station distribution ranges from 60 to 2744 m ASL. The spatial distribution of simulated precipitation was compared with the half-hourly Integrated Multi-satellite Retrievals for Global Precipitation Measurement (IMERG) level-3 data at 0.1° × 0.1° horizontal resolution (Huffman et al., 2019).

CTL simulated 550 nm Aerosol Optical Depth (AOD) is evaluated against the AOD retrievals from four ground-based Aerosol Robotic Network (AERONET version 3 level 2.0; Kathmandu Bode, Pokhara, Kanpur, and Jaipur; see **Fig. 4.1a**), satellite-based Moderate Resolution Imaging Spectroradiometer available at 10 km grid size [MODIS Terra (MOD04_L2; sensed at 1030 LST) and Aqua (MYD04_L2; sensed at 1330 LST)], and MERRA2 reanalysis product (three hourly; 0.5° × 0.625° spatial resolution). The spatial distribution of simulated AOD is compared with MODIS (level 3; 1°×1°) and MERRA2 reanalysis product (three hourly; 0.5° × 0.625° spatial resolution). The combined Dark Target and Deep Blue 550 nm AOD product from Terra and Aqua on-board MODIS satellite are used for comparison. AERONET AOD data were obtained for 1000 to 1100 LST (±30 minutes of Terra overpass time) and 1300 to 1400 LST (±30 minutes of Aqua overpass time) to match up the MODIS overpass times. For time consistency, we used 1045 LST (0500 UTC) and 1345 LST (0800 UTC) as the nearest simulated AOD times. The AERONET and MODIS retrievals of aerosol properties are limited during the monsoonal season since they provide the AOD data measured in cloud-free conditions.

Radiosonde observations from the http://weather.uwyo.edu/upperair/sounding.html at the Patna station (25.60°N, 85.1°E, 60 m ASL, only available at 00 UTC; see **Fig. 4.1a**) was used to evaluate temperature, zonal and meridional wind components, and mixing

ratio upper-air meteorological parameters. Sounding data was interpolated at 36 pressure levels between 100 and 975 hPa with an increment of 25 hPa.

4.3 Results and Discussion

4.3.1 Model Evaluation

Figure 4.3 shows the time series of the simulated AOD compared with the ground and satellited based AOD from AERONET and MODIS Aqua and Terra. Though limited data points are available for comparison, the CTL consistently underestimated the AOD, while D_AERO is comparable in magnitude with remotely sensed AOD (**Fig. 4.3**). **Figure 4.4** shows the spatial distribution of mean MODIS, MERRA2, and simulated AOD during the simulation period. Though the CTL underestimated the AOD in magnitude, it captured the spatial distribution of AOD compared to the MODIS (**Fig. 4.4a**) and MERRA2 (**Fig. 4.4b)**. Due to the higher emission rate, the aerosol is heavily concentrated over the foothills and the IGP compared to the higher elevation of the mountainous terrain. The variation in the AOD along with the topographical transect from lower to higher elevation is clearly illustrated in **Fig. 4.4**. Not surprisingly, simulated AOD is lower for the CLEAN simulation over the entire domain, with the differences being maximum in the lowlands (**Fig. 4.4b**). Although higher mountainous terrain is polluted compared to the CLEAN scenario, the CTL AOD shows that it remains pristine compared to IGP due to the strong stratification of aerosol emission with elevation and limited transport due to the topographical barrier. The doubling of the anthropogenic aerosols in D_AERO resulted in increased AOD comparable to the MODIS and MERRA2 products (**Fig. 4.4d)**. It should be noted that the MODIS and

MERRA2 are at coarser resolution and might have some biases related to the scale differences.

Underestimation of AOD by WRF-Chem is a well-known model bias and has also been reported in the east Asian monsoon region (Wu et al., 2013), Indian monsoon region (Soni et al., 2018; Govardhan et al., 2015), and Indo Gangetic Plain during monsoon by around 50% (Sarangi et al., 2015). Also, Regional Climate Model (RegCM4) underestimated AODs by a factor of 2 to 5 over south Asia in the period 2005 to 2007 (Nair et al., 2012). Mues et al. (2018) showed that the EDGAR HTAP v2.2 implemented with WRF-Chem underestimates the black carbon concentration over the Kathmandu valley by 80% in May of 2013, and one of the reasons might be the underrepresentation of traffic emissions. The lower estimation of the aerosol emission over Nepal by the global emission inventory is mainly due to the coarser resolution, emission factors, and lack of residential energy consumption consideration (Sadavarte et al., 2019). Other limitations that might contribute to the lower estimation of aerosol loading might be due to the different year used for emission inventory preparation (for 2010) and simulation in this study, the lack of representation of secondary organic aerosols, and not accounting for all major sources of emissions (e.g., emission due to infrastructure construction). Despite these well-known structural errors that have been attributed to emissions inventory and potentially result in low biases in the impact of aerosols, our results can provide meaningful insight into the role of aerosols in modulating the elevation dependence precipitation.

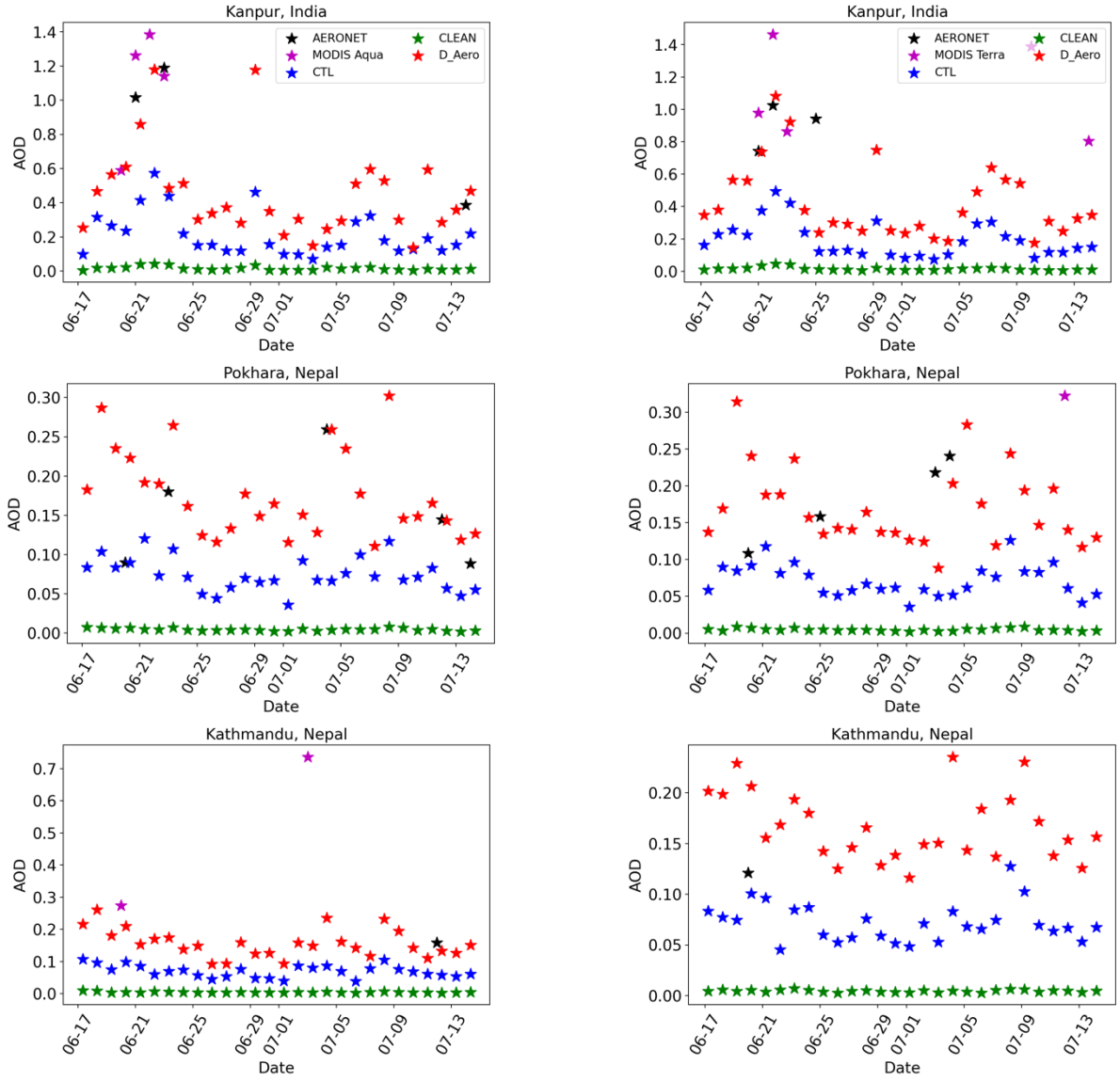

Figure 4.3: The simulated, AERONET and MODIS Aqua (first column) and Terra (second column) AOD at three AERONET stations (Kanpur, Pokhara, and Kathmandu; see Fig. 1a for location).

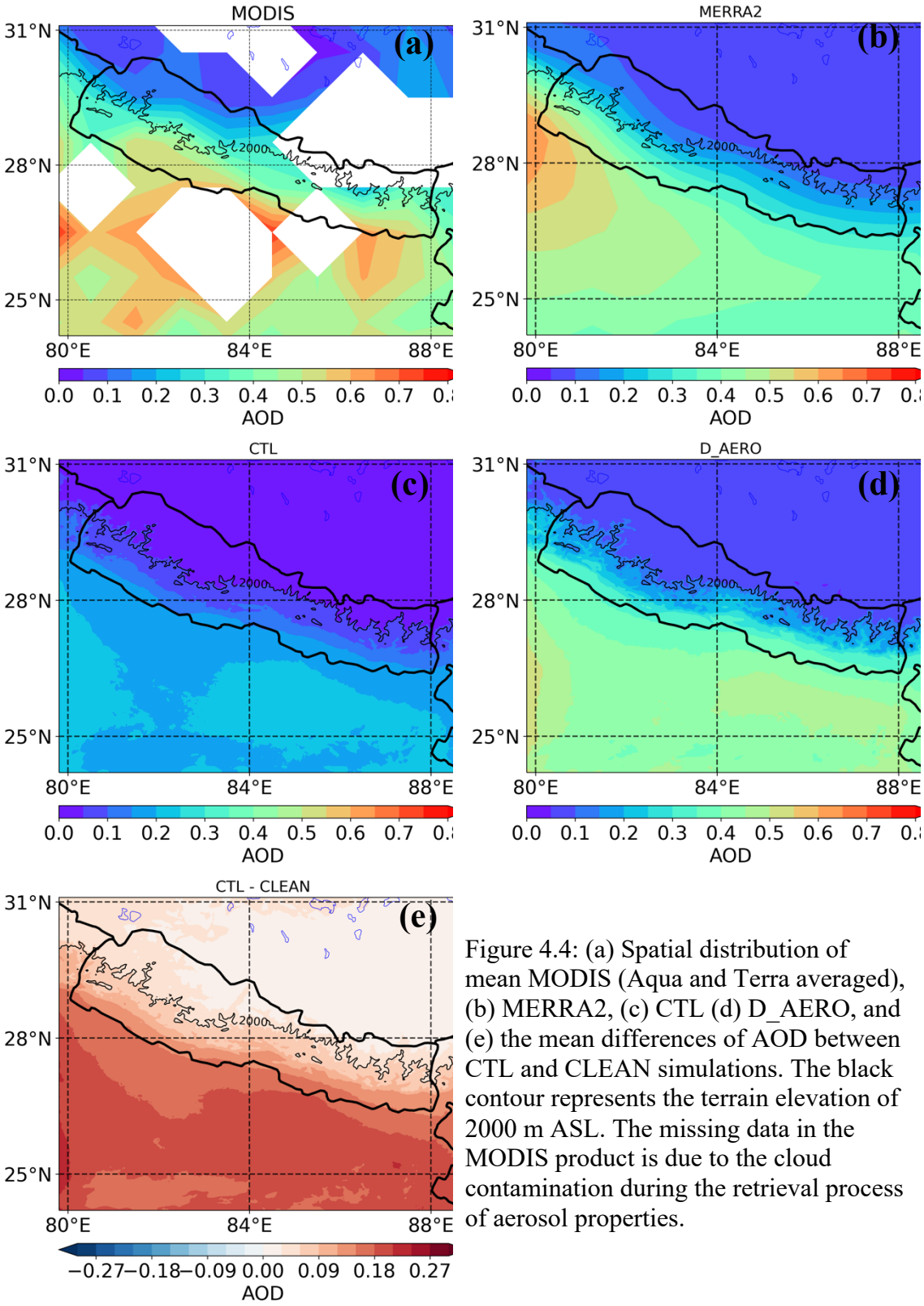

Figure 4.4: (a) Spatial distribution of mean MODIS (Aqua and Terra averaged), (b) MERRA2, (c) CTL (d) D_AERO, and (e) the mean differences of AOD between CTL and CLEAN simulations. The black contour represents the terrain elevation of 2000 m ASL. The missing data in the MODIS product is due to the cloud contamination during the retrieval process of aerosol properties.

The mean temperature, mixing ratio, and zonal and meridional wind bias profiles from the simulated output sampled from the upper air sounding observations at the Patna location are shown in **Fig. C4S2**. The model exhibits the systematic vertical easterly bias between 950 and 300 hPa. Above 900hPa, the systematic vertical dry bias (significant above 575 hPa) and minimal northerly biases are present. The cool bias prevails below 775 hPa, while the warm bias is present in the mid to upper troposphere. Though both the domains revealed a similar biases pattern, the cloud-resolving domain exhibited smaller biases.

Figure 4.5 shows the error statistics of daily precipitation at different gauge stations and simulated precipitation at the nearest grid point over Nepal. The biases in the simulated precipitation varied with elevation, where lowland (< 500 m ASL) depicted the larger bias, while the altitude between 500 and 1500 m exhibited the smallest bias. The mean bias estimation (MBE) across the rain gauge stations was lower by 0.29 mm/day with a mean root mean square error (RMSE) of 27.52 mm/day. The daily mean accumulated precipitation from the model correlated well with the gauge station data (Pearson correlation coefficient of 0.5). The maximum mean correlation was observed for the elevation between 500 and 1500 meters, the range of altitude that also depicted the minimum RMSE and MAE. Though some over or under estimation of the precipitation and higher RMSE, there is a good agreement between the onset and accumulated precipitation between the simulation and rain gauge stations (**Fig. 4.5 e-h**). Also, as suggested earlier, the lower concentration of aerosols can add up to the biases in the simulated precipitation. The manual recording of the gauge stations data and the under

catch or losses due to wind speed/direction can add up to the uncertainties in the precipitation data collection (Talchabhadel et al., 2017) and these model evaluation assessments. Also, since most rain gauge stations are over the valley floor, the precipitation simulated over the mountain top cannot be compared with the observational network.

Figure 4.6 shows the mean hourly precipitation estimates from IMERG, CTL, and the bias of CTL relative to the IMERG estimation. The model captured the overall feature of the precipitation distribution with higher precipitation over the mid-mountainous region of CenHim and leeward suppressed over northwestern Nepal and the TP. Compared to IMERG, the model underestimated the precipitation amount over the IGP, while the wet bias of the model is pronounced over the mountains of the CenHim. The overestimation of the precipitation by the WRF-Chem has also been reported in other studies over the Himalayan region (e.g., (Barman and Gokhale, 2022; Sicard et al., 2021; Adhikari and Mejia, 2022) and can be associated with the uncertainties from the physical parameterizations (e.g., Baró et al., 2015; Zhang et al., 2021). However, note that the finer resolution simulation better resolves the orographic forcing and can represent the precipitation over the complex terrain. Also, IMERG is at a coarser resolution than the model, and some biases might be related to the scale differences. The underprediction of accumulated precipitation by IMERG is evident over the rain gauge stations throughout the CenHim (**Fig. 4.5e-h**) and is consistent with the (Sharma et al., 2020a). The pronounced differences over the higher terrains of CenHim can also be associated with the underprediction of extreme precipitation events (> 25mm/day) by IMERG (Sharma et al., 2020b), which might be related to the weak detection of shallow orographic forced

precipitation event (Cao et al., 2018; Arulraj and Barros, 2019; Shige and Kummerow, 2016).

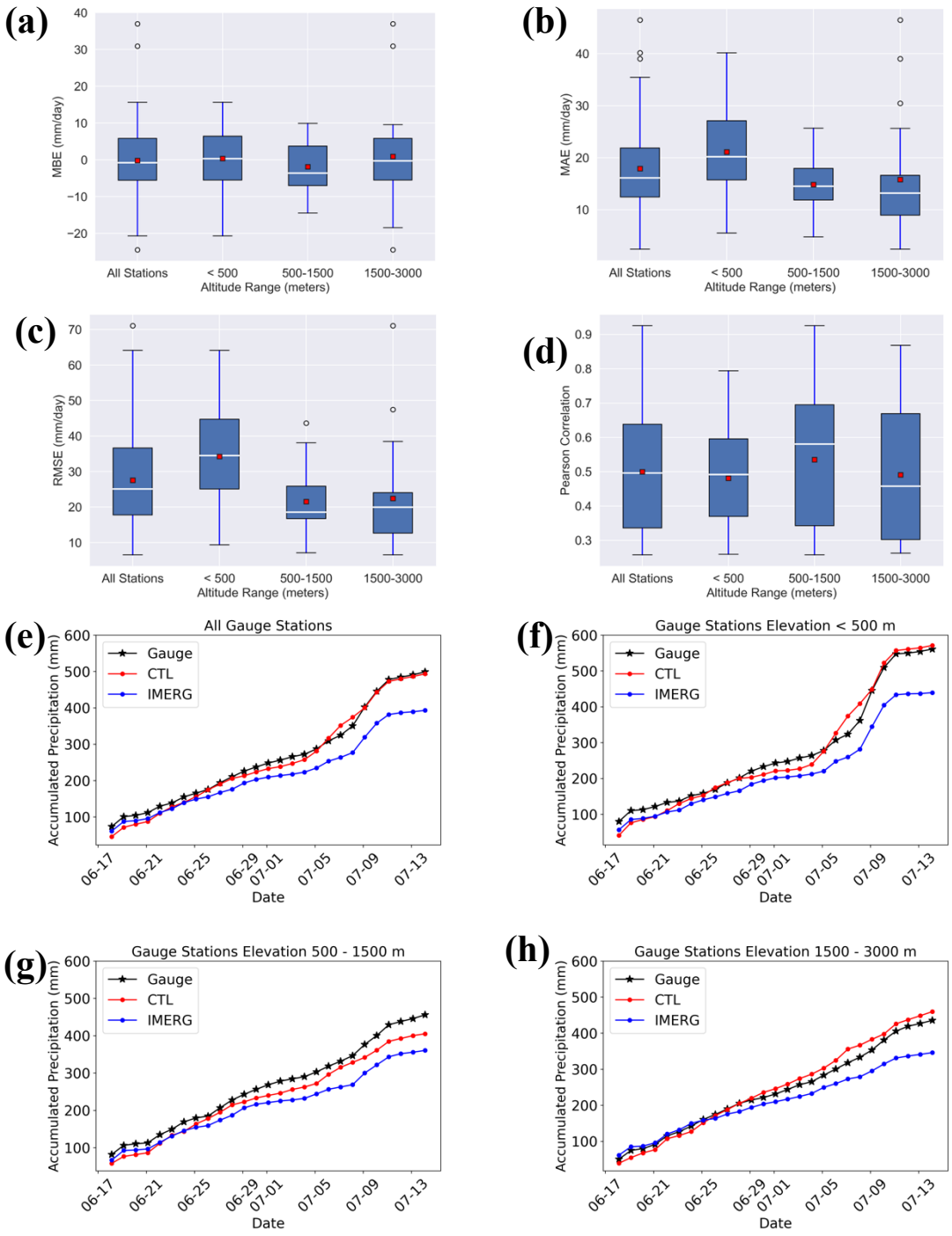

Figure 4.5 Box plots show the median, interquartile range, and extreme distribution for each of the error statistics [(**a)** MBE, (**b)** MAE, (**c)** RMSE, and (**d)** Pearson correlation] between the simulated and the rain gauge stations over Nepal, at an altitude that ranges below 500 m (41 stations), between 500 and 1500 m (28 stations), and between 1500 and 3000 m (21 stations). The red color marker at the center of the box represents the mean value. Time series of averaged accumulated precipitation at DHM rain gauge stations, CTL, and IMERG; **(e)** all rain gauge stations, stations located (**f)** below 500 m ASL, (**g)** between 500 and 1500 m, and (**h)** between 1500 and 3000 m terrain elevation.

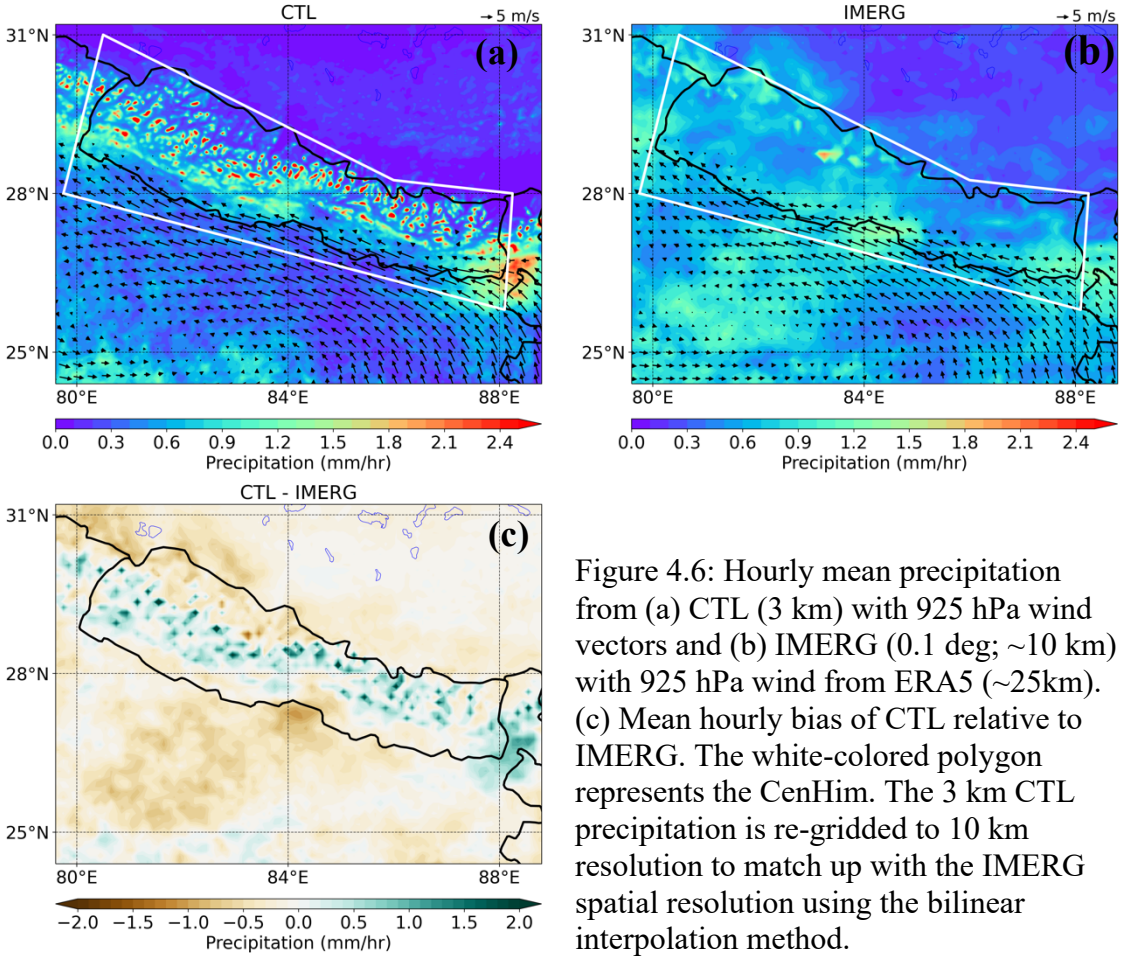

Figure 4.6: Hourly mean precipitation from (a) CTL (3 km) with 925 hPa wind vectors and (b) IMERG (0.1 deg; ~10 km) with 925 hPa wind from ERA5 (~25km). (c) Mean hourly bias of CTL relative to IMERG. The white-colored polygon represents the CenHim. The 3 km CTL precipitation is re-gridded to 10 km resolution to match up with the IMERG spatial resolution using the bilinear interpolation method.

4.3.2 Aerosol Effect on Precipitation

Figure 4.7 (a-c) shows the effect of aerosol on the spatial distribution of the mean hourly precipitation. Due to the total effect of aerosols, precipitation increases over the elevation

below 2000 m ASL except for the region just south of Nepal, with a pronounced enhancement by the ACI effect. At the same time, the reduced precipitation occurred over the high elevational region of the entire CenHim due to the combined effect of aerosol. **Figure 4.8a** shows the diurnal variation of precipitation as a function of terrain elevation. Minimum precipitation occurred throughout the elevations during the late morning (0900 to 1200 local time). The mid-altitude range, especially between 1000 and 2000 m ASL, of CenHim experiences double peaks with stronger daytime and weaker nighttime precipitation (**Fig. 4.8a**). The averaging of the entire CenHim might influence some of the diurnal features of intraregional precipitation; however, the diurnal pattern is consistent with the satellite-based findings of Fujinami et al. (2021). The surface heating and the orographic forcing enhance the convergence of daytime upslope moisture flow resulting in higher daytime precipitation over the southern slopes (Fujinami et al., 2021). In contrast, the adjacent foothills (below 600 m ASL) are characterized by single midnight to early morning peak due to the convergence of stronger nocturnal jets with the downslope winds (Fujinami et al., 2021; Terao et al., 2006). Precipitation over the higher elevation above 5000 m ASL and in the TP (rain shadow region of the Himalayas; not shown) is characterized by the afternoon peak and is consistent with Liu et al. (2022).

The diurnal variation of precipitation due to the aerosols effect as a function of elevation is presented in **Fig. 4.8 (b-d)** and shows an inconsistent response to the anthropogenic aerosols along the elevational gradient. Significant enhancement of precipitation occurred due to aerosols over the lower elevation (below 2000 m ASL) from the early morning to noon. In contrast, the aerosol suppressed afternoon (1400 to1800 local time) precipitation over the lower elevation. The significant suppression of

precipitation is observed over the higher terrain above 3000 m ASL during most of the day. Both the ARI and ACI effect of aerosols tend to reduce the precipitation over the higher elevation above 3000 m ASL. The afternoon suppression of precipitation over the lowlands (below 2000 m ASL) is dominated by the ARI effect **(Fig. 4.8c**). It is noteworthy that, though the ACI effect of aerosols suppressed the nighttime (after 1800 LST) precipitation below 1000 m ASL, it extended the enhancement of precipitation to the higher elevation up to 3600 m ASL (**Fig. 4.8d**). This can be attributed to the microphysical effect of aerosols delaying the conversion of smaller cloud droplets to raindrops and enhancing the cloud lifetime, resulting in larger advection time for orographic clouds, increasing the downwind precipitation (Givati and Rosenfeld, 2004; Choudhury et al., 2019).

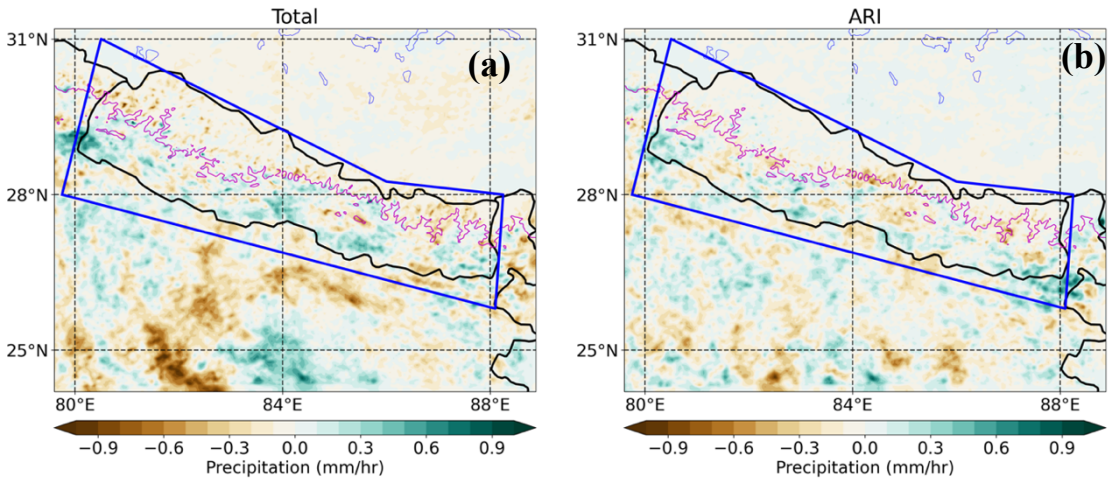

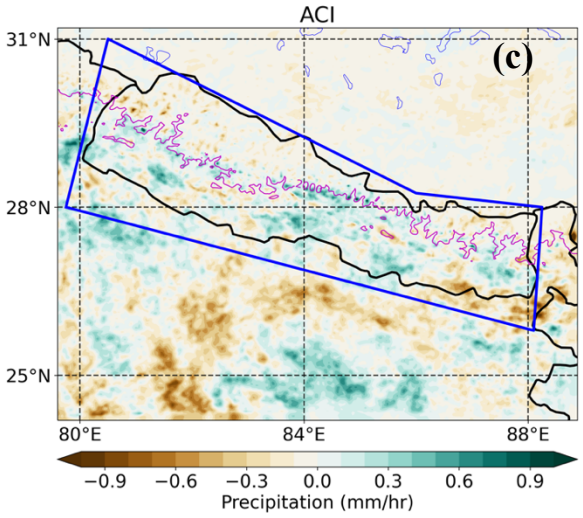

Figure 4.7: Spatial distribution of the differences in hourly mean precipitation due to the (a) aerosol effect (CTL - CLEAN), (b) ARI effect (CTL - NoARI), and (c) ACI effect (NoARI - CLEAN). The blue-colored polygon represents the CenHim, whereas the pink-colored contour indicates the 2000 m ASL terrain elevation.

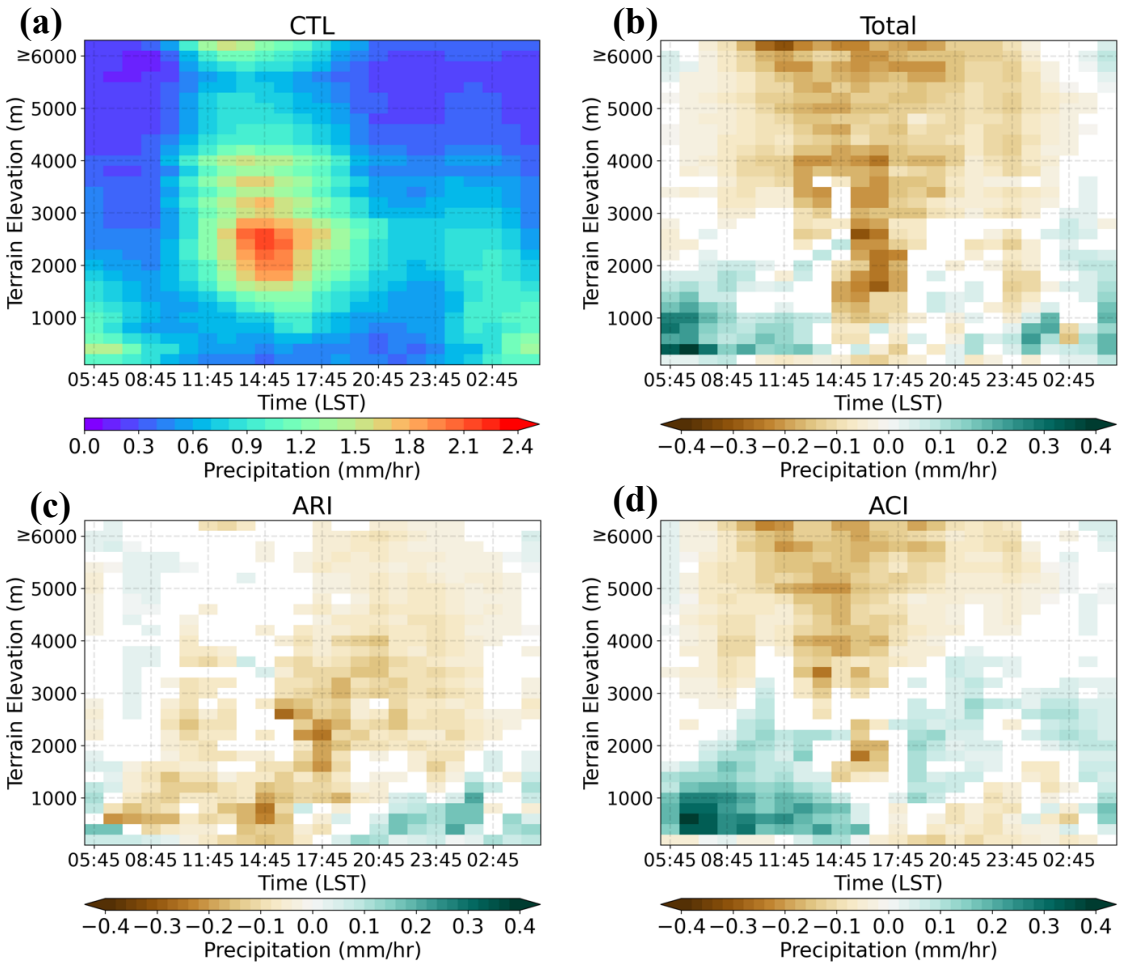

Figure 4.8: Diurnal-elevation (a) CTL precipitation, (b) aerosols effect (CTL-CLEAN), (c) ARI effect (CTL-NoARI), and (d) ACI effect (NoARI-CLEAN) and their diurnal variability. Only the differences that are significant at the 90 % confidence level based on the student t-test are plotted.

Variability in the amount of hourly precipitation increases from lower to higher altitudes (**Fig. 4.2b**), possibly due to the orographic feature associated with the abrupt change in the topographical gradient. To further investigate the response of elevational-dependent precipitation to the aerosols, we classified the mean precipitation intensity into heavy (> 1.04 mm/hr), moderate (between 0.42 and 1.04 mm/hr), and light (< 0.42 mm/hr) precipitation regime. A similar classification procedure has also been implemented by Sharma et al. (2020) for daily accumulated precipitation over Nepal Himalayas and for hourly precipitation over eastern China by Shao et al. (2022). **Figures 4.9** and **4.10** show the differences and relative change (%) in elevation dependence of the precipitation regime in precipitation due to different effects of aerosols and reveals a contrasting elevational response. Though the ACI effect slightly enhances the light precipitation below 1000 m ASL, the ARI effect dominates and monotonically suppresses the mean light precipitation by 17% over the CenHim. Whereas the ACI effect enhances the precipitation below 3000 m ASL and shows a most prominent impact on moderate to heavy precipitation regimes. Contrasting to the lower elevation, above 3000 m ASL, the ACI effect of aerosols suppressed all regimes of the precipitation intensity. The elevation between 1000 and 3000 m ASL acts as the region below and above which the different intensity of precipitation responds in the opposite direction to the effect of aerosols. The maximum increment (43%) in heavy precipitation due to the aerosol effect occurred over the elevation bin between 200-400 m ASL. Similarly, the total precipitation was

enhanced by 18% over the 200-400 m bin, while 5400-5600 m elevation experienced the maximum reduction (21%). Below 2000 m ASL, due to the combined effect of aerosols, the mean light precipitation is suppressed by 19%, while moderate and heavy precipitation is enhanced by 3% and 12%, respectively. In contrast, above 2000 m ASL, a significant suppression of all three categories of precipitation intensity is noticed with the 11% reduction in mean precipitation.

Other modeling studies over the mid-latitude mountains of the Great Alpine Region (Napoli et al., 2022) and Sierra Nevada (Wu et al., 2018) also reported the suppression of precipitation in a polluted environment over the higher elevation consistent with our findings. However, contrasting to enhanced precipitation in our result, these studies simulated the suppressed precipitation even in the lower elevations. This discrepancy might be associated with the differences in the aerosol concentration from the heavily polluted upwind region of IGP, enhanced moisture supply along with the monsoonal flow, and the steeper terrain of the Himalayas enhancing the orographic forcing and convection compared to the Great Alpine and the Sierra Nevada.

In comparison to the CLEAN scenario, the elevational-dependent precipitation showed a similar response in the diurnal cycle and spatial pattern to the increase in aerosols from CTL to D_AERO, besides the smaller changes in the magnitude (not shown). The doubling in aerosols resulted in increased monthly mean heavy precipitation below 2000 m ASL by 16% (4% higher compared to CTL run) and suppressed precipitation above the 2000 m ASL by 8% (similar to CTL run) compared to the CLEAN simulation. No significant differences were noted in the change in light precipitation due to the doubling of aerosols. It might be related to the non-linear

responses of aerosol concentration to the convective intensity, microphysical, and dynamical effect (Fan et al., 2013; Chang et al., 2015). Due to the stronger convection, the potentiality of the aerosol getting activated to cloud droplet increases, in the presence of higher concentration of aerosol.

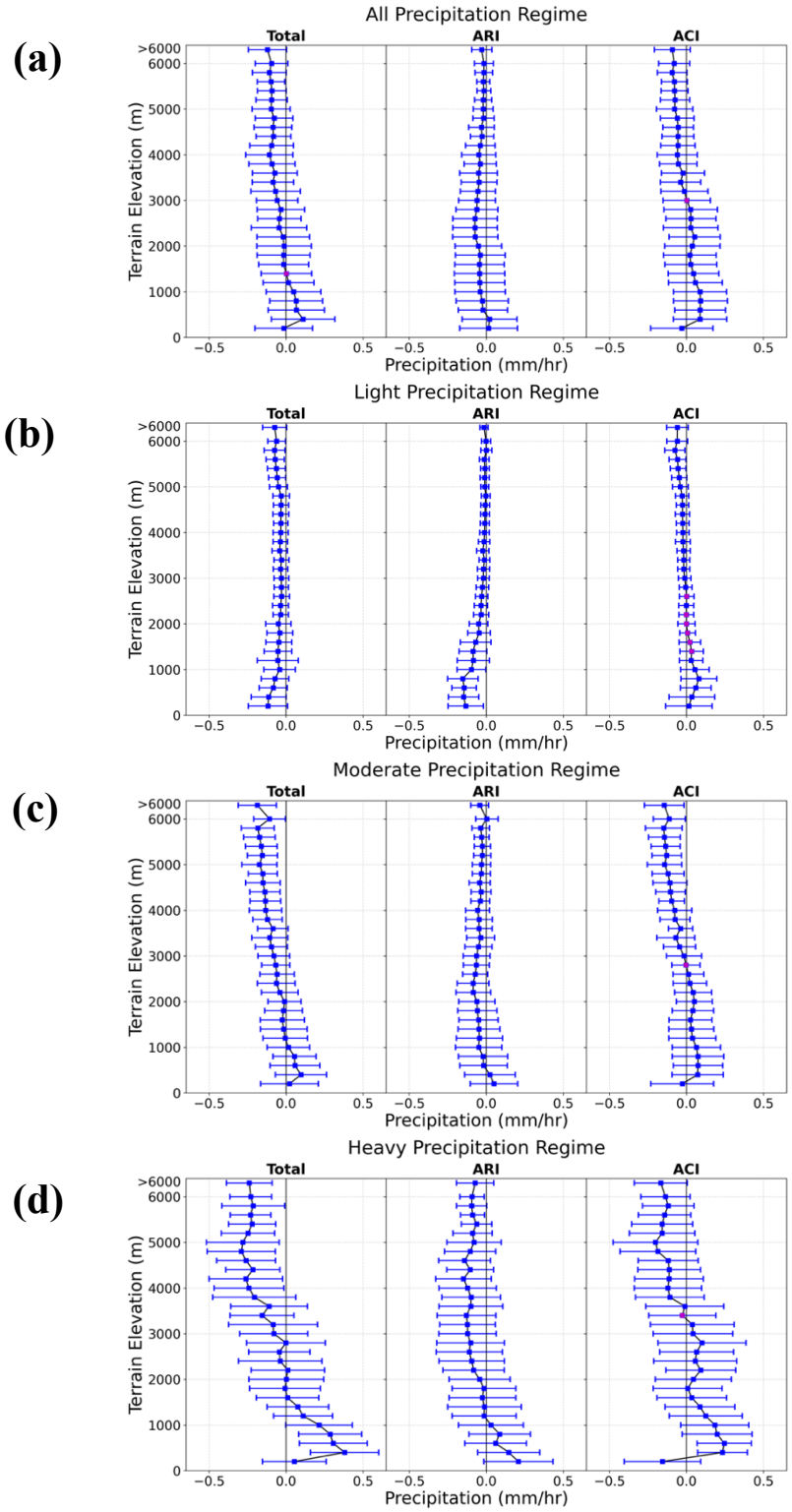

Figure 4.9: Elevational variability in different regimes [(a) all, (b) light, (c) moderate, and (d) heavy] precipitation differences due to aerosols. The blue dots and error bars respectively represent the mean

and ±1 standard deviation. The pink dot indicates that the differences between the two simulations are not significant at the 90% confidence interval based on the student t-test.

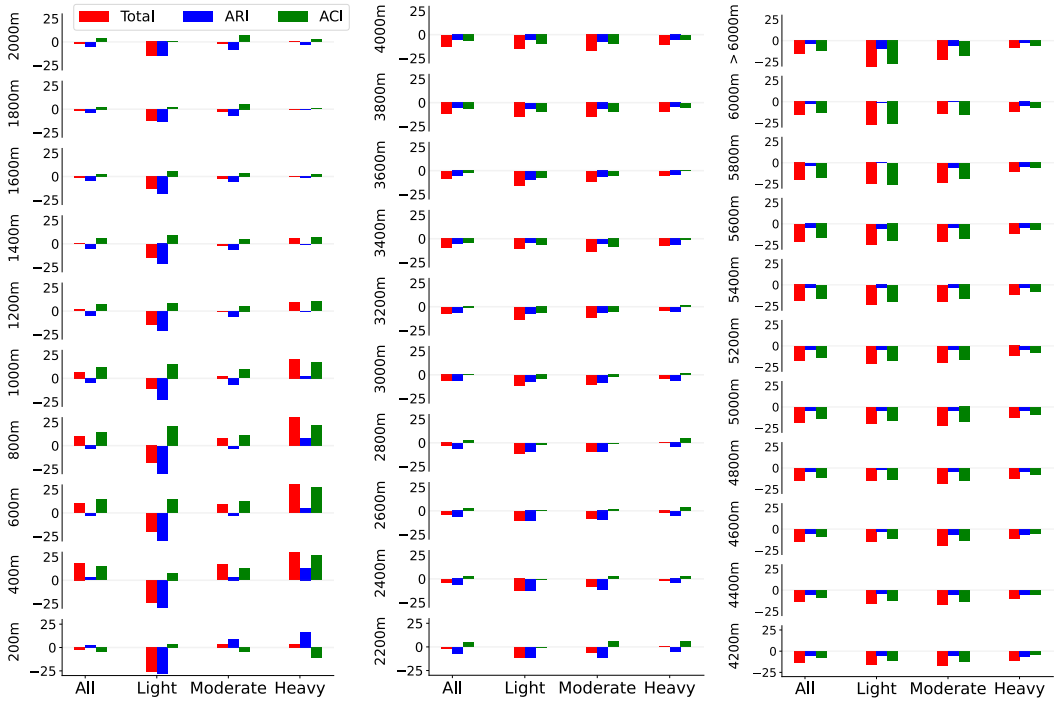

Figure 4.10: Relative change (%) in precipitation due to different effects of aerosols for all the elevational bins.

4.3.3 Aerosol Effect on Clouds

Figure 4.11a shows the CTL simulated diurnal-elevation of cloud fraction over the CenHim and resembles the diurnal precipitation pattern. The higher elevation above 4000 meters has the lower cloud coverage throughout the day due to the limited atmospheric moisture reaching the higher elevation. The ACI effect increases the cloud fraction (over most of the elevation throughout the day due to the enhanced activation of aerosol as cloud droplets (**Fig. 4.11d**). However, the ARI effect reduces the cloud coverage early in the morning below 2000 m ASL and the suppression propagate higher in elevation during the afternoon and evening (**Fig. 4.11c**), which might be associated with the weaker surface heating limiting the wind flows towards the slope of the

mountain and afternoon orographic cloud development. Although noisier and a less consistent diurnal-elevation relationship, the total aerosol effect is mostly that of enhancement of cloud cover. This result is consistent with long-term satellite retrieval of cloudiness during high aerosol concentration days (Adhikari and Mejia, 2021).

To further investigate the impact of anthropogenic aerosols on clouds and precipitation, the effect of aerosols on vertical velocity, LWP, and IWP is performed by dividing the terrain elevation below and above 2000 m ASL (**Fig. 4.12**), where the mean precipitation responded differently to the aerosols. Increased cloud coverage over the CenHim due to the aerosol effect is associated with the ACI effect resulting in enhanced cloud liquid water path (LWP) for all precipitation regimes (**Fig. 4.12c-d**). While ARI significantly contributes to the increase in ice water path (IWP; by 10%) below 2000 m ASL (**Fig. 4.12e**) along with the settle but upward 5% increase in mean vertical velocity (**Fig. 4.12a**). The ARI modulated increase in IWP below 2000 m ASL, where the amount of aerosol loading is higher, can be attributed to the warming of the atmosphere resulting in the evaporation of droplets and contributing to an increased upward moisture flux to the higher altitudes resulting in the formation of the ice. Other modeling studies have also reported an increment in the cloud ice water content due to the radiative heating effect of biomass burning (Liu et al., 2020) and dust aerosols (Dipu et al., 2013). While reduced IWP above 2000 m ASL due to ARI might be dominated by the surface cooling effect suppressing the cloud development. The minimal ACI effect in IWP is due to the lack of a model treating the activation of aerosol to ice nuclei.

The aerosol modulated vertical velocity below 2000 m ASL (**Fig. 4.12a**) suggests the convective strength is suppressed/enhanced for the light/heavy precipitation regime.

Additionally, due to the total aerosols effect, the number of strong updraft events (mean vertical velocity higher than 0.5 ms^{-1}) increased by 10% below 2000 m ASL (except for the lowest elevational bin below 200 m ASL) and reduced by 11% above 2000 m ASL (not shown). Along with the stronger convection, the enhanced IWP and LWP indicate the invigoration of the cloud resulting in increased heavier precipitation below 2000 m ASL. In contrast, the suppressed convection and more aerosol activated as a higher number of smaller cloud droplets resulted in a nonprecipitating cloud suppressing the light precipitation over the entire CenHim. The suppression of light and enhanced heavy precipitation due to modulated convective strength by anthropogenic aerosol is consistent with a simulated study over eastern China by Shao et al. (2022). The increased precipitation over the lower elevations with an invigorated convection is consistent with our other study based on satellite retrieval, showing an enhancement of precipitation due to the atmospheric aerosols over the southern slopes of the Central Himalayas (Adhikari and Mejia, 2021). Also, another satellite-based study by Choudhury et al. (2020) suggests the higher aerosol loading with the increased moist static energy significantly contributed to the enhancement of heavier precipitation over the Himalayan foothills.

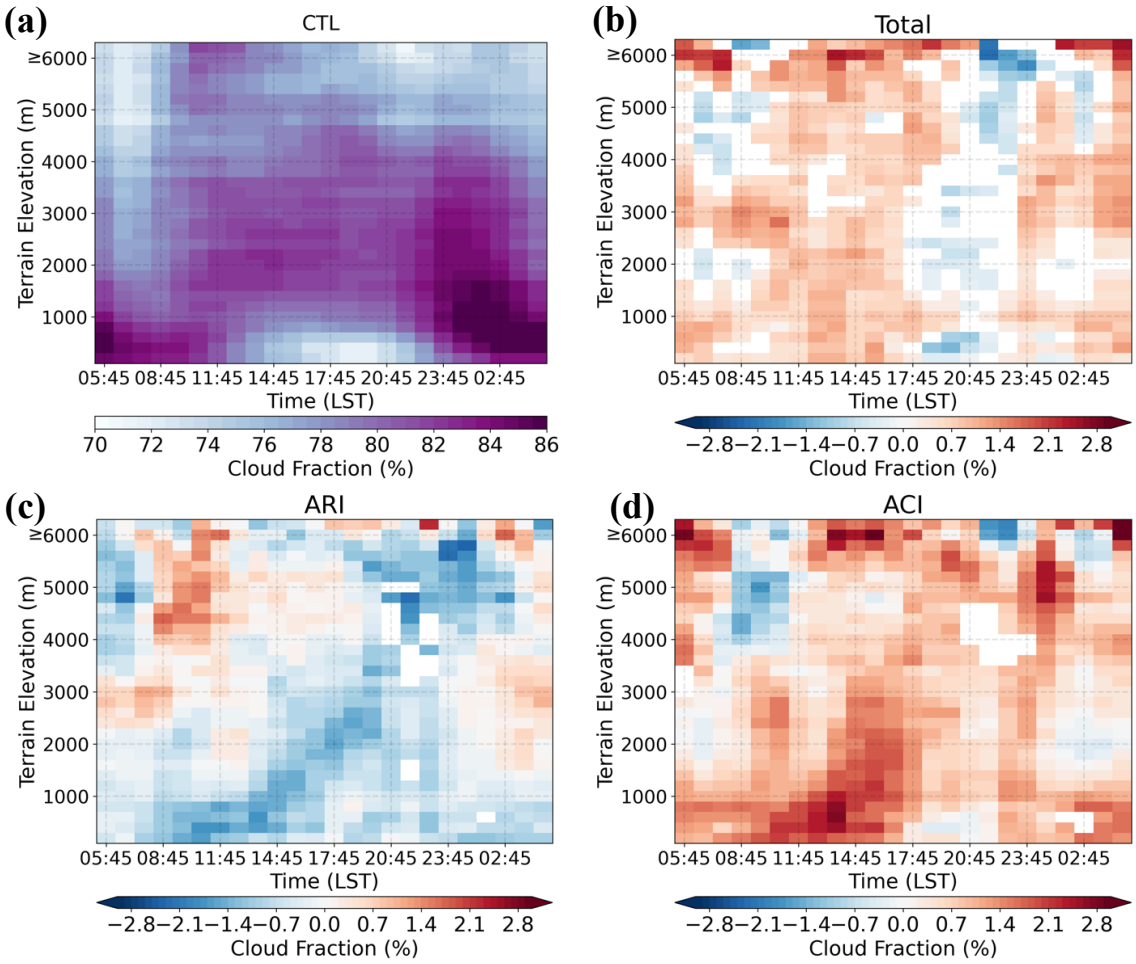

Figure 4.11: Diurnal-elevation of cloud fraction (a) CTL, and due to (b) aerosol effect (CTL - CLEAN), (c) ARI effect (CTL - NoARI), and (d) ACI effect (NoARI - CLEAN) and their diurnal variability. Only the differences that are significant at the 90 % confidence level based on the student t-test are plotted.

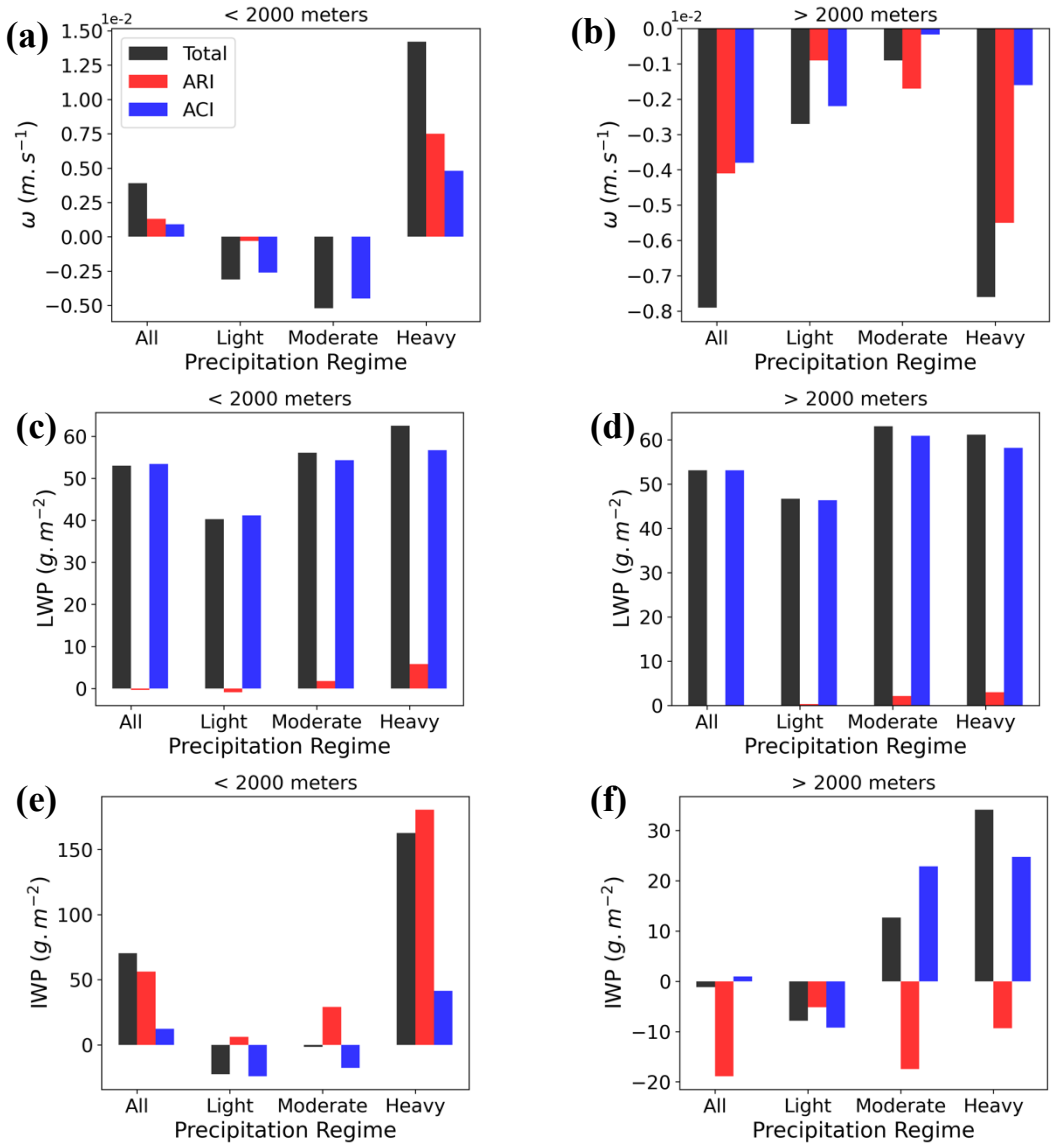

Figure 4.12: Monthly mean perturbation of (a, b) vertical velocity, (c, d) LWP, and (e, f) IWP over the CenHim region for the terrain elevation below (first column) and above (second column) surface elevation of 2000 m ASL, for total, light, moderate, and heavy precipitation regime.

4.3.4 Aerosol effect on Temperature and Radiation

Figure 4.13a shows the diurnal variation of decreasing temperature with increasing variability from low to high elevations. The diurnal-elevation surface cooling effect due to anthropogenic aerosols during the daytime is stronger throughout the elevational ranges (**Fig. 4.13b-d**). The daytime surface temperature cooling of -1.3 °C is likely due to the total effect of aerosols over the terrain elevation above 4000 m ASL, with the ACI effect contributing to most of the cooling (-1.1 °C). The daytime variation of change in surface temperature is consistent with all sky downwelling shortwave radiation flux at the surface (hereafter SW; **Fig. 4.14**). Over the Great Alpine Region of Europe, Napoli et al. (2022) reported simulated results showing similar high-elevation daytime surface cooling related to enhanced aerosol loadings. Another striking feature in **Fig. 4.14** is the smaller but significant nighttime surface temperature warming (+0.03 °C) above 2000 m ASL, likely related to enhanced cloudiness (**Fig. 4.11**) favoring trapping of the longwave radiation (**Fig. C4S3**). Our results indicate that the ACI effect of aerosols can significantly contribute to nighttime warming over the higher elevation.

A prominent increase in minimum temperature in the recent decades over the higher elevation of the Himalayan region has also been reported in the previous studies (e.g., Dimri et al., 2022; Liu et al., 2009). The enhanced nighttime minimum temperature has also been attributed to the enhanced cloud cover over the higher topographical elevation (Rangwala and Miller, 2012; Liu et al., 2009) and increased cloud liquid water path due to the aerosol indirect effect over East Asia (Huang et al., 2006b). Notably, the lack of aerosol snow interaction and deposition of light-absorbing aerosols on the snow surfaces in our simulation can add uncertainties in simulated temperature differences. The

deposition of absorbing aerosol on snow has a crucial impact on the snow darkening effect, the surface temperature, and the radiative forcing of the snowcapped Himalayan region (Qian et al., 2015; Sarangi et al., 2019). Also, Wu et al. (2018) showed that the inclusion of aerosol snow interaction in the simulation resulted in a significant increase in the surface temperature of the snowcapped mountain of Sierra Nevada.

Figure 4.14 (a-c) shows aerosol total, ARI, and ACI effects on diurnal-elevational variation of all sky SW, highlighting the stronger reduction of SW due to the aerosol effect at high elevations. The terrain elevation above 4000 m ASL noted the reduction of SW by -82.8 W m^{-2}, and most contribution is from the ACI effect of aerosols (**Fig. 4.14c**). The negative shortwave radiative perturbation at the surface due to the ACI effect is stronger and can be attributed to the higher cloud liquid water path (LWP) and enhanced cloud albedo due to more aerosols activated as condensation nuclei (Twomey, 1977). The stronger reduction of mid-day all sky SW over the higher elevation compared to the lower elevation is due to the ACI effect, which results in the formation of persistent polluted orographic clouds along with the upslope wind. A distinct difference in the impact of an elevational gradient in the SW for the clear sky (excluding cloud; **Fig. 4.14 d-f**) and all sky (including cloud) conditions are also noted. The reduction of the clear sky SW due to the aerosols at the terrain elevation below 1200 meters is stronger (-21 WM^{-2}), where the aerosol loadings are higher and is dominated by the ARI effect of aerosols. The higher elevation above 4000 m ASL experienced the smaller negative perturbation of clear sky SW radiation (> -5 Wm^{-2}). This change in clear sky SW in a relatively polluted environment at a higher elevation is consistent with a study by Marcq

et al. (2010) reporting a similar change near the base camp (5079 m ASL) of Mount Everest.

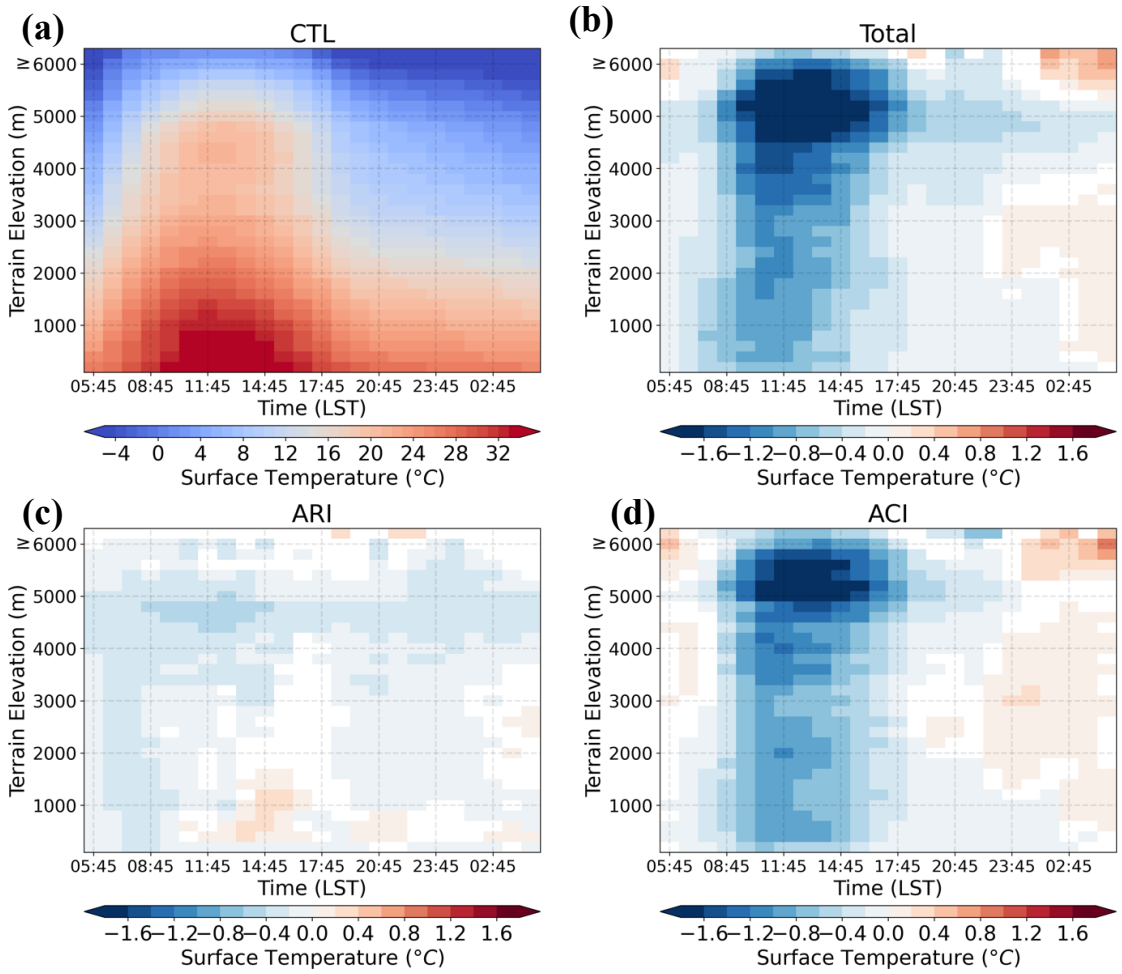

Figure 4.13: Diurnal-elevation of temperature (a) CTL simulated, and due to (b) aerosol effect (CTL - CLEAN), (c) ARI effect (CTL - NoARI), and (d) ACI effect (NoARI - CLEAN) and their diurnal variability. Only the differences that are significant at the 90 % confidence level based on the student t-test are plotted.

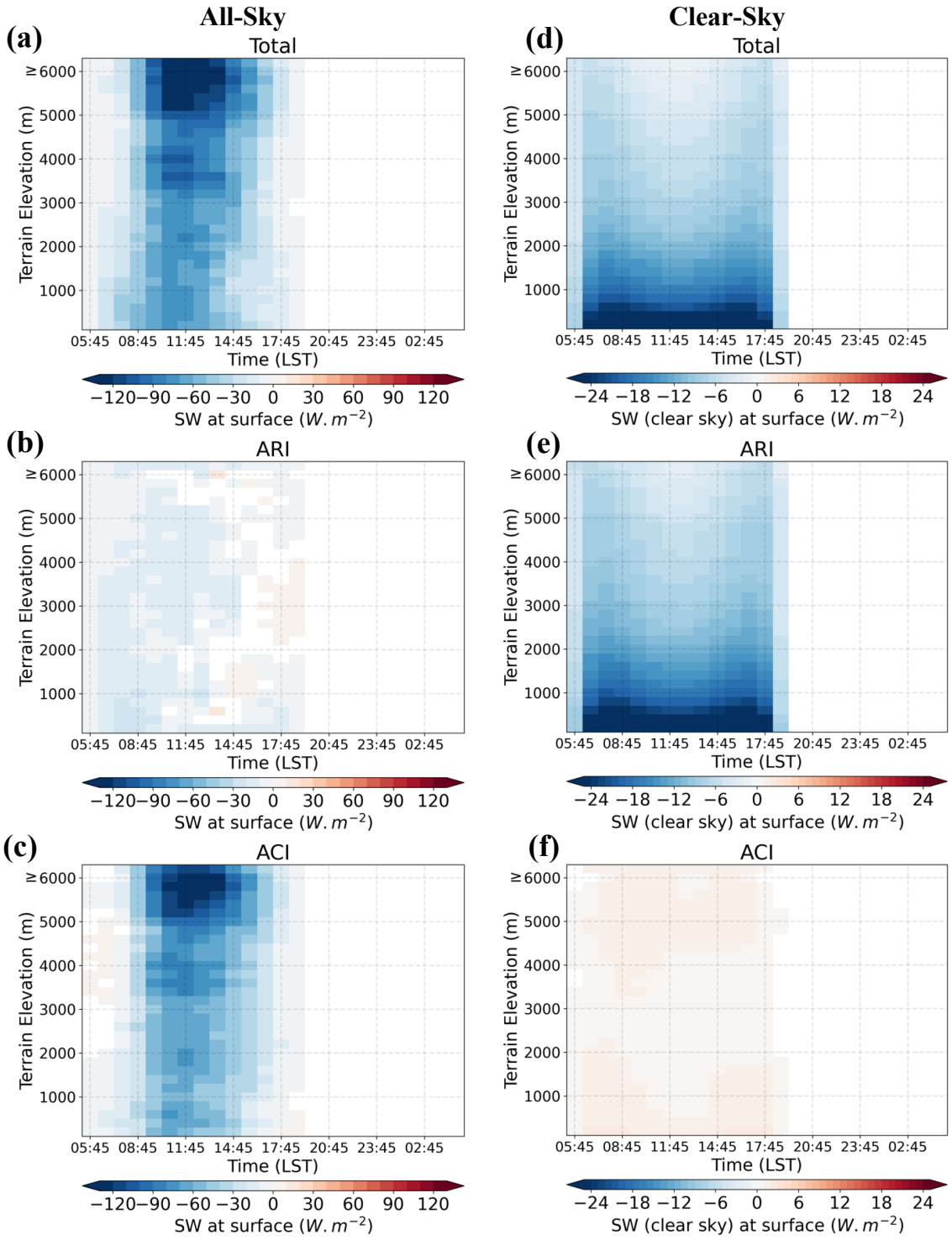

Figure 4.14: Diurnal-elevation all-sky (first column) and clear-sky (second column) downwelling shortwave radiation at the surface due to (a, c) aerosols (CTL - CLEAN), (b, d) ARI effect (CTL - NoARI), and (e, f) ACI effect (NoARI - CLEAN) and their

diurnal variability. Only the differences that are significant at the 90 % confidence level based on the student t-test are plotted.

The numerical simulation implemented in this study has several limitations. Few sensitivity simulations were only performed to assess the precipitation response to the different effect of aerosols, due to the limited computational resources. The lack of complete effects of aerosols in the model, such as INP activation and formation of secondary organic aerosols, can induce and add up the biases in our result. In this simulation, the contribution from the impact of aerosol snow interaction is not included, which can also play a part in modulating the mountain top surface temperature and orographic precipitation (Wu et al., 2018). The SNICAR (Snow, Ice, and Aerosol Radiation) model (Flanner et al., 2007), capable of simulating the snow surface albedo and aerosol radiative effect in snow, can be coupled with the WRF-Chem to study the aerosol-snow-interaction (Zhao et al., 2014). Also, it is noted that there are some biases in assessing the ACI effect associated with the presence of 10% aerosols and contribution from the fire and biogenic emissions in the CLEAN scenario. Furthermore, the 3 km grid sizes might be relatively coarser to resolve the orographic forcing and mountain-valley circulation of the steep and complex topography of the Himalayas. Advancement in the emission inventory and parameterization schemes is required to reduce the biases in the simulated AOD and precipitation for better quantifying elevation-dependent precipitation response to aerosols.

4.4 Conclusions

The presence of steep mountainous terrain and orographic distribution drives the very complex and non-linear precipitation system over the Central Himalayan region. Despite the importance on the hydrological processes of the Himalayas, the research studying the impact of aerosols in modulating the elevation-dependent precipitation over the Central Himalayas using cloud-resolving numerical simulation has not been performed. The first monsoonal month of 2013 (June 14 to July 15) is simulated using a high-resolution cloud-resolving WRF-Chem numerical modeling to understand the impact of aerosols on the elevation-dependent precipitation over the very complex terrain of the Central Himalayan region. In addition to explicitly resolving the cloud evolution, the detailed topographical representation by the cloud-resolving scale model better simulates the emission and transport processes of aerosols. So, the cloud-resolving simulation is important to provide better insight and quantify the impact of aerosol on elevation-dependent precipitation over the complex terrain. In addition to CTL (baseline) simulation, two different numerical experiments were performed similar to the CTL run but turning off the aerosol radiation feedback and reducing the anthropogenic aerosols to 10% of CTL. The comparison between the simulations allowed us to assess and discuss the relative impact of aerosol radiation and cloud interaction on the diurnal variation and different regimes of elevation-dependent precipitation and temperature.

The results show the total effect of anthropogenic aerosols cooled the daytime surface monotonically from lower to higher elevations. The higher elevation showed a strong diurnal variation in surface temperature, with a strong cooling above 4000 m ASL during the daytime (by -1.3°C) and above 2000m ASL, a nighttime warming (+0.03 °C).

The increased LWP and cloud coverage during daytime with higher aerosol concentration is attributed to the reduced SW and daytime temperature, while nighttime warming is due to the trapping of longwave radiation.

The simulated results show the contrasting response by diurnal and different regimes of precipitation to the anthropogenic aerosols. The total effect of aerosols tends to enhance the precipitation over the elevation below 2000 m ASL, while a significant reduction of precipitation occurred above 2000 m ASL with a dominating contribution from ACI effect. The mid elevation, generally between 1000 and 3000 m ASL, act as a threshold region below and above which the diurnal variation and various intensity of precipitation respond differently to the ARI, ACI, and total effect of aerosols. The combined impact of aerosols reduced the mean light precipitation across the CenHim region by 17%. However, along with the stronger convection below 2000 m ASL the ACI effect dominated and resulted in the enhancement of the heavy precipitation by 12%, contrasting to the reduction by 8% over the higher elevations. The result of our study can have broader impact and suggests enhanced heavy precipitation over the elevation below 2000 m ASL can increase the risk for extreme events (floods and landslides), while the suppressed high elevation precipitation can be critical for the regional supply of water resources (Immerzeel et al., 2010).

Despite some biases that exist in the simulation, our results underline the noticeable impact of aerosols on elevational-dependent precipitation. Though we simulated only the first month of the monsoon, our results indicate that the anthropogenic aerosol plays a significant role in enhancing (suppressing) the low elevation (high elevation) precipitation over the CenHim during the monsoon. To better understand the

seasonal and annual trend of atmospheric aerosols modulated elevation dependent precipitation over the CenHim, we need to perform long term simulations with a better parametrization scheme to include the maximum effect of aerosols. This could be the future scope and extension of this study.

References

Abdul-Razzak, H. and Ghan, S. J.: A parameterization of aerosol activation 3. Sectional representation, Journal of Geophysical Research: Atmospheres, 107, AAC 1-1-AAC 1-6, https://doi.org/10.1029/2001JD000483, 2002.

Ackerman, A. S., Toon, O. B., Stevens, D. E., Heymsfield, A. J., Ramanathan, V., and Welton, E. J.: Reduction of Tropical Cloudiness by Soot, Science, https://doi.org/10.1126/science.288.5468.1042, 2000.

Adhikari, P. and Mejia, J. F.: Influence of aerosols on clouds, precipitation and freezing level height over the foothills of the Himalayas during the Indian summer monsoon, Clim Dyn, https://doi.org/10.1007/s00382-021-05710-2, 2021.

Adhikari, P. and Mejia, J. F.: Impact of transported dust aerosols on precipitation over the Nepal Himalayas using convection-permitting WRF-Chem simulation, Atmospheric Environment: X, 15, 100179, https://doi.org/10.1016/j.aeaoa.2022.100179, 2022.

Albrecht, B. A.: Aerosols, Cloud Microphysics, and Fractional Cloudiness, Science, 245, 1227–1230, https://doi.org/10.1126/science.245.4923.1227, 1989.

Andreae, M. O. and Rosenfeld, D.: Aerosol–cloud–precipitation interactions. Part 1. The nature and sources of cloud-active aerosols, Earth-Science Reviews, 89, 13–41, https://doi.org/10.1016/j.earscirev.2008.03.001, 2008.

Andreae, M. O., Rosenfeld, D., Artaxo, P., Costa, A. A., Frank, G. P., Longo, K. M., and Silva-Dias, M. A. F.: Smoking rain clouds over the Amazon, Science, 303, 1337–1342, https://doi.org/10.1126/science.1092779, 2004.

Archer-Nicholls, S., Lowe, D., Schultz, D. M., and McFiggans, G.: Aerosol–radiation–cloud interactions in a regional coupled model: the effects of convective parameterisation and resolution, Atmos. Chem. Phys., 16, 5573–5594, https://doi.org/10.5194/acp-16-5573-2016, 2016.

Arulraj, M. and Barros, A. P.: Improving quantitative precipitation estimates in mountainous regions by modelling low-level seeder-feeder interactions constrained by Global Precipitation Measurement Dual-frequency Precipitation Radar measurements, Remote Sensing of Environment, 231, 111213, https://doi.org/10.1016/j.rse.2019.111213, 2019.

Barman, N. and Gokhale, S.: Aerosol influence on the pre-monsoon rainfall mechanisms over North-East India: A WRF-Chem study, Atmospheric Research, 268, 106002, https://doi.org/10.1016/j.atmosres.2021.106002, 2022.

Baró, R., Jiménez-Guerrero, P., Balzarini, A., Curci, G., Forkel, R., Grell, G., Hirtl, M., Honzak, L., Langer, M., Pérez, J. L., Pirovano, G., San José, R., Tuccella, P., Werhahn, J., and Žabkar, R.: Sensitivity analysis of the microphysics scheme in WRF-Chem contributions to AQMEII phase 2, Atmospheric Environment, 115, 620–629, https://doi.org/10.1016/j.atmosenv.2015.01.047, 2015.

Bradley, R. S., Keimig, F. T., Diaz, H. F., and Hardy, D. R.: Recent changes in freezing level heights in the Tropics with implications for the deglacierization of high mountain regions, Geophysical Research Letters, 36, https://doi.org/10.1029/2009GL037712, 2009.

Buchholz, R. R., Emmons, L. K., Tilmes, S., and The CESM2 Development Team: CESM2. 1/CAM-chem instantaneous output for boundary conditions, UCAR/NCAR-Atmospheric Chemistry Observations and Modeling Laboratory, https://doi.org/10.5065/NMP7-EP60, 2019.

Cao, Q., Painter, T. H., Currier, W. R., Lundquist, J. D., and Lettenmaier, D. P.: Estimation of Precipitation over the OLYMPEX Domain during Winter 2015/16, Journal of Hydrometeorology, 19, 143–160, https://doi.org/10.1175/JHM-D-17-0076.1, 2018.

Chang, D., Cheng, Y., Reutter, P., Trentmann, J., Burrows, S. M., Spichtinger, P., Nordmann, S., Andreae, M. O., Pöschl, U., and Su, H.: Comprehensive mapping

and characteristic regimes of aerosol effects on the formation and evolution of pyro-convective clouds, Atmospheric Chemistry and Physics, 15, 10325–10348, https://doi.org/10.5194/acp-15-10325-2015, 2015.

Chapman, E. G., Jr, W. I. G., Easter, R. C., Barnard, J. C., Ghan, S. J., Pekour, M. S., and Fast, J. D.: Coupling aerosol-cloud-radiative processes in the WRF-Chem model: Investigating the radiative impact of elevated point sources, Atmos. Chem. Phys., 20, 2009.

Cho, C., Li, R., Wang, S.-Y., Yoon, J.-H., and Gillies, R. R.: Anthropogenic footprint of climate change in the June 2013 northern India flood, Clim Dyn, 46, 797–805, https://doi.org/10.1007/s00382-015-2613-2, 2016.

Choudhury, G., Tyagi, B., Singh, J., Sarangi, C., and Tripathi, S. N.: Aerosol-orography-precipitation – A critical assessment, Atmospheric Environment, 214, 116831, https://doi.org/10.1016/j.atmosenv.2019.116831, 2019.

Choudhury, G., Tyagi, B., Vissa, N. K., Singh, J., Sarangi, C., Tripathi, S. N., and Tesche, M.: Aerosol-enhanced high precipitation events near the Himalayan foothills, Atmospheric Chemistry and Physics, 20, 15389–15399, https://doi.org/10.5194/acp-20-15389-2020, 2020.

Dey, S. and Di Girolamo, L.: A decade of change in aerosol properties over the Indian subcontinent, Geophysical Research Letters, 38, https://doi.org/10.1029/2011GL048153, 2011.

DHM Nepal: Monsoon onset and withdrawal date information. http://www.dhm.gov.np/uploads/climatic/841739888monsoon%20onset%20n%20withdrawal%20English_6%20June%202022.pdf, 2022.

Dimri, A. P., Palazzi, E., and Daloz, A. S.: Elevation dependent precipitation and temperature changes over Indian Himalayan region, Clim Dyn, https://doi.org/10.1007/s00382-021-06113-z, 2022.

Dipu, S., Prabha, T. V., Pandithurai, G., Dudhia, J., Pfister, G., Rajesh, K., and Goswami, B. N.: Impact of elevated aerosol layer on the cloud macrophysical properties prior to monsoon onset, Atmospheric Environment, 70, 454–467, https://doi.org/10.1016/j.atmosenv.2012.12.036, 2013.

Eidhammer, T., Barth, M. C., Petters, M. D., Wiedinmyer, C., and Prenni, A. J.: Aerosol microphysical impact on summertime convective precipitation in the Rocky Mountain region, Journal of Geophysical Research: Atmospheres, 119, 11,709-11,728, https://doi.org/10.1002/2014JD021883, 2014.

Emmons, L. K., Schwantes, R. H., Orlando, J. J., Tyndall, G., Kinnison, D., Lamarque, J.-F., Marsh, D., Mills, M. J., Tilmes, S., Bardeen, C., Buchholz, R. R., Conley, A., Gettelman, A., Garcia, R., Simpson, I., Blake, D. R., Meinardi, S., and Pétron, G.: The Chemistry Mechanism in the Community Earth System Model Version 2 (CESM2), Journal of Advances in Modeling Earth Systems, 12, e2019MS001882, https://doi.org/10.1029/2019MS001882, 2020.

Fan, J., Zhang, R., Li, G., and Tao, W.-K.: Effects of aerosols and relative humidity on cumulus clouds, Journal of Geophysical Research: Atmospheres, 112, https://doi.org/10.1029/2006JD008136, 2007.

Fan, J., Leung, L. R., Rosenfeld, D., Chen, Q., Li, Z., Zhang, J., and Yan, H.: Microphysical effects determine macrophysical response for aerosol impacts on deep convective clouds, PNAS, 110, E4581–E4590, https://doi.org/10.1073/pnas.1316830110, 2013.

Fan, J., Rosenfeld, D., Yang, Y., Zhao, C., Leung, L. R., and Li, Z.: Substantial contribution of anthropogenic air pollution to catastrophic floods in Southwest China, Geophysical Research Letters, 42, 6066–6075, https://doi.org/10.1002/2015GL064479, 2015.

Fan, J., Leung, L. R., Rosenfeld, D., and DeMott, P. J.: Effects of cloud condensation nuclei and ice nucleating particles on precipitation processes and supercooled

liquid in mixed-phase orographic clouds, Atmospheric Chemistry and Physics, 17, 1017–1035, https://doi.org/10.5194/acp-17-1017-2017, 2017.

Fast, J. D., Gustafson, W. I., Easter, R. C., Zaveri, R. A., Barnard, J. C., Chapman, E. G., Grell, G. A., and Peckham, S. E.: Evolution of ozone, particulates, and aerosol direct radiative forcing in the vicinity of Houston using a fully coupled meteorology-chemistry-aerosol model, Journal of Geophysical Research: Atmospheres, 111, https://doi.org/10.1029/2005JD006721, 2006.

Flanner, M. G., Zender, C. S., Randerson, J. T., and Rasch, P. J.: Present-day climate forcing and response from black carbon in snow, Journal of Geophysical Research: Atmospheres, 112, https://doi.org/10.1029/2006JD008003, 2007.

Fujinami, H., Fujita, K., Takahashi, N., Sato, T., Kanamori, H., Sunako, S., and Kayastha, R. B.: Twice-Daily Monsoon Precipitation Maxima in the Himalayas Driven by Land Surface Effects, Journal of Geophysical Research: Atmospheres, 126, e2020JD034255, https://doi.org/10.1029/2020JD034255, 2021.

Gery, M. W., Whitten, G. Z., Killus, J. P., and Dodge, M. C.: A photochemical kinetics mechanism for urban and regional scale computer modeling, Journal of Geophysical Research: Atmospheres, 94, 12925–12956, https://doi.org/10.1029/JD094iD10p12925, 1989.

Ghimire, S., Choudhary, A., and Dimri, A. P.: Assessment of the performance of CORDEX-South Asia experiments for monsoonal precipitation over the Himalayan region during present climate: part I, Clim Dyn, 50, 2311–2334, https://doi.org/10.1007/s00382-015-2747-2, 2018.

Givati, A. and Rosenfeld, D.: Quantifying Precipitation Suppression Due to Air Pollution, Journal of Applied Meteorology and Climatology, 43, 1038–1056, https://doi.org/10.1175/1520-0450(2004)043<1038:QPSDTA>2.0.CO;2, 2004.

Govardhan, G., Nanjundiah, R. S., Satheesh, S. K., Krishnamoorthy, K., and Kotamarthi, V. R.: Performance of WRF-Chem over Indian region: Comparison with measurements, J Earth Syst Sci, 124, 875–896, https://doi.org/10.1007/s12040-015-0576-7, 2015.

Grell, G. A. and Dévényi, D.: A generalized approach to parameterizing convection combining ensemble and data assimilation techniques, Geophysical Research Letters, 29, 38-1-38–4, https://doi.org/10.1029/2002GL015311, 2002.

Grell, G. A., Peckham, S. E., Schmitz, R., McKeen, S. A., Frost, G., Skamarock, W. C., and Eder, B.: Fully coupled "online" chemistry within the WRF model, Atmospheric Environment, 39, 6957–6975, https://doi.org/10.1016/j.atmosenv.2005.04.027, 2005.

Guenther, A., Karl, T., Harley, P., Wiedinmyer, C., Palmer, P. I., and Geron, C.: Estimates of global terrestrial isoprene emissions using MEGAN (Model of Emissions of Gases and Aerosols from Nature), Atmospheric Chemistry and Physics, 6, 3181–3210, https://doi.org/10.5194/acp-6-3181-2006, 2006.

Guenther, A. B., Jiang, X., Heald, C. L., Sakulyanontvittaya, T., Duhl, T., Emmons, L. K., and Wang, X.: The Model of Emissions of Gases and Aerosols from Nature version 2.1 (MEGAN2.1): an extended and updated framework for modeling biogenic emissions, Geoscientific Model Development, 5, 1471–1492, https://doi.org/10.5194/gmd-5-1471-2012, 2012.

Hallquist, M., Wenger, J. C., Baltensperger, U., Rudich, Y., Simpson, D., Claeys, M., Dommen, J., Donahue, N. M., George, C., Goldstein, A. H., Hamilton, J. F., Herrmann, H., Hoffmann, T., Iinuma, Y., Jang, M., Jenkin, M. E., Jimenez, J. L., Kiendler-Scharr, A., Maenhaut, W., McFiggans, G., Mentel, T. F., Monod, A., Prévôt, A. S. H., Seinfeld, J. H., Surratt, J. D., Szmigielski, R., and Wildt, J.: The formation, properties and impact of secondary organic aerosol: current and

emerging issues, Atmospheric Chemistry and Physics, 9, 5155–5236, https://doi.org/10.5194/acp-9-5155-2009, 2009.

Hansen, J., Sato, M., and Ruedy, R.: Radiative forcing and climate response, Journal of Geophysical Research: Atmospheres, 102, 6831–6864, https://doi.org/10.1029/96JD03436, 1997.

Haywood, J. and Boucher, O.: Estimates of the direct and indirect radiative forcing due to tropospheric aerosols: A review, Reviews of Geophysics, 38, 513–543, https://doi.org/10.1029/1999RG000078, 2000.

Hersbach, H., Bell, B., Berrisford, P., Hirahara, S., Horányi, A., Muñoz-Sabater, J., Nicolas, J., Peubey, C., Radu, R., Schepers, D., Simmons, A., Soci, C., Abdalla, S., Abellan, X., Balsamo, G., Bechtold, P., Biavati, G., Bidlot, J., Bonavita, M., De Chiara, G., Dahlgren, P., Dee, D., Diamantakis, M., Dragani, R., Flemming, J., Forbes, R., Fuentes, M., Geer, A., Haimberger, L., Healy, S., Hogan, R. J., Hólm, E., Janisková, M., Keeley, S., Laloyaux, P., Lopez, P., Lupu, C., Radnoti, G., de Rosnay, P., Rozum, I., Vamborg, F., Villaume, S., and Thépaut, J.-N.: The ERA5 global reanalysis, Quarterly Journal of the Royal Meteorological Society, 146, 1999–2049, https://doi.org/10.1002/qj.3803, 2020.

Hong, S.-Y., Noh, Y., and Dudhia, J.: A New Vertical Diffusion Package with an Explicit Treatment of Entrainment Processes, Mon. Wea. Rev., 134, 2318–2341, https://doi.org/10.1175/MWR3199.1, 2006.

Huang, J., Lin, B., Minnis, P., Wang, T., Wang, X., Hu, Y., Yi, Y., and Ayers, J. K.: Satellite-based assessment of possible dust aerosols semi-direct effect on cloud water path over East Asia, Geophysical Research Letters, 33, https://doi.org/10.1029/2006GL026561, 2006a.

Huang, Y., Dickinson, R. E., and Chameides, W. L.: Impact of aerosol indirect effect on surface temperature over East Asia, Proceedings of the National Academy of Sciences, 103, 4371–4376, https://doi.org/10.1073/pnas.0504428103, 2006b.

Huffman, G. J., Stocker, E. F., Bolvin, D. T., Nelkin, E. J., and Tan, J.: GPM IMERG Early Precipitation L3 Half Hourly 0.1 degree x 0.1 degree V06, Goddard Earth Sciences Data and Information Services Center (GES DISC), Greenbelt, MD, https://doi.org/10.5067/GPM/IMERG/3B-HH-E/06, 2019.

Iacono, M. J., Delamere, J. S., Mlawer, E. J., Shephard, M. W., Clough, S. A., and Collins, W. D.: Radiative forcing by long-lived greenhouse gases: Calculations with the AER radiative transfer models, Journal of Geophysical Research: Atmospheres, 113, https://doi.org/10.1029/2008JD009944, 2008.

Immerzeel, W. W., van Beek, L. P. H., and Bierkens, M. F. P.: Climate Change Will Affect the Asian Water Towers, Science, 328, 1382–1385, https://doi.org/10.1126/science.1183188, 2010.

IPCC: Climate change 2013: The Physical Science Basis: Working Group I Contribution to the Fifth Assessment Report of the Intergovernmental Panel on Climate, Cambridge University Press, 1553 pp., 2013.

Janssens-Maenhout, G., Crippa, M., Guizzardi, D., Dentener, F., Muntean, M., Pouliot, G., Keating, T., Zhang, Q., Kurokawa, J., Wankmüller, R., Denier van der Gon, H., Kuenen, J. J. P., Klimont, Z., Frost, G., Darras, S., Koffi, B., and Li, M.: HTAP_v2.2: a mosaic of regional and global emission grid maps for 2008 and 2010 to study hemispheric transport of air pollution, Atmospheric Chemistry and Physics, 15, 11411–11432, https://doi.org/10.5194/acp-15-11411-2015, 2015.

Ji, Z., Kang, S., Cong, Z., Zhang, Q., and Yao, T.: Simulation of carbonaceous aerosols over the Third Pole and adjacent regions: distribution, transportation, deposition, and climatic effects, Clim Dyn, 45, 2831–2846, https://doi.org/10.1007/s00382-015-2509-1, 2015.

Kang, S., Zhang, Q., Qian, Y., Ji, Z., Li, C., Cong, Z., Zhang, Y., Guo, J., Du, W., Huang, J., You, Q., Panday, A. K., Rupakheti, M., Chen, D., Gustafsson, Ö., Thiemens, M. H., and Qin, D.: Linking atmospheric pollution to cryospheric change in the

Third Pole region: current progress and future prospects, Natl Sci Rev, 6, 796–809, https://doi.org/10.1093/nsr/nwz031, 2019.

Kant, S., Panda, J., Rao, P., Sarangi, C., and Ghude, S. D.: Study of aerosol-cloud-precipitation-meteorology interaction during a distinct weather event over the Indian region using WRF-Chem, Atmospheric Research, 247, 105144, https://doi.org/10.1016/j.atmosres.2020.105144, 2021.

Kaul, D. S., Gupta, T., Tripathi, S. N., Tare, V., and Collett, J. L.: Secondary Organic Aerosol: A Comparison between Foggy and Nonfoggy Days, Environ. Sci. Technol., 45, 7307–7313, https://doi.org/10.1021/es201081d, 2011.

Khain, A., Lynn, B., and Shpund, J.: High resolution WRF simulations of Hurricane Irene: Sensitivity to aerosols and choice of microphysical schemes, Atmospheric Research, 167, 129–145, https://doi.org/10.1016/j.atmosres.2015.07.014, 2016.

Koren, I., Kaufman, Y. J., Rosenfeld, D., Remer, L. A., and Rudich, Y.: Aerosol invigoration and restructuring of Atlantic convective clouds, Geophysical Research Letters, 32, https://doi.org/10.1029/2005GL023187, 2005.

Kumar, M., Parmar, K. S., Kumar, D. B., Mhawish, A., Broday, D. M., Mall, R. K., and Banerjee, T.: Long-term aerosol climatology over Indo-Gangetic Plain: Trend, prediction and potential source fields, Atmospheric Environment, 180, 37–50, https://doi.org/10.1016/j.atmosenv.2018.02.027, 2018.

Lau, K. M., Kim, M. K., and Kim, K. M.: Asian summer monsoon anomalies induced by aerosol direct forcing: the role of the Tibetan Plateau, Clim Dyn, 26, 855–864, https://doi.org/10.1007/s00382-006-0114-z, 2006.

Lau, W. K. M., Kim, K.-M., Shi, J.-J., Matsui, T., Chin, M., Tan, Q., Peters-Lidard, C., and Tao, W. K.: Impacts of aerosol–monsoon interaction on rainfall and circulation over Northern India and the Himalaya Foothills, Clim Dyn, 49, 1945–1960, https://doi.org/10.1007/s00382-016-3430-y, 2017.

Li, Z., Lau, W. K.-M., Ramanathan, V., Wu, G., Ding, Y., Manoj, M. G., Liu, J., Qian, Y., Li, J., Zhou, T., Fan, J., Rosenfeld, D., Ming, Y., Wang, Y., Huang, J., Wang, B., Xu, X., Lee, S.-S., Cribb, M., Zhang, F., Yang, X., Zhao, C., Takemura, T., Wang, K., Xia, X., Yin, Y., Zhang, H., Guo, J., Zhai, P. M., Sugimoto, N., Babu, S. S., and Brasseur, G. P.: Aerosol and monsoon climate interactions over Asia, Reviews of Geophysics, 54, 866–929, https://doi.org/10.1002/2015RG000500, 2016.

Liu, L., Cheng, Y., Wang, S., Wei, C., Pöhlker, M. L., Pöhlker, C., Artaxo, P., Shrivastava, M., Andreae, M. O., Pöschl, U., and Su, H.: Impact of biomass burning aerosols on radiation, clouds, and precipitation over the Amazon: relative importance of aerosol–cloud and aerosol–radiation interactions, Atmospheric Chemistry and Physics, 20, 13283–13301, https://doi.org/10.5194/acp-20-13283-2020, 2020.

Liu, X., Cheng, Z., Yan, L., and Yin, Z.-Y.: Elevation dependency of recent and future minimum surface air temperature trends in the Tibetan Plateau and its surroundings, Global and Planetary Change, 68, 164–174, https://doi.org/10.1016/j.gloplacha.2009.03.017, 2009.

Liu, Z., Gao, Y., and Zhang, G.: How well can a convection-permitting-modelling improve the simulation of summer precipitation diurnal cycle over the Tibetan Plateau?, Clim Dyn, 58, 3121–3138, https://doi.org/10.1007/s00382-021-06090-3, 2022.

Lynn, E., Cuthbertson, A., He, M., Vasquez, J. P., Anderson, M. L., Coombe, P., Abatzoglou, J. T., and Hatchett, B. J.: Technical note: Precipitation-phase partitioning at landscape scales to regional scales, Hydrology and Earth System Sciences, 24, 5317–5328, https://doi.org/10.5194/hess-24-5317-2020, 2020.

Mahowald, N., Ward, D. S., Kloster, S., Flanner, M. G., Heald, C. L., Heavens, N. G., Hess, P. G., Lamarque, J.-F., and Chuang, P. Y.: Aerosol Impacts on Climate and

Biogeochemistry, Annual Review of Environment and Resources, 36, 45–74, https://doi.org/10.1146/annurev-environ-042009-094507, 2011.

Manoj, M. G., Lee, S.-S., and Li, Z.: Competing aerosol effects in triggering deep convection over the Indian Region, Clim Dyn, 56, 1815–1835, https://doi.org/10.1007/s00382-020-05561-3, 2021.

Marcq, S., Laj, P., Roger, J. C., Villani, P., Sellegri, K., Bonasoni, P., Marinoni, A., Cristofanelli, P., Verza, G. P., and Bergin, M.: Aerosol optical properties and radiative forcing in the high Himalaya based on measurements at the Nepal Climate Observatory-Pyramid site (5079 m a.s.l.), Atmos. Chem. Phys., 10, 5859–5872, https://doi.org/10.5194/acp-10-5859-2010, 2010.

Matin, M. A., Chitale, V. S., Murthy, M. S. R., Uddin, K., Bajracharya, B., and Pradhan, S.: Understanding forest fire patterns and risk in Nepal using remote sensing, geographic information system and historical fire data, Int. J. Wildland Fire, 26, 276–286, https://doi.org/10.1071/WF16056, 2017.

Morrison, H., Thompson, G., and Tatarskii, V.: Impact of Cloud Microphysics on the Development of Trailing Stratiform Precipitation in a Simulated Squall Line: Comparison of One- and Two-Moment Schemes, Mon. Wea. Rev., 137, 991–1007, https://doi.org/10.1175/2008MWR2556.1, 2009.

Mues, A., Lauer, A., Lupascu, A., Rupakheti, M., Kuik, F., and Lawrence, M. G.: WRF and WRF-Chem v3.5.1 simulations of meteorology and black carbon concentrations in the Kathmandu Valley, Geoscientific Model Development, 11, 2067–2091, https://doi.org/10.5194/gmd-11-2067-2018, 2018.

Nair, V. S., Solmon, F., Giorgi, F., Mariotti, L., Babu, S. S., and Moorthy, K. K.: Simulation of South Asian aerosols for regional climate studies, Journal of Geophysical Research: Atmospheres, 117, https://doi.org/10.1029/2011JD016711, 2012.

Napoli, A., Crespi, A., Ragone, F., Maugeri, M., and Pasquero, C.: Variability of orographic enhancement of precipitation in the Alpine region, Sci Rep, 9, 13352, https://doi.org/10.1038/s41598-019-49974-5, 2019.

Napoli, A., Desbiolles, F., Parodi, A., and Pasquero, C.: Aerosol indirect effects in complex-orography areas: a numerical study over the Great Alpine Region, Atmospheric Chemistry and Physics, 22, 3901–3909, https://doi.org/10.5194/acp-22-3901-2022, 2022.

Palazzi, E., Filippi, L., and von Hardenberg, J.: Insights into elevation-dependent warming in the Tibetan Plateau-Himalayas from CMIP5 model simulations, Clim Dyn, 48, 3991–4008, https://doi.org/10.1007/s00382-016-3316-z, 2017.

Pepin, N., Bradley, R. S., Diaz, H. F., Baraer, M., Caceres, E. B., Forsythe, N., Fowler, H., Greenwood, G., Hashmi, M. Z., Liu, X. D., Miller, J. R., Ning, L., Ohmura, A., Palazzi, E., Rangwala, I., Schöner, W., Severskiy, I., Shahgedanova, M., Wang, M. B., Williamson, S. N., Yang, D. Q., and Mountain Research Initiative EDW Working Group: Elevation-dependent warming in mountain regions of the world, Nature Climate Change, 5, 424–430, https://doi.org/10.1038/nclimate2563, 2015.

Pincus, R. and Baker, M. B.: Effect of precipitation on the albedo susceptibility of clouds in the marine boundary layer, Nature, 372, 250–252, https://doi.org/10.1038/372250a0, 1994.

Prein, A. F. and Heymsfield, A. J.: Increased melting level height impacts surface precipitation phase and intensity, Nature Climate Change, 10, 771–776, https://doi.org/10.1038/s41558-020-0825-x, 2020.

Qian, Y., Yasunari, T. J., Doherty, S. J., Flanner, M. G., Lau, W. K. M., Ming, J., Wang, H., Wang, M., Warren, S. G., and Zhang, R.: Light-absorbing particles in snow and ice: Measurement and modeling of climatic and hydrological impact, Adv. Atmos. Sci., 32, 64–91, https://doi.org/10.1007/s00376-014-0010-0, 2015.

Ramanathan, V. and Carmichael, G.: Global and regional climate changes due to black carbon, Nature Geosci, 1, 221–227, https://doi.org/10.1038/ngeo156, 2008.

Ramanathan, V., Chung, C., Kim, D., Bettge, T., Buja, L., Kiehl, J. T., Washington, W. M., Fu, Q., Sikka, D. R., and Wild, M.: Atmospheric brown clouds: Impacts on South Asian climate and hydrological cycle, Proceedings of the National Academy of Sciences, 102, 5326–5333, https://doi.org/10.1073/pnas.0500656102, 2005.

Rangwala, I. and Miller, J. R.: Climate change in mountains: a review of elevation-dependent warming and its possible causes, Climatic Change, 114, 527–547, https://doi.org/10.1007/s10584-012-0419-3, 2012.

Rangwala, I., Miller, J. R., Russell, G. L., and Xu, M.: Using a global climate model to evaluate the influences of water vapor, snow cover and atmospheric aerosol on warming in the Tibetan Plateau during the twenty-first century, Clim Dyn, 34, 859–872, https://doi.org/10.1007/s00382-009-0564-1, 2010.

Rosenfeld, D.: TRMM observed first direct evidence of smoke from forest fires inhibiting rainfall, Geophysical Research Letters, 26, 3105–3108, https://doi.org/10.1029/1999GL006066, 1999.

Rosenfeld, D., Lohmann, U., Raga, G. B., O'Dowd, C. D., Kulmala, M., Fuzzi, S., Reissell, A., and Andreae, M. O.: Flood or Drought: How Do Aerosols Affect Precipitation?, Science, 321, 1309–1313, https://doi.org/10.1126/science.1160606, 2008.

Sadavarte, P., Rupakheti, M., Bhave, P., Shakya, K., and Lawrence, M.: Nepal emission inventory – Part I: Technologies and combustion sources (NEEMI-Tech) for 2001–2016, Atmospheric Chemistry and Physics, 19, 12953–12973, https://doi.org/10.5194/acp-19-12953-2019, 2019.

Sarangi, C., Tripathi, S. N., Tripathi, S., and Barth, M. C.: Aerosol-cloud associations over Gangetic Basin during a typical monsoon depression event using WRF-Chem simulation, Journal of Geophysical Research: Atmospheres, 120, 10,974-10,995, https://doi.org/10.1002/2015JD023634, 2015.

Sarangi, C., Qian, Y., Rittger, K., Bormann, K. J., Liu, Y., Wang, H., Wan, H., Lin, G., and Painter, T. H.: Impact of light-absorbing particles on snow albedo darkening and associated radiative forcing over high-mountain Asia: high-resolution WRF-Chem modeling and new satellite observations, Atmospheric Chemistry and Physics, 19, 7105–7128, https://doi.org/10.5194/acp-19-7105-2019, 2019.

Shao, T., Liu, Y., Wang, R., Zhu, Q., Tan, Z., and Luo, R.: Role of anthropogenic aerosols in affecting different-grade precipitation over eastern China: A case study, Science of The Total Environment, 807, 150886, https://doi.org/10.1016/j.scitotenv.2021.150886, 2022.

Sharma, S., Chen, Y., Zhou, X., Yang, K., Li, X., Niu, X., Hu, X., and Khadka, N.: Evaluation of GPM-Era Satellite Precipitation Products on the Southern Slopes of the Central Himalayas Against Rain Gauge Data, Remote Sensing, 12, 1836, https://doi.org/10.3390/rs12111836, 2020a.

Sharma, S., Khadka, N., Hamal, K., Shrestha, D., Talchabhadel, R., and Chen, Y.: How Accurately Can Satellite Products (TMPA and IMERG) Detect Precipitation Patterns, Extremities, and Drought Across the Nepalese Himalaya?, Earth and Space Science, 7, e2020EA001315, https://doi.org/10.1029/2020EA001315, 2020b.

Shige, S. and Kummerow, C. D.: Precipitation-Top Heights of Heavy Orographic Rainfall in the Asian Monsoon Region, Journal of the Atmospheric Sciences, 73, 3009–3024, https://doi.org/10.1175/JAS-D-15-0271.1, 2016.

Sicard, P., Crippa, P., De Marco, A., Castruccio, S., Giani, P., Cuesta, J., Paoletti, E., Feng, Z., and Anav, A.: High spatial resolution WRF-Chem model over Asia:

Physics and chemistry evaluation, Atmospheric Environment, 244, 118004, https://doi.org/10.1016/j.atmosenv.2020.118004, 2021.

Sijikumar, S., Aneesh, S., and Rajeev, K.: Multi-year model simulations of mineral dust distribution and transport over the Indian subcontinent during summer monsoon seasons, Meteorol Atmos Phys, 128, 453–464, https://doi.org/10.1007/s00703-015-0422-0, 2016.

Soni, P., Tripathi, S. N., and Srivastava, R.: Radiative effects of black carbon aerosols on Indian monsoon: a study using WRF-Chem model, Theor Appl Climatol, 132, 115–134, https://doi.org/10.1007/s00704-017-2057-1, 2018.

Talchabhadel, R., Karki, R., and Parajuli, B.: Intercomparison of precipitation measured between automatic and manual precipitation gauge in Nepal, Measurement, 106, 264–273, https://doi.org/10.1016/j.measurement.2016.06.047, 2017.

Terao, T., Islam, Md. N., Hayashi, T., and Oka, T.: Nocturnal jet and its effects on early morning rainfall peak over northeastern Bangladesh during the summer monsoon season, Geophysical Research Letters, 33, https://doi.org/10.1029/2006GL026156, 2006.

Tewari, M., Chen, F., Wang, W., Dudhia, J., LeMone, M. A., Mitchell, K., Ek, M., Gayno, G., Wegiel, J., and Cuenca, R. H.: Implementation and verification of the unified NOAH land surface model in the WRF model, in: 20th conference on weather analysis and forecasting/16th conference on numerical weather prediction, 2165–2170, 2004.

Twomey, S.: The Influence of Pollution on the Shortwave Albedo of Clouds, J. Atmos. Sci., 34, 1149–1152, https://doi.org/10.1175/1520-0469(1977)034<1149:TIOPOT>2.0.CO;2, 1977.

Vernier, J.-P., Thomason, L. W., and Kar, J.: CALIPSO detection of an Asian tropopause aerosol layer, Geophysical Research Letters, 38, https://doi.org/10.1029/2010GL046614, 2011.

Wang, S., Zhang, M., Pepin, N. C., Li, Z., Sun, M., Huang, X., and Wang, Q.: Recent changes in freezing level heights in High Asia and their impact on glacier changes, Journal of Geophysical Research: Atmospheres, 119, 1753–1765, https://doi.org/10.1002/2013JD020490, 2014.

Wu, L., Su, H., and Jiang, J. H.: Regional simulation of aerosol impacts on precipitation during the East Asian summer monsoon, Journal of Geophysical Research: Atmospheres, 118, 6454–6467, https://doi.org/10.1002/jgrd.50527, 2013.

Wu, L., Gu, Y. (ORCID:0000000234120794), Jiang, J. H., Su, H., Yu, N., Zhao, C., Qian, Y., Zhao, B. (ORCID:0000000184389188), Liou, K.-N., and Choi, Y.-S.: Impacts of aerosols on seasonal precipitation and snowpack in California based on convection-permitting WRF-Chem simulations, Atmospheric Chemistry and Physics (Online), 18, https://doi.org/10.5194/acp-18-5529-2018, 2018.

Yang, Q., W. I. Gustafson Jr., Fast, J. D., Wang, H., Easter, R. C., Morrison, H., Lee, Y.-N., Chapman, E. G., Spak, S. N., and Mena-Carrasco, M. A.: Assessing regional scale predictions of aerosols, marine stratocumulus, and their interactions during VOCALS-REx using WRF-Chem, Atmos. Chem. Phys., 11, 11951–11975, https://doi.org/10.5194/acp-11-11951-2011, 2011.

Zaveri, R. A. and Peters, L. K.: A new lumped structure photochemical mechanism for large-scale applications, Journal of Geophysical Research: Atmospheres, 104, 30387–30415, https://doi.org/10.1029/1999JD900876, 1999.

Zaveri, R. A., Easter, R. C., Fast, J. D., and Peters, L. K.: Model for Simulating Aerosol Interactions and Chemistry (MOSAIC), Journal of Geophysical Research: Atmospheres, 113, https://doi.org/10.1029/2007JD008782, 2008.

Zhang, Y. and Guo, Y.: Variability of atmospheric freezing-level height and its impact on the cryosphere in China, Annals of Glaciology, 52, 81–88, https://doi.org/10.3189/172756411797252095, 2011.

Zhang, Y., Fan, J., Li, Z., and Rosenfeld, D.: Impacts of cloud microphysics parameterizations on simulated aerosol–cloud interactions for deep convective clouds over Houston, Atmospheric Chemistry and Physics, 21, 2363–2381, https://doi.org/10.5194/acp-21-2363-2021, 2021.

Zhao, C., Chen, S., Leung, L. R., Qian, Y., Kok, J. F., Zaveri, R. A., and Huang, J.: Uncertainty in modeling dust mass balance and radiative forcing from size parameterization, Atmospheric Chemistry and Physics, 13, 10733–10753, https://doi.org/10.5194/acp-13-10733-2013, 2013.

Zhao, C., Hu, Z., Qian, Y., Ruby Leung, L., Huang, J., Huang, M., Jin, J., Flanner, M. G., Zhang, R., Wang, H., Yan, H., Lu, Z., and Streets, D. G.: Simulating black carbon and dust and their radiative forcing in seasonal snow: a case study over North China with field campaign measurements, Atmospheric Chemistry and Physics, 14, 11475–11491, https://doi.org/10.5194/acp-14-11475-2014, 2014.

Supplementary Information for Chapter 4

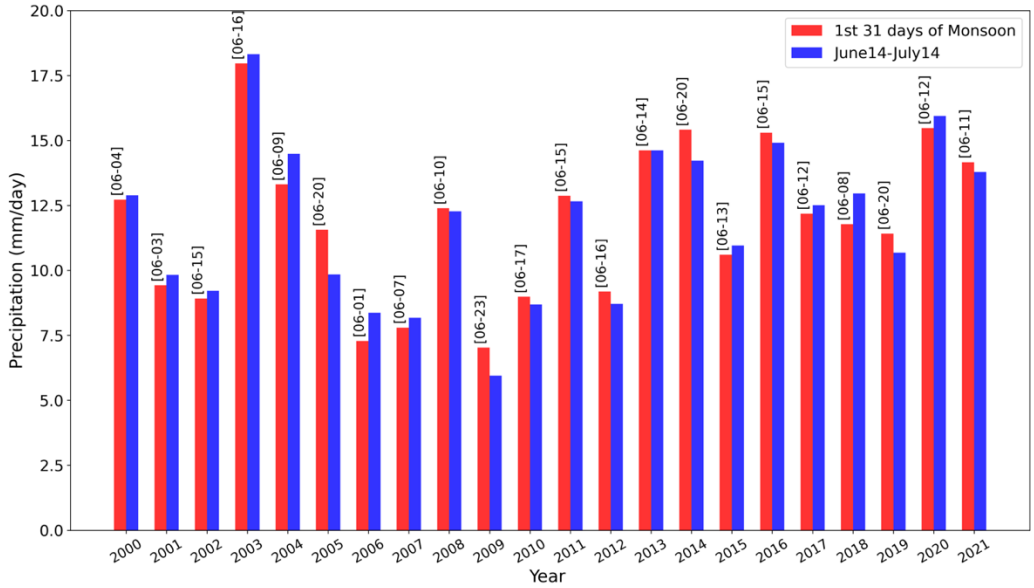

Figure C4S1: The 22 years of mean monsoonal precipitation for the first month (31 days after the monsoon onset) using IMERG data over the CenHim region. In 2013 the monsoon onset occurred on June 14th from eastern Nepal according to DHM. June 14th to July 14th is the period of our simulation, which includes the first 31 days after monsoonal onset for 2013 (or first month of monsoon). The dates shown in bracket at the top of the bar indicates the date of monsoon onset over Nepal for that respective year.

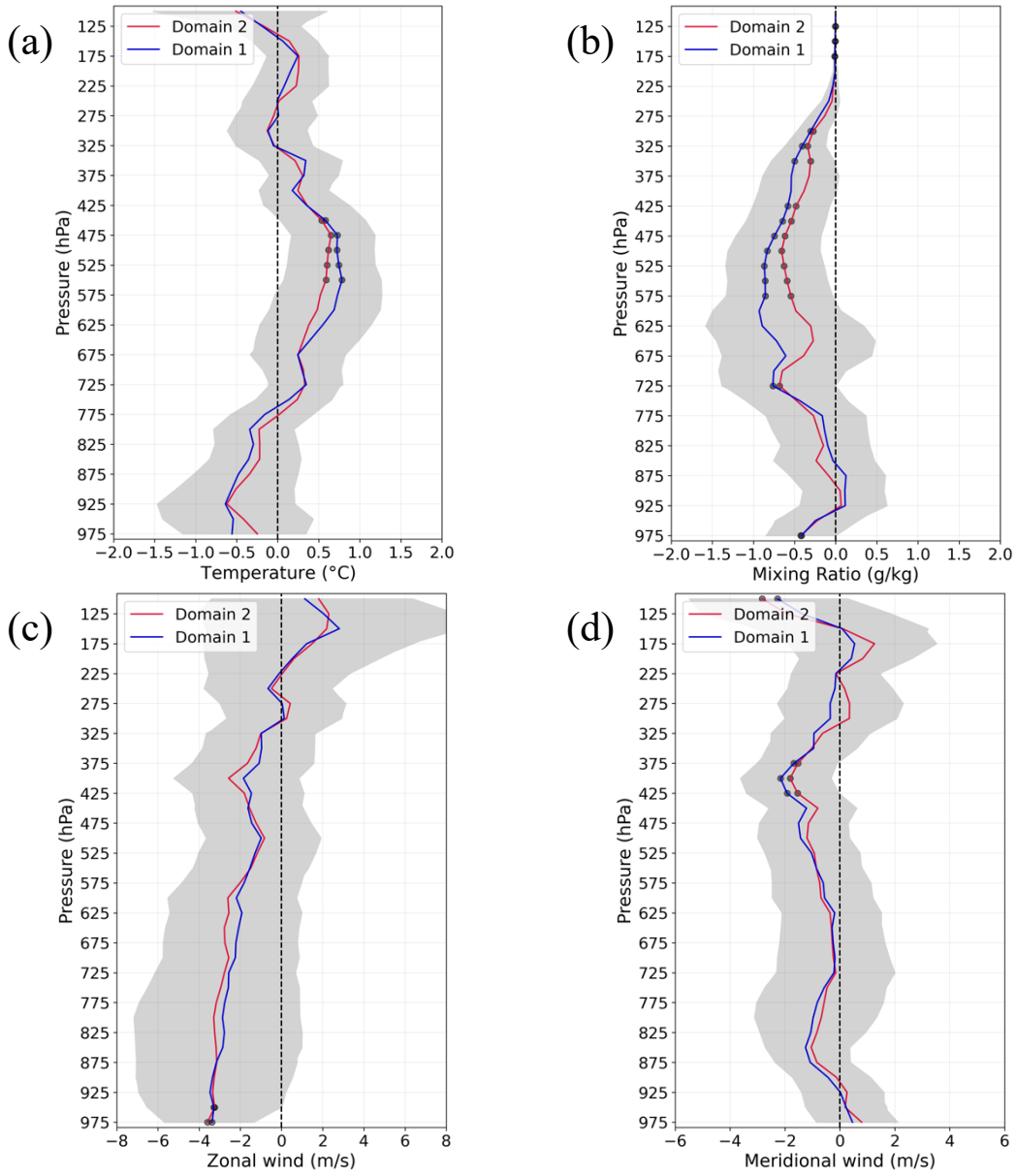

Figure C4S2: The mean (June 17 – July 14, except July 5th and 9th) (a) temperature, (b) mixing ratio, (c) zonal, and (d) meridional wind bias (CTL – Observation) profiles from the simulated (CTL) output sampled at the nearest grid cell location from the upper air sounding observation location at Patna location. Shaded regions represent the 95% confidence interval of the difference between the model and observation. The dot indicates that the differences between the observation and model are only significantly different at those levels.

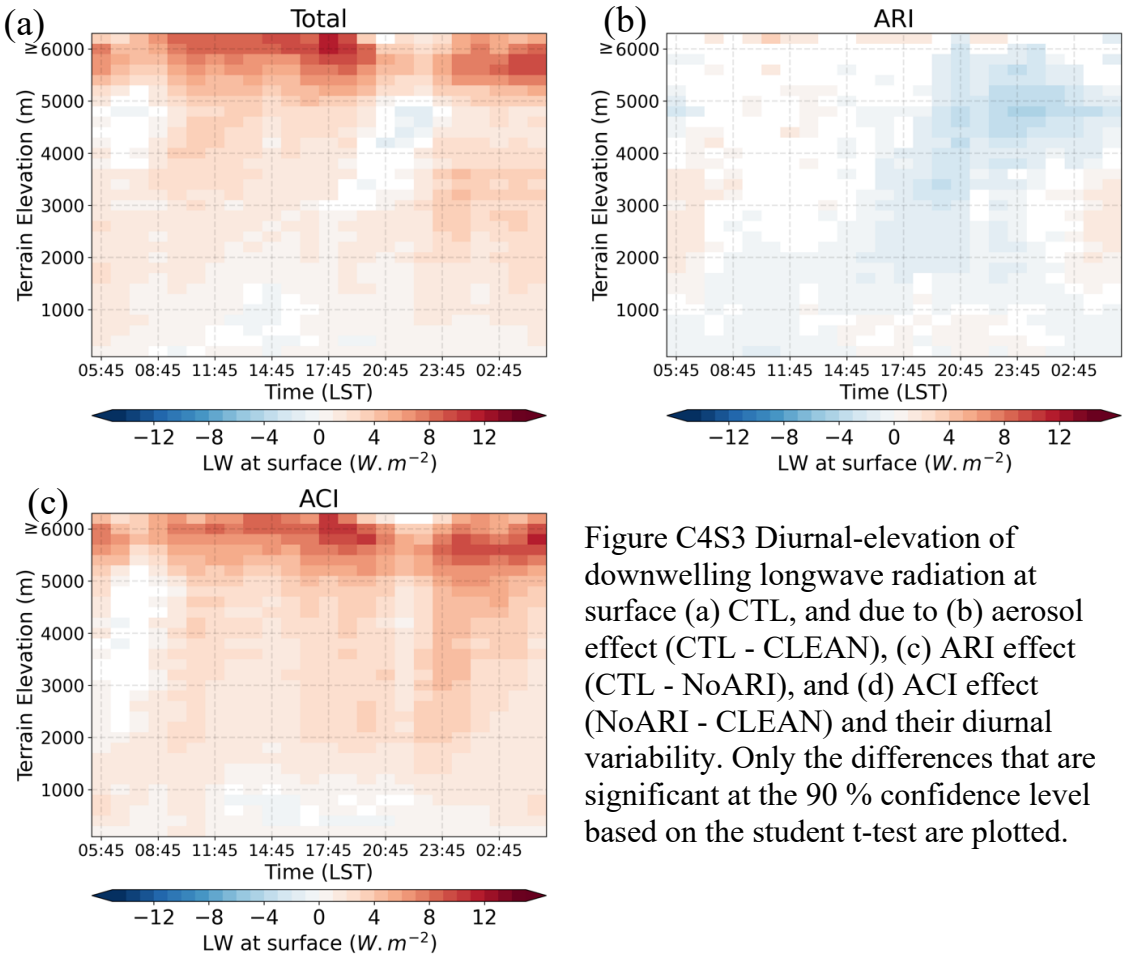

Figure C4S3 Diurnal-elevation of downwelling longwave radiation at surface (a) CTL, and due to (b) aerosol effect (CTL - CLEAN), (c) ARI effect (CTL - NoARI), and (d) ACI effect (NoARI - CLEAN) and their diurnal variability. Only the differences that are significant at the 90 % confidence level based on the student t-test are plotted.

Chapter 5: Summary and Conclusions

The primary objective of this dissertation is to study the impact of atmospheric aerosols, from natural and anthropogenic sources, in modulating the monsoonal precipitation, cloud processes, and freezing isotherm over the central Himalayas. Because the Indian monsoon region is collocated in the heavily polluted region of the IGP due to its topographical features and the intensive anthropogenic activities, it is important to advance the understanding on the contribution of aerosols in modulating the monsoonal precipitation over the downwind Himalayan region. This study implemented the sixteen years of remote sensing and reanalysis datasets (Chapter 2) and cloud-resolving scale numerical modeling (Chapters 3 and 4) to improve the understanding of the role of aerosols in perturbating the convective processes and hence the precipitation intensity and distribution over the Central Himalayas.

The main objective of chapter two was to assess the impact of aerosols on the cloud properties, precipitation, and freezing isotherm during the Indian summer monsoon season in the daily and interannual timescale over the foothills and the southern slopes of the Himalayas (SSFH). The satellite-based and reanalysis datasets from 2002 to 2017 were implemented to identify the polluted and relatively cleaner days based on the ±1 standard deviation from the mean sixteen-year monsoonal AOD over the SSFH region. Compared to clean days, polluted days were characterized by the presence of broader and taller clouds and enhanced precipitation. The direct relationship of AOD with cloud invigoration and precipitation remained consistent, regardless of the meteorological forcing (relative humidity and vertical velocity). Higher aerosol loading showed a positive correlation between deeper clouds and precipitation over the SSFH region during

both wet and dry monsoonal years. Also, the higher concentration of aerosols over the SSFH increased the mean FLH by 136.2 ±18.82 meters, which can be critical for the snowline altitude and impact the hydroclimate of the Himalayas. The results of this chapter indicate that the impact of aerosol in modulating the regional monsoonal precipitation and freezing isotherm can be crucial for the hydroclimate of the Himalayas.

Due to the challenges and limitations of satellite-based observational study in isolating the impact of aerosols from different sources and their interaction with radiation and cloud the findings from chapter one demanded the higher resolution regional numerical modeling. Larger biases in the global climate models are associated with the convective parameterization, as the coarser-resolution simulation limits the simulation of the life cycle of the convective precipitation processes. Also, the global climate model cannot capture the detailed topographical structure that influences the transport of moisture and aerosol processes, especially over the complex terrain, and limits our understanding of aerosol-cloud-precipitation interaction. Unlike climate models, the high-resolution cloud-resolving scale models can better simulate comprehensive cloud evolution, associated thermodynamics, and optical properties, which are essential in the determination of atmospheric and surface energy distribution. Furthermore, it also better represents the aerosol emissions and transport, which are crucial for understanding and quantifying the aerosol impact on precipitation and climate.

To further understand and better quantify the impact of locally emitted and transported natural and anthropogenic aerosols on the regional precipitation through radiative and microphysical pathways, in chapters 3 and 4, we implemented a cloud-resolving scale WRF-Chem, which can represent the aerosols from different sources and

simulate the interaction of aerosol with radiation and clouds. The objective of this chapter was to assess the impact of the long-range transported dust aerosols after an episodic and significant dust storm event, which occurred from 12 to 15 June 2018 in the Thar desert located in northwestern India, on the precipitation and convective process over the Nepal Himalayas. The transported dust aerosols were isolated in a sensitivity study by zeroing out the dust aerosols from lateral boundary conditions but keeping all other locally emitted and transported aerosols. Dust aerosols activated as CCN enhanced the convection by increasing the updraft with the release of latent heat of condensation. Long-range transported dust aerosols significantly impacted the microphysical properties and enhanced the precipitation by 9.3% over the southern slopes of the Nepal Himalayas. The enhanced FLH (+58.5 m) over the Central Himalayan region due to the dust aerosols is comparable (+136.2 m) to the findings from chapter one. The simulation isolated the role of dust aerosols alone from other aerosols, so it is possible that the tropospheric warming by the proportional effect of the total atmospheric aerosols is larger than the simulated warming signal. Though we analyzed only one episodic dust transport event in this chapter, it highlights the significant importance of remote dust aerosols in impacting the cloud microphysical properties and precipitation over the Nepal Himalayas, which can significantly modulate the Himalayan hydrology.

In chapter 4, we simulated the first monsoonal month of 2013 (June 14 to July 15) using a cloud-resolving WRF-Chem to understand the impact of aerosols on elevational-dependent temperature and precipitation over the Central Himalayan region. We performed three different sensitivity experiments CTL (baseline simulation with all anthropogenic and natural aerosols), NoARI (similar to CTL but excluding aerosol

radiation feedback), and CLEAN (similar to CTL but reducing the aerosols to 10%). The higher elevation showed a strong diurnal variation in surface temperature, with a strong aerosol driven cooling above 4000 m ASL during the daytime (by -1.3°C) and above 2000 m ASL during the nighttime warming (+0.03 °C). The simulated results show a contrasting influence of aerosol on the elevation-dependent precipitation. The mid-elevation, generally between 1000 and 3000 meters, acted as the threshold elevation below and above which the diurnal variation and precipitation of various intensities (light, moderate, and heavy) responded differently for ARI, ACI, and the combined effect of aerosols. The aerosol effect reduced the mean light precipitation by 17% over the CenHim with a dominating response due to the ARI effect. Along with the stronger convection, the ACI effect dominated and resulted in enhanced heavy precipitation by 12% below 2000 m ASL, which can potentially increase the risk for extreme events (floods and landslides). In contrast, the suppressed precipitation due to aerosols above 2000 m ASL can be critical for the regional supply of water resources. The mean FLH due to the total aerosol effect is reduced by 9 m, but the difference is not statistically significant and contrasts with our findings in chapters two and three. The non-significant difference in FLH might be associated with the lower concentration of radiation-absorbing aerosols. Sensitivity studies on the magnitude of the radiation-absorbing anthropogenic aerosols and long-term simulation can provide further insight into the role of aerosols in modulating the FLH.

The synopsis of the study suggests that the natural and anthropogenic aerosols significantly modulate the convective processes, monsoonal precipitation, and freezing isotherm over the Central Himalayan region, which could pose significant consequences

to the changing climatic conditions of the Himalayas. The Himalayan and Tibetan Plateau region, which modulates the hydroclimate of south and east Asia, are highly sensitive to the rapidly changing climate. The enhanced FLH over the higher elevation can be crucial to the upward movement of snowline altitude, snow to rainfall ratio, melting of the snowpack, and reduction in the higher elevation surface albedo. Also, the aerosol-enhanced nighttime warming due to increased cloud coverage over the high-elevation can significantly increases the minimum temperature. The warming of the minimum temperature can have a more critical impact during the winter/spring, and our results suggest elaborating the investigation to quantify the effect of aerosols in elevation-dependent warming during other seasons. The enhanced/suppressed precipitation over the low/high elevations of the Central Himalayas has important implications in terms of frequency and intensity of extreme weather events, altering the snow water equivalent and surface runoff, and regional water supply. The aerosol-induced enhanced FLH, increased warming, and precipitation can further intensify the streamflow and exacerbates the downstream flooding concern. These can directly influence the Himalayan ecosystem and the large population residing downstream of the Himalayan region. Our results reinforce the global need for a systematic approach to deaccelerate anthropogenic activities to minimize the future risk to the Himalayan climate.

5.1 Future Recommendations

Due to the complex dynamic and physical processes and larger uncertainties involved in the aerosol-cloud-precipitation-climate interaction, it is very challenging to isolate the impact of individual mechanisms and components. In this study, we

investigated the link between natural and anthropogenic aerosols in modulating the convective processes and monsoonal precipitation over the Central Himalayan region. Also, we found that the atmospheric aerosols could increase the freezing level height, which can be crucial for the change in snowline altitude and snowpack melting, which can pose a significant consequence to the changing Himalayan hydroclimate. However, further research and investigation are needed to continuously advance the understanding of the impact of aerosol on the Himalayan hydroclimate.

Our results underline the need for an improved representation of terrain-induced convective processes over the complex topography to understand further and quantify the complete impact of aerosol on cloud microphysics, precipitation, and the regional climate. Additional dust storm case studies should be simulated to improve the physical understanding of the remotely transported mineral dust aerosols in the Himalayan hydrology via aerosol-cloud-radiation-interaction and the deposition over the snowpack. Our findings also demand a further detailed investigation of the role of aerosol loading in modulating the FLH, especially over the high mountains of the world located downwind of the polluted region. Due to the inhomogeneity in the aerosol distribution over the complex topography, improved emission inventory together with its diurnal distribution will help elaborate and advance further the current findings on the diurnal impact of aerosols on temperature distribution and convective/precipitation system. A long-term simulation with the inclusion of feedback processes associated with aerosol-snow-interaction will better assess and advance the understanding of the diurnal to interannual responses of elevation-dependent temperature and precipitation over the highly vulnerable Himalayan region.

The biases of the global and regional model may be overemphasized because of inaccuracies and uncertainties associated with the limited observations. There is a need for continuous data collection from a more dense distribution of observational networks (e.g., AERONET and weather stations) with more meteorological variables along the elevational transect of the Himalayan topography, especially over the high elevation region. It not only quantifies the long-term trend and pattern of the sensitive regions but also will help evaluate and constrain numerical modeling studies in complex terrain.